

OXYGEN ISOTOPES AND VOLATILES IN  
MARTIAN METEORITES

Thesis by  
Melanie Beth Channon

In Partial Fulfillment of the Requirements for the  
Degree of  
Doctor of Philosophy



CALIFORNIA INSTITUTE OF TECHNOLOGY  
Pasadena, California  
2013  
(Defended October 22, 2012)

© 2013  
Melanie B. Channon  
All Rights Reserved

## ACKNOWLEDGEMENTS

I would like to thank my dear husband Mike Newman for introducing me to the world of academia and supporting me the entire way through my undergraduate and graduate studies, with much sacrifice to himself, including taking the hardest bar exam in the country, working at a miserable job for two years, and living long distance for three years. If we survived all this, we can survive anything.

I would like to thank my advisers John Eiler and Ed Stolper for accepting me as a student, believing in me, and never making me feel like I was not meant to be in graduate school at Caltech. It should also go without saying (although it won't) that their guidance has made me a much better scientist. I am honored to have been advised by such brilliant minds.

I would like to thank George Rossman, Paul Asimow, and Ken Farley for always having an open door policy with me and being so willing and excited to talk about science.

I would like to thank Jeremy Boyce, John Beckett, and Mike Baker for not only their invaluable advice and insightful discussions about science, but also for their genuine friendship and reminders that great science is balanced by great recreation.

I would like to thank Magalie Bonifacie, Lindsey Hedges, Nami Kitchen, Marion Le Voyer, Ma Chi, and Yunbin Guan for their vital roles in my development of skills in the laboratory and in using analytical instruments.

Last but not least, I would like to thank my dear friend June Wicks for her endless encouragement and her irreplaceable friendship.

## ABSTRACT

Oxygen isotopes were measured in mineral separates from martian meteorites using laser fluorination and were found to be remarkably uniform in both  $\delta^{18}\text{O}$  and  $\Delta^{17}\text{O}$ , suggesting that martian magmas did not assimilate aqueously altered crust regardless of any other geochemical variations.

Measurements of Cl, F, H, and S in apatite from martian meteorites were made using the SIMS and NanoSIMS. Martian apatites are typically higher in Cl than terrestrial apatites from mafic and ultramafic rocks, signifying that Mars is inherently higher in Cl than Earth. Apatites from basaltic and olivine-phyric shergottites are as high in water as any terrestrial apatite from mafic and ultramafic rocks, implying the possibility that martian magmas may be more similar in water abundance to terrestrial magmas than previously thought. Apatites from lherzolitic shergottites, nakhlites, chassignites, and ALH 84001 (all of which are cumulate rocks) are all lower in water than the basaltic and olivine-phyric shergottites, indicating that the slow-cooling accumulation process allows escape of water from trapped melts where apatite later formed. Sulfur is only high in some apatites from basaltic and olivine-phyric shergottites and low in all other SNCs from this study, which could mean that cumulate SNCs are low in all volatiles and that there are other controlling factors in basaltic and olivine-phyric magmas dictating the inclusion of sulfur into apatite.

Sulfur  $K\alpha$  X-rays were measured in SNC apatites using the electron probe. None of the peaks in the SNC spectra reside in the same position as anhydrite (where sulfur is 100% sulfate) or pyrite (where sulfur is 100% sulfide), but instead all SNC spectra peaks lie in between these two end member peaks, which implies that SNC apatites may be substituting

some sulfide, as well as sulfate, into their structure. However, further work is needed to verify this hypothesis.

## TABLE OF CONTENTS

List of Figures and Tables.....	viii
<b>Introduction:</b> Mars and Martian Meteorites.....	1
<b>Chapter I:</b> Oxygen Isotope Compositions of Mineral Separates from SNC Meteorites: Constraints on the Origin and Evolution of Martian Magmas .....	4
Introduction .....	4
Previous Studies .....	10
Values of $\delta^{18}\text{O}$ .....	10
Values of $\Delta^{17}\text{O}$ .....	11
Sample Materials, Preparation, and Analytical Techniques.....	13
Results .....	16
Discussion.....	19
Cleaning Study .....	19
Measurements of $\delta^{18}\text{O}$ .....	22
Comparison of the Present Study with Previous Data .....	23
Shergottites.....	29
DaG 476 Olivine and NWA 4468 Maskelynite .....	32
Nakhlites, Chassignite, and ALH 84001 .....	34
Measurements of $\Delta^{17}\text{O}$ .....	35
Conclusions .....	39
<b>Chapter II:</b> Abundance of Cl, F, H, and S in Apatites from SNC Meteorites.....	42
Introduction .....	42
Materials and Methods .....	45
Results .....	48
NanoSIMS Images .....	48
SNC Apatite Spot Analyses.....	50
Discussion.....	62

H <sub>2</sub> O Contamination.....	62
H <sub>2</sub> O versus Rock Type.....	70
Sulfur.....	74
Summary/Conclusions .....	77
<b>Chapter III: Speciation of Sulfur in Apatites from SNC Meteorites.....</b>	<b>78</b>
Introduction .....	78
Materials and Methods .....	79
Data Reduction .....	81
Results .....	81
Discussion.....	92
Sulfur Speciation.....	92
Sulfur Concentrations .....	96
Conclusions .....	98
Bibliography .....	101
Appendix A: Raw Data for Chapter I .....	122
Appendix B: Raw Data and Calibration Curves for Chapter II .....	130
Appendix C: Supplementary Data, Spectra, and Calibration Curves for Chapter III.....	162

## LIST OF FIGURES AND TABLES

	<i>Page</i>
Figure 1.1. Previous $\delta^{18}\text{O}$ studies of SNCs.....	9
Table 1.1. Oxygen isotope data of SNC mineral separates from this study.....	17
Table 1.2. Oxygen isotope data on mineral separates from the cleaning experiment.....	23
Figure 1.2. Measurements of $\delta^{18}\text{O}$ of SNC mineral separates from this study .....	24
Figure 1.3. Histogram of $\Delta^{17}\text{O}$ measurements of SNC mineral separates from this study.....	25
Figure 1.4. Comparison of $\delta^{18}\text{O}$ SNC mineral separates from this study with theoretically and experimentally predicted $\delta^{18}\text{O}$ of coexisting minerals at equilibrium and terrestrial samples.....	26
Figure 1.5. Comparisons of $\delta^{18}\text{O}$ measurements of SNCs from this study to those from other laboratories .....	27
Figure 1.6. Comparisons of $\Delta^{17}\text{O}$ measurements of SNCs form this study to those from other laboratories .....	36
Figure 2.1. Composition of SNC apatites compared to terrestrial apatites .....	44
Figure 2.2. NanoSIMS images of apatite 2 from shergottite JaH 479 .....	49
Figure 2.3. NanoSIMS images of apatite 6 from shergottite JaH 479 .....	50
Figure 2.4. NanoSIMS images of apatite 7 from shergottite JaH 479 .....	51
Figure 2.5. NanoSIMS images of apatite 4 from shergottite NWA 6710.....	52

Figure 2.6. NanoSIMS images of olivine from shergottite NWA 6710 .....	53
Figure 2.7. NanoSIMS images of pyroxene from shergottite NWA 6710 .....	54
Figure 2.8. NanoSIMS images of maskelynite from shergottite NWA 6710 .....	55
Figure 2.9. NanoSIMS images of apatite 1 from shergottite Dhofar 019 .....	56
Figure 2.10. NanoSIMS images of pyroxene from shergottite Dhofar 019 .....	57
Table 2.1. Measurements of Cl, F, H <sub>2</sub> O, and S in SNC apatites from this study .....	58
Table 2.2. Measurements of H <sub>2</sub> O in SNC and terrestrial olivines from this study .....	60
Figure 2.11. Abundance of chlorine in apatites from SNCs.....	62
Figure 2.12. Abundance of H <sub>2</sub> O in apatites from SNCs.....	63
Figure 2.13. Abundance of H <sub>2</sub> O in apatites and olivines from SNCs and terrestrial samples.....	64
Figure 2.14. Ternary diagram for the composition of apatite in SNCs and terrestrial samples.....	65
Figure 2.15. Abundance of sulfur in apatites from SNCs .....	66
Figure 2.16. Calibration curves for OH in apatite and olivine .....	68
Figure 2.17. Hydrogen versus carbon for measurements made in this study ..	70
Figure 2.18. Composition of SNC apatites compared to terrestrial apatites ....	74
Figure 2.19. NanoSIMS and back-scattered electron images of apatite 7 from shergottite JaH 479 .....	75

Table 3.1. Peak positions of sulfur X-rays and the estimated percent of sulfide in apatites from session 1 .....	82
Table 3.2. Peak positions of sulfur X-rays and the estimated percent of sulfide in apatites form session 2 .....	82
Table 3.3. Peak positions of sulfur X-rays and the estimated percent of sulfide in apatites from session 3 .....	83
Figure 3.1. Spectra of terrestrial standards for each analytical session.....	84
Figure 3.2. Percent of sulfur estimated to be sulfide for all apatites measured in this study.....	87
Figure 3.3. Sulfur X-ray peak positions for all measurements from this study for spectrometer 3.....	88
Figure 3.4. Spectra of apatites from shergottite JaH 479 on spectrometer 3 ...	89
Figure 3.5. Spectra of apatites from shergottite NWA 856 on spectrometer 3 .....	91
Figure 3.6. Spectra of apatites from shergottite NWA 2986 on spectrometer 3 .....	92
Figure 3.7. Spectra of apatites from shergottite Shergotty on spectrometer 3 .....	93
Figure 3.8. Spectra of apatites from shergottite RBT 04262 on spectrometer 3 .....	94
Figure 3.9. Spectra of apatites from shergottite NWA 1950 on spectrometer 3 .....	95
Figure 3.10. Example of varying spectral intensities .....	96

Table 3.4. Estimated intensities of sulfur X-rays and sulfur abundances .....	97
Figure 3.11. Peak intensity versus S abundance for spectrometer 3 in session 1 .....	98
Table 3.5. Calculated concentrations from this study.....	99
Table A.1. Raw data from all Delta sessions .....	123
Table A.2. Raw data from all MAT 252 sessions.....	128
Table B.1. Raw data from the SIMS session .....	131
Figure B.1. Calibration curve for OH during the SIMS session .....	135
Figure B.2. Calibration curve for Cl during the SIMS session .....	135
Figure B.3. Calibration curve for F during the SIMS session .....	136
Figure B.4. Calibration curve for S during the SIMS session .....	136
Table B.2. Raw data from the June 2011 NanoSIMS session.....	137
Figure B.5. Calibration curve for OH during the June 2011 NanoSIMS session .....	140
Figure B.6. Calibration curve for Cl during the June 2011 NanoSIMS session .....	140

Figure B.7. Calibration curve for F during the June 2011 NanoSIMS session .....	141
Figure B.8. Calibration curve for S during the June 2011 NanoSIMS session .....	141
Table B.3. Raw data from the December 2011 NanoSIMS session .....	142
Figure B.9. Calibration curve for OH during the December 2011 NanoSIMS session .....	144
Figure B.10. Calibration curve for Cl during the December 2011 NanoSIMS session .....	144
Figure B.11. Calibration curve for F during the December 2011 NanoSIMS session .....	145
Figure B.12. Calibration curve for S during the December 2011 NanoSIMS session .....	145
Table B.4. Raw data from the February 2012 NanoSIMS session .....	146
Figure B.13. Calibration curve for OH during the February 2012 NanoSIMS session .....	149
Figure B.14. Calibration curve for Cl during the February 2012 NanoSIMS session .....	149

Figure B.15. Calibration curve for F during the February 2012 NanoSIMS session .....	150
Figure B.16. Calibration curve for S during the February 2012 NanoSIMS session .....	150
Table B.5. Raw data from the May 2012 NanoSIMS session.....	151
Figure B.17. Calibration curve for OH in apatite during the May 2012 NanoSIMS session .....	155
Figure B.18. Calibration curve for OH in olivine during the May 2012 NanoSIMS session .....	155
Table B.6. Raw data from the June 2012 NanoSIMS session.....	156
Figure B.19. Calibration curve for OH in apatite during the June 2012 NanoSIMS session .....	159
Figure B.20. Calibration curve for OH in olivine during the June 2012 NanoSIMS session .....	159
Figure B.21. Calibration curve for Cl in apatite during the June 2012 NanoSIMS session .....	160
Figure B.22. Calibration curve for F in apatite during the June 2012 NanoSIMS session .....	160

Figure B.23. Calibration curve for S in apatite during the June 2012 NanoSIMS session .....	161
Table C.1. Analyses from session 1 that were removed.....	162
Figure C.1. Spectra of apatites from shergottite JaH 479 on spectrometer 1 .....	163
Figure C.2. Spectra of apatites from shergottite JaH 479 on spectrometer 2 .....	164
Figure C.3. Spectra of apatites from shergottite JaH 479 on spectrometer 5 .....	166
Figure C.4. Spectra of apatites from shergottite NWA 856 on spectrometer 1 .....	167
Figure C.5. Spectra of apatites from shergottite NWA 856 on spectrometer 2 .....	168
Figure C.6. Spectra of apatites from shergottite NWA 856 on spectrometer 5 .....	169
Figure C.7. Spectra of apatites from shergottite NWA 2986 on spectrometer 1 .....	170
Figure C.8. Spectra of apatites from shergottite NWA 2986 on spectrometer 2 .....	171

Figure C.9. Spectra of apatites from shergottite NWA 2986 on spectrometer 5 .....	172
Figure C.10. Spectra of apatites from shergottite Shergotty on spectrometer 1 .....	173
Figure C.11. Spectra of apatites from shergottite Shergotty on spectrometer 2 .....	173
Figure C.12. Spectra of apatites from shergottite Shergotty on spectrometer 5 .....	174
Figure C.13. Spectra of apatites from shergottite RBT 04262 on spectrometer 2 .....	174
Figure C.14. Spectra of apatites from shergottite RBT 04262 on spectrometer 5 .....	175
Figure C.15. Spectra of apatites from shergottite NWA 1950 on spectrometer 1 .....	175
Figure C.16. Spectra of apatites from shergottite NWA 1950 on spectrometer 2 .....	176
Figure C.17. Spectra of apatites from shergottite NWA 1950 on spectrometer 5 .....	176

Figure C.18. Peak intensity versus S abundance for spectrometer 2 in session 1 .....	177
Figure C.19. Peak intensity versus S abundance for spectrometer 5 in session 1 .....	178
Figure C.20. Peak intensity versus S abundance for spectrometer 1 in session 2 .....	179
Figure C.21. Peak intensity versus S abundance for spectrometer 2 in session 2 .....	180
Figure C.22. Peak intensity versus S abundance for spectrometer 3 in session 2 .....	181
Figure C.23. Peak intensity versus S abundance for spectrometer 5 in session 2 .....	182
Table C.2. Calculated sulfur concentration data.....	183

## *Introduction*

### MARS AND MARTIAN METEORITES

Martian (SNC) meteorites are the only physical samples we have from the planet Mars. They provide a valuable way to explore martian geochemistry as well as to test theoretical models and to corroborate observations and measurements made on Mars, either remotely from orbit or from ground-based landers and rovers. Some of the most impactful observations and measurements include liquid-carved (most likely water) geomorphological features on the martian surface (Carr 2012 and references therein); spectra indicating the presence of carbonates, hematite, sulfates, halides, and phyllosilicates (Christensen et al. 2001; Squyres et al. 2004; Bibring et al. 2006; Ming et al. 2006; Ehlmann et al. 2008; Mustard et al. 2008; Morris et al. 2010; Jensen and Glotch 2011), which are all produced in the presence of water; and a wealth of volatiles, some of which, such as chlorine and sulfur, appear to be more abundant on Mars than on Earth (Clark and Baird 1979; Dreibus and Wanke 1985, 1987; Haskin et al. 2005; King and McLennan 2010).

To date, there are 67 known martian meteorites, and they are petrographically grouped into six types of rocks: Basalts, olivine-phyric basalts, lherzolites (these first three are known as shergottites named after the type specimen Shergotty), clinopyroxenites (known as nakhlites named after the type specimen Nakhla), one orthopyroxenite (named ALH 84001), and dunites (known as chassignites named after the type specimen Chassigny). They span a wide range of ages from 175 Ma to 4.1 Ga (Borg et al. 1997; Nyquist et al.

2001; Borg et al. 2003; Bouvier et al. 2005, 2008; Symes et al. 2008; Bouvier et al. 2009; Nyquist et al. 2009; Park et al. 2009; Lapen et al. 2010), and are thought to come from various parts of the martian surface. Although some alteration materials and volatile elements have been found in the SNCs (Bridges et al. 2001; Filiberto and Treiman 2009), they do not exhibit abundant evidence of martian magmas being wet. They do not contain nominally hydrous minerals or anomalously high volatiles like what is observed remotely.

The focus of my studies at Caltech has been to use indirect techniques to investigate the presence of water and volatiles that may have existed on the martian surface and in the magmas that generated these meteorites. Specifically, I measured oxygen isotopes in mineral separates from many of the martian meteorites to detect whether magmas had assimilated crust that had been aqueously altered. This would be evident by variation in oxygen isotopes between meteorites, and would contribute to remote observations that suggest past liquid water on the martian surface.

I also measured Cl, F, H, and S in apatite from these meteorites, in order to test for high water abundance as well as to assess whether they were uniformly high in Cl, and anomalously high in S, similar to soil measurements made by the Viking lander. Apatite is a retentive, igneous mineral that can stoichiometrically incorporate Cl, F, and/or OH in what is known as the X site of its atomic structure, and include S as a substitution trace element. High H abundance in apatite would confirm the presence of water in martian magmas, which has been more difficult to establish than the presence of water on the surface. High Cl and S in apatites would suggest that their high abundances on the surface

is because Mars is inherently high in volatiles rather than the result of surficial processes driving Cl and S to concentrate in particular areas on the surface.

Sulfur is a unique volatile compared to Cl, F, and H in that it can vary in its oxidation state depending on the oxygen fugacity of the magma that the apatite is generated from. Apatite is thought to accommodate sulfur strictly as sulfate groups replacing phosphate, but it is possible that sulfur might also substitute as sulfide on the X site. Measuring sulfur in apatite also gave me the opportunity to explore whether apatite in martian meteorites is harboring sulfur in both its oxidized and reduced states, as the range of oxygen fugacities estimated for martian magmas extend from conditions where both sulfate and sulfide exist in the magma to conditions where only sulfide exists. In either case, sulfur is a good potential tool to contribute to the estimation of oxygen fugacity in the magmas where these meteorites were produced.

*Chapter I*OXYGEN ISOTOPE COMPOSITIONS OF MINERAL SEPARATES FROM SNC  
METEORITES: CONSTRAINTS ON THE ORIGIN AND EVOLUTION OF  
MARTIAN MAGMAS**Introduction**

Martian (SNC) meteorites currently comprise 67 (unpaired) mafic and ultramafic igneous rocks that are classified as shergottites, nakhlites, chassignites, and ALH 84001. The shergottites are subdivided into three petrographic types (basaltic, olivine-phyric, and lherzolitic) that crystallized at 175 – 575 Ma (e.g., Nyquist et al. 2001; Borg et al. 2003; Symes et al. 2008; Nyquist et al. 2009) or possibly 4.1 – 4.3 Ga (Bouvier et al. 2005, 2008, 2009). Nakhlites and chassignites are cumulates (clinopyroxenites and dunites, respectively) that formed at ca. 1.3 Ga (Nyquist et al. 2001; Bouvier et al. 2009; Park et al. 2009). ALH 84001 is an orthopyroxenite that formed at either 4.5 Ga (e.g., Nyquist et al. 2001) or 4.1 Ga (Bouvier et al. 2009; Lapen et al. 2010).

The shergottites have been subdivided into depleted, moderately depleted, and enriched groups based on their light rare earth element (LREE) to heavy rare earth element (HREE) ratios, with the depleted group having the lowest ratios and the enriched group having the highest ratios (e.g., Borg et al. 2002; Bridges and Warren 2006). The ratios of LREE to HREE in these meteorites are correlated with several radiogenic isotope ratios (e.g., positively with  $^{87}\text{Sr}/^{86}\text{Sr}$  and negatively with  $^{143}\text{Nd}/^{144}\text{Nd}$ ) and with oxygen fugacity, which

increases by three log<sub>10</sub> units from the depleted group to the enriched group (Wadhwa 2001; Herd, Borg, et al. 2002; Herd 2003; McCanta et al. 2004; Herd 2006). In addition, whole rock  $\delta^{18}\text{O}$  values of shergottites correlate positively with oxygen fugacity and enrichment (Herd 2003).

On Earth,  $\delta^{18}\text{O}$  values of mantle peridotites and primitive mafic magmas are generally similar, but they differ systematically from sedimentary, weathered, and hydrothermally altered components of the crust due to low-temperature fractionations between these crustal materials and coexisting water. The distinctive oxygen isotope ratios of crustal materials can influence the  $\delta^{18}\text{O}$  values of mantle-derived magmas either by mixing into the mantle sources of basalts via subduction or delamination or by assimilation as these magmas pass through the crust or altered mantle lithosphere (Taylor 1980; Eiler 2001 and references therein). These processes are known to occur on Earth, and they lead to ranges of up to ~5 per mil in the  $\delta^{18}\text{O}$  values of unaltered terrestrial igneous rocks and to correlations between  $\delta^{18}\text{O}$  values and other geochemical variables (e.g., Taylor 1980; Davidson et al. 2005). These processes are sufficiently common that oxygen isotope measurements of a random sampling of several dozen terrestrial igneous rocks would likely make it obvious that the Earth's crust is rich in sedimentary and aqueously altered materials. Based on this terrestrial analogy, a straightforward interpretation of the positive correlations between  $\delta^{18}\text{O}$  values, LREE/HREE ratios, and oxidation in the shergottites is that they reflect variable amounts of crustal assimilation into mantle-derived magmas; that is, the depleted shergottites reflect partial melts of martian mantle uncontaminated by altered crustal rocks, while the incompatible-element-enriched, oxidized shergottites crystallized from magmas

that either assimilated high- $\delta^{18}\text{O}$  crustal rocks that had experienced aqueous alteration at low temperatures or mixed with partial melts of such crustal rocks.

There is considerable evidence that at least parts of the martian crust have been altered by exposure to liquid water: e.g., martian valley networks, outflow channels, gullies, deltas, etc. (Carr 2012 and references therein); the presence of carbonates, hematite, sulfates, halides, and phyllosilicates in the SNC meteorites (Bridges et al. 2001; McCubbin et al. 2009); and the identification of similar phases on the martian surface (e.g., Squyres et al. 2004; Ming et al. 2006; Morris et al. 2010), or by remote sensing (e.g., Christensen et al. 2001; Bibring et al. 2006; Ehlmann et al. 2008; Mustard et al. 2008; Jensen and Glotch 2011). Although the extent of these processes and their effects on the  $^{18}\text{O}/^{16}\text{O}$  ratios of martian crustal rocks are unknown, if aqueous alteration has been widespread, it could also have modified the oxidation states of multivalent cations in the crust and thus could also explain the oxidation of enriched, relative to depleted, magmas. Interaction of mantle-derived magmas with altered crust could thus explain why enriched shergottites have elevated  $\delta^{18}\text{O}$  values relative to the depleted shergottites and that these values appear to correlate with trace element ratios, oxidation state, and radiogenic isotope ratios (Taylor 1980). Although current data are consistent with correlations expected for such an assimilative process when whole rock  $\delta^{18}\text{O}$  values are compared to oxygen fugacity and trace element ratios (Herd 2003), whole rock  $\delta^{18}\text{O}$  values of the shergottites do not necessarily correspond to those of the liquids from which they precipitated because many of these meteorites are cumulates (e.g., McSween 1994; Bridges and Warren 2006; Papike et al. 2009); i.e., they contain proportions of minerals that are not representative of the normative mineralogy of their parent magmas, and because igneous minerals differ from

one another in their mineral-melt oxygen isotope fractionations, it is likely that whole rock cumulates have  $\delta^{18}\text{O}$  values different from the liquids from which they precipitated (Eiler 2001 and references therein). Many of the SNCs also contain alteration phases (e.g., Bridges et al. 2001), which differ in  $\delta^{18}\text{O}$  from coexisting igneous minerals (Clayton and Mayeda 1983; Valley et al. 1997; Farquhar et al. 1998; Romanek et al. 1998). Acid leaching is a relatively common practice to remove (or at least test for the effects of) alteration phases prior to oxygen isotope analysis, but the effects of alteration on published whole rock  $\delta^{18}\text{O}$  values of SNC meteorites are difficult to evaluate because most authors did not report whether or not they performed acid leaching or other purification procedures.

In addition to studies of  $\delta^{18}\text{O}$  values in SNC meteorites,  $\Delta^{17}\text{O}$  values in the SNCs have been studied extensively, and indeed the systematic deviation of these meteorites from the terrestrial fractionation line was a critical factor in lumping the SNC meteorites (previously thought of as three separate groups of meteorites) into one group likely from a single parent body (Clayton and Mayeda 1983, 1996). A detailed investigation of  $\Delta^{17}\text{O}$  values in SNC whole rocks and mineral separates has detected variations that have been used to suggest the assimilation of near-surface alteration materials (Rumble and Irving 2009). However, interpretations of variability in  $\Delta^{17}\text{O}$  values in SNCs are difficult to connect quantitatively with inferences based on  $\delta^{18}\text{O}$  values, trace element ratios, or oxygen fugacity because observed variations in  $\Delta^{17}\text{O}$  have not yet been shown to correlate with other geochemical parameters.

The goal of the work reported here is to test previously proposed relationships between the SNC meteorites by constraining the  $\delta^{18}\text{O}$  and  $\Delta^{17}\text{O}$  values of mineral separates in the SNCs

(i.e., rather than basing these relationships on whole rock measurements). Although, as summarized above, there have been many previous measurements of these parameters for martian meteorites, and results from different laboratories differ beyond stated error bars (even for the same meteorite) with the result that the collective dataset of  $\delta^{18}\text{O}$  (for shergottites in particular) is variable and confusing (see figure 1.1 and the previous studies section below). Our work differs from previous studies by (1) analyzing mineral separates (i.e., pyroxene, olivine, and maskelynite) rather than whole rocks so as to constrain the  $\delta^{18}\text{O}$  values of the liquids from which cumulate phases crystallized (discussed below); (2) analyzing many of the known SNC meteorites in a single laboratory, thereby minimizing issues associated with interlaboratory comparisons that may account for some of the variability in currently available data; (3) utilizing recent analytical advances in laser fluorination techniques and extensively replicating analyses, thereby minimizing uncertainties in the measurements; and (4) attempting to evaluate the effects of alteration phases on measured oxygen isotope ratios through the use of various sample preparation protocols. We emphasize (1) in particular because the focus on mineral separates allows direct comparison between the same phase from different meteorites permits assessment of whether equilibrium has been achieved among coexisting phases in a single meteorite (Eiler 2001), and minimizes potentially confusing effects of variations in whole rock oxygen isotope ratios that would arise between a series of cogenetic cumulates that vary only in their phase proportions.

Overall, our goal is to address the question of whether the sources of enriched, oxidized shergottites differ in  $\delta^{18}\text{O}$  and  $\Delta^{17}\text{O}$  from those of depleted shergottites and thereby to address the possible role of aqueously altered crustal materials in their petrogenesis. The

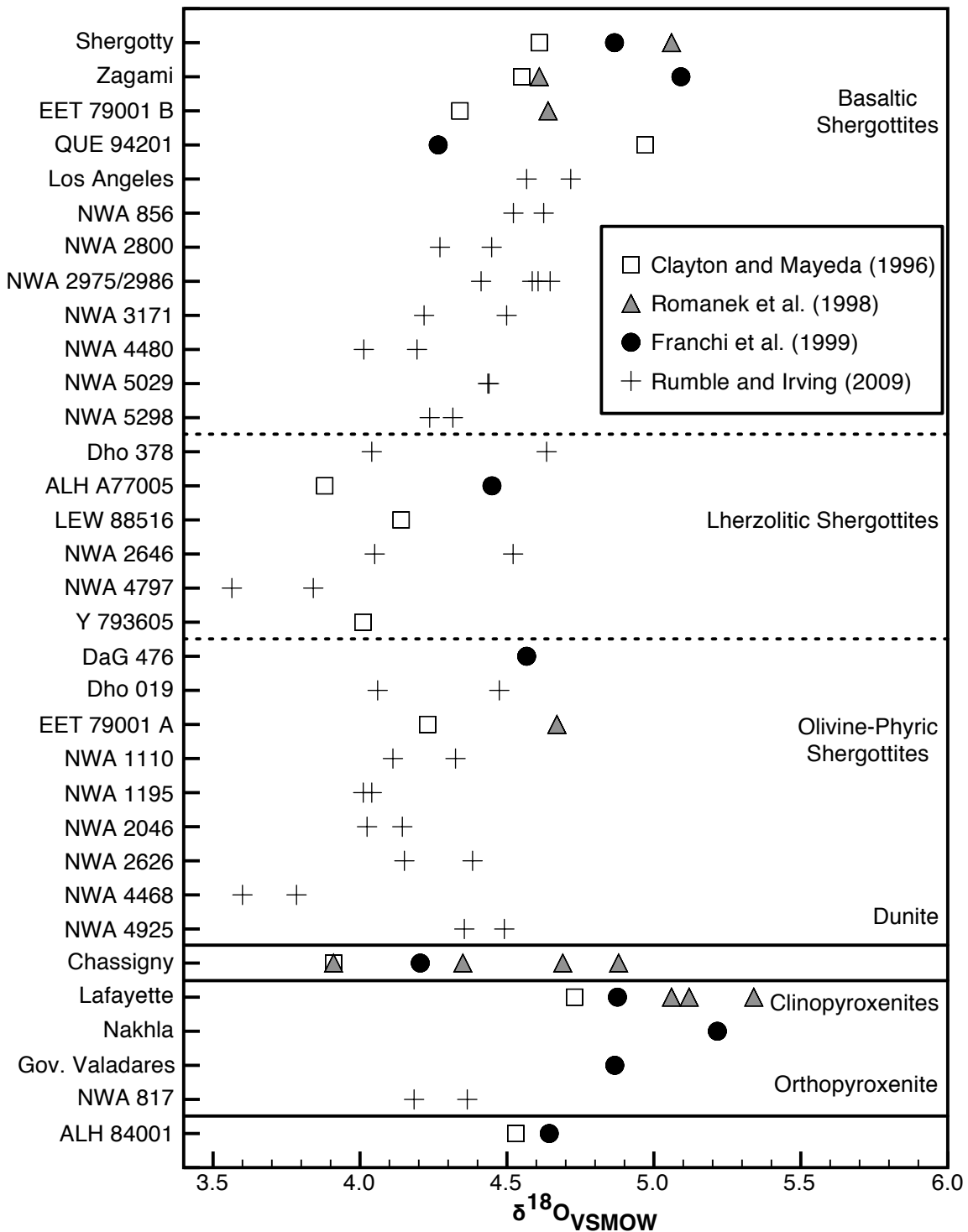


Figure 1.1. Previous oxygen isotope studies.

key result is that we have been unable to confirm the correlation between  $\delta^{18}\text{O}$  of mineral separates and concentrations of incompatible elements or indexes of oxidation state that

previous workers have found based on whole rock  $\delta^{18}\text{O}$  analyses. Instead we have found uniformity in  $\delta^{18}\text{O}$  from the same minerals (and  $\Delta^{17}\text{O}$  from all phases) among the shergottites. We also measured nakhlites, a chassignite, and ALH 84001 to assess their oxygen isotopic compositions relative to the shergottites and previous whole rock analyses, and we found them to differ from the shergottites, but by much less than what has been suggested previously. Preliminary results of this study were reported in Channon et al. (2009, 2010).

## **Previous Studies**

### Values of $\delta^{18}\text{O}$

Taylor et al. (1965) found negligible differences in  $\delta^{18}\text{O}$  of pyroxene separates between Shergotty, Lafayette, and Nakhla (a range of 0.2 per mil). Clayton and Mayeda (1996) found a whole rock standard deviation of 0.35 per mil ( $1\sigma$ ; all errors reported hereafter are  $1\sigma$ ) among all the SNCs in their study, but attributed it to different modal abundances of major minerals in each meteorite and concluded that there is no isotopic evidence for crustal, water-dominated processes that affect the petrogenesis of these rocks. Romanek et al. (1998) and Franchi et al. (1999) observed ranges between meteorites in whole rock  $\delta^{18}\text{O}$  values similar to those observed by Clayton and Mayeda (1996), but in general, the three whole rock studies differ systematically by up to 0.4 per mil in the average value of their ranges (figure 1.1). Franchi et al. (1999) attributed these value discrepancies to different reference gas calibration methods by the three different laboratories (described below). A preliminary oxygen isotope study by Rumble and Irving (2009), performed at a different laboratory than any of the three previous whole rock studies, yields a similar range in

whole rock  $\delta^{18}\text{O}$  between meteorites, with values most closely resembling those of Clayton and Mayeda (1983). All other available  $\delta^{18}\text{O}$  data come from one of these laboratories or various others for the purpose of individual sample characterization and/or meteorite classification (Clayton and Mayeda 1983, 1986; Valley et al. 1997; Farquhar and Thiemens 2000; Rubin et al. 2000; Barrat, Gillet, et al. 2002; Gnos et al. 2002; Jambon et al. 2002; Sautter et al. 2002; Taylor et al. 2002; Gillet et al. 2005; Beck et al. 2006; Treiman and Irving 2008). The combined dataset of all available  $\delta^{18}\text{O}$  measurements span a range of up to 2 per mil and do not form any trends with incompatible-element enrichment or oxygen fugacity.

#### Values of $\Delta^{17}\text{O}$

Several previous oxygen isotope analyses of the SNCs have had as their primary goal the measurement of  $^{17}\text{O}$  anomalies as a tool for meteorite categorization. Clayton and Mayeda (1996) demonstrated that the SNCs have a uniform  $\Delta^{17}\text{O}$  of  $0.28 \pm 0.07\text{‰}$  (note that the standard deviation of  $0.07\text{‰}$  is comparable to the uncertainty for the conventional fluorination methods used in their study), suggesting that they all come from the same parent body. Romanek et al. (1998), using a laser fluorination method, reproduced six of these whole rock measurements and made measurements on mineral and alteration separates from Lafayette,  $\Delta^{17}\text{O} = 0.30 \pm 0.06\text{‰}$  (calculated from table 2 in Romanek et al. 1998). Franchi et al. (1999) generated a higher precision laser fluorination dataset with an even more tightly defined  $\Delta^{17}\text{O}$  value for martian igneous rocks of  $0.32 \pm 0.013\text{‰}$  ( $n = 11$ ). They concluded that the larger variability in  $\Delta^{17}\text{O}$  observed in previous whole rock studies resulted from analytical uncertainty and that SNCs have no inherent differences in  $\Delta^{17}\text{O}$ .

above laser fluorination uncertainty. However, since then, more SNCs have been discovered and analyzed in several different laboratories, largely for meteorite classification. All of these newer data sets exhibit the same  $\sim 0.3\text{‰}$  average offset from the terrestrial fractionation line observed in previous data, but the standard deviation in  $\Delta^{17}\text{O}$  of the composite data set (61 meteorites) is comparable to that found in the initial studies of Clayton and Mayeda (1996) and Romanek et al. (1998) (i.e.,  $\pm 0.05\text{‰}$ ). The larger uncertainty of all data now available relative to the study of Franchi et al. (1999) could reflect poor interlaboratory precision or real variations in  $\Delta^{17}\text{O}$  among samples not considered by Franchi et al. (1999). Rumble and Irving (2009) addressed this issue by examining 22 SNCs using a laser fluorination technique similar to that used by Franchi et al. (1999), and they found an average  $\Delta^{17}\text{O}$  of  $0.33 \pm 0.04\text{‰}$ ; the uncertainty is larger than the  $0.01\text{‰}$  uncertainty observed by Franchi et al. (1999), consistent with the notion that Franchi et al. (1999) analyzed a smaller set of samples that simply happened to be less variable. Moreover, Rumble and Irving (2009) also found significant variations between splits of the same meteorite (a range of  $0.1\text{‰}$  in NWA 856). They attempted to minimize the effects of terrestrial weathering as a source of this variability by acid washing their samples; they attribute sample-to-sample variability to different amounts of assimilation of crustal alteration phases by ascending magmas, and they attribute heterogeneity within a single meteorite to the lack of isotopic equilibration of the assimilated material within the magma.

## Sample Materials, Preparation, and Analytical Techniques

Portions of 10 shergottites, 3 nakhlites, NWA 2737 (a chassignite), and ALH 84001 were crushed in air in a stainless steel mortar and pestle and sieved to separate out 200 – 500  $\mu\text{m}$  grain-size fractions (a few samples with smaller crystal sizes were sieved to separate out a 100 – 500  $\mu\text{m}$  grain-size fraction). This was followed by hand picking olivine (*ol*), pyroxene (*px*), and maskelynite (*msk*) separates under a binocular microscope. The purity of the separates is estimated to be >90% based on Raman spectroscopy and scanning electron microscopy (SEM). No effort was made to distinguish augite (*aug*), pigeonite (*pig*), and orthopyroxene (*opx*) during hand picking, and the pyroxenes in shergottites were therefore measured as mixtures. Pyroxene in nakhlites is primarily *aug*, and *px* in ALH 84001 is primarily *opx*.

Three terrestrial samples were analyzed in this study; UWG-2 garnet was used as the main standard (Valley et al. 1995), and *ol* and *opx* (enstatite) from a San Carlos lherzolite were monitored as internal, check standards and treated as unknown samples. John Valley provided the UWG-2 garnet, and the San Carlos lherzolite was obtained from the Geological and Planetary Science Division sample collection at the California Institute of Technology. For this study the lherzolite was crushed and sieved in the same manner as the meteorites, and *ol* and *opx* were separated by hand under an optical microscope.

Cleaning studies were performed on *px* (presumably mostly *aug*) separates from sample NWA 998, a highly altered nakhlite that has experienced both martian and terrestrial weathering (Treiman and Irving 2008), and less-altered *opx* from the San Carlos lherzolite as a terrestrial analogue. The San Carlos lherzolite contains both *opx* and *cpx* (Cr-diopside),

which were easily separated because the *cpx* is bright green. Aliquots of the hand-picked pyroxene separates from the 200 – 500 mm size fractions of both NWA 998 and San Carlos were washed in 2.5M HCl for 20 minutes at 90°C. A subset of these HCl-washed separates were additionally washed in 5% HF for 10 minutes at room temperature, rinsed with 2.5M HCl, and then rinsed with deionized H<sub>2</sub>O. All of the washed samples were dried in an oven prior to analysis.

All oxygen isotope measurements were performed at the California Institute of Technology by laser fluorination using a CO<sub>2</sub> laser, BrF<sub>5</sub> reagent, and a purification apparatus using cryogenic traps and a Hg-diffusion pump (Sharp 1990; Elsenheimer and Valley 1993). All samples were prefluorinated with BrF<sub>5</sub> at room temperature for at least 12 hours to remove adsorbed water and trace surface contaminants prior to analysis.

For the  $\Delta^{17}\text{O}$  analyses, O<sub>2</sub> released by fluorination was recovered first by adsorption onto a liquid-nitrogen-cooled 13X molecular sieve following the methods of Miller et al. (1999) and Wiechert et al. (2001). The liquid nitrogen trap was replaced by an ethanol – dry ice slush (similar to Clayton and Mayeda 1983) to keep fluorination by-products such as NF<sub>3</sub> and CF<sub>4</sub> trapped on the 13X molecular sieve while releasing O<sub>2</sub>. The released O<sub>2</sub> was then adsorbed onto a liquid-nitrogen-cooled 5A molecular sieve inside a pyrex glass finger, after which the glass finger was isolated from the rest of the extraction line, and the O<sub>2</sub> was released and measured with a Finnigan MAT 252 mass spectrometer. This method also gave  $\delta^{18}\text{O}$  analyses, but most  $\delta^{18}\text{O}$  measurements reported in this study were made by converting O<sub>2</sub> to CO<sub>2</sub> using a heated graphite rod based on designs by Sharp (1990) and

Elsenhimer and Valley (1993) rather than trapping it onto a liquid-nitrogen-cooled 13X molecular sieve, and analyzed by a ThermoFinnigan Delta<sup>PLUS</sup> XL mass spectrometer.

A total of 17 measurements (two of which were for the cleaning study—one where the sample was leached only with HCl and the other with both HCl and HF) were made on 11 SNC meteorites during 8 separate sessions spread over an 11-month period using the O<sub>2</sub> method for analysis on the MAT 252; a single MAT 252 session took one day and typically included 3 analyses of UWG-2 garnet, 1 analysis of either San Carlos *ol* or *opx*, and 2 SNC analyses. A total of 77 measurements on 15 SNC meteorites were made during 16 separate analytical sessions using the CO<sub>2</sub> method for analysis on the Delta; a single Delta session lasted one day and typically included 6 analyses of UWG-2 garnet, 4 analyses of San Carlos *ol* and/or *opx*, and 5 meteorite analyses. Raw data for all sessions can be found in Appendix A. All measured  $\delta^{18}\text{O}$  values are reported using the VSMOW scale, and were standardized to UWG-2 garnet using the oxygen isotopic composition of  $\delta^{18}\text{O}_{\text{VSMOW}} = 5.800\text{‰}$  (Valley et al. 1995). All  $\delta^{17}\text{O}_{\text{VSMOW}}$  values were standardized using UWG-2 = 3.046‰ (Spicuzza et al., 2007). We calculated  $\Delta^{17}\text{O}$  using equations and methods of Miller (2002), with a high-temperature silicate slope  $\lambda$  of 0.5259 (Spicuzza et al. 2007). Variation of UWG-2 garnet over the course of any one session was on average  $\pm 0.07\text{‰}$  for  $\delta^{18}\text{O}_{\text{VSMOW}}$  and  $\pm 0.03\text{‰}$  for  $\delta^{17}\text{O}_{\text{VSMOW}}$ . Over the course of this study  $\delta^{18}\text{O}_{\text{VSMOW}}$  values of  $5.23 \pm 0.16\text{‰}$  (n = 28) and  $5.72 \pm 0.11\text{‰}$  (n = 34) were obtained for San Carlos *ol* and *opx*. The San Carlos *ol* value is similar to  $5.23 \pm 0.15\text{‰}$  (n = 11—from F<sub>2</sub> fluorination) and  $4.99 \pm 0.18\text{‰}$  (n = 7—from BrF<sub>5</sub> fluorination) reported by Rumble et al. (1997), and  $5.26 \pm 0.05\text{‰}$  (n = 7) reported by Eiler et al. (1996). Both of these studies use similar UWG-2 garnet values. San Carlos *opx* is not typically used as a standard, so it is not compared to

other labs. However, the  $\sim 0.50\%$  difference in  $\delta^{18}\text{O}$  between San Carlos *ol* and *opx* agrees with independent estimates of the equilibrium fractionation between these two phases at magmatic temperatures (Eiler 2001 and references therein). The San Carlos *ol* and *opx* gave  $\Delta^{17}\text{O}$  values of  $0.000 \pm 0.019\%$  ( $n = 8$ ) and  $0.003 \pm 0.019\%$  ( $n = 5$ ) respectively.

## Results

Oxygen isotope compositions of all SNC mineral separates measured in this study are presented in table 1.1. Errors in parentheses are standard error of the mean of all analyses for that phase per meteorite; all others are the standard deviation ( $1\sigma$ ) of the UWG-2 garnet standard used during the same session. Analyses of  $\delta^{18}\text{O}$  yield similar results whether measured as  $\text{CO}_2$  on the Delta<sup>PLUS</sup> XL or as  $\text{O}_2$  on the MAT 252. The cleaning study showed that there is little difference in  $\delta^{18}\text{O}$  of measurements of NWA 998 *px* whether the separates were unleached or leached using HCl or HF (table 1.2).

Measurements of  $\delta^{18}\text{O}_{\text{VSMOW}}$  of *ol* in shergottites (with the exception of DaG 476) and chassignite NWA 2737 average to  $4.36 \pm 0.12\%$  (table 1.1 and figure 1.2). The exception, *ol* from DaG 476, is  $\sim 1\%$  higher; it is also higher than all SNC *px* and *msk* measurements from this study. We discuss below the possibility that DaG 476 *ol* has undergone subsolidus alteration that modified its  $\delta^{18}\text{O}$ . Olivine in the nakhlites is  $0.35\%$  higher in  $\delta^{18}\text{O}_{\text{VSMOW}}$  than *ol* in the shergottites and chassignite.

The average  $\delta^{18}\text{O}_{\text{VSMOW}}$  of shergottite *px*'s is  $4.71 \pm 0.13\%$ . However, DaG 476, Dho 019, and SaU 005 are outliers at the higher end of the  $\delta^{18}\text{O}$  shergottite range; the *px* from these three meteorites have an average  $\delta^{18}\text{O}_{\text{VSMOW}}$  value of  $4.88 \pm 0.09\%$  (figure 1.2). Excluding

Table 1.1. Data from this study obtained by CO<sub>2</sub> and O<sub>2</sub> analyses.

Meteorite	phase	$\delta^{17}\text{O}_{\text{VSMOW}}$	error	$\delta^{18}\text{O}_{\text{VSMOW}}$	error	$\Delta^{17}\text{O}$	error	
<b>Basaltic Shergottites</b>								
Shergotty	pyroxene			4.81	0.09			
				4.79	0.03			
		*	2.75	0.02	4.66	0.03	0.306	0.015
		<b>Average</b>			<b>4.75</b>	<b>(0.05)</b>		
	maskelynite				5.14	0.09		
				5.33	0.03			
				5.27	0.07			
	<b>Average</b>			<b>5.25</b>	<b>(0.06)</b>			
Zagami	pyroxene			4.65	0.12			
				4.58	0.07			
		*	2.74	0.01	4.60	0.02	0.323	0.010
		<b>Average</b>			<b>4.61</b>	<b>(0.02)</b>		
	maskelynite				5.04	0.12		
				5.16	0.07			
		<b>Average</b>			<b>5.10</b>	<b>(0.06)</b>		
NWA 2986	pyroxene			4.56	0.09			
				4.70	0.09			
		*	2.72	0.01	4.62	0.01	0.288	0.004
		<b>Average</b>			<b>4.63</b>	<b>(0.04)</b>		
	maskelynite				5.16	0.09		
				5.10	0.09			
				5.43	0.07			
	<b>Average</b>			<b>5.23</b>	<b>(0.10)</b>			
NWA 4468	pyroxene			4.61	0.12			
				4.75	0.11			
		*	2.86	0.01	4.82	0.01	0.327	0.004
		<b>Average</b>			<b>4.73</b>	<b>(0.06)</b>		
	maskelynite				4.95	0.12		
				4.96	0.07			
		<b>Average</b>			<b>4.96</b>	<b>(0.01)</b>		

\*Measurements made using the O<sub>2</sub> method on the MAT 252; all others were made using the CO<sub>2</sub> method on the Delta. Methods are described in the sample materials preparation, and analytical techniques section.

these three samples, the average  $\delta^{18}\text{O}_{\text{VSMOW}}$  of shergottite *px*'s is  $4.67 \pm 0.10\%$ . The  $\delta^{18}\text{O}_{\text{VSMOW}}$  of *px* in the nakhlites average to  $4.87 \pm 0.10\%$ ; i.e., like the three anomalous shergottite *px* values, they are also  $\sim 0.2\%$  higher than the mean value of the typical

Table 1.1 continued.

Meteorite	phase	$\delta^{17}\text{O}_{\text{VSMOW}}$	error	$\delta^{18}\text{O}_{\text{VSMOW}}$	error	$\Delta^{17}\text{O}$	error
<b>Olivine/Pyroxene-Phyric Shergottites</b>							
DaG 476	pyroxene			4.78	0.08		
				4.82	0.07		
				5.00	0.07		
	<b>Average</b>			<b>4.87</b>	<b>(0.07)</b>		
	olivine			5.38	0.11		
				5.32	0.07		
				<b>5.35</b>	<b>(0.03)</b>		
Dho 019	pyroxene			4.96	0.07		
SaU 005	pyroxene			4.86	0.12		
	olivine			4.29	0.12		
NWA 2046	pyroxene			4.76	0.06		
				4.58	0.08		
				<b>4.67</b>	<b>(0.09)</b>		
	olivine			4.15	0.06		
				4.49	0.08		
				4.42	0.11		
	<b>Average</b>			<b>4.35</b>	<b>(0.10)</b>		

\*Measurements made using the  $\text{O}_2$  method on the MAT 252; all others were made using the  $\text{CO}_2$  method on the Delta. Methods are described in the sample materials preparation, and analytical techniques section.

shergottite *px*'s. The  $\delta^{18}\text{O}_{\text{VSMOW}}$  of *px* in ALH 84001 is  $5.02 \pm 0.11\text{‰}$ , which is  $\sim 0.35\text{‰}$  higher than the average of typical shergottite *px* and  $\sim 0.15\text{‰}$  higher than nakhlite *px*.

Excluding *msk* from NWA 4468, shergottite *msk* has an average  $\delta^{18}\text{O}_{\text{VSMOW}} = 5.20 \pm 0.13\text{‰}$  (table 1.1 and figure 1.2). Maskelynite from NWA 4468 is  $0.15\text{‰}$  lower than the others.

The average of the  $\Delta^{17}\text{O}$  analyses of SNC mineral separates is  $0.313 \pm 0.015\text{‰}$  (table 1.1 and figure 1.3). Except for the  $\Delta^{17}\text{O}$  of HF-leached NWA 998 *px*, which is  $\sim 0.03\text{‰}$  higher (figure 1.3) than HCl-leached and untreated NWA 998 *px*, there are no systematic variations within or between samples.

Table 1.1 continued.

Meteorite	phase	$\delta^{17}\text{O}_{\text{VSMOW}}$	error	$\delta^{18}\text{O}_{\text{VSMOW}}$	error	$\Delta^{17}\text{O}$	error		
<b>Peridotitic ("Lherzolithic") Shergottites</b>									
ALH A77005	pyroxene			4.77	0.07				
				4.49	0.11				
		<b>Average</b>			<b>4.63</b>	<b>(0.14)</b>			
	olivine			4.39	0.12				
				4.16	0.16				
				4.26	0.16				
				4.32	0.04				
				4.50	0.09				
				4.31	0.08	0.321	0.010		
		<b>Average</b>			<b>4.32</b>	<b>(0.05)</b>			
NWA 1950	pyroxene			4.58	0.12				
				4.80	0.16				
				4.61	0.16				
				4.71	0.04				
		<b>Average</b>			<b>4.68</b>	<b>(0.05)</b>			
	olivine			4.41	0.12				
				4.46	0.16				
				4.50	0.09				
				4.33	0.04				
				4.39	0.15	0.287	0.024		
			4.29	0.03	0.321	0.020			
	<b>Average</b>			<b>2.58</b>	<b>(0.01)</b>	<b>4.40</b>	<b>(0.03)</b>	<b>0.304</b>	<b>(0.017)</b>

\*Measurements made using the O<sub>2</sub> method on the MAT 252; all others were made using the CO<sub>2</sub> method on the Delta. Methods are described in the sample materials preparation, and analytical techniques section.

## Discussion

### Cleaning Study

Pyroxene separates from NWA 998 typically have spots of red-orange stains or films on their surfaces. It was a concern that this contamination might contribute to the relatively high values of  $\delta^{18}\text{O}$  we observe for the nakhlites. However, after the leaching experiments (described above), visual inspection of the separates showed that HCl and HF baths had

Table 1.1 continued.

Meteorite	phase	$\delta^{17}\text{O}_{\text{VSMOW}}$	error	$\delta^{18}\text{O}_{\text{VSMOW}}$	error	$\Delta^{17}\text{O}$	error	
<b><u>Nakhlites</u></b>								
Lafayette	pyroxene			4.93	0.12			
				4.80	0.16			
				4.76	0.16			
				5.03	0.09			
		*	2.83	0.01	4.83	0.02	0.293	0.010
		<b>Average</b>			<b>4.87</b>	<b>(0.05)</b>		
Lafayette	olivine			4.51	0.16			
				4.92	0.09			
				4.69	0.04			
				4.83	0.09			
		<b>Average</b>			<b>4.74</b>	<b>(0.09)</b>		
Nakhla	pyroxene			5.00	0.03			
				4.74	0.06			
				4.68	0.08			
		*	2.82	0.01	4.76	0.03	0.319	0.020
		<b>Average</b>			<b>4.80</b>	<b>(0.07)</b>		

\*Measurements made using the  $\text{O}_2$  method on the MAT 252; all others were made using the  $\text{CO}_2$  method on the Delta. Methods are described in the sample materials preparation, and analytical techniques section.

removed the surface contamination (the appearance of San Carlos *opx* did not change—the surface appeared clean both before and after the experiments), and yet  $\delta^{18}\text{O}$  measurements remained the same (table 1.2—where all errors are  $1\sigma$  of the UWG-2 garnet standard from that session) at a 95% confidence level using the Mann-Whitney U test. It is possible this is because  $\text{BrF}_5$  pretreatment removes the contaminant (i.e., leaching in acids prior to introduction to the laser fluorination sample chamber just removes constituents that would have been removed during pretreatment). Or, the surface impurities do not meaningfully contribute to the oxygen isotopic composition, either due to their low abundance or similarity in oxygen isotope composition to the mineral substrates. Measurements of  $\Delta^{17}\text{O}$  appear to be influenced by HF leaching, at least in the one sample on which this was

Table 1.1 continued.

Meteorite	phase	$\delta^{17}\text{O}_{\text{VSMOW}}$	error	$\delta^{18}\text{O}_{\text{VSMOW}}$	error	$\Delta^{17}\text{O}$	error	
<b><u>Nakhlites Continued</u></b>								
NWA 998	pyroxene			4.94	0.04			
				5.01	0.04			
				5.00	0.04			
				4.97	0.04			
		*	2.83	0.05	4.78	0.08	0.324	0.010
		*	2.83	0.05	4.81	0.08	0.306	0.010
		*	2.90	0.03	4.91	0.05	0.317	0.008
		*	2.79	0.07	4.73	0.14	0.309	0.012
		<b>Average</b>	<b>2.84</b>	<b>(0.02)</b>	<b>4.89</b>	<b>(0.04)</b>	<b>0.314</b>	<b>(0.005)</b>
		HCl-treated			4.96	0.04		
		pyroxene			4.95	0.04		
					4.92	0.04		
					4.82	0.04		
		*	2.92	0.03	4.95	0.05	0.317	0.008
	<b>Average</b>			<b>4.92</b>	<b>(0.03)</b>			
	HF-treated			4.98	0.06			
	pyroxene			4.85	0.06			
				4.82	0.06			
				4.74	0.06			
	*	2.86	0.07	4.79	0.14	0.342	0.012	
	<b>Average</b>			<b>4.84</b>	<b>(0.04)</b>			
	<b>all pyroxene</b>	<b>2.85</b>	<b>(0.02)</b>	<b>4.89</b>	<b>(0.02)</b>	<b>0.319</b>	<b>(0.005)</b>	
	olivine			4.41	0.16			
				4.86	0.09			
				4.58	0.04			
				4.74	0.09			
	<b>Average</b>			<b>4.65</b>	<b>(0.10)</b>			

\*Measurements made using the O<sub>2</sub> method on the MAT 252; all others were made using the CO<sub>2</sub> method on the Delta. Methods are described in the sample materials preparation, and analytical techniques section.

attempted. However, only one measurement of this kind was made, therefore conclusions are unclear at this time.

Table 1.1 continued.

Meteorite	phase	$\delta^{17}\text{O}_{\text{VSMOW}}$	error	$\delta^{18}\text{O}_{\text{VSMOW}}$	error	$\Delta^{17}\text{O}$	error	
<b><u>Chassignite</u></b>								
NWA 2737	olivine			4.37	0.12			
		*	2.62	0.01	4.36	0.02	0.325	0.010
	<b>Average</b>			<b>4.37</b>	<b>(0.01)</b>			
<b><u>Orthopyroxenite</u></b>								
ALH 84001	pyroxene			5.18	0.03			
				4.92	0.03			
				5.03	0.06			
		*	2.92	0.02	4.97	0.03	0.305	0.015
	<b>Average</b>			<b>5.03</b>	<b>(0.06)</b>			

\*Measurements made using the  $\text{O}_2$  method on the MAT 252; all others were made using the  $\text{CO}_2$  method on the Delta. Methods are described in the sample materials preparation, and analytical techniques section.

#### Measurements of $\delta^{18}\text{O}$

Except for DaG 476 *ol*, all  $\delta^{18}\text{O}$  values of SNC minerals from this study display relationships that broadly agree with equilibrium fractionations in oxygen isotope ratios among these minerals at igneous temperatures (figure 1.2). Maskelynites show the highest values, olivines show the lowest, and pyroxenes are in the middle. Figure 1.4 illustrates the mineral – mineral fractionations for various coexisting mineral pairs (olivine – pyroxene and maskelynite – pyroxene pairs from the same rock) analyzed in this study, and compares these data with similar mineral pairs from terrestrial mafic igneous rocks (where plagioclase is included as a point of comparison to maskelynite), and to fractionations predicted based on previous experimental constraints on mineral – mineral fractionation factors (Rosenbaum and Matthey 1995; Eiler 2001). Most terrestrial data appear to be slightly out of equilibrium compared to experimental and theoretical determinations, either because the experiments are slightly in error or because phenocryst assemblages in mafic igneous rocks are typically slightly out of equilibrium. Almost all martian data from this

Table 1.2. Results of cleaning study.

	$\delta^{18}\text{O}_{\text{VSMOW}}$					
	untreated	error	HCl	error	HF	error
NWA 998	4.94	0.04	4.96	0.04	4.98	0.06
	5.01	0.04	4.95	0.04	4.85	0.06
	5.00	0.04	4.92	0.04	4.82	0.06
	4.97	0.04	4.82	0.04	4.74	0.06
<b>Average</b>	<b>4.98</b>	<b>0.03</b>	<b>4.91</b>	<b>0.06</b>	<b>4.85</b>	<b>0.10</b>
SCOL	5.77	0.04				
	5.78	0.04	5.79	0.06		
	5.69	0.04	5.59	0.06	5.84	0.06
	5.75	0.06	5.89	0.06	5.75	0.06
	5.55	0.06	5.82	0.06	5.64	0.06
	5.75	0.06	5.65	0.06	5.67	0.06
<b>Average</b>	<b>5.72</b>	<b>0.09</b>	<b>5.75</b>	<b>0.12</b>	<b>5.73</b>	<b>0.09</b>

study are comparable to terrestrial data and most are within predicted ranges of equilibrium fractionations. However, the *ol* – *px* fractionation in DaG 476 and the *px* – *msk* fractionation in NWA 4468 fall outside both the predicted range for magmatic equilibrium and the majority of the terrestrial dataset we considered.

#### Comparison of the Present Study with Previous Data

Figure 1.5 compares  $\delta^{18}\text{O}$  values of SNCs from this study to previous measurements. It is noteworthy that we observe a significantly smaller range in  $\delta^{18}\text{O}$  for any one phase than was observed in previous studies. There are three factors that may be contributing to this finding. First, most of these rocks are cumulates. Bulk measurements of a lherzolithic shergottite that consists of mostly *ol* and *px* will result in a lower  $\delta^{18}\text{O}$  than a basaltic shergottite that consists of *px* and *msk* even if they had parent magmas that were identical in  $\delta^{18}\text{O}$  and had closely similar  $\delta^{18}\text{O}$  values of pyroxenes. This is due to oxygen isotope

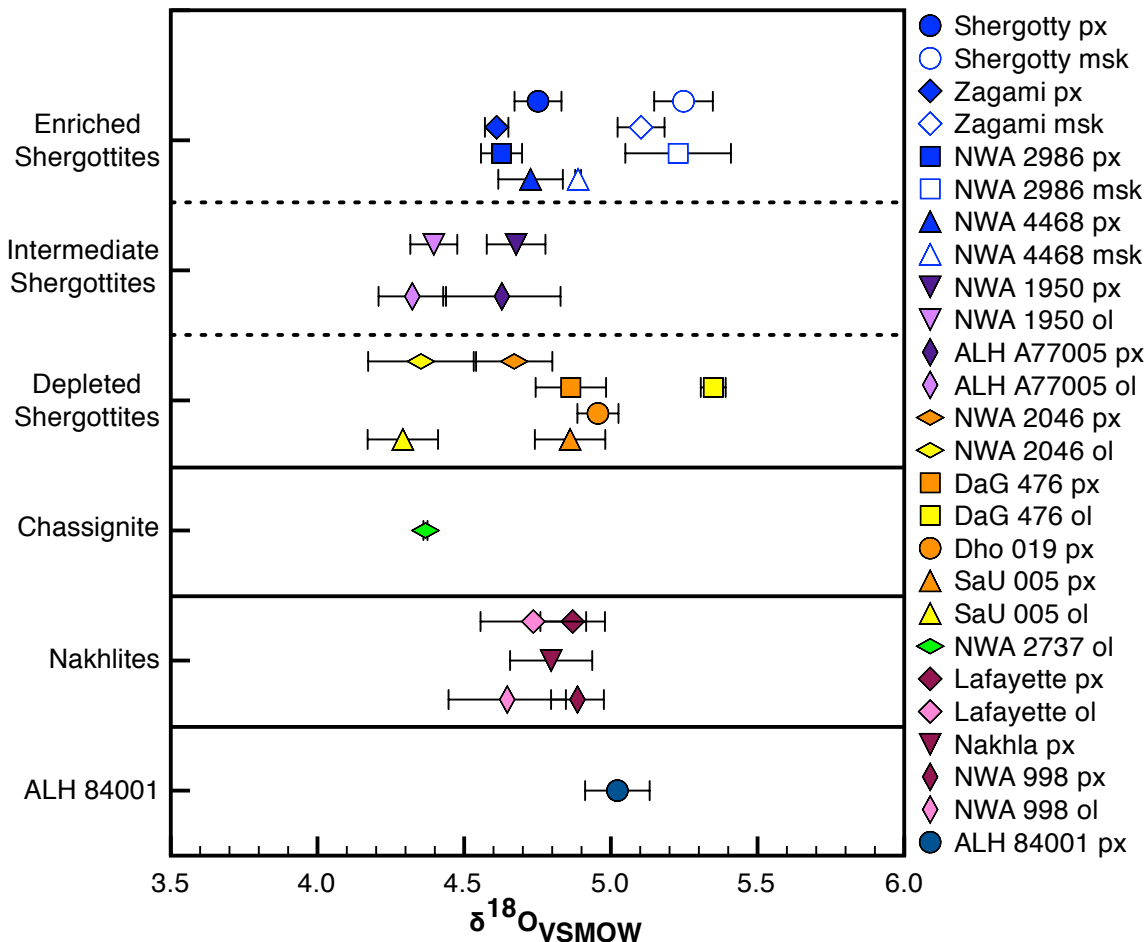


Figure 1.2. Measurements from this study. The shergottites are grouped according to depletion. All error bars are 1σ standard deviation.

fractionation among coexisting phases in magmas. Clayton and Mayeda (1996) attributed all variations of  $\delta^{18}\text{O}$  values of SNC whole rock samples in their study to this factor.

Second, different laboratories use different sample preparation techniques and prefluorination conditions. Neither Romanek et al. (1998) nor Franchi et al. (1999) report acid washing as a sample preparation technique, but Rumble and Irving (2009) do report acid washing. Measurements of bulk rocks might include contaminants, such as terrestrial weathering products and/or martian alteration phases that are not present in mineral separates. Acid leaching is intended to remove these contaminants, though it is not clear

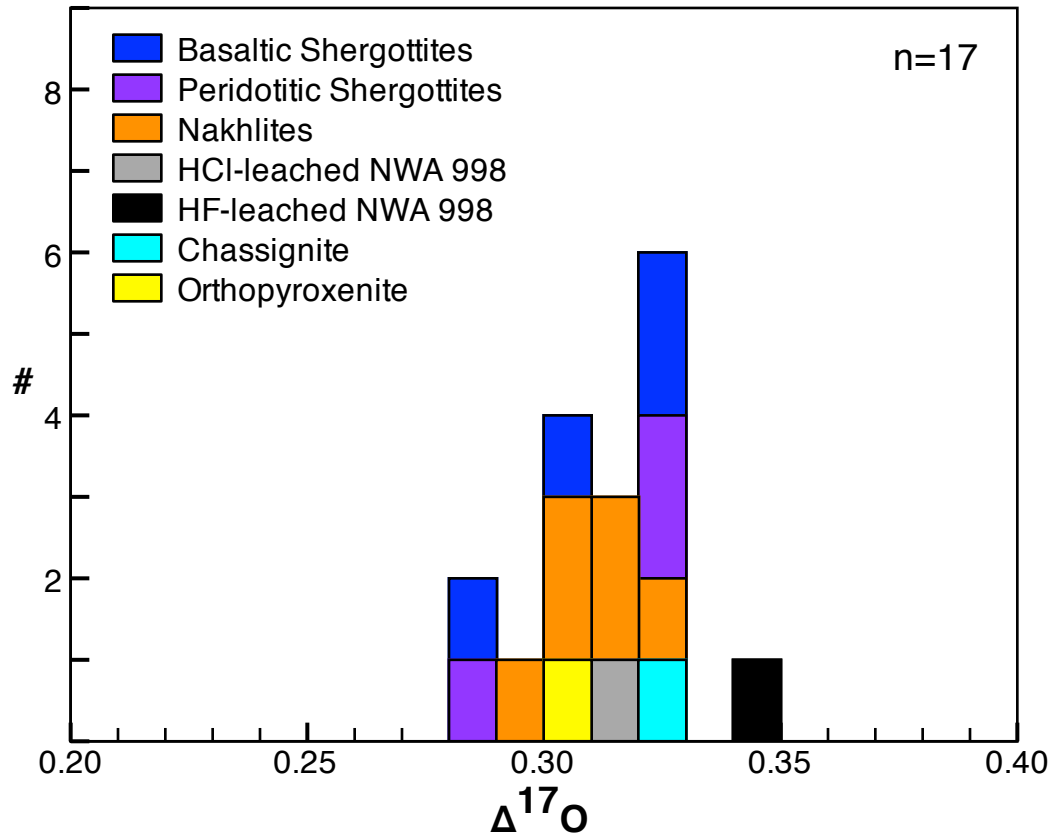


Figure 1.3. Histogram of all  $\Delta^{17}\text{O}$  measurements made on SNC mineral separates from this study.

that it does so with perfect efficiency. Furthermore, acid leaching might actually degrade the quality of oxygen isotope measurements in some cases. Olivine can transform to an amorphous “gel” when exposed to acids. It is unknown whether or not this causes an effect on  $\delta^{18}\text{O}$  (or  $\Delta^{17}\text{O}$ ) measurements, but there is a possibility that acid leaching a bulk sample that contains a lot of olivine may have an effect. Measurements of the same sample prepared in various ways made in one lab, and on one instrument (similar to the cleaning experiments performed on NWA 998 pyroxenes in this study) may be able to resolve whether some of the cleaning methods used in prior studies subtly influence  $\delta^{18}\text{O}$  (or  $\Delta^{17}\text{O}$ ) values.

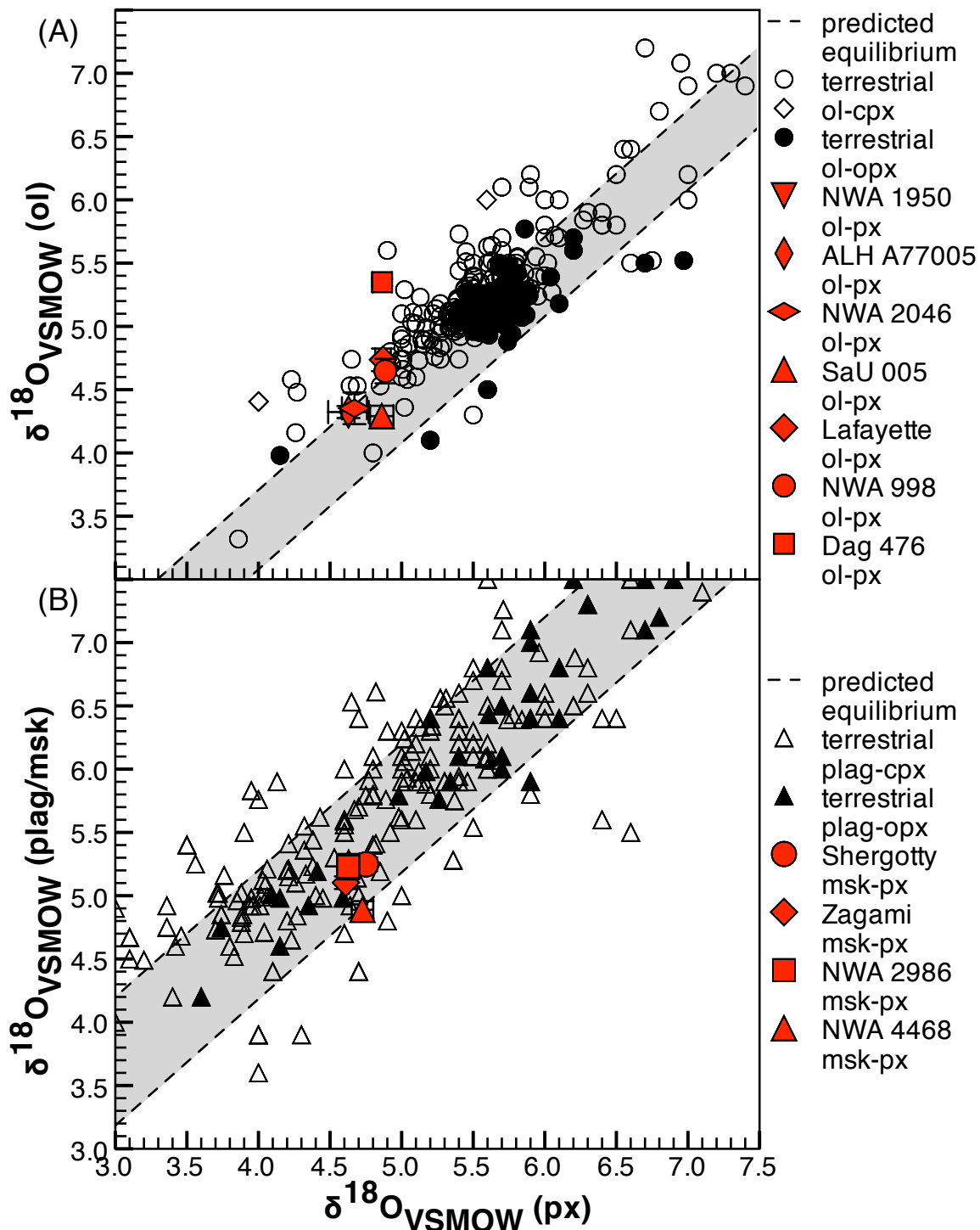


Figure 1.4. (A) Ol – px equilibrium pairs. (B) Plag/msk – px pairs. Data from this study compared with terrestrial samples. Black and open symbols are from terrestrial samples (from GEOROC); red symbols are from this study. Grey regions denote equilibrium based on experimental and theoretical data (Rosenbaum and Matthey 1995; Eiler 2001).

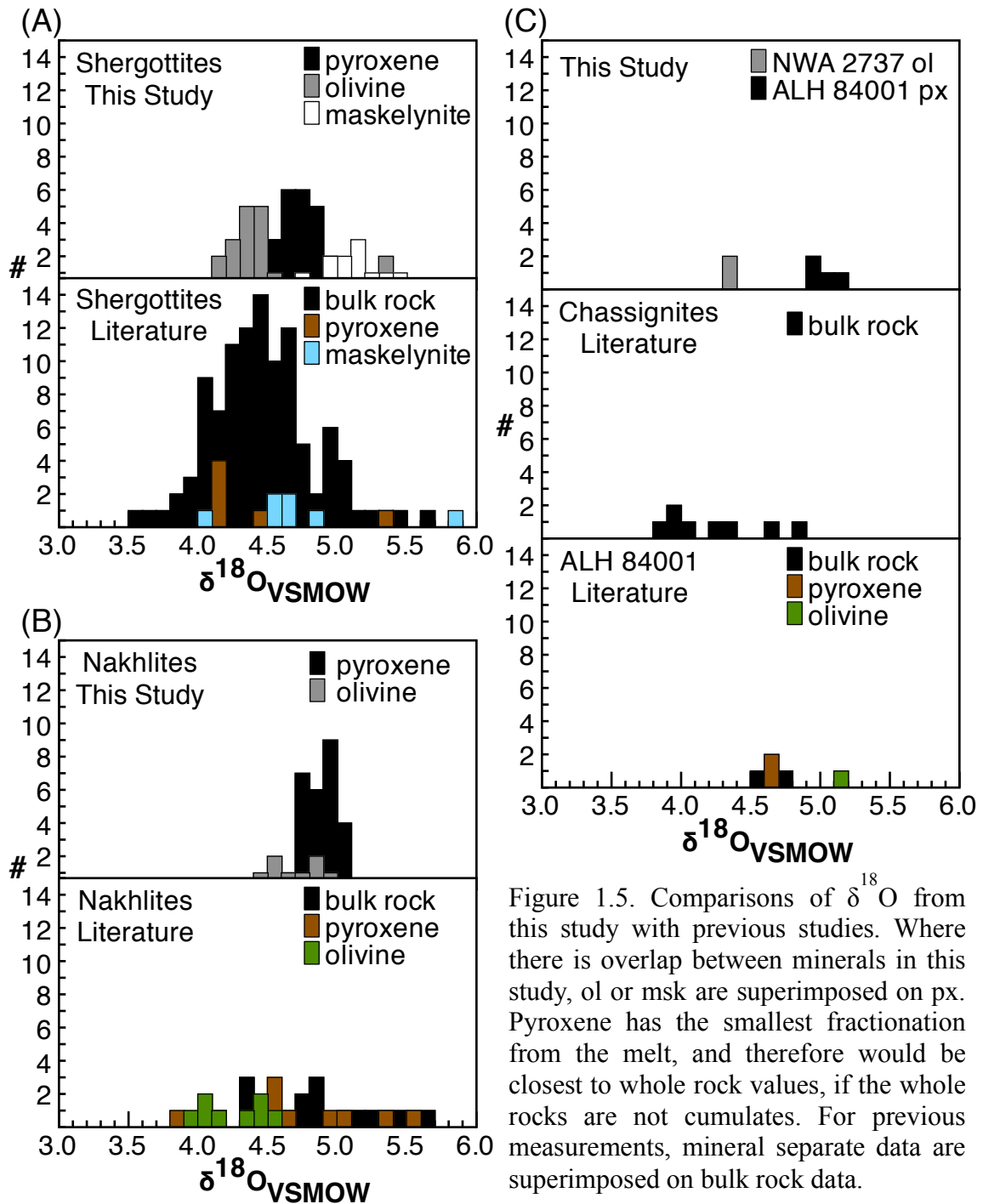


Figure 1.5. Comparisons of  $\delta^{18}\text{O}$  from this study with previous studies. Where there is overlap between minerals in this study, ol or msk are superimposed on px. Pyroxene has the smallest fractionation from the melt, and therefore would be closest to whole rock values, if the whole rocks are not cumulates. For previous measurements, mineral separate data are superimposed on bulk rock data.

Prefluorination of the sample chamber in this study and at the Geophysical Laboratory (GL—laboratory used by Rumble and Irving 2009) is done overnight at room temperature (Rumble et al. 2007), whereas at Open University (OU—laboratory used by Franchi et al.

1999) the sample chamber is evacuated overnight at elevated temperature and then prefluorinated at room temperature prior to analysis (Franchi et al. 1999). Romanek et al. (1998) prefluorinated for one hour at an elevated temperature, presumably following methods of Clayton and Mayeda (1963).

Third, not all studies have followed the same practices in calibrating measurements to the VSMOW scale. Laboratories that make calibrations based on international silicate standards (this study and that of Romanek et al. 1998) obviously depend on the accepted value for that standard. Kusakabe and Matsuhisa (2008) have demonstrated that different laboratories are not reporting the same values for some standards. Franchi et al. (1999), and Clayton and Mayeda (1983) report data for silicate standards that are lower than those from Romanek et al. (1998), and this study (e.g.,  $\delta^{18}\text{O}$  of UWG-2 = 5.4‰ vs. 5.8‰). The conference abstract of Rumble and Irving (2009) does not report standard data. However, even after one corrects for different silicate standard values, scatter still exists in the data, even for the same meteorite. Franchi et al. (1999) and Clayton and Mayeda (1963) report data relative to a working gas that has been independently calibrated to VSMOW (i.e., as opposed to the difference with respect to an interlaboratory silicate standard). It is unclear how data were calibrated to the VSMOW scale for the Rumble and Irving (2009) abstract. Surveying the various approaches to calibration for obtaining  $\delta^{18}\text{O}$  values, we conclude that one cannot compile a data set of  $\delta^{18}\text{O}$  measurements of SNC meteorites among different laboratories without introducing systematic errors on the order of tenths of per mil due to variations in methods and materials for calibration to the VSMOW scale (and this is likely generally true for silicate  $\delta^{18}\text{O}$  values). Nevertheless, when one attempts to correct for these differences (i.e., by adding 0.4‰ to data from the Franchi et al. 1999 and Clayton and

Mayeda 1983 to make them consistent with our calibration), significant interlaboratory differences still exist in data for the SNC meteorites, even for whole rock measurements of the same meteorite. This implies that differences in analytical or sample preparation procedures are at least partially responsible. Nevertheless, we again emphasize the general lack of variation in  $\delta^{18}\text{O}$  in this study and the one done at OU (Franchi et al. 1999); a large enough range of samples are considered in that work that we consider it unlikely variations in  $\delta^{18}\text{O}$  observed among other studies reflect true variations among primary martian silicate minerals.

### Shergottites

Pyroxene is a major phase in SNC meteorites and was analyzed in the largest number and diversity of samples in this study, and so serves as the simplest point of reference for estimating differences in  $\delta^{18}\text{O}$  between samples. Figures 1.2 and 1.5 summarize these data for our sample suite, which covers the whole range in shergottites, from depleted and reduced to enriched and oxidized. These figures suggest that liquids from which the shergottites crystallized span a significantly smaller range in  $\delta^{18}\text{O}_{\text{VSMOW}}$  (0.35‰) than previously inferred from whole rock measurements (~2‰), and that the process responsible for the trends between  $\delta^{18}\text{O}$  and enrichment and oxygen fugacity among the shergottites (Herd 2003) do not reflect compositional trends among the SNC parent magmas; they must instead be fortuitous results of analytical errors, sample preparation artifacts and/or systematic differences in mineral proportions of cumulate rocks. In any event, our oxygen isotope data provide little to no evidence that the oxidation state or enrichment of shergottites is associated with oxygen isotope signals, and thus do not provide any

indication that the shergottite parent magmas assimilated or mixed with aqueously altered mantle or crustal components.

Pyroxenes in DaG 476, Dho 019, and SaU 005 (that is, three of the four depleted shergottites that we analyzed) are slightly higher in  $\delta^{18}\text{O}$  (by  $\sim 0.2\text{‰}$ ) than pyroxenes from other shergottites. A  $0.2\text{‰}$  difference in  $\delta^{18}\text{O}$  among shergottite pyroxenes may be too small to support any confident conclusions. But it is among the only statistically significant variations we observe in our otherwise uniform data set, so we discuss possible explanations below.

It is imaginable that this reflects a high proportion of  $\delta^{18}\text{O}$ -rich alteration phases in pyroxene separates from these samples. None of these samples were acid washed, and both DaG 476 and Dho 019 exhibit terrestrial weathering; however, SaU 005 does not exhibit terrestrial weathering. And, our cleaning study of NWA 998 (also higher in  $\delta^{18}\text{O}$  by  $0.2\text{‰}$ ) suggests that acid leaching makes no significant difference to the measurements of pyroxenes that contain visible alteration products. We conclude that there is little evidence that alteration products could be responsible for this difference.

The depleted shergottites are relatively rich in low-Ca pyroxene (mostly *pig* with some *opx*, and little *aug*). It is known that *opx* is higher in  $\delta^{18}\text{O}$  than coexisting high-Ca *cpx* when they form in mutual equilibrium. It is not obvious whether this reflects a chemical or structural difference, and so it is not clear whether the low-Ca, clinopyroxene *pig* should exhibit an oxygen isotope fractionation resembling *opx* or calcic *cpx*. If the fractionation of  $\delta^{18}\text{O}$  in pyroxene depends on Ca content (i.e., *pig* behaves more like *opx*) one could argue that the *px* from these three depleted shergottites are high in  $\delta^{18}\text{O}$  because they contain more low-

Ca *px* than high-Ca *px*. However, in this case, we would have expected the lherzolitic shergottites (the lherzolitic shergottites measured in this study are intermediately enriched), which have the lowest Ca *px*'s of all the shergottites, to be even higher in  $\delta^{18}\text{O}$ , which they are not (figure 1.2). If instead,  $\delta^{18}\text{O}$  fractionation among the pyroxenes depends on structure (i.e., *pig* behaves like *cpx*), then these three depleted shergottites should have had  $\delta^{18}\text{O}$  values similar to basaltic shergottites (all basaltic shergottites in this study are enriched and are abundant in *cpx*) rather than the slightly elevated values we observe. Additionally, because lherzolitic shergottites (where *px* is mostly *opx* and *pig*) have the same  $\delta^{18}\text{O}$  values as basaltic shergottites (which have roughly equal *aug* and *pig*), it is unlikely that variations in oxygen isotope fractionation behavior among various end member pyroxenes are responsible for the subtle differences among bulk pyroxene separates we analyzed in this study.

Alternatively, the higher  $\delta^{18}\text{O}$  of pyroxenes from DaG 476, Dho 019, and SaU 005 could reflect a slightly higher  $\delta^{18}\text{O}$  of the sources of depleted shergottites (perhaps approaching the  $\delta^{18}\text{O}$  values of nakhlites; see below). It would be counterintuitive if this difference reflected altered crustal components to those sources, as these should lead to elevated  $\delta^{18}\text{O}$  coupled with enriched geochemical signatures. Thus, it is more plausible that this difference exists between the mantle sources of depleted shergottites and the rest of the shergottites. The one counter indication of this hypothesis is that NWA 2046 has also been classified as a depleted shergottite but does not display elevated  $\delta^{18}\text{O}$ . However, there is no REE, Rb/Sr, or Sm/Nd data for NWA 2046, and its classification as depleted is based on secondary evidence from olivine trace element abundances and maskelynite major element compositions (Shearer et al. 2008; Papike et al. 2009). It is worth exploring whether NWA

2046 shares the depleted source characteristics of DaG 476, Dho 019, and SaU 005 (i.e., it is possible that the depleted shergottites are, in fact, universally slightly elevated in  $\delta^{18}\text{O}$ , and NWA 2046 is not actually a depleted shergottite). Depleted shergottites studied by Bouvier et al. (2009) define a trend in Pb isotope space that differs from that defined by the moderate and enriched shergottites (both of which share the same trend), which indicates that the shergottites come from at least two reservoirs that have remained separate for over four billion years. Additionally, Sm-Nd isotopes show that DaG 476, Dho 019, and QUE 94201 share a pseudoisochron with nakhlites Nakhla, Lafayette, and Governador Valadares, while enriched and intermediate shergottites share a separate pseudoisochron (Nyquist et al. 2001). Although the depleted shergottites are much younger than the Nakhlites, they are also several hundred million years older than other shergottites. Perhaps there is no relationship between any of the shergottite types, and the observed trend between enrichment and oxidation is not from mixing two reservoirs, but rather from a magma ocean stratification process in the mantle that is zoned with depth, similar to conclusions of Symes et al. (2008).

#### DaG 476 Olivine and NWA 4468 Maskelynite

Olivine megacrysts in DaG 476 have the most obviously anomalous  $\delta^{18}\text{O}$  value among the shergottites in that they are higher than both *px* and *msk* from the same rock, rather than lower as expected for equilibrium partitioning at magmatic temperatures, and thus higher than any plausible equilibrium magmatic value for olivine in these rocks. DaG 476 and its pairs were found in the desert and display abundant terrestrial weathering. Wadhwa et al. (2001) reported in situ SIMS REE patterns in DaG *ol* that exhibit a LREE enrichment they

argue is specific to terrestrial alteration. However, Edmunson et al. (2005) attribute this enrichment to mobilization of oxygen during impact on Mars that creates defects and allows incorporation of larger, incompatible elements into their structures (i.e., it may be a consequence of subsolidus processes on Mars). Oxygen isotope exchange during terrestrial alteration processes at near surface temperatures generally increases the  $\delta^{18}\text{O}$  in altered solids. In the case of martian meteorites, terrestrial weathering should also decrease their  $\Delta^{17}\text{O}$  values (though this may only be noticeable if alteration is severe). It is possible that shock impact created defects in megacrystic *ol* grains without affecting smaller *px* and *plag* in the same manner, thus leaving *ol* more susceptible to terrestrial weathering. This scenario would be consistent with the fact that we observe a difference in  $\delta^{18}\text{O}$  between *px* and *msk* in DaG 476 consistent with magmatic equilibrium, but a higher  $\delta^{18}\text{O}$  value in olivine.

Similarly, NWA 4468 exhibits a difference in  $\delta^{18}\text{O}$  between *msk* and *px* that differs from the equilibrium fractionation between plagioclase and pyroxene at magmatic temperatures (figure 1.4). The relatively low  $\delta^{18}\text{O}$  value of *msk* in NWA 4468 may reflect the earlier growth of *opx* from the parent melt. NWA 4468 contains large *opx*-cored oikocrysts, and *msk* is an interstitial phase in this poikilitic rock. Crystallization of *opx* (and possibly *plg*) from basaltic melt is predicted to reduce the  $\delta^{18}\text{O}$  of residual basaltic liquid. Thus, growth of plagioclase from a late-stage, interstitial melt after growth of *opx* could lead to *msk-px* fractionations that are smaller than equilibrium at magmatic temperatures.

Nakhlites, Chassignite, and ALH 84001

Olivine in the nakhlites is higher in  $\delta^{18}\text{O}$  than *ol* in all the other SNCs (apart from DaG 476, which we suggest is influenced uniquely by subsolidus alteration). Pyroxene in the nakhlites is higher in  $\delta^{18}\text{O}$  than *px* in all the enriched and moderate shergottites but similar in  $\delta^{18}\text{O}$  to *px* in the depleted shergottites, Dag 476, Dho 019, and SaU 005. High  $\delta^{18}\text{O}$  in minerals from the nakhlites could be a product of exchange with late-stage evolved melts that coexisted with these cumulate rocks. Olivine in the nakhlites is out of Fe/Mg equilibrium with coexisting *px* and is thought to have undergone diffusive chemical exchange with the evolving magma during slow cooling (Longhi and Pan 1989). Iron and magnesium interdiffusion is much faster than oxygen self-diffusion in olivine (e.g., Ryerson et al. 1989; Dohmen et al. 2007), and so it is not obvious that this slow cooling had to affect the oxygen isotope compositions of these grains, though it could have if cooling were slow enough. Self-diffusion of oxygen occurs faster in pyroxene than in olivine. Crystallization of oxides, high-Ca *cpx*, and *ol* in basaltic melts increases  $\delta^{18}\text{O}$  of the residual magma. Therefore, oxygen exchange between an early formed cumulate phase and an evolved magma could increase the  $\delta^{18}\text{O}$  of the earlier formed olivine and pyroxene. Olivine in all other SNCs is thought to have crystallized early and have undergone subsolidus equilibration to a much smaller degree that only affects *ol* rims. Therefore, this process is only suspected to have affected the nakhlites. Thus, if slow cooling in the presence of evolved melt explains the high  $\delta^{18}\text{O}$  of nakhlite minerals, their similarity to the somewhat high  $\delta^{18}\text{O}$  in *px* from depleted shergottites DaG 476, Dho 019, and SaU 005 must be coincidental.

Instead, this could be consistent with the nakhlites and depleted shergottites being products of partial melting of a shared or similar, high  $\delta^{18}\text{O}$  reservoir—an idea supported by the fact that these rocks collectively define a  $^{147}\text{Sm}$ - $^{143}\text{Nd}$  whole-rock “isochron” of 1.3 Ga (Nyquist et al. 2001) and have similar  $\epsilon^{142}\text{Nd}$  (Foley et al. 2005). Other constraints on this hypothesis are that nakhlites are LREE enriched (Wadhwa and Crozaz 1995) whereas the depleted shergottites are not, and Rb-Sr whole-rock ages for these samples are 4.5 Ga.

Olivine from the chassignite, NWA 2737 is similar in  $\delta^{18}\text{O}$  to olivine from the enriched and intermediate shergottites, and is not relatively high like the nakhlites. This is consistent with Wadhwa and Crozaz’s (1995) suggestion that chassignites and nakhlites are not from the same source magma.

Pyroxene from ALH 84001 is the only *px* separate that consists of mostly *opx* rather than *cpx* (*pig* and *aug*), and has the highest  $\delta^{18}\text{O}$  value. The difference in  $\delta^{18}\text{O}$  between *px* from ALH 84001 and *px* from all the other SNCs is similar to the difference expected for  $\delta^{18}\text{O}$  fractionation between *cpx* and *opx* at magmatic temperatures. Thus, the parent melt of ALH 84001 may have had a  $\delta^{18}\text{O}$  value closely similar to those of other SNCs.

#### Measurements of $\Delta^{17}\text{O}$

The standard deviation in  $\Delta^{17}\text{O}$  ( $\pm 0.015\%$ ) of SNCs from this study is similar to the  $\pm 0.013\%$  standard deviation reported by Franchi et al. (1999) (figure 1.6). Franchi et al. (1999) calculated values of  $\Delta^{17}\text{O}$  using the expression:  $\Delta^{17}\text{O} = \delta^{17}\text{O} - 0.52 \delta^{18}\text{O}$  (Clayton and Mayeda 1996) whereas this study uses the logarithmic equations of Miller (2002),  $\Delta^{17}\text{O} = 1000\ln((\delta^{17}\text{O}/1000) + 1) - \lambda 1000\ln((\delta^{18}\text{O}/1000) + 1)$ , and a mass law exponent,  $\lambda$ ,

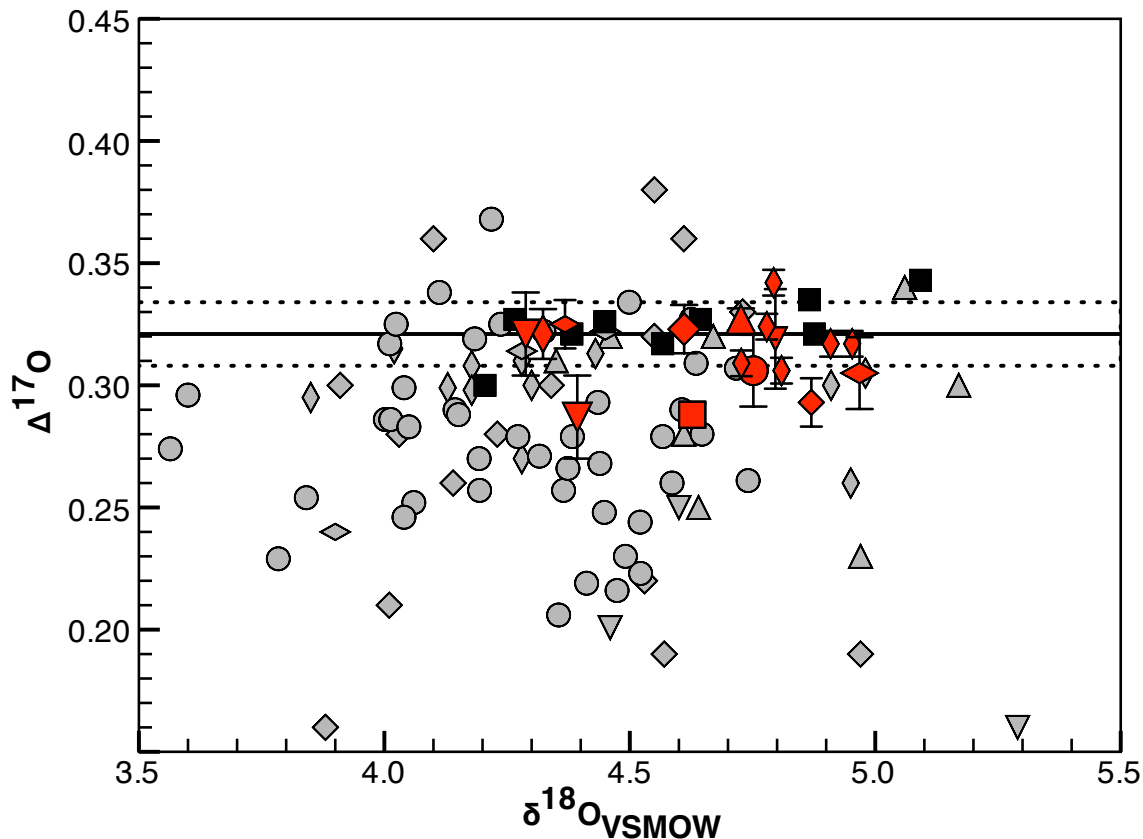


Figure 1.6. Measurements from this study (red) compared with those from other laboratories. The solid and dashed black lines are the martian fractionation line and associated error reported by Franchi et al. (1999). The variation in this study is similar to that of Franchi et al. (1999). Black squares, Franchi et al. (1999) study; grey diamonds, Clayton and Mayeda (1996) study; grey triangles, Romanek et al. (1998) study; grey circles, Rumble and Irving (2009) study; grey vertical diamonds, additional data from Open University (2000 – 2008); grey upside-down triangles, additional data from Geophysical Laboratory. Red symbols from this study: circle, Shergotty *px*; square, NWA 2986 *px*; large diamond, Zagami *px*; small diamond, Lafayette *px*; triangle, NWA 4468 *px*; large upside-down triangle, NWA 2950 *ol*; small upside-down triangle, Nakhla *px*; large vertical diamond, ALH A77005 *ol*; horizontal diamond, NWA 2737 *ol*.

of 0.5259 (Spicuzza et al. 2007). These two methods result in closely similar results because of the small variations in  $\delta^{18}\text{O}$  among SNC samples and the relatively modest differences between SNC samples and terrestrial standards; i.e., the linear approximation is suitable. Nevertheless, we use the power law expression throughout this study in order to be consistent with current evaluations of the terrestrial fractionation line.

We can think of no obvious explanation as to why we found a uniform, precisely defined  $\Delta^{17}\text{O}$  value for SNC meteorite components, other than that the minerals in question (and their parent magmas) are, in fact, invariant in  $\Delta^{17}\text{O}$  (i.e., it seems unlikely that such a null result could arise fortuitously or through an analytical artifact). This conclusion implies that the variations in  $\Delta^{17}\text{O}$  found in some previous studies are analytical artifacts or a consequence of terrestrial or martian alteration products that we successfully removed by pretreatment. This is unsurprising in the case of Clayton and Mayeda (1996), who used a resistance-heated fluorination technique with analytical errors no better than  $\pm 0.07\text{‰}$  (based on analyses of standards from Clayton and Mayeda 1996). However, the discrepancies among the other published studies need more explanation, as Franchi et al. (1999), Romanek et al. (1998), and Rumble and Irving (2009) used the laser fluorination technique as was used in this study. In addition to different sample techniques and prefluorination conditions between laboratories described above, different labs also used different  $\text{O}_2$  extraction methods. After heating the sample with a laser in the presence of  $\text{BrF}_5$ , Romanek et al. (1998), Franchi et al. (1999), and Rumble and Irving (2009) (as reported in Rumble et al. 2007) expose the sample gas product to  $\text{KBr}$  to remove any excess  $\text{F}$ , whereas in this study the gas is transferred through a  $\text{Hg}$ -diffusion pump where excess  $\text{F}$  will react with heated  $\text{Hg}$ . After exposure to  $\text{KBr}$ , Rumble and Irving (2009) also transfer the gas through a  $\text{Hg}$ -diffusion pump (Rumble et al. 2007). The gas is then trapped by freezing it onto a 13X molecular sieve in this study and at the Open University labs (Franchi et al. 1999); a 5A molecular sieve at Geophysical Laboratory (Rumble et al. 2007); and in a flow-through  $\text{He}$  cryostat by Romanek et al. (1998). In this study, the gas is further purified by slightly raising the temperature of the 13X molecular sieve trap (we

replace liquid nitrogen with an ethanol slush, similar to methods of Clayton and Mayeda (1983) to keep other fluorination by-products such as  $\text{NF}_3$  and  $\text{CF}_4$  trapped while releasing  $\text{O}_2$ , and then refreeze onto a 5A molecular sieve. These fluorination by-products can cause interferences for mass-to-charge ratio ( $m/z$ ) 33, and are dealt with at OU by scanning  $m/z = 52$  ( $\text{NF}_2^+$ ) on the mass spec and, if necessary, refreezing the sample gas onto a separate 13X molecular sieve, and adjusting the temperature with insulated heating tape so that the  $\text{NF}_3$  is retained on the trap but  $\text{O}_2$  is released (Miller et al. 1999). At GL, the use of a 5A molecular sieve is helpful in preferentially adsorbing the interfering molecules, and their laboratory is known to monitor interference by scanning  $m/z = 52$  and  $69$  ( $\text{CF}_3^+$ ) (Wiechert et al. 2001). Romanek et al. (1998) does not discuss this issue.

Most available  $\Delta^{17}\text{O}$  measurements of SNC meteorites come from University of Chicago—the lab used by Clayton and Mayeda (1996), the OU, or the GL, whose respective methods are described above. However, a significant amount of available data comes from various other laboratories, and most of this has been reported only in meteoritical bulletins and/or conference abstracts, omitting methodological details. Although the same approximate  $\Delta^{17}\text{O}$  value of  $\sim 0.3\%$  is reported for all SNCs by all laboratories, it seems possible to us that subtle variability about this value observed in a subset of the data reflects inter- and intralaboratory artifacts. Now that standard deviations in  $\Delta^{17}\text{O}$  of  $0.015\%$  or less are found in two separate studies that cover a broad range of SNCs (this one and that of Franchi et al. 1999), we think it unlikely that the variation in  $\Delta^{17}\text{O}$  of other existing data is characteristic of primary silicate minerals in martian samples.

## Conclusions

Though we have made some effort to explain subtle variations in  $\delta^{18}\text{O}$  among the SNCs, the key result of this study is that the SNCs, taken as a group, are remarkably uniform in oxygen isotope composition, and most of the subtle variations that are observed can be understood as consequences of crystallization differentiation or (in the case of *ol* in DaG 476) terrestrial weathering. This homogeneity is even clearer in  $\Delta^{17}\text{O}$ , which is uniform within analytical precision. Our results are explicitly inconsistent with the correlation between  $\delta^{18}\text{O}$  and indices of enrichment noted by Herd (2003), and we suggest that result reflected the combined effects of fortuitous analytical errors and systematic effects of crystal accumulation on whole rock  $\delta^{18}\text{O}$  values. In any event, no such correlation exists among the parent magmas of the SNCs. We conclude that there is no oxygen isotope evidence that the enriched shergottites are derived from an aqueously altered source or assimilated or mixed with a component of altered crust.

The apparent uniformity in oxygen isotope compositions of martian magmas (at least, as sampled by igneous minerals in the SNC meteorites) is remarkable when compared with terrestrial, lunar, and other meteoritic materials. The variability in  $\delta^{18}\text{O}$  of terrestrial basaltic and gabbroic rocks exceeds that of martian equivalents by more than an order of magnitude—a testament to the important role of aqueous alteration and authigenic sediments in the geochemical evolution of the crust, which is sampled by terrestrial basaltic magmas as subducted source components and lithospheric contaminants. Though it is challenging to reach general conclusions about martian geology based on our sampling of rocks in the known SNC meteorite collection, it would appear that these phenomena do not

operate on Mars. It seems inevitable that martian magmatism must expose hot magmas to the walls of magmatic plumbing systems, and so stoping, crustal melting, and assimilation must occur. The absence of an oxygen isotope signature of assimilation in the SNCs suggests that the crust of Mars is simply very poor in aqueous alteration products. This implies that clays, sulfates, carbonates, and oxides observed at the surface of Mars and found in trace quantities as martian weathering products in the SNCs make up a relatively small fraction of the martian crust overall. While this argument is based on indirect, negative evidence, it is one of the only insights available to us today regarding the distribution of aqueous alteration products beneath the martian surface.

Martian magmas seem to be more homogeneous in  $\delta^{18}\text{O}$ , by greater than a factor of 2, than lunar magmas (Wiechert et al. 2001; Spicuzza et al. 2007). However, the majority of heterogeneity in  $\delta^{18}\text{O}$  of mare basalts appears to be from an offset between high- and low-Ti basalts. Similar to conclusions of Spicuzza et al. (2007), we suggest this is an indication of the distinctive role of oxide-rich cumulates in the early differentiation history of the moon. Even at magmatic temperatures, oxide minerals are markedly lower in  $\delta^{18}\text{O}$  than coexisting silicates. This effect could readily explain why high-Ti basalts are, on average,  $\sim 0.2\%$  lower in  $\delta^{18}\text{O}$  than low-Ti basalts (Spicuzza et al. 2007).

Parent magmas of the SNCs are much more homogeneous in  $\delta^{18}\text{O}$ , by nearly a factor of 4, than previous measurements of the HED meteorites (Wiechert et al. 2004; Scott et al. 2009). Most of this heterogeneity seems to come from the cumulate eucrites (Scott et al. 2009), but unfortunately the HED meteorites have not yet been subjected to a high-precision study of the oxygen isotope compositions of mineral separates. Therefore, there

remain several possible explanations for their  $\delta^{18}\text{O}$  variation—analytical errors, contaminants, mixing of minerals having different partitioning behavior, and actual heterogeneity in  $\delta^{18}\text{O}$  of the HED parent body, or bodies. We suggest this is an attractive target for future study.

DaG 476 exhibits abundant terrestrial weathering that may have had more of an effect on impact-fractured, megacrystic *ol* than other nonfractured phases. This could explain why *ol* from DaG 476 is higher in  $\delta^{18}\text{O}$  than expected for equilibrium with coexisting phases at magmatic temperatures. Similarly, *px* and *msk* are slightly out of isotopic equilibrium in NWA 4468 and may reflect the early growth of *opx* phenocrysts that relatively depleted the residual melt of  $^{18}\text{O}$  by the time plagioclase crystallized.

*Chapter II*

## ABUNDANCES OF CL, F, H, AND S IN APATITES FROM SNC METEORITES

**Introduction**

The abundances of volatiles (e.g. H<sub>2</sub>O, CO<sub>2</sub>, S, F, Cl, etc.) in silicate magmas have a strong effect on their phase equilibria and physical properties, such as density and viscosity, both of which influence magmatic composition and behavior during crystallization, melting, ascent, and eruption (Roggensack et al. 1997; Webster et al. 1999; Behrens and Webster 2011; Zajacz et al. 2012). Additionally, outgassing of igneous volatiles plays a critical role in atmospheric composition and climate (Devine et al. 1984; Symonds et al. 1988; Wallace and Gerlach 1994; Thordarson and Self 2003; Behrens and Webster 2011; Zelenski and Taran 2012).

Several lines of evidence suggest that the martian surface is richer in chlorine and sulfur than Earth (Clark and Baird 1979; Dreibus and Wanke 1985, 1987; Haskin et al. 2005; King and McLennan 2010), and that water persisted on the surface at least long enough to carve out many geomorphologic features (Carr 2012 and references therein). However, there is little understanding of the connections between these observations regarding the geology of the martian surface and the abundances and forms of volatiles released by martian magmas during their eruption and intrusion. We have few constraints on current and past volatile abundances in the martian mantle and their effects on magmatic processes, and on the contributions of magmatic volatiles to the atmosphere and surface of Mars

(Dreibus and Wanke 1985, 1987; Johnson et al. 1991; Watson et al. 1994; Jakosky and Jones 1997; Dann et al. 2001; Lentz et al. 2001; McSween et al. 2001; Patiño Douce and Roden 2006; Nekvasil et al. 2007; Filiberto and Treiman 2009; Gaillard and Scaillet 2009; Righter et al. 2009; King and McLennan 2010; McCubbin et al. 2012).

One way to acquire information on the volatiles Cl, F, OH, and S in magmas is through analyses of the mineral apatite— $\text{Ca}_5(\text{PO}_4)_3(\text{Cl},\text{F},\text{OH})$  (Piccoli and Candela 2002; Parat and Holtz 2004). Apatite is a late-crystallizing mineral in igneous systems and is more retentive of these volatile elements than glasses and silicate melts (Roegge et al. 1974; Brenan 1994; Streck and Dilles 1998; Tepper and Kuehner 1999). In addition to sequestering Cl, F, and OH, apatite can also incorporate sulfur as sulfate by substituting it for phosphate (Pan and Fleet 2002; Parat et al. 2011). However, sulfate is only present in magmas where oxygen fugacity is greater than  $\sim 1$  log unit below the quartz-fayalite-magnetite (QFM) buffer (Carroll and Rutherford 1988; Wallace and Carmichael 1994; Jugo et al. 2005; Baker and Moretti 2011), and Peng et al. (1997) have observed increasing abundance of sulfur in apatite with increasing oxygen fugacity. The oxygen fugacities of SNC magmas have been estimated to be between 5 log units below and 1 log unit above the QFM buffer (Herd et al. 2001; Wadhwa 2001; Herd, Borg, et al. 2002; Goodrich et al. 2003; Herd 2003; McCanta et al. 2004; Herd 2006; Karner et al. 2007; McCanta et al. 2009), thus we should only expect to observe sulfur in apatites from the more oxidized end of the spectrum of SNCs.

Previous measurements show that Cl is higher in most SNC apatites than in terrestrial apatites from mafic and ultramafic rocks (figure 2.1), which is consistent with the high chlorine contents found in martian soils (Clark and Baird 1979; Dreibus and Wanke 1985,

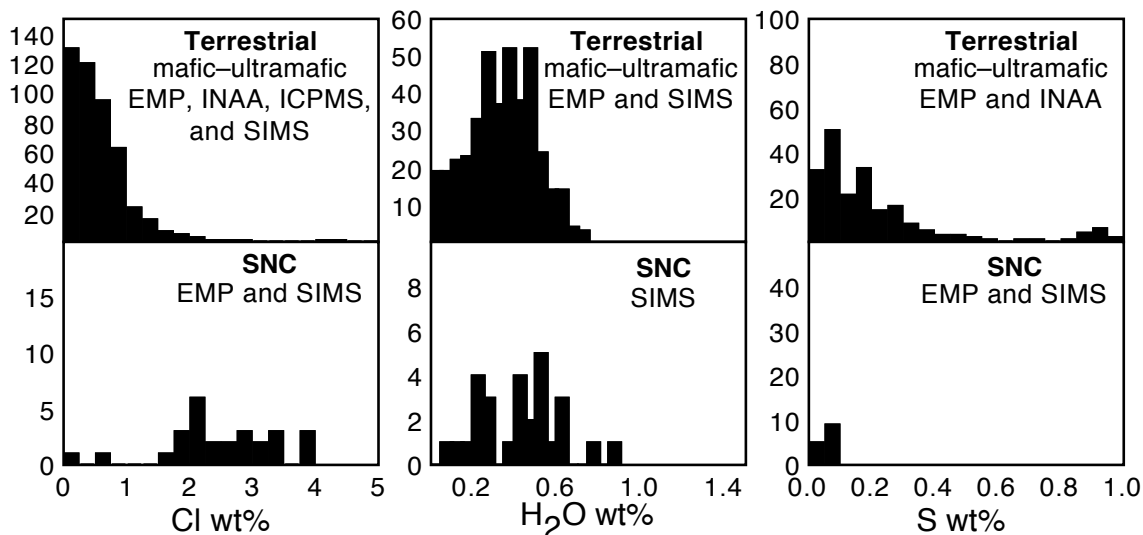


Figure 2.1. SNC apatites compared to terrestrial apatites from mafic and ultramafic rocks. SNC data are from Jagoutz and Wänke (1986), Harvey et al (1993), McCoy et al. (1999), Leshin (2000), Barrat, Gillet et al. (2002), Taylor et al. (2002), Xirouchakis et al. (2002), Boctor et al. (2003), Greenwood et al (2003), Guan et al. (2003), Warren et al. (2004), Beck et al. (2006), Treiman et al. (2007), Greenwood et al. (2008), Treiman and Irving (2008), Sharp et al. (2011), McCubbin et al. (2012), and terrestrial data are from GEOROC.

1987). Previous measurements also show that SNC apatites have a similar range in H<sub>2</sub>O as terrestrial apatites, and they are lower in S than terrestrial apatites. This would suggest that there is more water in martian magmas than previously believed, and that the oxygen fugacities are too low for apatite to incorporate much sulfur. However, the data are too sparse to support any general conclusions regarding the diversity of volatile contents among the various types of martian igneous rocks and, by inference, their mantle sources. Here, we report measurements of Cl, F, H, and S from a relatively large and representative set of SNC apatites, obtained in order to better constrain the volatile contents of martian magmas.

## Materials and Methods

Analyses of Cl, F, H, (reported as H<sub>2</sub>O), and S were measured in apatite and olivine [(Mg,Fe)<sub>2</sub>SiO<sub>4</sub>] in martian and terrestrial samples, which were prepared both as polished thin sections (PTS) and as polished grains or rock fragments pressed into indium. Twenty-one apatite grains in PTSs of three basaltic shergottites (JaH 479, NWA 856, and NWA 2986), one lherzolic shergottite (NWA 1950), and one nakhlite (NWA 998) were analyzed using the Cameca IMS 7f-GEO secondary ion mass spectrometer (SIMS) at the Center for Microanalysis at Caltech. Fourteen apatite grains in PTSs from one basaltic shergottite (Shergotty), two olivine-phyric shergottites (Dho 019 and NWA 6710), one chassignite (NWA 2737), and one terrestrial sample from a Kilauea Iki lava lake drill core (NMNH 116771-178) were measured using the Cameca NanoSIMS 50L also at the Center for Microanalysis at Caltech. Seven olivine grains in PTSs of two olivine-phyric shergottites (two in Dho 019 and one in NWA 6710) and the Kilauea Iki sample, and sixteen olivine grains were also analyzed on the on the NanoSIMS, from rock fragments mounted in indium from one basaltic shergottite (JaH 479), one lherzolic shergottite (NWA 1950), one olivine-phyric shergottite (NWA 6710), and olivine separates mounted in indium from a terrestrial peridotite (San Carlos). The analyses of olivine in PTSs were compared to analyses of olivine mounted in indium in order to test the effect, if any, the thin sections had on the hydrogen background. Additionally, the NanoSIMS was used to generate elemental images of seven apatite grains in one basaltic shergottite (JaH 479) and two olivine-phyric shergottites (Dho 019 and NWA 6710), one olivine grain in NWA 6710, two pyroxene grains (one in Dho 019 and one in NWA 6710), and one maskelynite grain in NWA 6710 in order to assess the homogeneity of such grains.

All thin sections were previously carbon coated in order to locate phosphate grains using the JEOL JXA-8200 electron probe at Caltech. Back-scattered electron (BSE) and secondary electron (SE) images were made of apatite grains after their composition was verified using the Oxford X-MAX SDD X-ray energy dispersive spectrometer (EDS) system on the Zeiss 1550VP field emission scanning electron microscope (FE SEM) at Caltech. Carbon coats were removed by polishing them with 0.25- $\mu\text{m}$  grit diamond paste. Thin sections were then cleaned by sonication in deionized water for 30 seconds, and then rinsed with ethanol. Once dry, they were then sputter coated with 30 – 50 nm of gold. They were held in the airlock of either the 7f-GEO or NanoSIMS 50L for 12 – 72 hours prior to analysis.

For measurements made with the Cameca IMS-7f GEO, a  $\text{Cs}^+$  primary ion beam was rastered over a  $\sim 20 \times 20 \mu\text{m}$  area, and a 100  $\mu\text{m}$  field aperture was used to collect ions from the central 8 – 10  $\mu\text{m}$  of the sputtered region. The beam current was 3.5 nA with an impact energy of 20 kV, and the mass resolving power was  $\sim 5000$  ( $M/\Delta M$ ). We routinely inspected the secondary ion image of carbon after ten seconds of presputtering (to establish that the carbon coat was removed) and  $\sim 3$  minutes of tuning (in the same spot of analysis), and then collected fifteen cycles through the mass sequence  $^{12}\text{C}$ ,  $^{16}\text{O}^1\text{H}$ ,  $^{18}\text{O}$ ,  $^{19}\text{F}$ ,  $^{31}\text{P}$ ,  $^{32}\text{S}$ , and  $^{35}\text{Cl}$  using an electron multiplier detector for all masses.

For spot analyses using the Cameca NanoSIMS 50L, a  $\text{Cs}^+$  primary ion beam was rastered over a  $2 \times 2 \mu\text{m}$  area, and electrostatic gating of the secondary ion beam was used to restrict collected ions to the central area of  $1.1 \times 1.1 \mu\text{m}$ . The beam current was 9 pA with an impact energy of 16 kV, and a mass resolving power of  $>8000$ . Because most apatite

grains in the SNCs were small ( $\sim 30 \times 30 \mu\text{m}$ ), tuning prior to each measurement was done on the spot intended for analysis; therefore presputtering was only 10 seconds. We measured 100 cycles of  $^{12}\text{C}$ ,  $^{16}\text{O}^1\text{H}$ ,  $^{18}\text{O}$ ,  $^{19}\text{F}$ ,  $^{31}\text{P}$ ,  $^{32}\text{S}$ , and  $^{35}\text{Cl}$ , where all masses were simultaneously collected.

For NanoSIMS elemental mapping images, a  $\text{Cs}^+$  primary beam current of 3 pA was rastered over areas from  $35 \times 35$  to  $50 \times 50 \mu\text{m}$ , with total image acquisition times of 15 to 30 minutes.

We measured four independently analyzed natural apatites, Ap003, Ap004, Ap005, and Ap018 (abundances reported in McCubbin et al. 2012) and synthetic fluorapatite and chlorapatite (abundances reported in Boyce et al. 2012) and plotted measured ion ratios against reported abundances in order to create a calibration curve for converting measured ion ratios of our samples to elemental abundances (raw data and calibration curves can be found in appendix B). Another natural apatite from Durango, Mexico was used as an in-house laboratory check standard. We used eight independently analyzed olivine grains (one synthetic), grr997, grr999a, grr1012-1, grr1017, grr1629-2, grr1695-2, grr1784e, and rom177 (Mosenfelder et al. 2011) as olivine standards. All spot analyses were made after examining secondary ion images of carbon (typically associated with contaminants) to identify and avoid cracks. Additionally, the cracks were analyzed and compared to nominally crack-free samples to better recognize sample measurements that accidentally included cryptic crack-associated contaminants. Finally, we rejected any apatite analyses in which measured H, Cl, and F summed to significantly less (0.85) or greater than one (1.10) atom per formula unit (i.e., they violated the stoichiometric constraints on measurements of

apatite and thus likely included signals from materials other than apatite). The lower limit was set farther from nominal stoichiometry in order to allow grains that might have substantial trace element substitutions to pass the filter. Thirty sample apatite analyses out of eighty-three were rejected for one or more of these reasons and can be found in appendix B.

## **Results**

### NanoSIMS Images

The ion images generated for apatites in samples JaH 479 (an enriched basaltic shergottite) and NWA 6710 (an enriched olivine-phyric shergottite) show that all measured volatiles have high signal intensities in cracks and along grain boundaries, but are relatively homogenous throughout grain interiors for volatiles other than sulfur (which is commonly heterogeneous within apatite grains; figures 2.2 through 2.5). Sulfur enrichments are observed in linear features in the interiors of apatite grains. These may represent microcracks along which sulfur pervaded apatites. These linear S enrichments do not appear to be associated with enrichments in other volatiles. Ion NanoSIMS images of an NWA 6710 olivine show three features: (1) oscillatory zoning in phosphorus in the outer edges of the crystal, preserving evidence of faceted growth; (2) increased abundance in both Cl and S in smaller cracks and (3) increased abundances of all volatiles in larger cracks (figure 2.6). Similarly; an ion image of pyroxene in NWA 6710 shows that OH is homogeneously distributed throughout the grain but high in abundance in large cracks and grain boundaries, and increased abundances of all other volatiles in microcracks (figure 2.7). An ion image of maskelynite in NWA 6710 shows a relatively homogenous

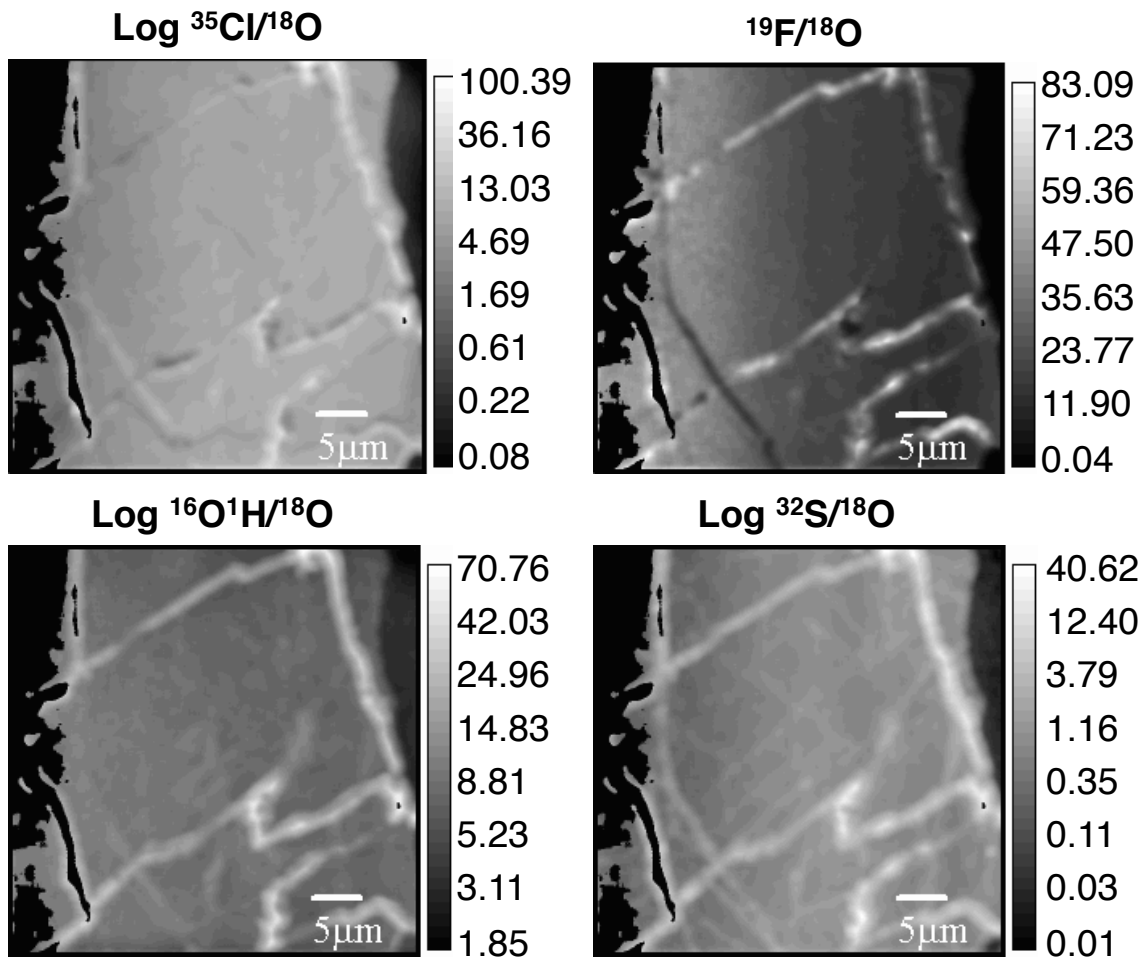


Figure 2.2. JaH 479 apatite 2. Note that a logarithmic scale is not used for the fluorine image.

distribution of all volatiles within grain interiors with some increased concentrations towards grain boundaries, and complete homogeneity in phosphorus (figure 2.8). The ion image of apatite in Dhofar 019 (a depleted olivine-phyric shergottite) shows heterogeneity and penetration into microcracks from all volatiles (figure 2.9). A Dho 019 pyroxene image shows the same distribution as the apatite, except that it also shows penetration into microcracks by phosphorus as well (figure 2.10).

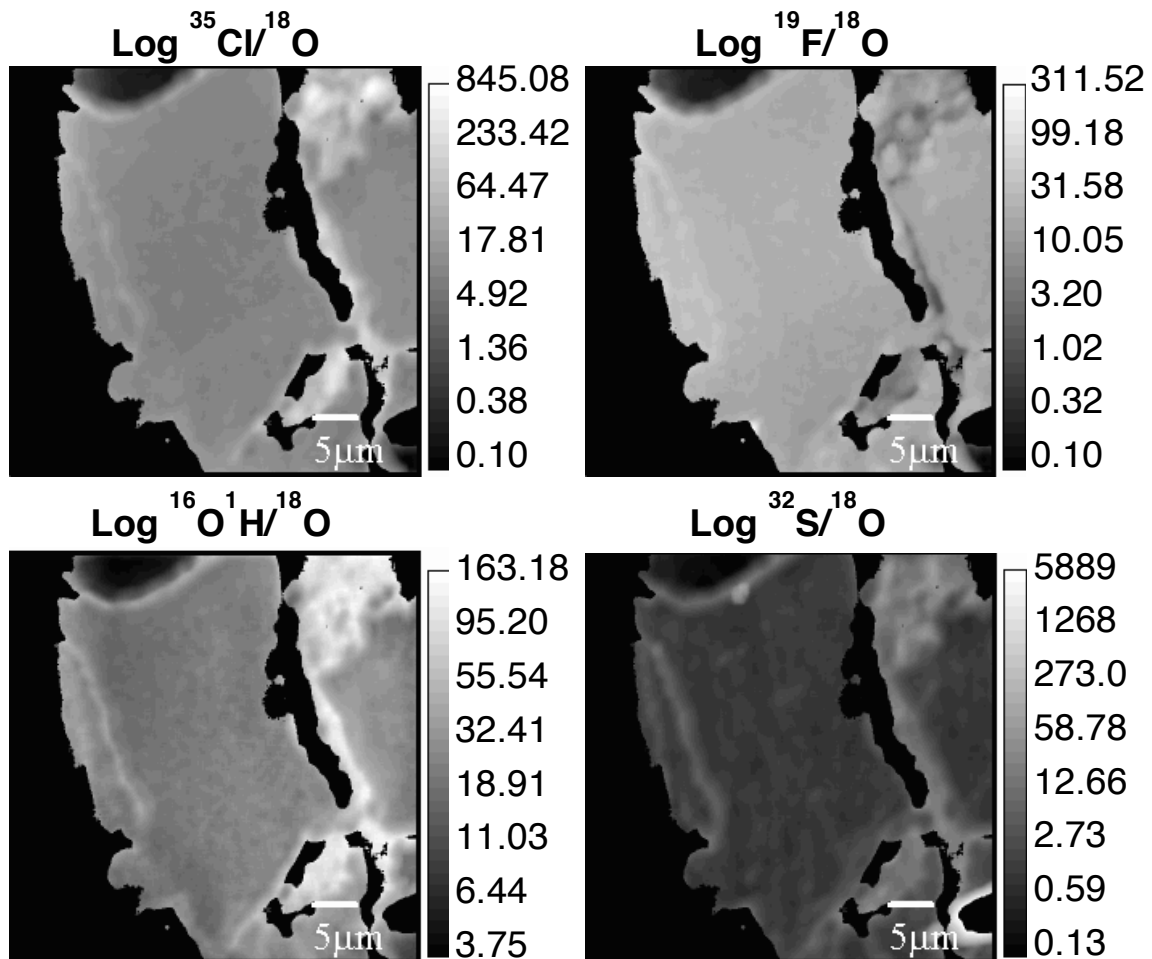


Figure 2.3. JaH 479 apatite 6.

### SNC Apatite Spot Analyses

Data for all apatite spot analyses can be found in table 2.1 (where the MS column indicates which mass spectrometer was used, either the 7f or the NanoSIMS—NS), and all olivine spot analyses can be found in table 2.2. Most SNC apatites, in both this study and previous studies using various techniques, have chlorine abundances between 1 and 3 wt%, but rare samples are outside this range, spanning from nearly 0 to just under 4 wt% (figure 2.11). This is an extraordinary range, though we emphasize it appears to be a consistent feature across multiple independent studies: Chlorine concentrations reported here are generally 1

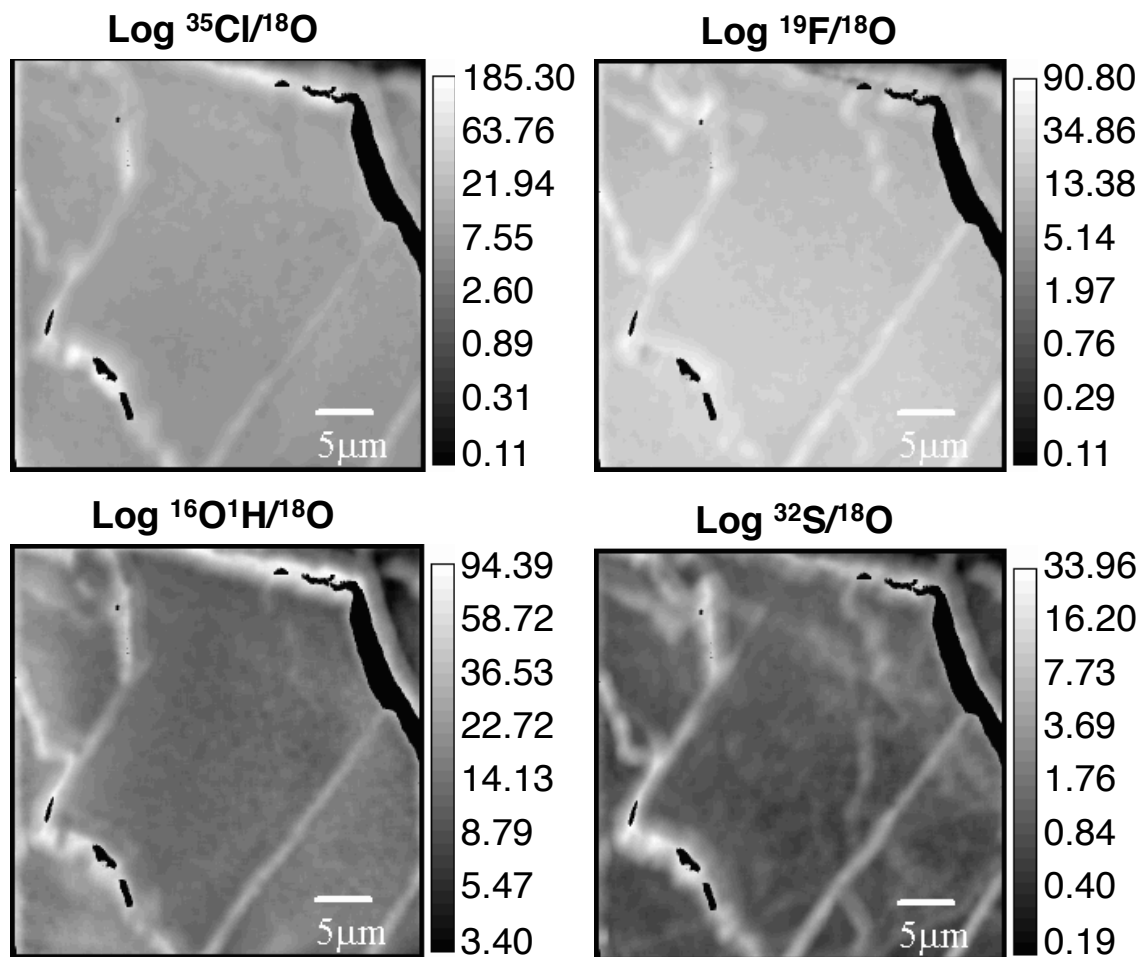


Figure 2.4. JaH 479 apatite 7.

wt% or less than previously reported values for SNC meteorites with the same petrographic lithology. Both this study and previous data show that SNC apatites are typically higher in Cl than terrestrial apatites from mafic and ultramafic rock types (with a few outliers).

Apatites from basaltic shergottites have  $\text{H}_2\text{O}$  abundances that average  $0.50 \pm 0.15$  wt% and range between 0.12 and 0.87 wt% (again, considering both data from this study and from previous studies; figure 2.12). Apatites from the two olivine-phyric shergottites examined in this study average  $0.86 \pm 0.10$  wt%  $\text{H}_2\text{O}$ . Apatites from lherzolithic shergottites (including both measurements in this study and one previous study) have average  $\text{H}_2\text{O}$  abundances of

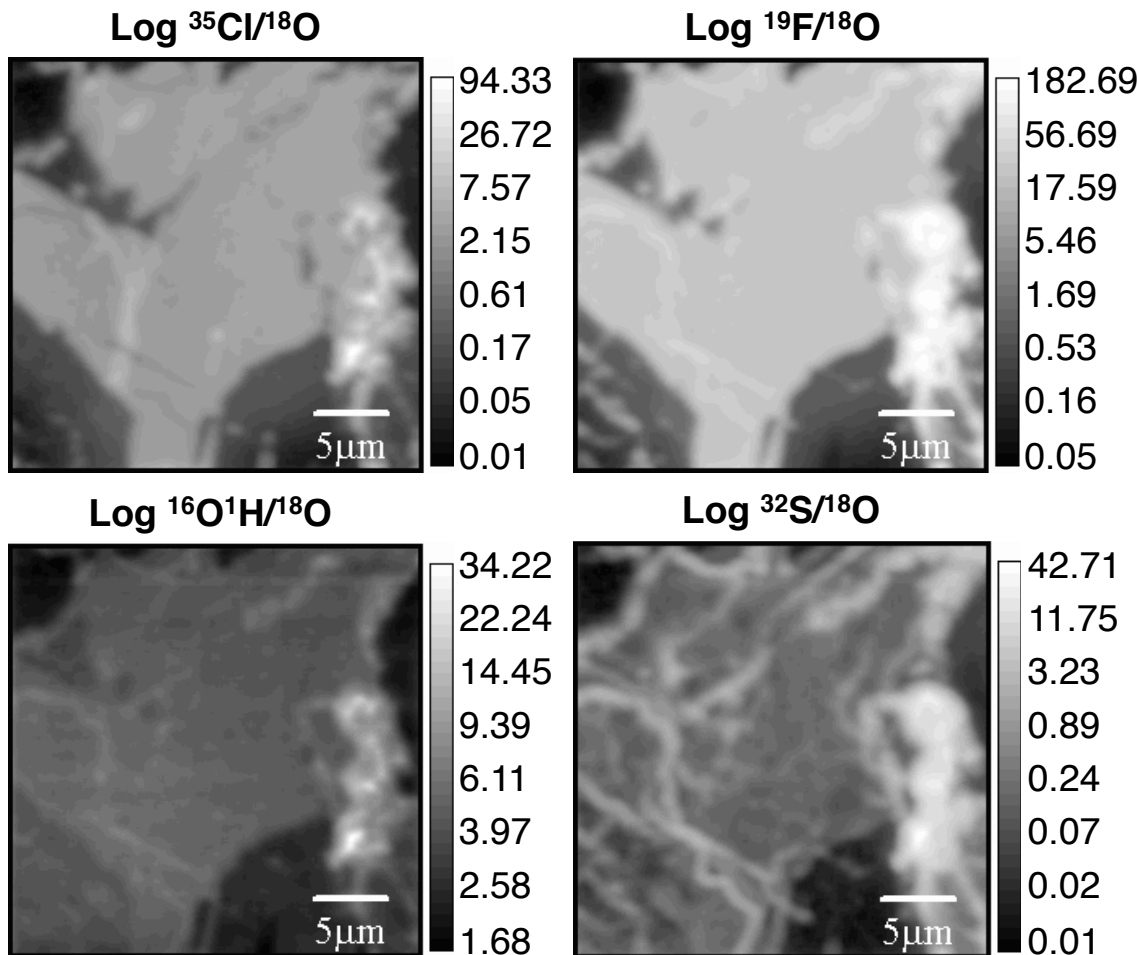


Figure 2.5. NWA 6710 apatite 4.

$0.22 \pm 0.17$  wt%. However, note that the lherzolitic shergottite from this study (NWA 1950) has apatite  $\text{H}_2\text{O}$  contents at least 0.15 wt% less than the apatite from a previously analyzed lherzolitic shergottite, GRV 99027 (Guan et al. 2003). Apatites from clinopyroxenite NWA 998, dunites Chassigny and NWA 2737, and orthopyroxenite ALH 84001 (all analyzed in this study; we are aware of no previous measurements of water contents of apatites from cumulate SNCs) have an average  $\text{H}_2\text{O}$  abundance of  $0.13 \pm 0.06$  wt%. Measurements from this study and previous SNC studies differ by no more than 0.19 wt%  $\text{H}_2\text{O}$  among apatites from meteorites that share the same petrographic lithology.

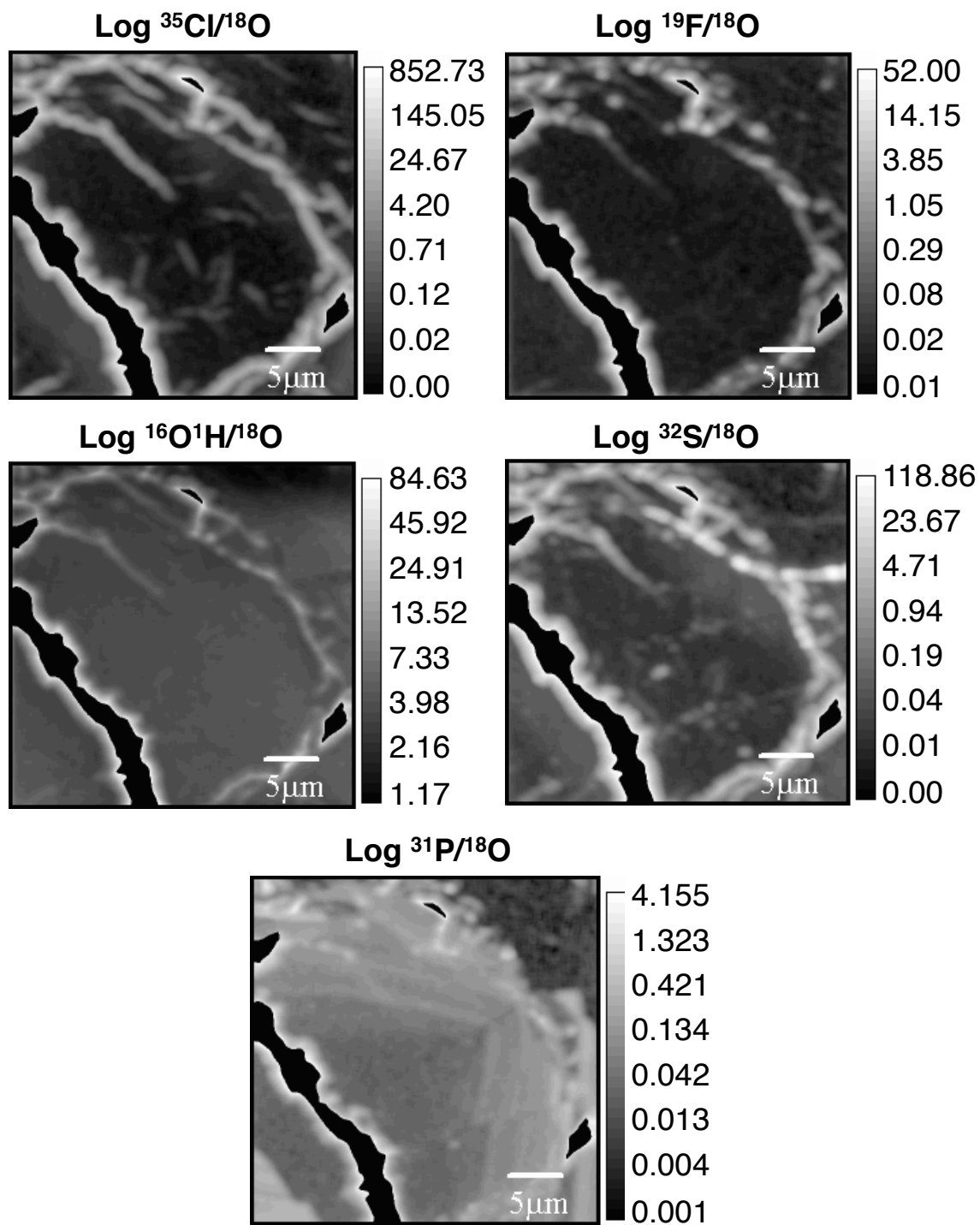


Figure 2.6. NWA 6710 olivine.

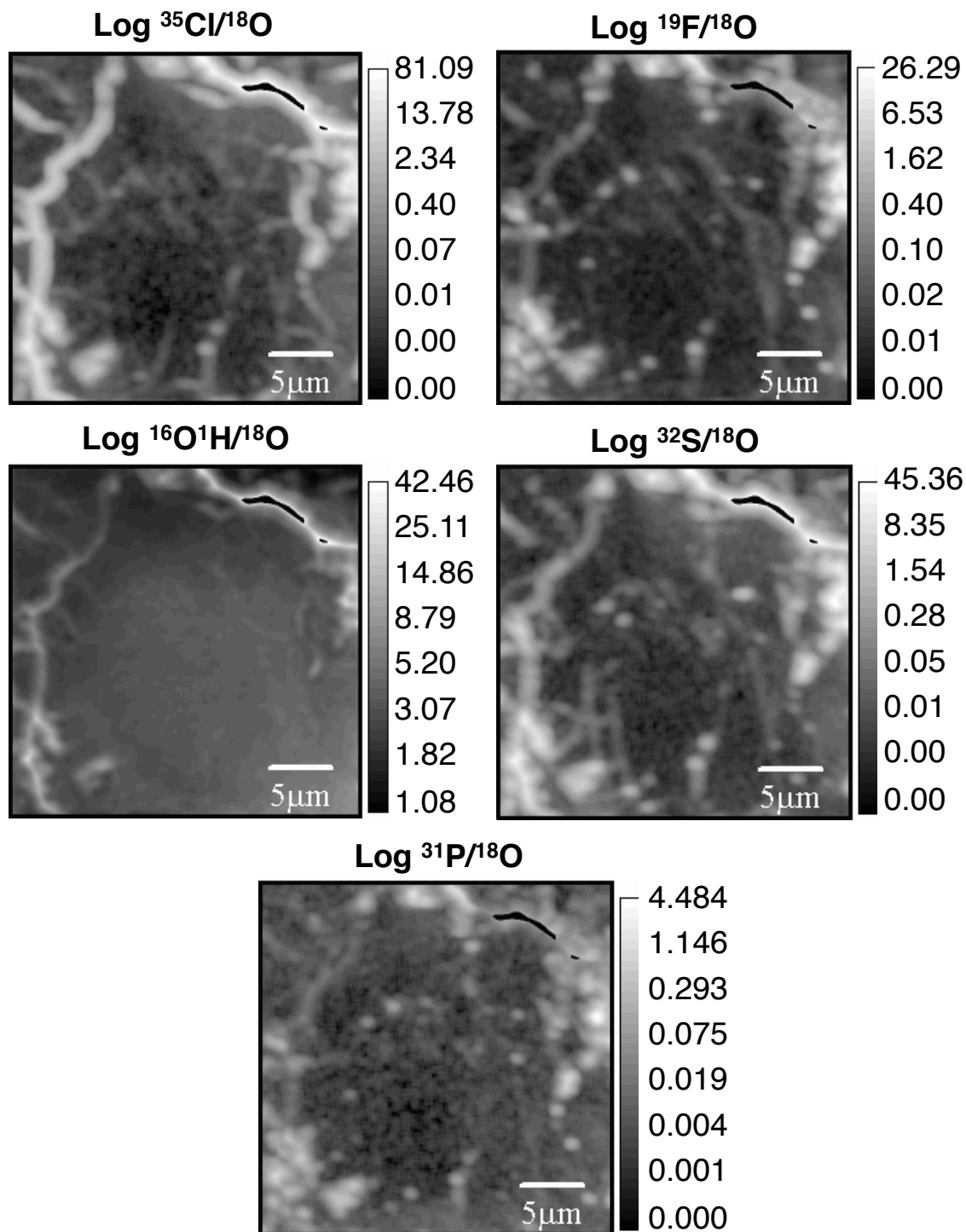


Figure 2.7. NWA 6710 pyroxene.

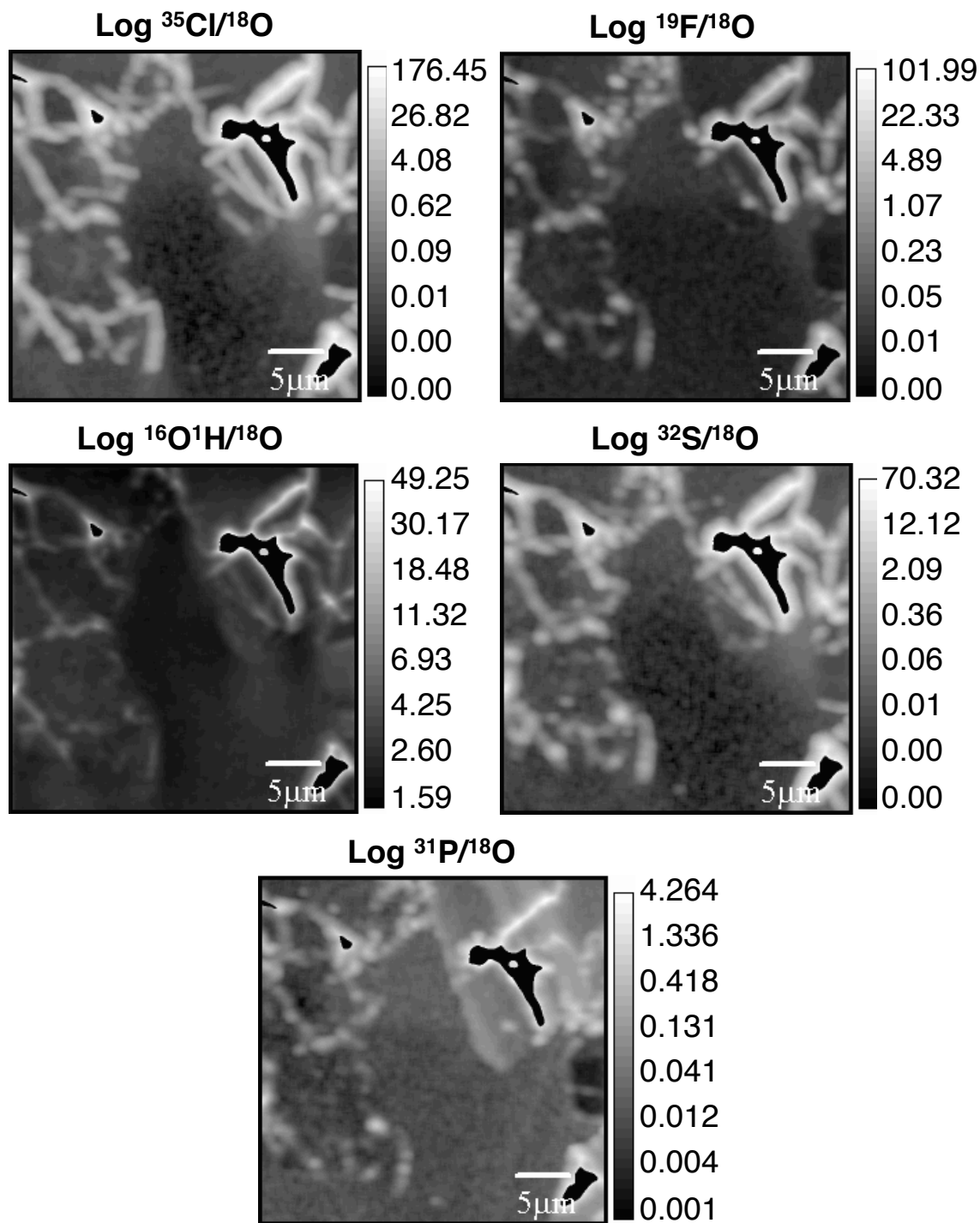


Figure 2.8. NWA 6710 maskelynite.

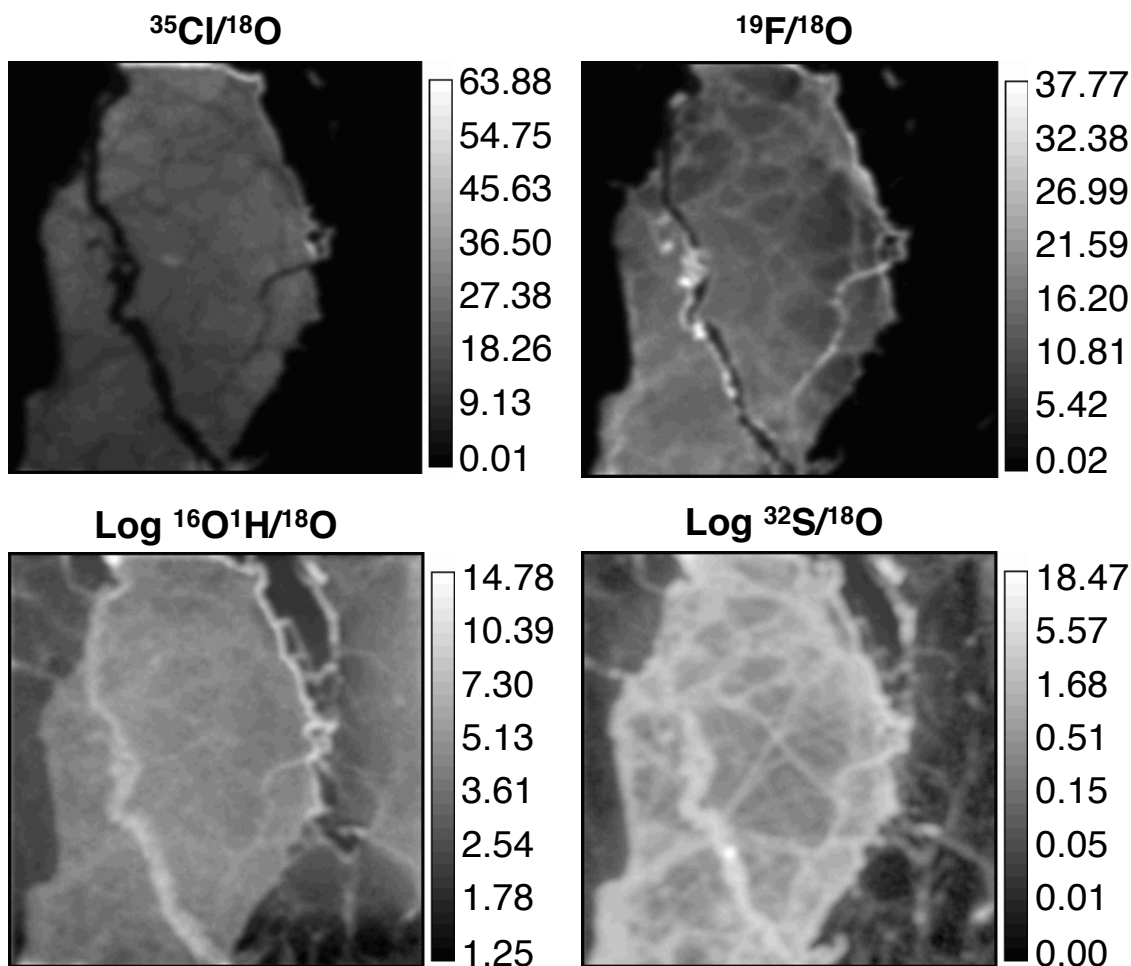


Figure 2.9. Dhofar 019 apatite 1. Note that a logarithmic scale is not used for the chlorine and fluorine images.

Martian apatites show a similar range in  $\text{H}_2\text{O}$  content as terrestrial apatites from mafic and ultramafic rocks, excepting apatites from the two olivine-phyric shergottites, which show higher  $\text{H}_2\text{O}$  contents than terrestrial apatites from mafic and ultramafic rocks.

The abundances of  $\text{H}_2\text{O}$  in olivines from SNCs and terrestrial samples are shown in figure 2.13. Note that our results depend strongly on the sample preparation techniques. The average abundance of  $\text{H}_2\text{O}$  in all the SNC olivines that were mounted in indium is  $1090 \pm 620$  ppm. This is significantly in excess of the water contents of typical terrestrial igneous

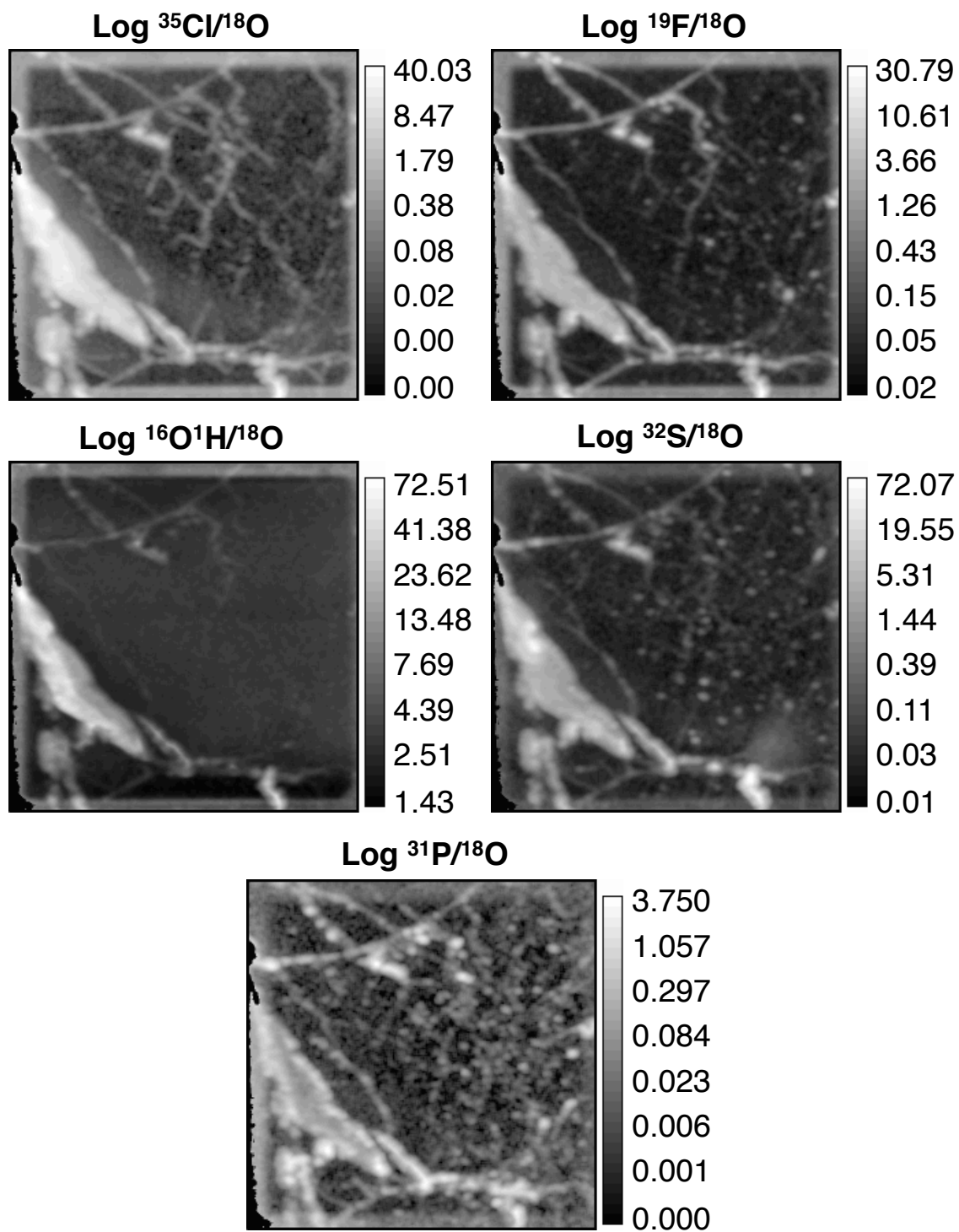


Figure 2.10. Dhofar 019 pyroxene.

Table 2.1. All SNC apatite measurements from this study.

Meteorite	Grain	MS	Cl		F		H <sub>2</sub> O		S		Cl+	
			(wt%)	2 $\sigma$	(wt%)	2 $\sigma$	(wt%)	2 $\sigma$	(wt%)	2 $\sigma$	F+	
Basaltic Shergottites												
<b>JaH 479</b>	1_1	7f	2.20	0.11	1.49	0.03	0.42	0.05	0.13	0.02	0.95	
	2_1b	7f	1.14	0.07	1.28	0.09	0.87	0.16	0.10	0.02	0.98	
	2_3	NS	1.79	0.10	1.63	0.18	0.64	0.06	0.12	0.01	1.04	
	3_1	7f	2.04	0.10	1.46	0.02	0.49	0.05	0.21	0.02	0.95	
	6_1a	7f	1.51	0.07	1.70	0.02	0.58	0.06	0.09	0.03	0.98	
	6_1b	7f	1.60	0.11	1.76	0.05	0.63	0.07	0.10	0.02	1.04	
				1.56		1.73		0.60		0.09		1.01
	7_1a	7f	2.20	0.09	1.39	0.02	0.42	0.04	0.16	0.02	0.92	
	8_1	7f	1.45	0.08	1.79	0.02	0.47	0.04	0.10	0.01	0.94	
	8_2	7f	1.59	0.07	1.83	0.02	0.38	0.04	0.08	0.01	0.92	
	8_3	7f	1.95	0.08	1.42	0.02	0.48	0.05	0.13	0.01	0.93	
	9_1	7f	1.57	0.07	1.93	0.03	0.37	0.03	0.10	0.01	0.94	
	9_2a	7f	1.74	0.10	1.83	0.03	0.53	0.11	0.13	0.02	1.03	
	10_1	7f	1.86	0.09	1.41	0.03	0.49	0.05	0.14	0.01	0.91	
	11_1	7f	1.26	0.07	2.41	0.05	0.36	0.04	0.10	0.01	1.02	
<b>NWA 856</b>	1_1	7f	2.35	0.15	0.62	0.01	0.57	0.06	0.03	0.01	0.97	
	1_2	7f	2.96	0.18	0.59	0.03	0.59	0.07	0.05	0.01	0.91	
	3_1	7f	1.34	0.06	1.94	0.02	0.36	0.03	0.03	0.00	0.91	
<b>NWA 2986</b>	1_2	7f	1.88	0.08	1.25	0.03	0.53	0.05	0.09	0.01	0.89	
	2_1	7f	2.93	0.19	0.88	0.02	0.43	0.04	0.06	0.00	0.90	
	3_1	7f	1.79	0.08	1.74	0.02	0.32	0.03	0.14	0.08	0.90	
	4_1	7f	2.59	0.14	1.23	0.03	0.31	0.03	0.05	0.00	0.88	
	5_1	7f	1.97	0.12	1.30	0.03	0.44	0.04	0.05	0.00	0.87	
<b>Shergotty</b>	5_1	NS	2.42	0.15	1.59	0.16	0.60	0.12	0.04	0.01	1.10	
	5_2	NS	2.42	0.15	1.60	0.16	0.60	0.12	0.04	0.01	1.10	
	6_1	NS	2.55	0.16	1.41	0.15	0.54	0.11	0.07	0.01	1.04	
	6_2	NS	2.36	0.15	1.53	0.16	0.58	0.12	0.06	0.02	1.07	
	6_3	NS	2.36	0.14	1.53	0.16	0.59	0.12	0.05	0.01	1.07	

Table 2.1 continued.

Meteorite	Grain	MS	Cl		F		H <sub>2</sub> O		S		Cl+
			(wt%)	2 $\sigma$	(wt%)	2 $\sigma$	(wt%)	2 $\sigma$	(wt%)	2 $\sigma$	F+
Olivine-Phyric Shergottites											
NWA 6710	1a_2	NS	0.20	0.03	2.05	0.41	0.94	0.20	0.04	0.01	1.08
	1b_1	NS	0.43	0.04	1.89	0.39	0.83	0.17	0.02	0.01	1.02
	2_1	NS	0.05	0.02	1.83	0.39	0.92	0.19	0.01	0.01	0.99
	9_2	NS	0.47	0.03	1.77	0.19	0.93	0.09	0.03	0.01	1.04
	11_1	NS	1.56	0.08	1.48	0.18	0.75	0.07	0.02	0.01	1.03
	11_2	NS	1.26	0.06	1.53	0.18	0.74	0.07	0.02	0.01	0.99
Dho 019	2_3	NS	3.18	0.18	1.08	0.17	0.99	0.09	0.21	0.02	1.03
	2_4	NS	3.52	0.17	1.05	0.17	0.72	0.06	0.09	0.01	0.99
Lherzolithic Shergottites											
NWA 1950	1_1	7f	2.28	0.10	2.02	0.02	0.07	0.01	0.02	0.00	0.91
	1_2	7f	1.73	0.16	2.54	0.04	0.10	0.02	0.01	0.00	0.98
	2_1a	7f	0.31	0.02	2.92	0.04	0.27	0.03	0.01	0.00	0.97
	2_1b	7f	0.47	0.02	2.88	0.07	0.28	0.03	0.01	0.00	0.99
				0.39		2.90		0.28		0.01	
Nakhlites											
NWA 998	1_1	7f	3.06	0.14	1.74	0.02	0.07	0.01	0.00	0.00	0.95
	2_1a	7f	3.05	0.13	1.84	0.02	0.07	0.01	0.00	0.00	0.97
	3_1	7f	3.11	0.11	1.71	0.02	0.11	0.01	0.01	0.00	0.97
Chassignites											
NWA 2737	1_1	NS	2.46	0.11	2.31	0.18	0.15	0.06	0.00	0.01	1.06
	1_3	NS	1.95	0.11	2.40	0.19	0.12	0.06	0.00	0.01	0.99
	2_1a	NS	2.27	0.11	2.43	0.19	0.16	0.06	0.00	0.01	1.06
	2_1b	NS	2.28	0.11	2.44	0.19	0.16	0.61	0.00	0.01	1.07
				2.27		2.43		0.16		0.00	

olivines, so we suspect these high average values and large range reflects variable contamination (possibly during martian weathering, terrestrial weathering and/or sample preparation and storage). The analysis of the olivine grain in the thin section of NWA 6710

Table 2.2 All olivine measurements from this study.

Meteorite	Olivine Medium	H <sub>2</sub> O (ppm)	2 $\sigma$
<b>Basaltic Shergottite</b>			
<b>JaH 479</b>	2_1 indium	1630	830
	4_1 indium	2320	1690
	5_1 indium	1540	650
<b>Olivine-Phyric Shergottites</b>			
<b>Dho 019</b>	1_1 thin section	2070	450
	2_1 thin section	2830	600
<b>NWA 6710</b>	1_1 thin section	5800	910
	1_1 indium	1730	710
	1_2 indium	1050	340
	2_1 indium	1630	710
	3_1 indium	740	690
	4_1 indium	980	340
	5_1 indium	1330	610
<b>Lherzolithic Shergottite</b>			
<b>NWA 1950</b>	1_1 indium	520	180
	1_2 indium	400	130
	3_1 indium	900	360
	4_1 indium	50	50
	5_1 indium	320	100
	6_1 indium	1140	400

gave an apparent H<sub>2</sub>O abundance of 5800 ppm—an extraordinarily high value that almost certainly reflects the high degree of H contamination. The contrast between this result and results for SNC olivines mounted in indium suggests that most of the contamination present in nominally anhydrous minerals in thin sections was introduced during the thin section preparation process (not surprising,

given the use of epoxy in sample mounting for thin sectioning). Similarly, the olivine grains in the thin section of Dho 019 give an average apparent water content of  $2450 \pm 540$  ppm, or  $\sim 1360$  ppm higher than the average SNC olivine mounted in indium. We further examined the contamination associated with thin sections by analyzing a thin section mount of olivine from Kilauea Iki drill core (sample 116771-178). Our measurement of this

Figure 2.2 continued.

Sample	Olivine Medium		H <sub>2</sub> O	2σ
			(ppm)	
Terrestrial				
NMNH 116771-178	1_1	thin section	210	100
	1_2	thin section	230	110
	2_1	thin section	290	120
	4_1	thin section	170	90
	5_1	thin section	370	140
San Carlos	1_1	indium	0	60
	1_2	indium	0	60
	1_3	indium	0	60
	2_1	indium	10	60
	2_2	indium	10	70

olivine yielded an average of  $250 \pm 80$  ppm, which is 250 ppm higher than the average of the San Carlos olivine grains (0 ppm) that were mounted in indium. It is noteworthy to mention that olivine in the SNCs has undergone shock

metamorphism, which might increase its vulnerability to H contamination (both on Mars and on Earth, and during thin section preparation). Nevertheless, this experiment makes it clear that thin sections are more vulnerable to H contamination than indium mounted grains. We discuss the implications of this artifact for our measurements of H<sub>2</sub>O (and other volatiles) in apatite in the following sections.

Figures 2.12 and 2.14 illustrate systematic variations in H<sub>2</sub>O abundance of apatite by rock type. Basaltic shergottites and olivine-phyric shergottites have higher H<sub>2</sub>O contents than the lherzolithic shergottites, nakhlite, chassignites, and ALH 84001. Figure 2.14 also supports previous observations (figure 2.11) that SNC apatites typically have more Cl (as well as less F) than terrestrial igneous apatites from mafic and ultramafic rocks.

Sulfur in SNC apatites ranges from zero to 0.21 wt%, which is higher than previous measurements by at least 0.13 wt% (figure 2.15). As with H<sub>2</sub>O, S abundances are lower in

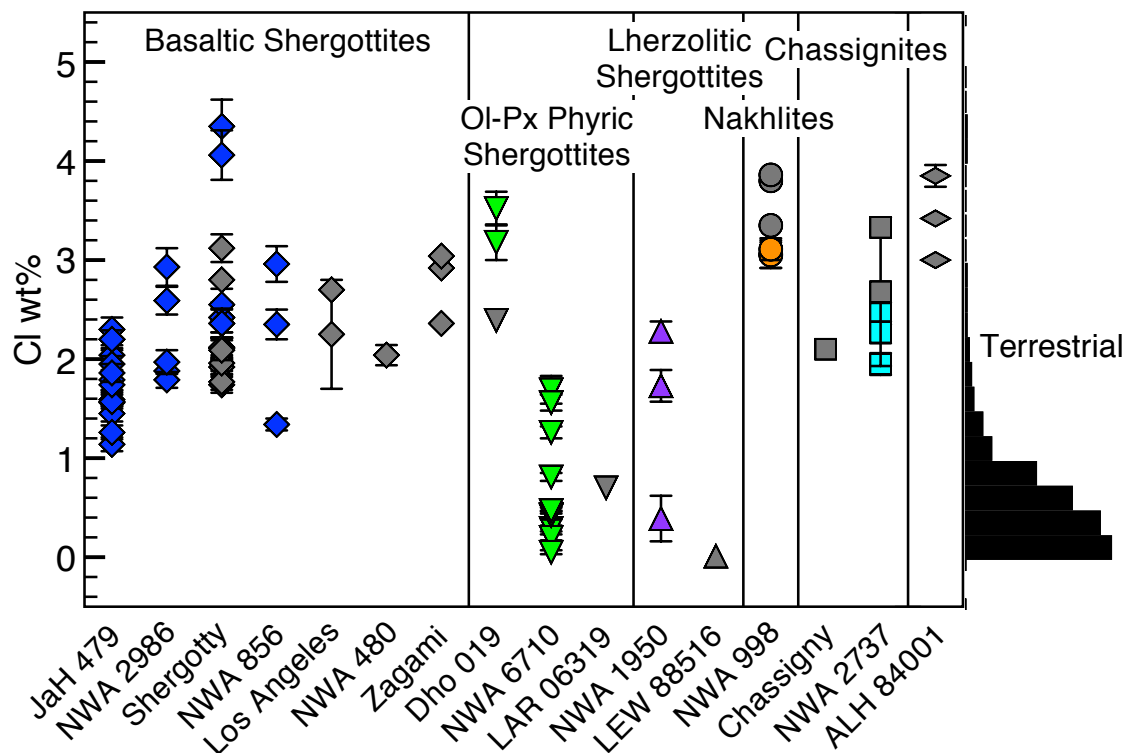


Figure 2.11. Chlorine abundance in apatites from SNCs grouped according to rock type and compared to a histogram of terrestrial apatites from mafic and ultramafic rocks. Symbols in color are measurements from this study; symbols in grey are from previous studies (Jagoutz and Wänke 1986; Harvey et al. 1993; McCoy et al. 1999; Barrat, Gillet et al. 2002; Taylor et al. 2002; Boctor et al 2003; Greenwood et al. 2003; Warrant et al. 2004; Beck et al. 2006; Treiman et al. 2007; Treiman and Irving 2008; Sharp et al. 2011; McCubbin et al. 2012); terrestrial data are from GEOROC.

apatites from the lherzolitic shergottites, nakhlite, and chassignite than in those from the basaltic shergottites, and olivine-phyric shergottites.

## Discussion

### H<sub>2</sub>O Contamination

The ion images of apatites in SNC meteorites suggest the distribution of H within them is relatively homogeneous (figures 2.2 through 2.5, and 2.9). Additionally, we screened all

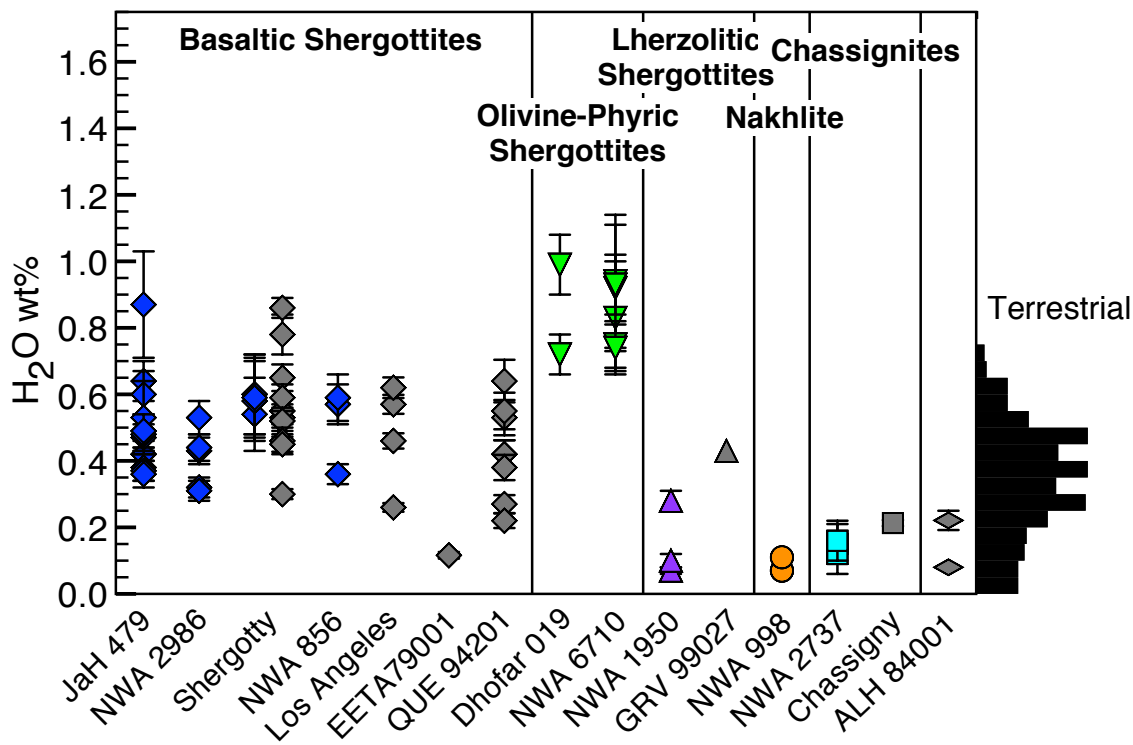


Figure 2.12. H<sub>2</sub>O abundance in SNC apatites grouped according to rock type and compared to a histogram of terrestrial apatites from mafic and ultramafic rocks. Symbols in color are measurements from this study; symbols in grey are from previous studies (Leshin 2000; Boctor et al. 2003; Guan et al. 2003; Greenwood et al. 2008; McCubbin et al. 2012); terrestrial data are from GEOROC.

the analysis sites with secondary ion images of carbon and positioned the sample stage such that the ion beam would not overlap carbon-contaminated cracks during analysis. Additionally, the H<sub>2</sub>O abundances we obtained for samples that have been previously measured in other laboratories are nearly identical (figure 2.12). And, we rejected all analyses where measurements of Cl, F, and OH summed to greater than 1.10 per formula unit. These precautions were all taken to increase our confidence that our H<sub>2</sub>O measurements of the apatites reflect those of the apatite itself rather than surface or crack contaminants. However, these precautions were unsuccessful in many of the SNC olivines, indicating that H contamination occurs in these samples and could be present in the SNC

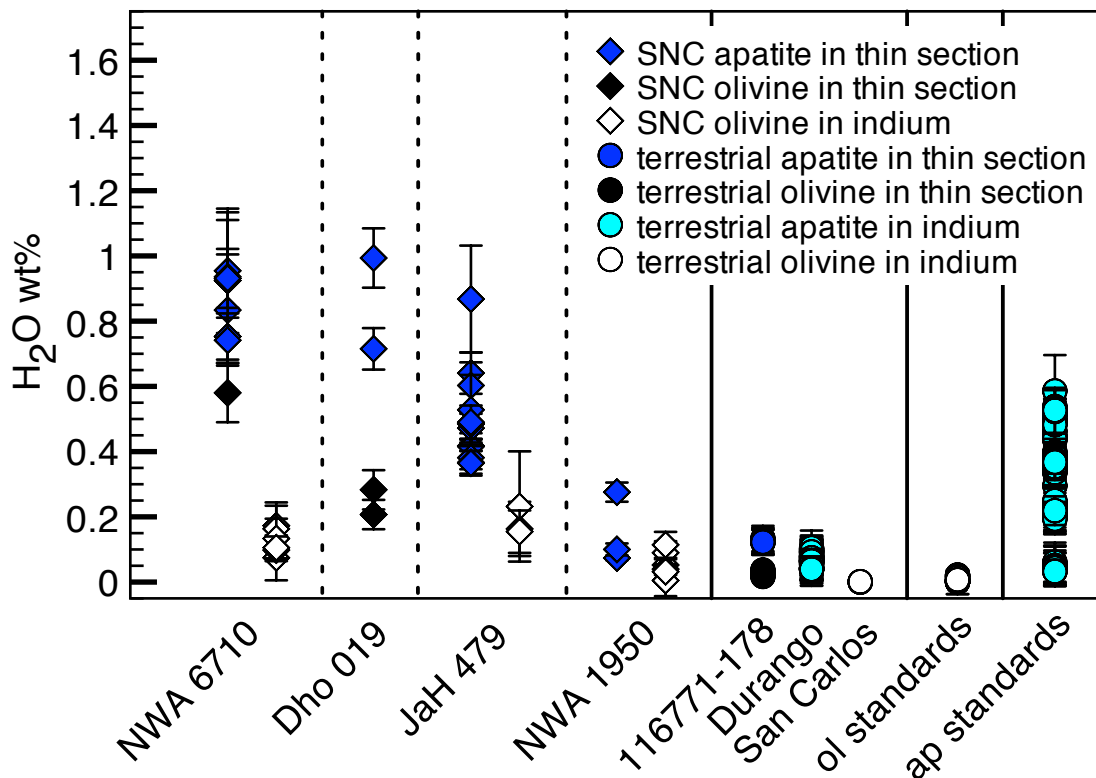


Figure 2.13. Measurements of apatites and olivines from both thin sections and indium mounts from this study, including standards.

apatites. Some of this contamination may simply be increased instrumental background levels of OH from thin section degassing compared to indium mounts. It is not clear why this contribution would be higher in the SNC thin sections than in the terrestrial thin section, but this clearly could be the case. We know most about H contamination in SNC sample NWA 6710, in which olivine was analyzed both in thin section and mounted in indium and the H contamination is unusually high (table 2.2 and figure 2.13). There is no obvious artifact in the measurements of olivine in the thin section of NWA 6710 that would lead us to reject the analyses on technical grounds; <sup>18</sup>O counts were steady and similar to other olivines. It is possible that olivine in this sample contains cryptic cracks (either healed, or just below the surface) that provided unusual opportunities for contamination

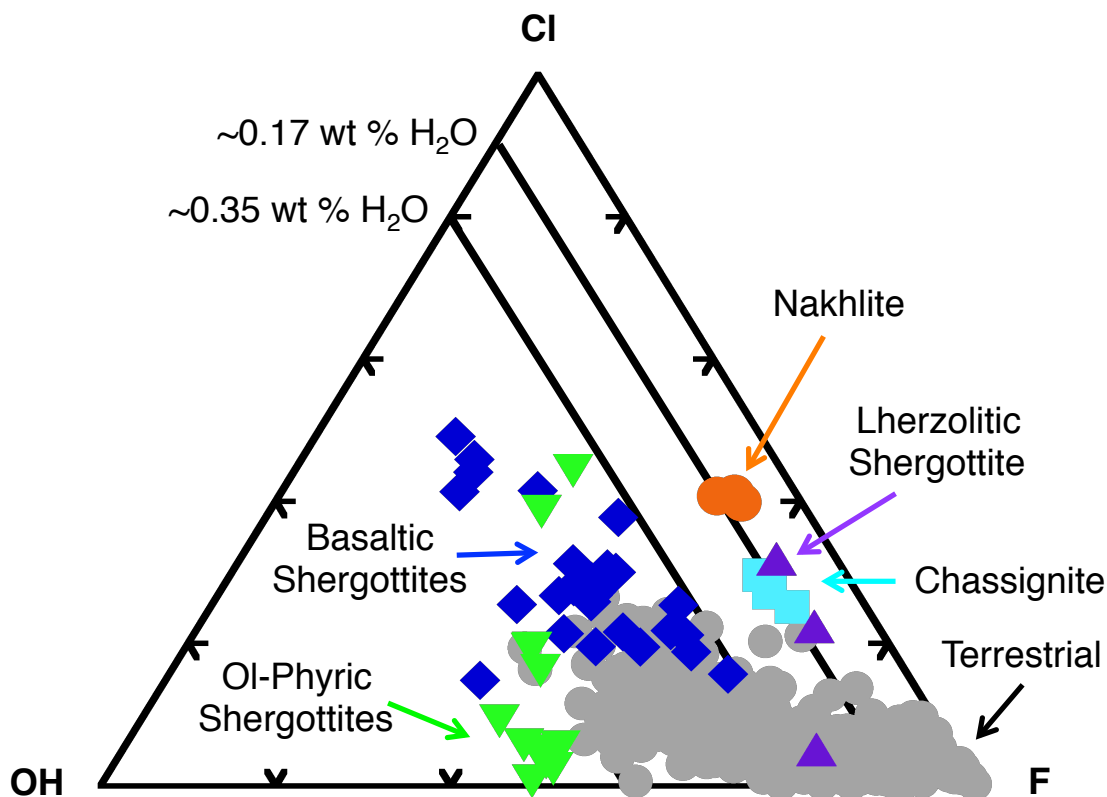


Figure 2.14. Ternary plot showing the occupancy distribution of the halogen site in apatite normalized to  $F + Cl + OH = 1$ . All SNC data are from this study, and all terrestrial data are from GEOROC.

(whether on Mars, Earth or in sample preparation). Future work should attempt to replicate the measurement in the same olivine and several others in the NWA 6710 thin section and perhaps explore the possible sources of this H using D/H ratio measurements (I consider it possible that some component of this H is martian).

Not only is the difference in  $H_2O$  of olivine between thin sections and indium mounts greater for SNCs than for terrestrial rocks, the  $H_2O$  abundance of SNC olivines mounted in indium is also greater than terrestrial olivines mounted in indium. This leads me to suspect that at least some minerals from the SNCs contain H contamination that has nothing to do

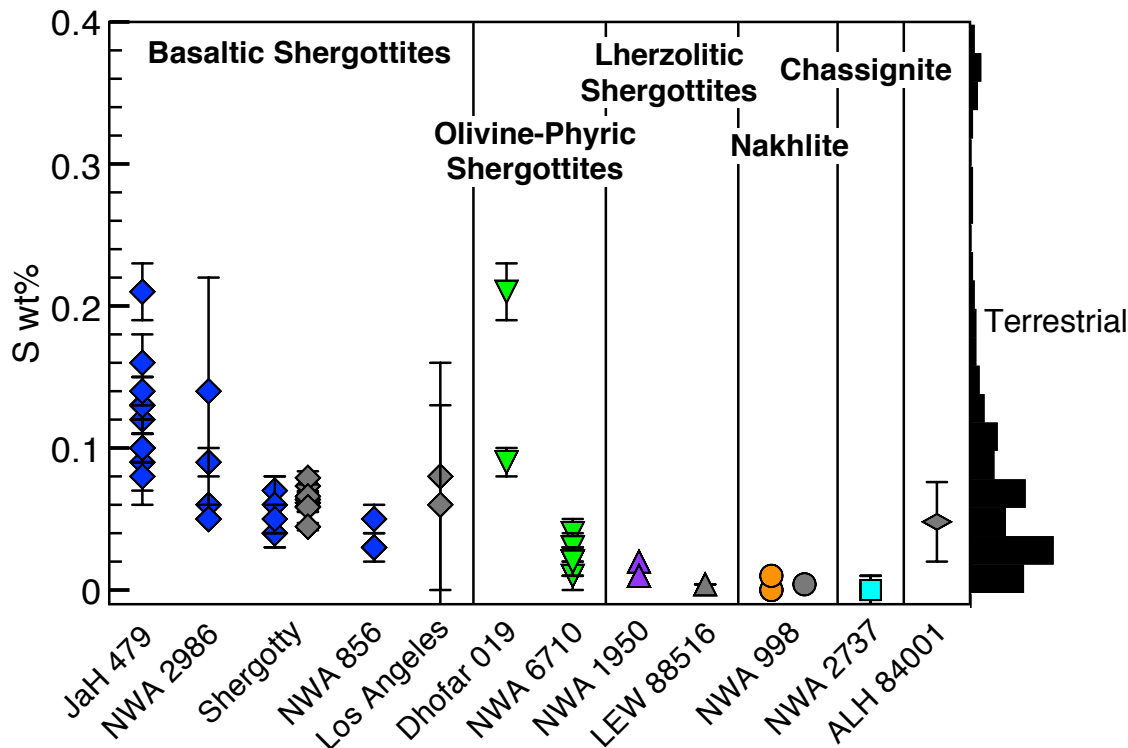


Figure 2.15. Sulfur abundances in SNC apatites grouped according to rock type and compared to a histogram of terrestrial apatites from mafic and ultramafic rocks. Symbols in color are measurements from this study; grey symbols are from previous studies (Harvey et al. 1993; Xirouchakis et al. 2002; Greenwood et al. 2003; Treiman and Irving 2008; McCubbin et al. 2012); terrestrial data are from GEOROC.

with epoxy or thin sectioning, and is either an intrinsic property of these martian minerals or was acquired during their residence on earth. The lherzolithic shergottite NWA 1950 is the only meteorite that I measured that has olivines with hydrogen contents similar to terrestrial olivines, and it also has low water contents in the apatites. This suggests the possibility that the meteorites that have apatites with high water abundance could have high water abundance throughout the rock. One difference between the terrestrial olivine mounts and the SNC mounts that might contribute to this phenomenon is that the terrestrial mounts are of olivine separates, whereas the SNC mounts are polished rock fragments that may contain glasses and/or interstitial phases that may be degassing in the NanoSIMS sample

chamber and adding to the background. SNC olivines in indium are ~1000 ppm higher in H<sub>2</sub>O than the terrestrial olivines, which again, is similar to the uncertainty in SNC apatite H<sub>2</sub>O abundance for the H<sub>2</sub>O-enriched apatites, and thus is not believed to be a major factor in the H measurements of SNC apatites.

One other factor to consider here for the SNC olivine measurements is the accuracy of our calibrations of water contents of olivines. Our terrestrial olivine standards exhibit a smaller range in apparent H<sub>2</sub>O abundance than the SNC olivines we studied. The calibration curve for olivine is relatively steep (i.e., high inferred H<sub>2</sub>O abundance for a given measured OH-ion intensity), and we lack olivine standards having high H<sub>2</sub>O abundances so the extrapolation of the calibration curve to high water contents may involve relatively large errors. Hence, any increase in OH counts due to contamination, outgassing of glasses and/or interstitial phases in the rock fragments, etc., will lead to exaggerated inferred water contents (i.e., much higher than if the same contaminant was encountered when analyzing a phase, like apatite, having a gentler slope to its calibration curve).

A key question for our study is whether contamination that clearly impacted analyses of H in olivine has influenced our measurements of H or other volatiles in apatite. It has not been possible for us to find and analyze apatite in indium mounts, so it is difficult to directly assess the effect of thin section mounting on volatile abundances in apatites. Instead, we must make indirect arguments based on the effects on olivines and the relative volatile abundances and slopes of calibration curves between the two phases (figure 2.16). The most important fact to note is that olivine has a much higher slope to its calibration curve than does apatite (at least in our work), and so a uniform contaminant applied to both

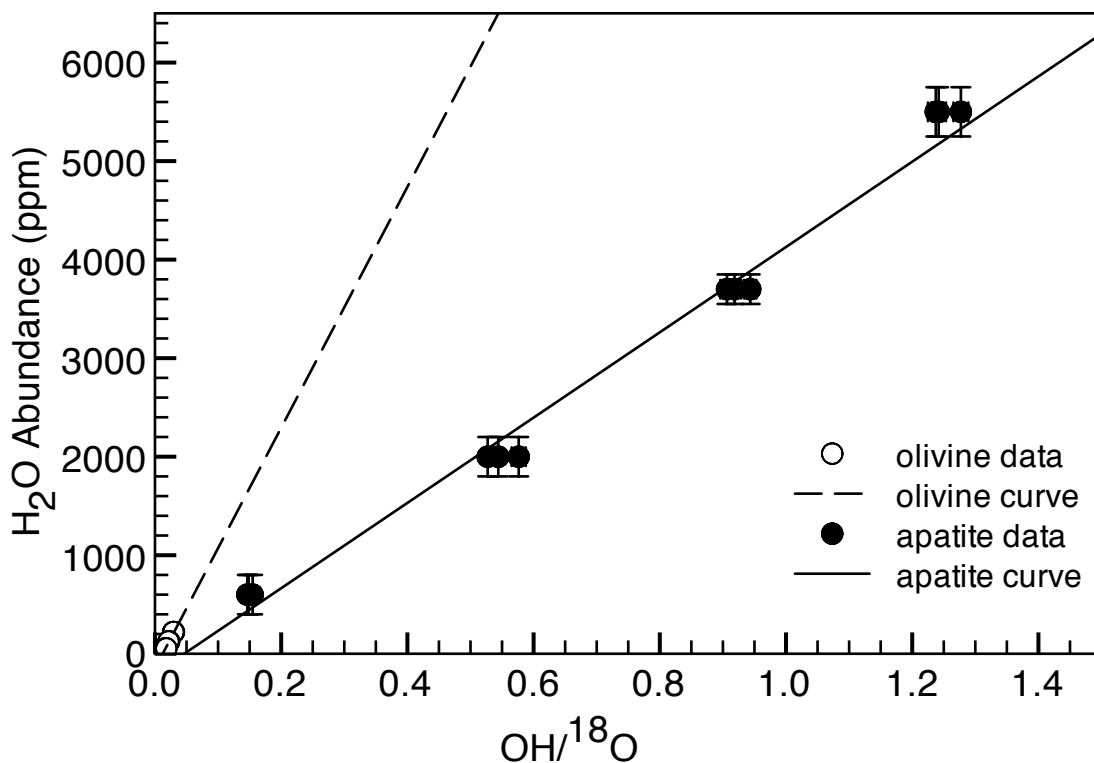


Figure 2.16. Calibration curves for OH in apatite and olivine during one of the NanoSIMS sessions.

phases will lead to thousands of ppm artificial enrichments in olivine but only hundreds of ppm enrichments in apatite. And, because apatite appears to be intrinsically much higher in H<sub>2</sub>O content than olivines, that contamination is added to a larger true amount, leading to a smaller proportional enrichment. For this reason, I did not make any corrections to the H<sub>2</sub>O abundances in SNC apatites reported in table 2.2 to account for the H contamination observed in olivine. Nevertheless, I believe this issue should be reevaluated by finding and mounting SNC apatites in indium in order to analyze them free of at least the one source of contamination we know we can control—thin section contaminants. And, if possible, SNC olivine separates (as opposed to apatite bearing rock fragments) should be mounted in indium in order to discern the contribution of glasses and/or interstitial phases to the

background of the apatite measurements. Finally, future work should measure D/H of SNC apatites and olivines to at least distinguish whether H<sub>2</sub>O is from a terrestrial source, which could indicate contamination from weathering in the terrestrial desert prior to meteorite discovery and collection, or is instead martian.

Finally, we examined whether apparent H<sub>2</sub>O abundances in SNC apatites are correlated with elevations in carbon. Carbon can be a structural constituent of some apatites, but is very low in abundance in mafic igneous rocks. In contrast, carbon is generally very abundant in common contaminants, and so is potentially an indication of contamination (figure 2.17). The Ap003 and Ap004 standards were also plotted for comparison, as they were the two standards that had the highest and lowest H<sub>2</sub>O abundance. Figure 2.17 spans four analytical sessions, one on the 7f and three on the NanoSIMS, and are denoted in the NanoSIMS plot as S1, S2, and S3 at the end of the sample or standard name. Most of the SNC apatites have more carbon than the standards, as well as more variation in carbon than the standards. This could be evidence that the SNC apatites are relatively rich in organic contaminants (not surprising given that they were prepared as epoxy mounted thin sections). Or, it could be an indication that carbonate is substituting for phosphate in the SNCs. The variability of the data yields only ambiguous evidence as to how they should be best interpreted: The highest <sup>16</sup>OH/<sup>18</sup>O measurements are not the highest <sup>12</sup>C/<sup>18</sup>O measurements, suggesting carbon abundances have little to do with H<sub>2</sub>O abundances. There does appear to be a general correlation between carbon and OH in the NanoSIMS plot, but it is not confirmed in the 7f plot and the location of the basaltic shergottites are the same in both plots. These plots seem to neither confirm nor definitively rule out contamination in the SNCs.

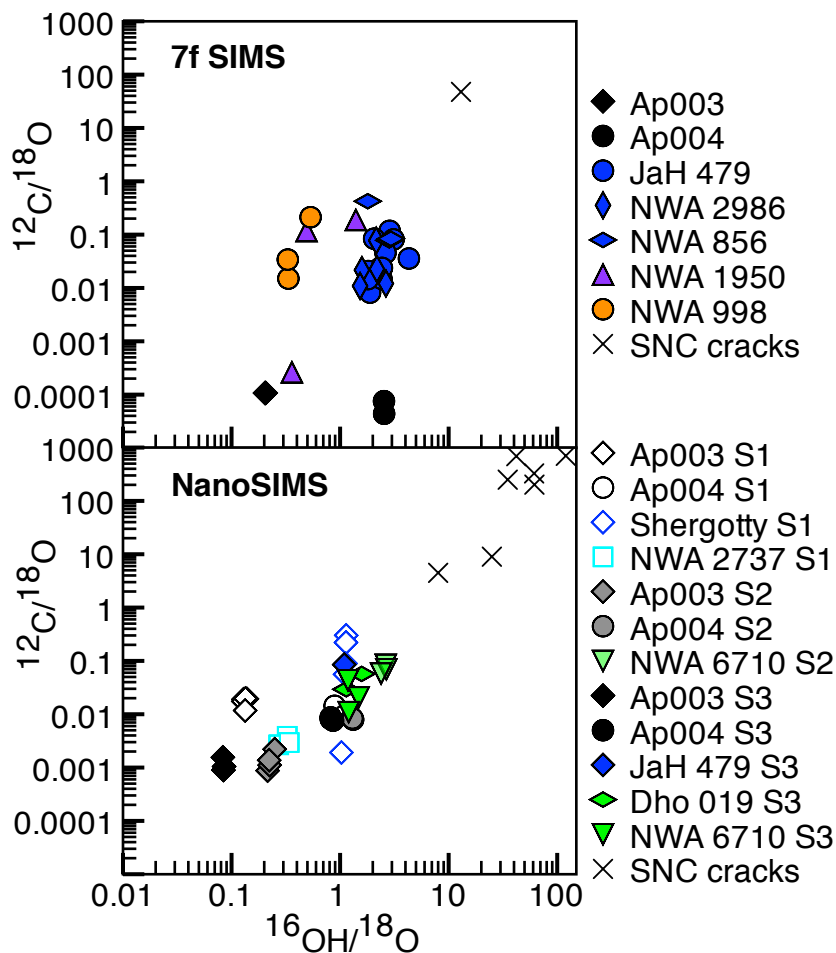


Figure 2.17. SNC apatite measurements from this study compared to cracks in SNC thin sections and the apatite standards with the highest and lowest H<sub>2</sub>O abundances.

As mentioned previously, plans for future work are in place in an effort to assess possible contamination of the SNC apatites. These efforts will be continued until the issue is resolved prior to publication. However, since measurements of the basaltic shergottites are the same as previous studies from different

laboratories, and because stoichiometric closure has been met, I will continue discussing what these results, as they are, might mean.

### H<sub>2</sub>O versus Rock Type

The correlation between rock type and H<sub>2</sub>O abundance observed in this study (figures 2.12 and 2.14) could reflect (1) different water contents in the source magmas of the SNCs, (2) different extents of crystallization prior to apatite formation, or (3) different degassing or

cooling histories. If H<sub>2</sub>O contents of apatites faithfully record the relative H<sub>2</sub>O contents of their source magmas, the similarities between apatites in basaltic and olivine-phyric shergottites and terrestrial basalts could signify similar water contents in the sources of basalts on these two planets. However, this is complicated because, aside from the petrographic difference that divides shergottites, there also exists a geochemical ordering of shergottites into depleted, enriched, and intermediate shergottites based on rare earth element patterns, and Rb/Sr and Sm/Nd systematics. The petrographic groups (i.e., the different water abundances) do not align with the geochemical groups. For example, there exist both enriched and depleted basaltic shergottites. Therefore, it would have to be a coincidence that all the basaltic shergottite sources have the same water contents even though they have different incompatible element contents.

Again, the extent of crystallization prior to apatite formation depends on source composition, therefore scenario (2) has a problem similar to scenario (1). The phosphorus content of magmas generally dictates when apatite will crystallize within the cooling sequence of a particular magma body. This would predict an inverse correlation between bulk rock phosphorus content and apatite H<sub>2</sub>O content; however, bulk rock phosphorus in basaltic and olivine phyric shergottites is either higher than or similar to that in cumulate rock types.

Scenario (3) is most compelling because the correlation between rock type and H<sub>2</sub>O abundance in apatite also coincides with the low-H<sub>2</sub>O apatites prevailing in rock types that are cumulates. Lherzolic shergottites, nakhlites, chassignites, and ALH 84001 are all considered to be cumulate rocks that are missing major mineral components typically

found in basalts (Reid and Bunch 1975; Floran et al. 1978; Lundberg et al. 1990; Harvey et al. 1993; McSween 1994; Mittlefehldt 1994; Nyquist et al. 2001; Bridges and Warren 2006). Lherzolites are made of early accumulation minerals from primary basaltic magmas formed in large, shallow, subsurface reservoirs or large lava lakes (Harvey et al. 1993; Ikeda 1994; McSween 1994). Nakhilites and chassignites are believed to have formed by accumulation of layers of clinopyroxene and olivine (respectively) in thick lava flows or lava lakes, or shallow subsurface sills (McSween 1994; McSween and Treiman 1998; Friedman Lentz et al. 1999; Treiman 2005), and ALH 84001 is considered to be accumulated orthopyroxene from a subsurface magma reservoir (Mittlefehldt 1994; Treiman 1998).

On the other hand, olivine-phyric and basaltic shergottites are basalts that contain additional cumulus crystals rather than only consisting of accumulated early mineral phases. Olivine-phyric shergottites contain megacrysts of either xenocrystic or phenocrystic cumulus olivine (McSween and Jarosewich 1983; Mittlefehldt et al. 1999; Zipfel et al. 2000; Wadhwa et al. 2001; Barrat, Jambon et al. 2002; Herd, Schwandt et al. 2002; Goodrich 2003; Shearer et al. 2008; Basu Sarbadhikari et al. 2009; Usui et al. 2009), while most basaltic shergottites contain cumulus pyroxene (e.g., McSween 1994 and references therein). Basaltic shergottite QUE 94201 may be the only martian meteorite to represent a primary liquid composition (McSween et al. 1996). Basaltic and ol-phyric shergottites are thought to have formed either entirely extrusively or intrusively, or have a two-stage history of early crystallization in large magma chambers followed by quicker cooling in dikes and sills or lava flows that entrain the earlier formed crystals.

The correlation between rock type and H<sub>2</sub>O abundance in apatite could be due to the different formation histories in the slower-cooling cumulate rocks compared to the phyric and aphyric basaltic rocks. Perhaps the slow cooling of deeper cumulate rocks has allowed redistribution of H<sub>2</sub>O away from interstitial regions where apatite later formed. This does not; however, explain why apatites from olivine-phyric shergottites are higher in H<sub>2</sub>O than apatites from basaltic shergottites. Yet, it is interesting to note that all of the apatite data for the olivine-phyric shergottites show stoichiometries where Cl+F+OH are either nearly one, or higher than one (table 2.2). It is not a rule that all apatites from this study that have high H<sub>2</sub>O contents have stoichiometries close to one, or that all apatites that have stoichiometries close to one also have high H<sub>2</sub>O contents. However, it is true that all olivine-phyric shergottite apatite measurements have high H<sub>2</sub>O abundances and have stoichiometries that are 0.99 or greater. If future work to determine exact contributions to the OH background by either thin sections or interstitial phases can reconcile the difference in H<sub>2</sub>O abundance of apatites between basaltic and olivine-phyric shergottites, this scenario may be plausible for explaining the systematic correlation of rock type and apatite H<sub>2</sub>O abundance.

No matter which scenario is favored, the addition of data from this study to existing data clearly shows that H<sub>2</sub>O contents of SNC apatites span a remarkably similar range to apatites from terrestrial mafic and ultramafic rocks (figures 2.12 and 2.18). This may indicate that H<sub>2</sub>O contents in martian magmas are more similar to terrestrial magmas than previously thought.

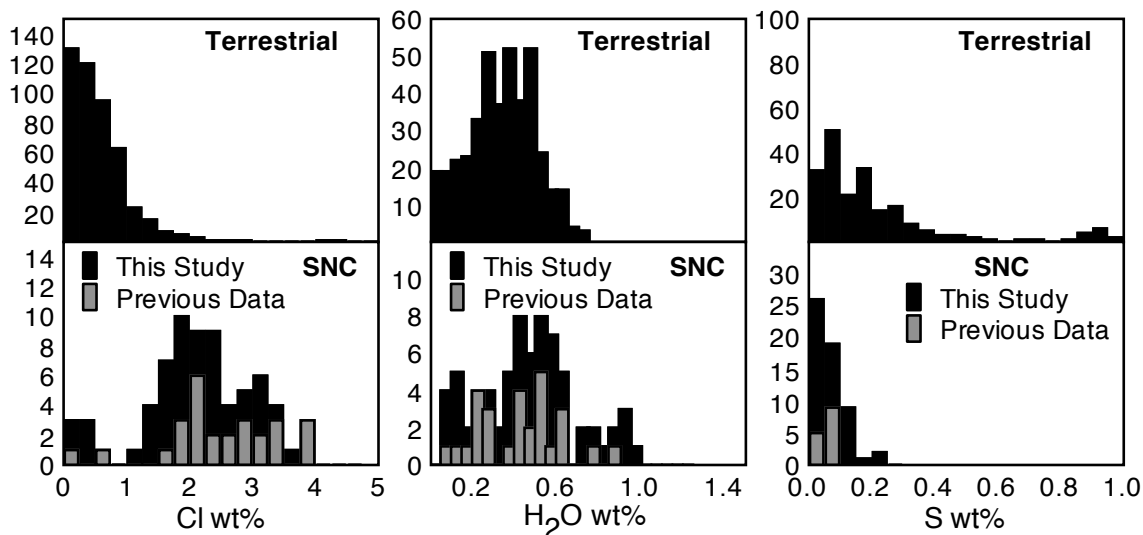


Figure 2.18. SNC apatite data from this study added to previous SNC apatite data, and compared to terrestrial apatite data.

### Sulfur

Because S appears to penetrate microcracks in SNC grains that other volatiles do not penetrate, and we cannot use stoichiometry as an additional constraint for the validity of S measurements, caution has been used in the interpretation of the S data. However, figure 2.19 shows that most of the microcracks are visible in the back-scattered electron images, and therefore would have been avoided for point analyses. The exception to this is the meteorite Dho 019, which is highly weathered from both terrestrial and martian alteration processes. Aside from Dho 019, I will still make efforts to interpret the S data as a constraint on the S contents of martian magmatic rocks.

The major observation in the S data is that there is very low abundance in the apatites from lherzolites, the nakhlite, and the chassignite, and variable abundance in the apatites from basaltic shergottites, olivine-phyric shergottites, and ALH 84001. All of these apatites have

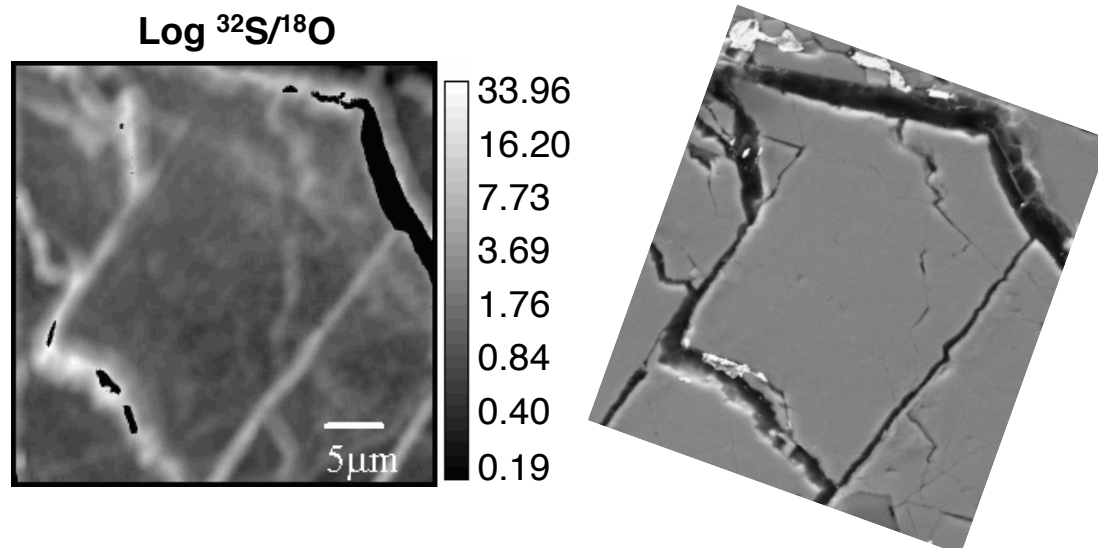


Figure 2.19. NanoSIMS image of JaH 479 apatite 7 on the left compared to a back-scattered electron image of the same grain on the right.

somewhat discrete sulfur abundances that when put together form an array with a similar range to terrestrial apatites from mafic and ultramafic rocks. Aside from ALH 84001, this is consistent with the possibility that the cumulate SNC apatites, which we also found to be low in  $\text{H}_2\text{O}$ , are low in volatiles in general. However, sulfur is more complicated because its incorporation into apatite is partly controlled by oxygen fugacity. The Iherzolithic shergottites are too low in oxygen fugacity (QFM-3.1 to QFM-1.9) to incorporate sulfate (McCanta et al. 2009), which generally happens at  $\sim$ QFM-1 or greater. However, some nakhlites (QFM-2.4 to QFM-0.3), basaltic shergottites (QFM-5 to QFM-0.92), and olivine-phyric shergottites (QFM-4.2 to QFM+0.92) may be high enough in oxygen fugacity to incorporate some sulfate. The oxygen fugacity for chassignites and ALH 84001 is unknown, however it has been estimated that ALH 84001 formed at an oxygen fugacity of either QFM-3.5 or at the QFM buffer. Specifically from this study, Shergotty is between QFM-1.6 and QFM -0.92, depending on the method used to determine oxygen fugacity (Herd et al. 2001; Wadhwa 2001; McCanta et al. 2004), and the rest of the meteorites from

this study have unknown oxygen fugacities, which indicates that they may be high enough to incorporate some sulfate. Perhaps the measurement of S in apatite could be a more sensitive oxygen fugacity barometer for meteorites with oxygen fugacity estimates greater than  $\sim$ QFM-1.0.

Another possible explanation is that, similar to H<sub>2</sub>O content, there could simply be different S abundances in the source magmas, and the array of discrete abundances could signify reservoir mixing between a high-S reservoir and a low-S reservoir. However, as we argued in the case of H<sub>2</sub>O abundances, S abundances are not correlated with other variables commonly used to assign magmatic source compositions to SNCs, such as radiogenic isotopes and rare earth element enrichment.

There is also a possibility that apatite is able to sequester sulfide into the halogen site. If this is true, I imagine it might be possible to use S speciation measurements in estimating oxygen fugacity for these meteorites. This possibility will be discussed in detail in chapter III.

In any case, finding SNC apatites with sulfur abundances of up to 0.2 wt% makes the high sulfur abundance found in martian soils less anomalous than previously believed. Even if most of the sulfur has degassed out of these magmas prior to complete crystallization, the record of high S in some SNC apatites shows that there existed some high-S magmas and that the high-S soils are not just a product of weathering processes that increased the concentration in the soils.

## **Summary/Conclusions**

The prominent findings of this study are the low water contents of apatites from the cumulate rock types (lherzolitic shergottites, the nakhlite, chassignites, and ALH 84001) and the high S abundance in some of the SNCs. Additionally, the ranges in SNC apatite H<sub>2</sub>O contents are similar to the ranges in apatites from terrestrial mafic and ultramafic rocks. This is more clearly illustrated in the abundance histograms that include the measurements from this study as well as all other available data (figure 2.18).

*Chapter III*

## SPECIATION OF SULFUR IN APATITES FROM SNC METEORITES

**Introduction**

Chapter II illustrates that sulfur is abundant (up to 2100 ppm) in some martian apatites. Apatite is thought to incorporate sulfur only as  $S^{6+}$  ions (in the form of sulfate) substituting for  $P^{5+}$  ions (in the form of phosphate) (Pan and Fleet 2002; Parat et al. 2011). Dissolved  $S^{6+}$  only exists in appreciable quantities in magmas where the oxygen fugacity is greater than one log unit below the quartz-fayalite-magnetite (QFM) buffer, below which sulfur is predominantly  $S^{2-}$  (Carroll and Rutherford 1988; Wallace and Carmichael 1994; Jugo et al. 2005; Baker and Moretti 2011). Martian magmas are believed to have oxygen fugacities that range from about one log unit above the QFM buffer to well below the QFM buffer (by five log units) (Herd et al. 2001; Wadhwa 2001; Herd, Borg, et al. 2002; Goodrich et al. 2003; Herd 2003; McCanta et al. 2004; Herd 2006; Karner et al. 2007; McCanta et al. 2009). It is possible that all the martian apatites containing sulfur from chapter II are from the more oxidized magmas on Mars. The oxygen fugacity of Shergotty has been estimated to be between QFM-1.6 and QFM-0.92 depending on the method used (Herd et al. 2001; Wadhwa 2001), therefore the Shergotty magma may have had high enough oxygen fugacity for sulfate to be present at the time of apatite crystallization. However, oxygen fugacity of the magmas from which the other high-S bearing apatites in chapter II crystallized from has not yet been determined and may be lower than QFM-1, as the majority of the magmas that the martian meteorites crystallized from have been estimated

to be. In the same vein, lunar apatites have been shown to contain sulfur (310 – 460 ppm, Boyce et al. 2010), and their magmas are thought to be too reducing to contain oxidized sulfur. Therefore, it is possible that both lunar and martian apatites are incorporating  $S^{2-}$  ions into the halogen site; a substitution mechanism never previously observed in nature. On the other hand, the last gasp of melt from which apatite crystallizes in the mesostasis in lunar and martian rocks could be more oxidizing than the oxygen fugacities calculated from other phenocrysts in the same samples. Or perhaps sulfur is simply present as a contaminant in healed cracks and inclusions.

The oxidation state of sulfur in minerals has been determined by measuring the  $K\alpha$  X-ray wavelength of sulfur, which exhibits a peak shift between  $S^{6+}$  and  $S^{2-}$  (Carroll and Rutherford 1988; Rowe et al. 2007). Our goal is to measure the peak positions of sulfur  $K\alpha$  X-rays in apatites from martian meteorites in order to better understand their high sulfur contents in these SNCs. Additionally, the sulfur wavelengths in martian apatites, relative to  $S^{6+}$  and  $S^{2-}$  standards, may be used to determine the relative proportions of the two species. And finally, I explore whether the relative peak intensities combined with sulfur abundance measurements from chapter II can be used as a calibration curve to determine the sulfur abundance in apatites with unknown sulfur concentration.

## **Materials and Methods**

A total of twenty apatites from six SNC thin sections were analyzed; four of those were basaltic shergottites (JaH 479, NWA 856, NWA 2986, and Shergotty), one was an olivine-phyric shergottite (RBT 04262), and one was a lherzolitic shergottite (NWA 1950). The sulfur  $K\alpha$  X-rays were measured over three separate sessions (martian samples were

measured only in the first and last of these sessions) on the Caltech JEOL 8200 electron microprobe with a 15 kV, 300 nA beam for 2 – 60 seconds/step (shorter count times were for the two standards with high S abundance) for L values (distance from the crystal to the sample that theoretically corresponds to wavelengths between 0.5276 and 0.5464 nm, respectively where  $L = 280\sin\theta \approx 320\lambda$ ) between 169 and 175 with PET diffracting crystals and ~280 mm Rowland circles. The beam was defocused to 15  $\mu\text{m}$ , and sulfur  $\text{K}\alpha$  X-rays were measured using either 3 or 4 PET crystals simultaneously. For session 1, L value step sizes were between 0.01 and 0.03, with shorter step sizes for low-sulfur intensities and larger step sizes for high-sulfur intensities. Step sizes were constant at 0.001 for session 2, and 0.015 for session 3. Unfortunately, we had no independently measured apatites to use for calculating  $\text{S}^{6+}/\text{S}^{2-}$  ratios. Instead, we used anhydrite and pyrite as relative standards for peak positions that we defined to be 100% sulfate and 100% sulfide, respectively and then applied a linear relationship between the two to estimate the percent of sulfide present in apatite samples. A terrestrial apatite crystal from Durango, Mexico was used to test the reproducibility of the relationship between apatite peak positions and the two standard end-member peak positions. The same crystals of Durango apatite and the two end-member standards were used for all the sessions. In order to avoid sulfur generated from sources other than apatite, we made every possible attempt to avoid cracks, grain boundaries, and apatites adjacent to sulfide minerals. Although every effort was made to avoid sources of potential contamination, it is possible that contamination from cryptic sources such as healed cracks or melt inclusions may have affected some or all of these analyses.

## Data Reduction

In order to determine peak positions, the raw spectra were corrected using linear backgrounds and Gaussian curves in the program Igor. Another control used to test the validity of the data was the agreement or disagreement of relative peak positions of samples compared to the standard peak positions (calculated percent sulfide) from spectrometer to spectrometer within a session. We rejected four sample analyses (that can be found in appendix C) that varied widely in percent sulfide between spectrometers.

Corrected peak height intensities were combined with sulfur abundances from chapter II, and stoichiometrically calculated sulfur abundances for anhydrite and pyrite to determine sulfur concentrations of SNC apatites that had not been measured in chapter II. A weighted, least-squares linear regression was calculated to find the best-fit line for the data (Reed 1992) for each spectrometer in each session and averaged to determine the final concentration result per measurement.

## Results

All peak position data and percent sulfide estimates can be found in tables 3.1 through 3.3 (divided by electron probe session). Figure 3.1 (also divided by session) shows the spectra and peak positions of Durango apatite and the two end-member standards, anhydrite and pyrite, for all the spectrometers used during each session. This figure shows that the position of the Durango peak is in a different relative position to anhydrite and pyrite for each session, which changes the estimated percent of sulfide present in Durango by up to 49%. For example, for spectrometer 3 Durango is calculated to have 13% sulfide in session

Table 3.1. Corrected S K $\alpha$  X-ray peak positions and estimated percent sulfide from session 1.

<b>Session 1</b>							
<b>Sample</b>	<b>Peak Position</b>			<b>% Sulfide</b>			
	<b>spec 2</b>	<b>spec 3</b>	<b>spec 5</b>	<b>spec 2</b>	<b>spec 3</b>	<b>spec 5</b>	
<b><u>Standards</u></b>							
<b>anhydrite</b>	172.093	172.007	172.072	0	0	0	
<b>pyrite</b>	172.151	172.068	172.131	100	100	100	
<b>Durango</b>	172.098	172.015	172.080	9	13	14	
<b><u>Basaltic Shergottites</u></b>							
<b>JaH 479</b>	1	172.107	172.031	172.087	24	39	25
	3	172.104	172.018	172.088	19	18	27
	9	172.098	172.018	172.086	9	18	24
	10	172.102	172.018	172.086	16	18	24
<b>NWA 856</b>	2	172.102	172.018	172.098	16	18	44
	4	172.113	172.025	172.084	34	30	20
<b>NWA 2986</b>	1	172.110	172.026	172.073	29	31	2
<b><u>Olivine-Phyric Shergottite</u></b>							
<b>RBT 04262</b>	1	172.102	172.011	172.080	16	7	14
	2	172.103	172.018	172.081	17	18	15

Table 3.2. Corrected S K $\alpha$  X-ray peak positions and estimated percent sulfide from session 2.

<b>Session 2</b>								
<b>Standard</b>	<b>Peak Position</b>				<b>% Sulfide</b>			
	<b>spec 1</b>	<b>spec 2</b>	<b>spec 3</b>	<b>spec 5</b>	<b>spec 1</b>	<b>spec 2</b>	<b>spec 3</b>	<b>spec 5</b>
<b>anhydrite</b>	172.167	172.125	172.028	172.031	0	0	0	0
<b>pyrite</b>	172.223	172.181	172.077	172.105	100	100	100	100
<b>Durango</b>	172.188	172.147	172.052	172.059	37	39	49	38

1 and 62% sulfide in session 3. Figure 3.1 C also shows that anhydrite spectra are not always reproducible in the same session. Figure 3.2 shows that the apatites from basaltic shergottites possibly display a similar shift in estimated percent sulfide from

Table 3.3. Corrected K $\alpha$  X-ray peak positions and estimated percent sulfide from session 3.

<b>Session 3</b>									
<b>Sample</b>	<b>Peak Position</b>				<b>% Sulfide</b>				
	<b>spec 1</b>	<b>spec 2</b>	<b>spec 3</b>	<b>spec 5</b>	<b>spec 1</b>	<b>spec 2</b>	<b>spec 3</b>	<b>spec 5</b>	
<b><u>Standards</u></b>									
<b>anhydrite</b>	172.070	172.000	171.988	171.955					
	172.074	171.980	171.963	171.894					
	172.072	171.990	171.976	171.925	0	0	0	0	
<b>pyrite</b>	172.169	172.074	172.054	171.993					
	172.160	172.066	172.047	171.988					
	172.165	172.070	172.051	171.991	100	100	100	100	
<b>Durango</b>	172.123	172.031	172.017	171.950	55	51	55	39	
	172.120	172.029	172.015	171.950	52	49	53	39	
<b><u>Basaltic Shergottites</u></b>									
<b>JaH 479</b>	3	172.128	172.036	172.016	171.952	61	58	54	42
	8	172.114	172.016	172.001	171.940	45	32	34	23
<b>NWA 856</b>	1	172.105	172.029	172.013	171.943	36	49	50	28
	3	172.089	171.995	171.995	171.927	18	6	26	4
<b>NWA 2986</b>	3	172.109	172.015	171.993	171.926	40	31	23	2
	4	172.100	172.009	171.990	171.924	30	24	19	-1
<b>Shergotty</b>	3	172.116	172.036	172.014	171.938	48	58	51	20
	6	172.122	172.038	172.019	171.945	54	60	58	31
<b><u>Lherzolic Shergottites</u></b>									
<b>NWA 1950</b>	1	172.068	171.995	171.976	171.902	-4	6	1	-34
	2	172.097	172.024	172.018	171.954	27	42	57	45

session 1 to session 3 to that observed for Durango, particularly for JaH 479. Detected peak positions for anhydrite, pyrite, Durango, and JaH 479 apatite 3 (the only SNC apatite grain measured in both session 1 and session 3) are most similar between sessions on spectrometer 3. Therefore, using absolute peak positions from spectrometer 3 rather than percent sulfide relative to anhydrite and pyrite, figure 3.3 shows that there is less of a discrepancy between session 1 and session 3 for the basaltic shergottites and Durango.

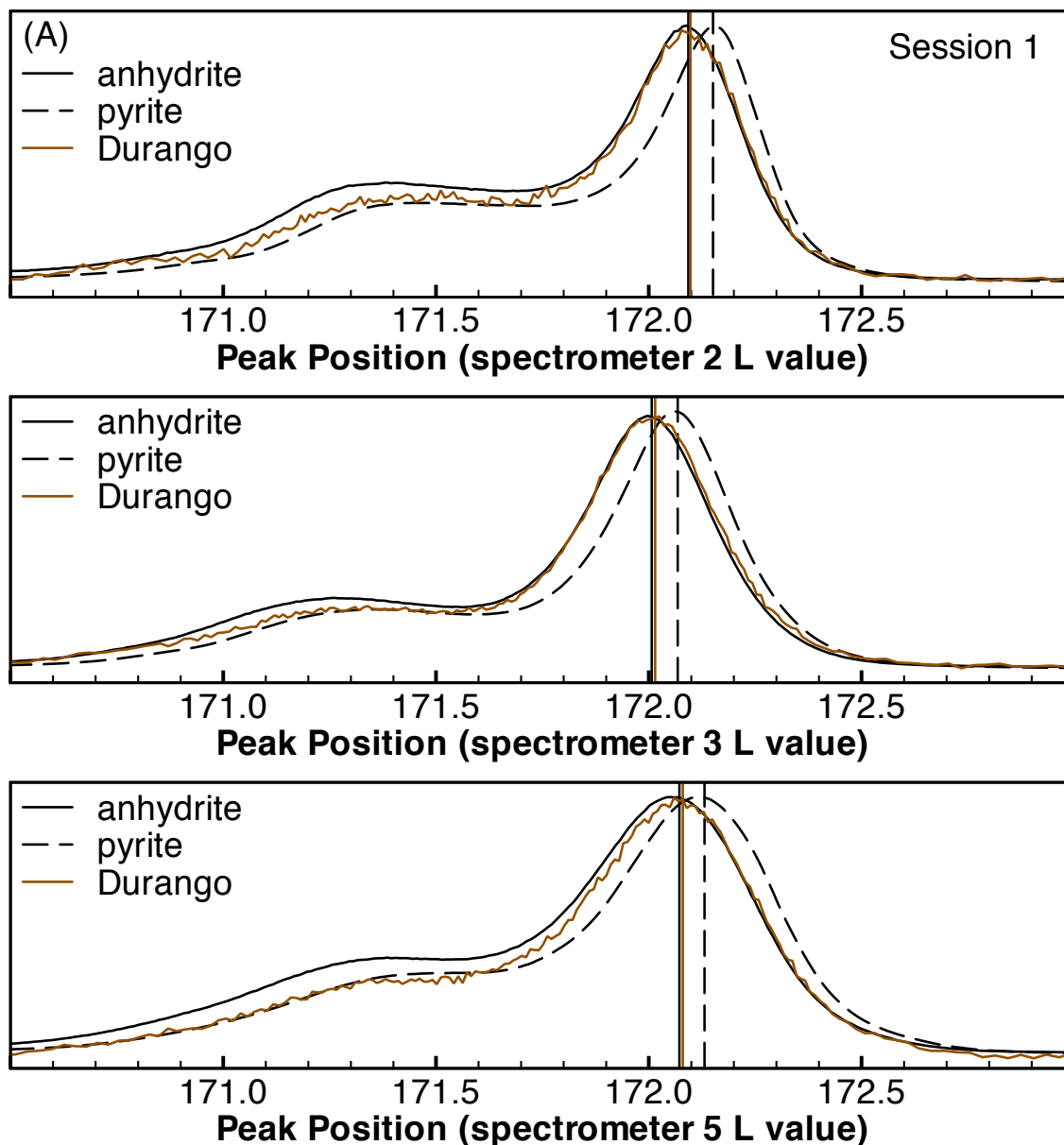


Figure 3.1. Spectra of standards from all spectrometers used during a session. Vertical scale is arbitrary intensity; the scale was changed for each spectrum such that the peak heights would match and peak positions could be more easily compared. (A) session 1, (B) session 2, and (C) session 3.

However, the standards are not reproducible between session 1 and 3, especially not anhydrite. Additionally, peak positions for the standards and Durango in session 2 are different than in the other sessions. Not only are the peak positions different for the same samples from session to session, but the distance between anhydrite and pyrite, and the

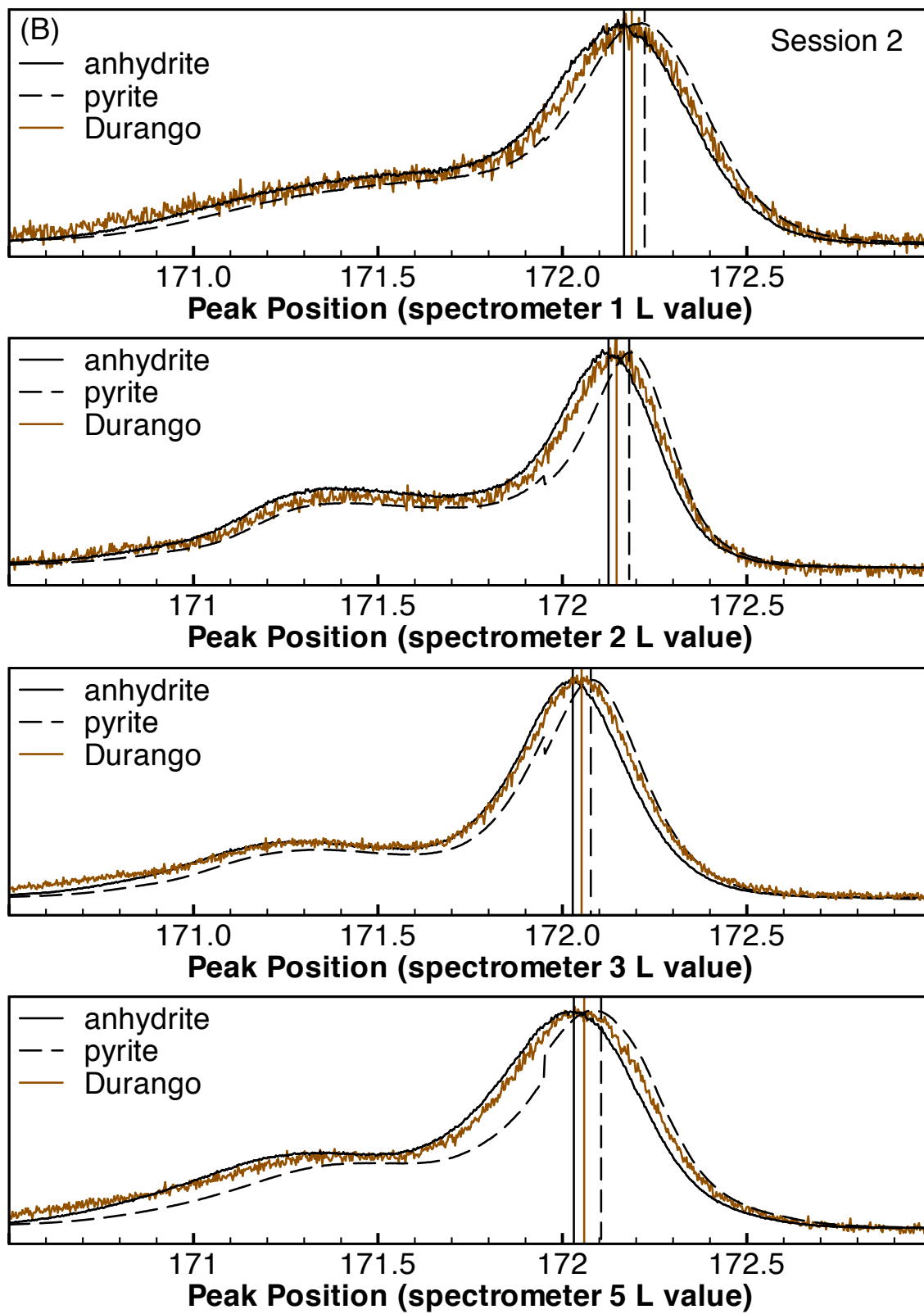


Figure 3.1 continued.

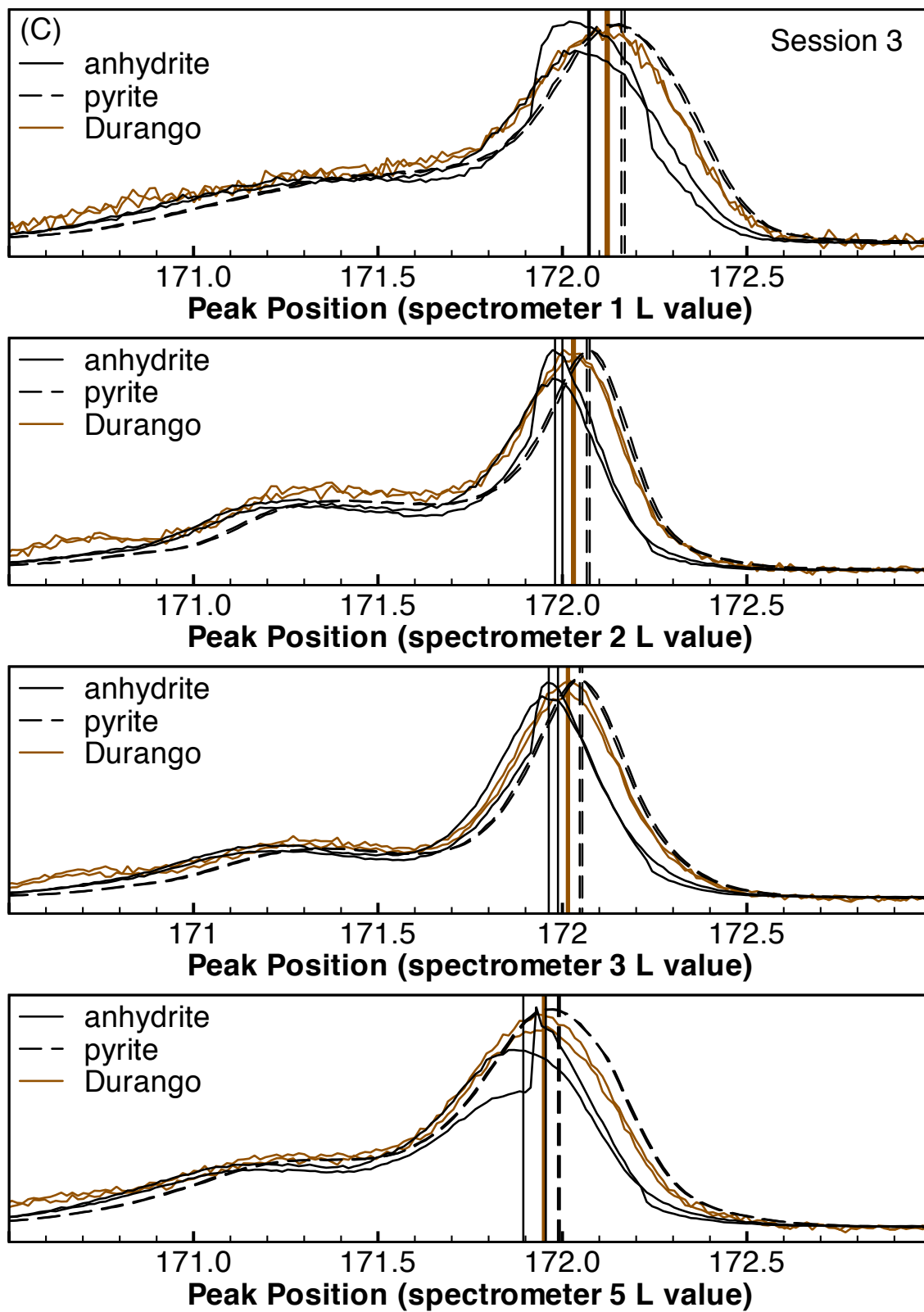


Figure 3.1 continued.

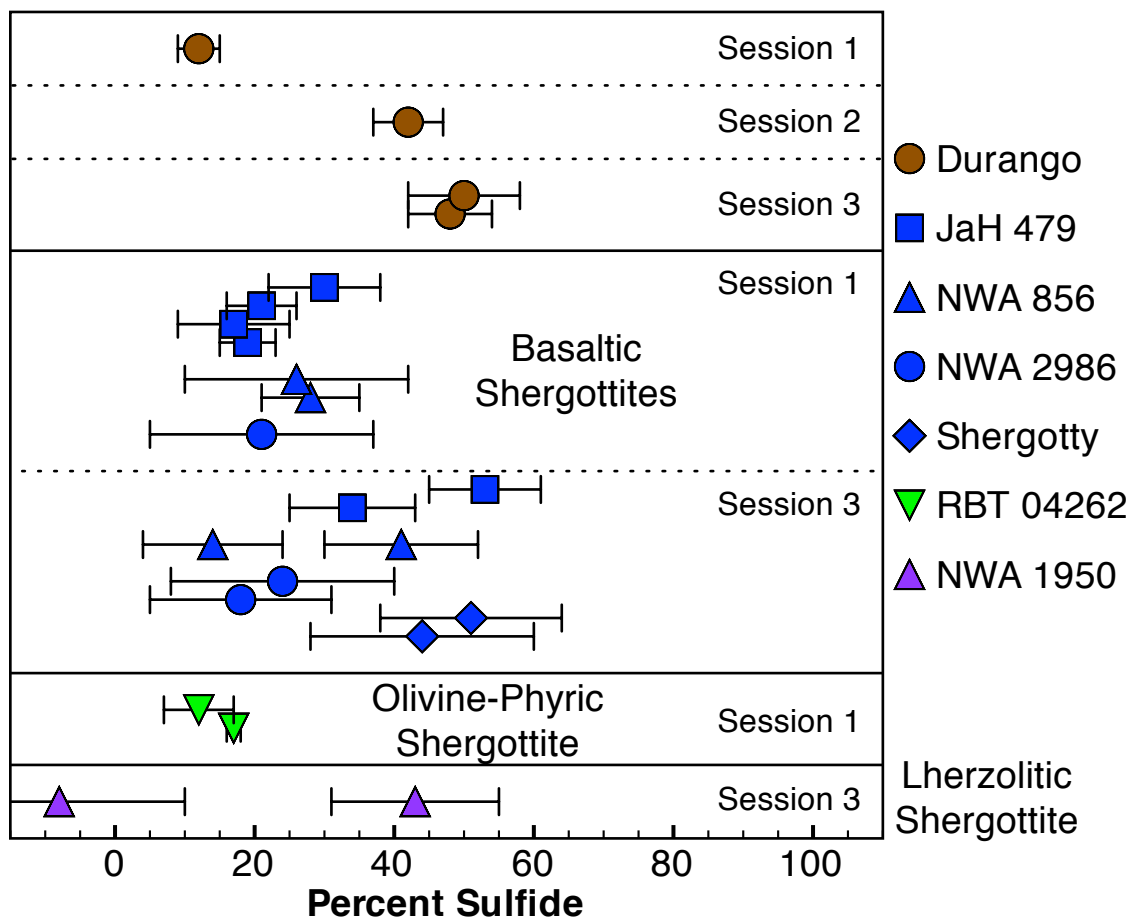


Figure 3.2. Estimated percent sulfide of each Durango and SNC analysis grouped according to sample type and session. Each plotted point represents the average of percent sulfide values calculated for each spectrometer used during an analysis. Error bars are one standard deviation.

relative peak position of Durango between them is different from session to session as well. The one consistency is that all the apatite peak positions fall between the anhydrite and pyrite peak positions within a session (or slightly outside of anhydrite, correlating to less than -10% percent sulfide when the calculated percent sulfide from all spectrometers are averaged).

Because spectrometer 3 yields the most similar peak positions for the apatites between sessions 1 and 3 (the only two sessions where SNC apatites were measured), only spectra

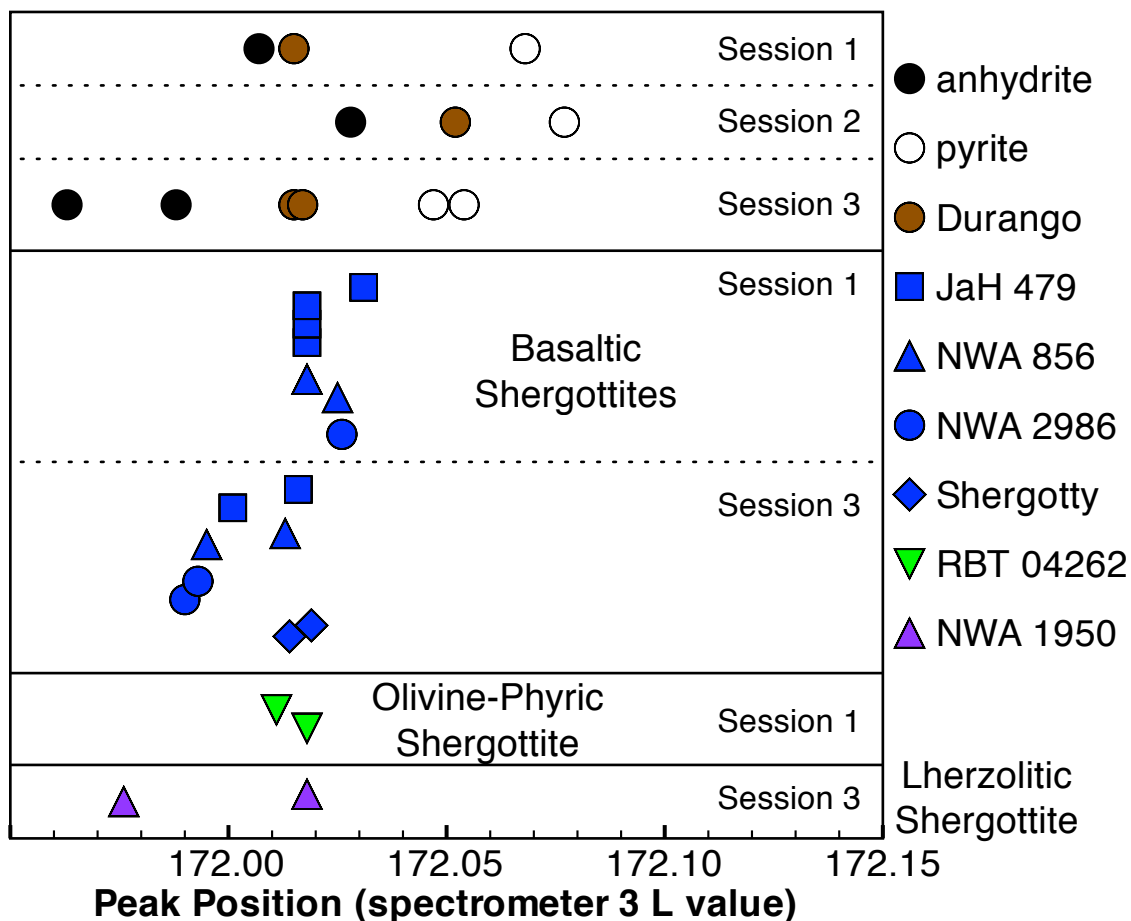


Figure 3.3. Peak positions from spectrometer 3 of all grains analyzed in this study grouped according to sample type and session.

from that spectrometer are used for the figures in the rest of this chapter to make visual comparisons easiest. Figures of spectra from all the other spectrometers besides 3 can be found in appendix C. Figures 3.4 through 3.9 show the spectra and peak positions for the SNC apatites relative to the standard end-members. The vertical scale on all spectra figures is arbitrary; the scale was changed for each spectrum such that the peak height would be the same for all spectra within a figure. This was done after calculating peak positions, and has no bearing on the data presented in tables 3.1 through 3.3. An example of the variation between peak intensity for different samples can be seen in figure 3.10. Background-

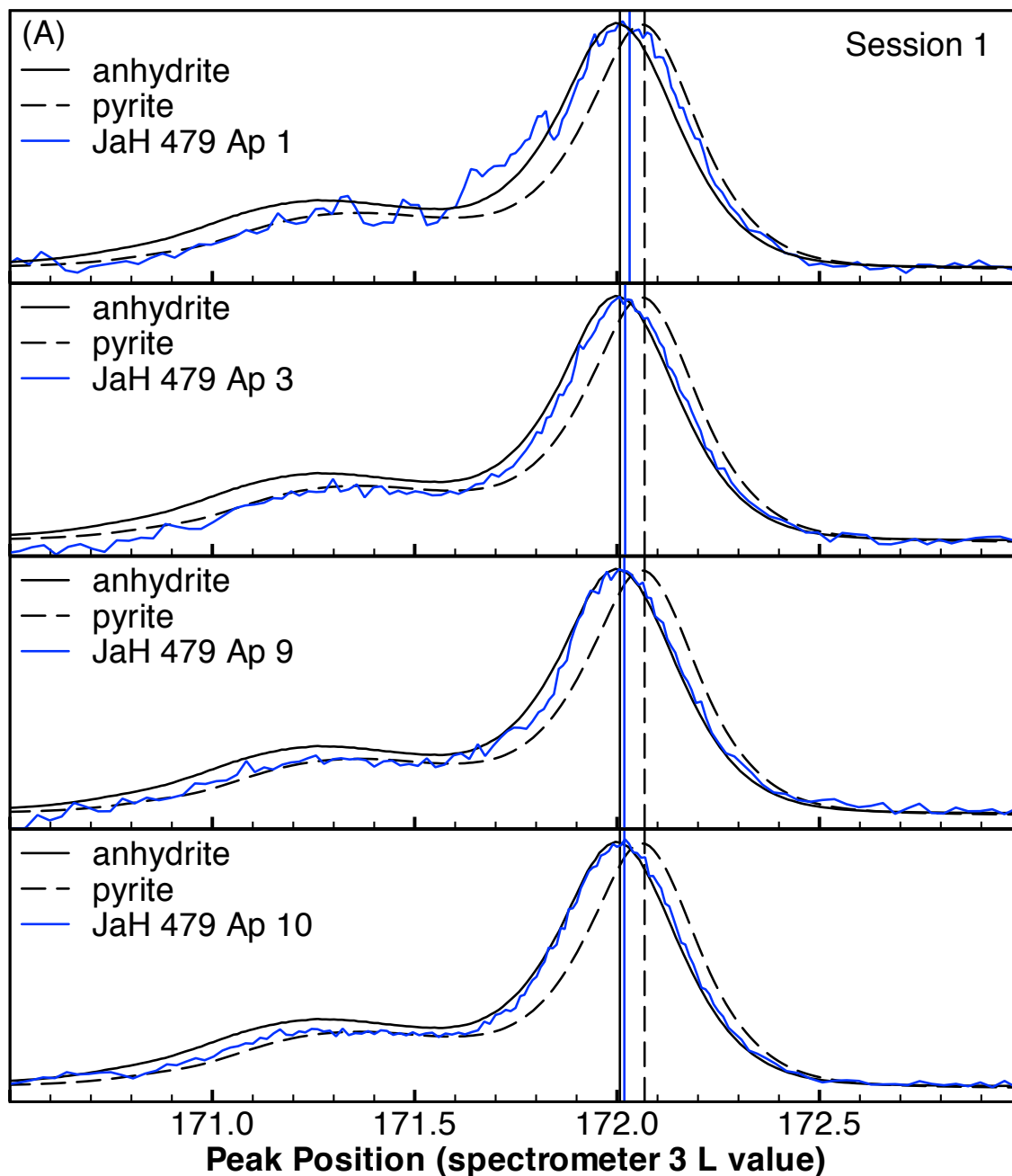


Figure 3.4. Spectrometer 3 spectra of all apatite grains from basaltic shergottite JaH 479 measured during session 1 and session 3. Vertical scale is arbitrary intensity; the scale was changed for each spectrum such that the peak heights would match and peak positions could be more easily compared. (A) session 1, and (B) session 3.

corrected peak intensities and sulfur abundances are listed in table 3.4, and an example of the calibration curve is plotted in figure 3.11 with data from session 1 and spectrometer 3. The rest of the calibration curves can be found in appendix C. The best-fit lines from each

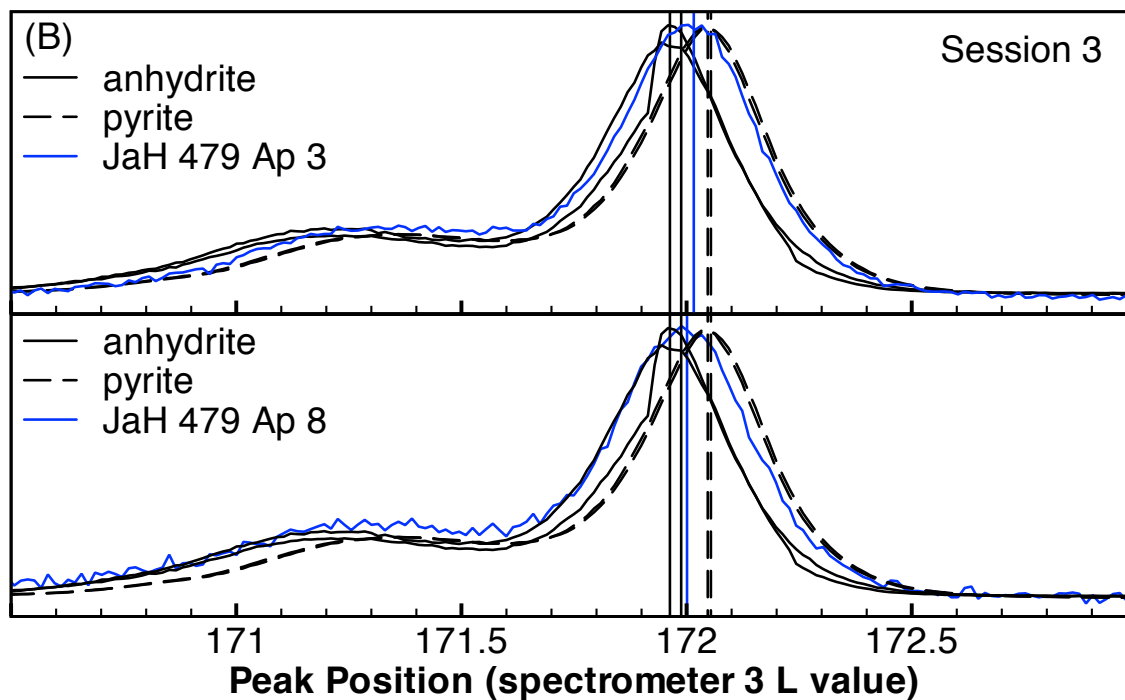


Figure 3.4 continued.

spectrometer were used to calculate independent sulfur concentrations, and those concentrations were averaged to get the final concentration shown in table 3.4. All calculated sulfur concentration data can be found in appendix C. Concentrations were determined for NWA 856 apatites 2 and 4, Shergotty apatite 3, and RBT 04262 apatites 1 and 2. The estimated sulfur concentrations for apatites 2 and 4 in NWA 856 agree well with the ion probe concentration measurements of apatites 1 and 3 for NWA 856 from chapter II. The estimated sulfur abundance for Shergotty apatite 3 agrees well with the ion probe concentration measurements of apatites 5 and 6 from chapter II. The estimated sulfur abundance for RBT 04262 apatites are within the range of apatite sulfur concentrations in all basaltic and olivine-phyric shergottites measured by the ion probe in chapter II.

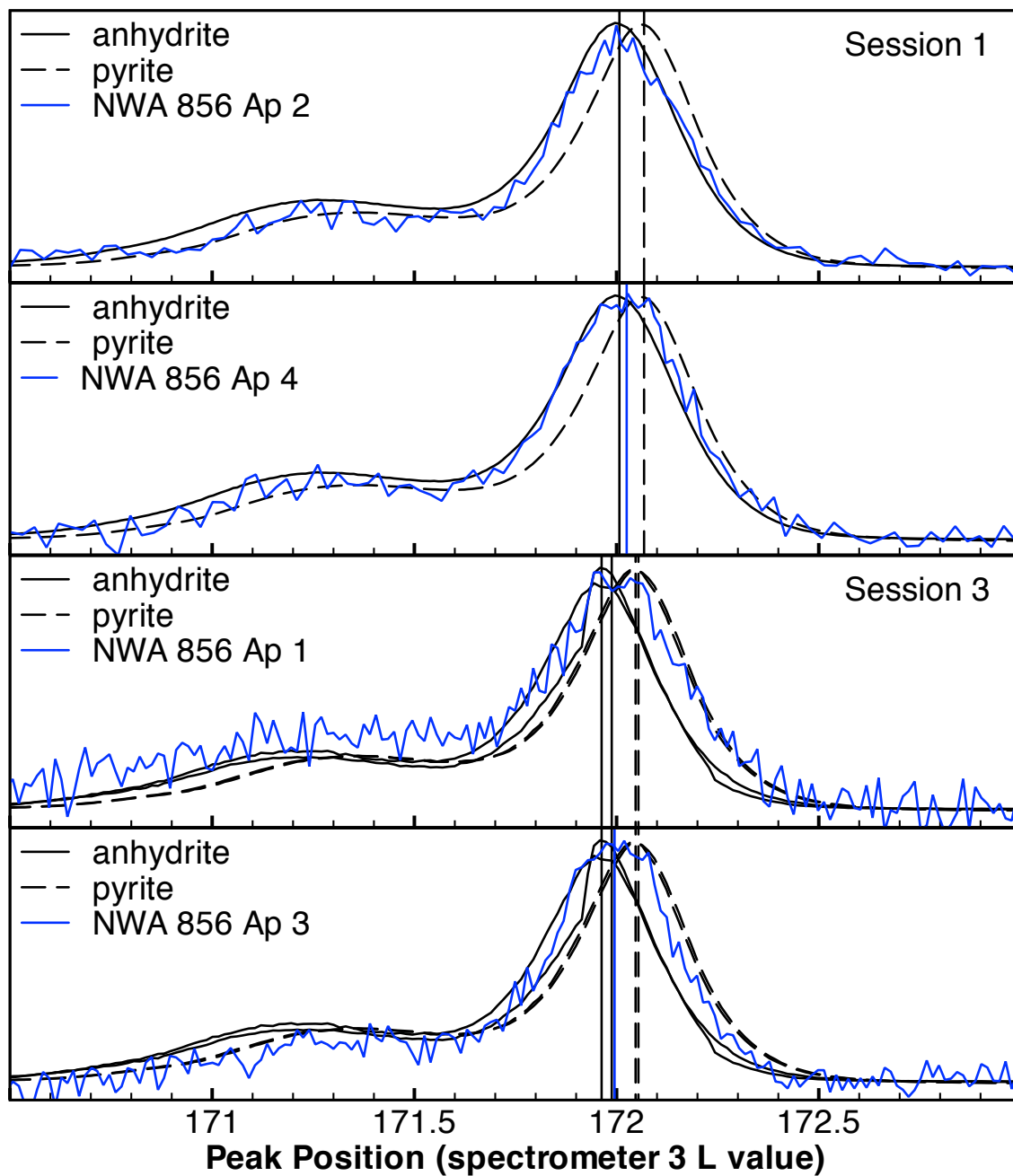


Figure 3.5. Spectrometer 3 spectra of all apatite grains from basaltic shergottite NWA 856 measured during session 1 and session 3. Vertical scale is arbitrary intensity; the scale was changed for each spectrum such that the peak heights would match and peak positions could be more easily compared.

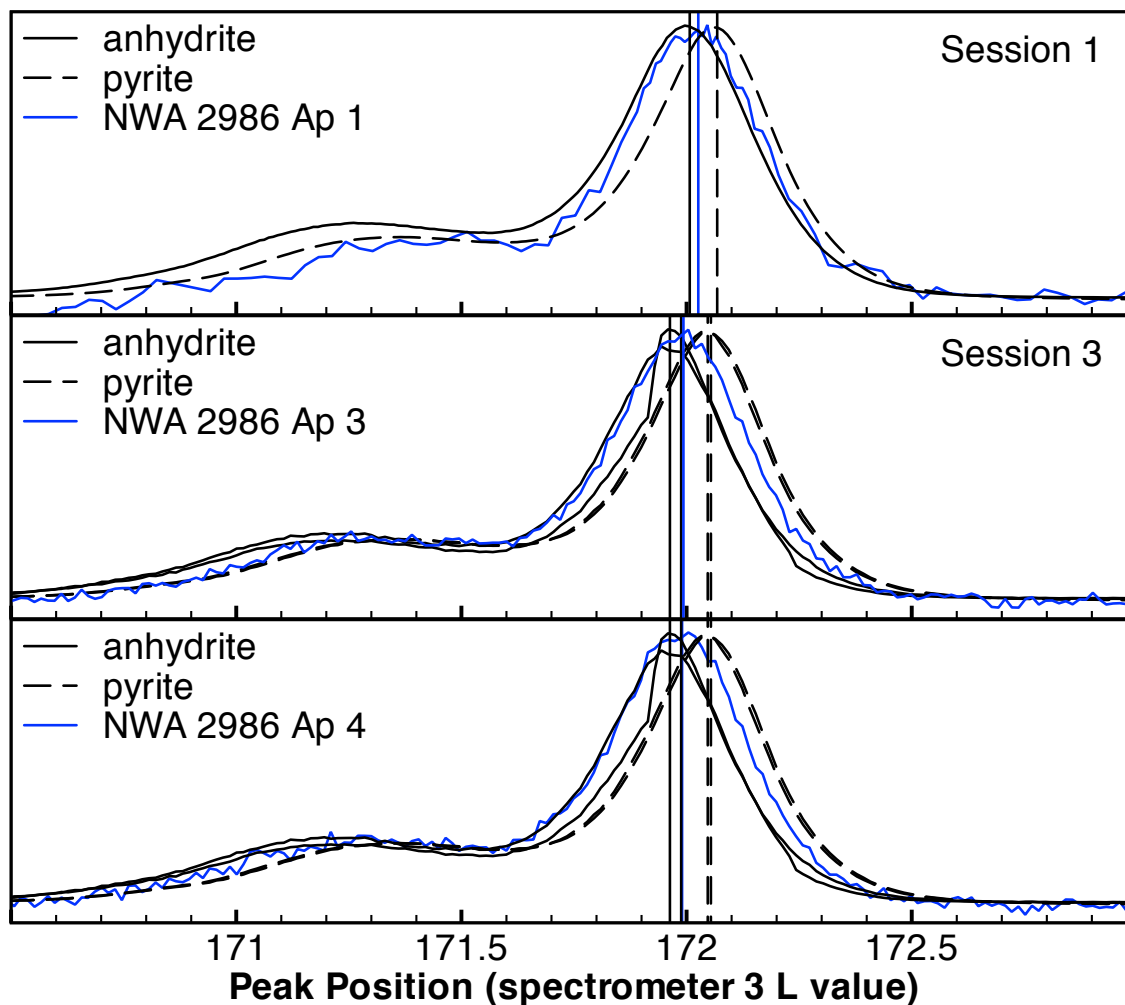


Figure 3.6. Spectrometer 3 spectra of all apatite grains from basaltic shergottite NWA 2986 measured during session 1 and session 3. Vertical scale is arbitrary intensity; the scale was changed for each spectrum such that the peak heights would match and peak positions could be more easily compared.

## Discussion

### Sulfur Speciation

Spectrometer 3 appears to be the most consistent from session to session. However, it appears to only be consistent for apatite, and not for anhydrite or pyrite. The exception to this is Durango apatite in session 2; it also appears to be inconsistent with Durango

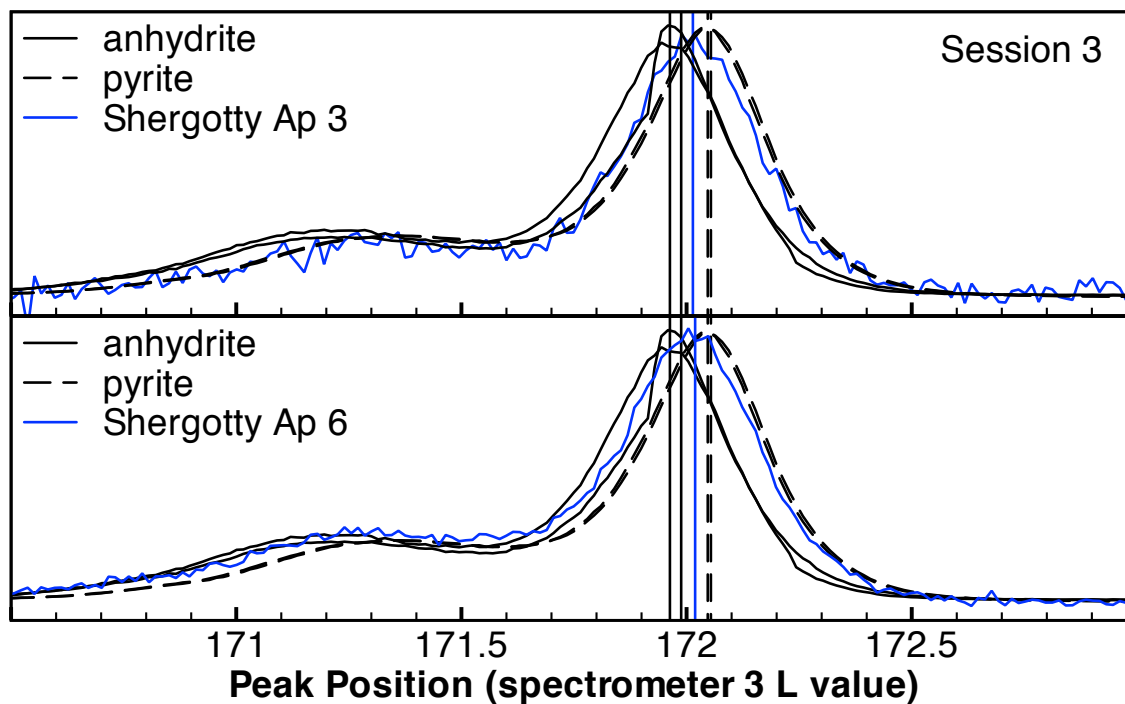


Figure 3.7. Spectrometer 3 spectra of apatite grains from basaltic shergottite Shergotty measured during session 3. Vertical scale is arbitrary intensity; the scale was changed for each spectrum such that the peak heights would match and peak positions could be more easily compared.

measurements from the other sessions. It is not expected that the peak positions between sessions should be consistent, but it is expected that the relative peak positions of Durango within the end member peaks should be consistent, unless the sulfide percent of Durango is heterogeneous within the crystal. Therefore, it is not feasible to calculate sulfide percentages from the data at this time. Anhydrite appears to be the least reproducible from session to session (figure 3.3), which perhaps suggests that the anhydrite standard is heterogeneous and is the leading problem to tackle going forward.

Aside from the irreproducibility of the standards, an encouraging result is that all the basaltic shergottite apatites are similar to each other in peak position. An additional promising result is that all the apatite peak positions (both Durango and the SNCs) reside within the anhydrite and pyrite end-member peaks, which indeed indicates the possibility

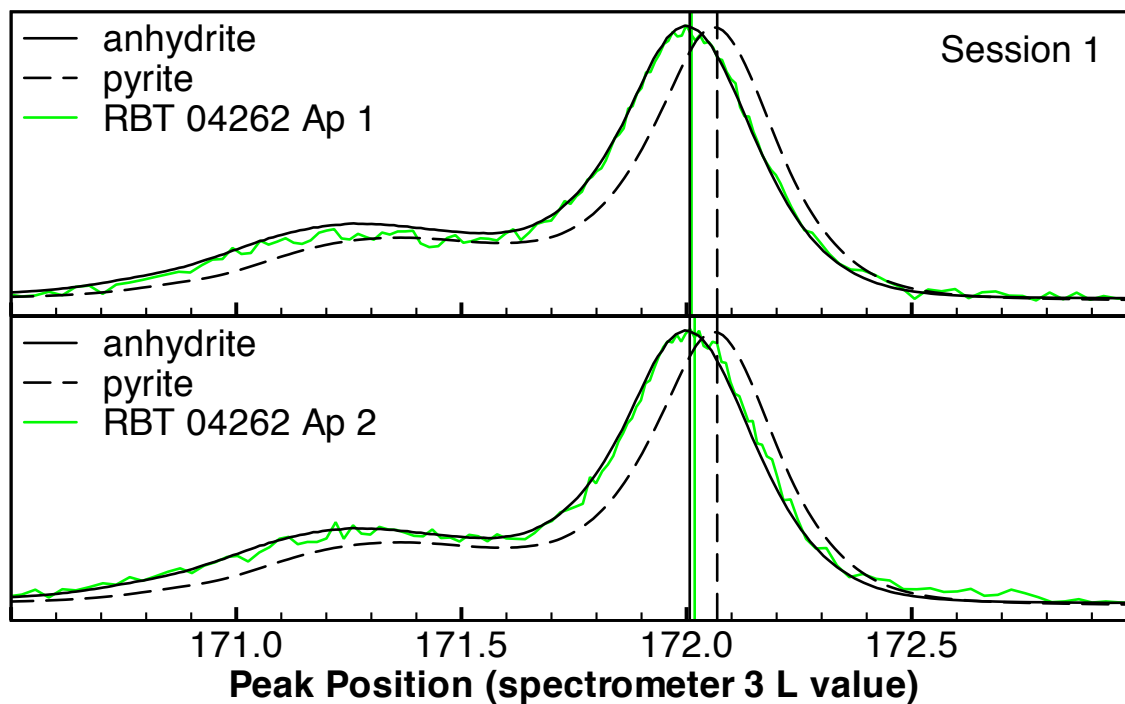


Figure 3.8. Spectrometer 3 spectra of all apatite grains from olivine-phyric shergottite RBT 04262 measured during session 1. Vertical scale is arbitrary intensity; the scale was changed for each spectrum such that the peak heights would match and peak positions could be more easily compared.

that apatites are incorporating both sulfate (mostly likely substituting for phosphate) and sulfide (most likely substituting in the halogen site). However, in order to determine how much of each they are taking up, either the inability to reproduce the standards from session to session needs to be resolved, or different standards should be used. It is also possible that measurement of this sort would be more successful using XANES, however electron probe measurements have been used in the past to determine sulfur speciation (Carroll and Rutherford 1988; Rowe et al. 2007), and if they can be resolved here it would be a more cost-effective and time-efficient way to conduct this research.

One difference in methods between sessions in this study was the L value step size. This seems the least likely cause for different peak calculations, however in order to be rigorous it should be ruled out and it is the easiest next step. Simply setting up another session to use

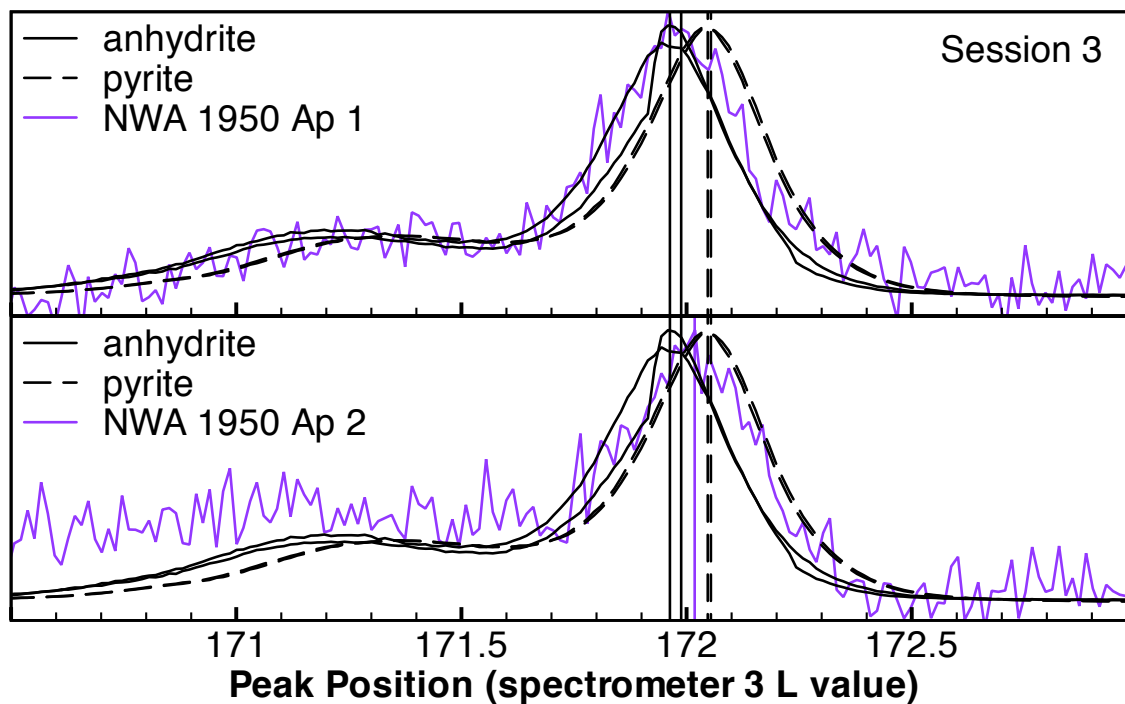


Figure 3.9. Spectrometer 3 spectra of all apatites from lherzolitic shergottite NWA 1950 measured during session 3. Vertical scale is arbitrary intensity; the scale was changed for each spectrum such that the peak heights would match and peak positions could be more easily compared.

the same step size as one of the previous sessions to determine if the anhydrite and pyrite peak positions can be replicated (or at least if the distance between the anhydrite and pyrite peak positions and the relative Durango peak position between them can be reproduced) should clarify if this is the cause for the discrepancy.

In the direction of using new standards, either a synthetic cesanite,  $\text{Na}_6\text{Ca}_4(\text{SO}_4)_6(\text{OH})_2$ , or caracolite,  $\text{Na}_6\text{Pb}_4(\text{SO}_4)_6\text{Cl}_2$  could be an acceptable alternative to anhydrite (Pan and Fleet 2002). Pyrite seems to be more robust than apatite, but a sulfoapatite,  $\text{Ca}_{10}(\text{PO}_4)_6\text{S}$ , has been synthesized in the laboratory (Henning et al. 2000), and if it can be synthesized again or obtained from Henning, may be a good standard to use here instead of pyrite.

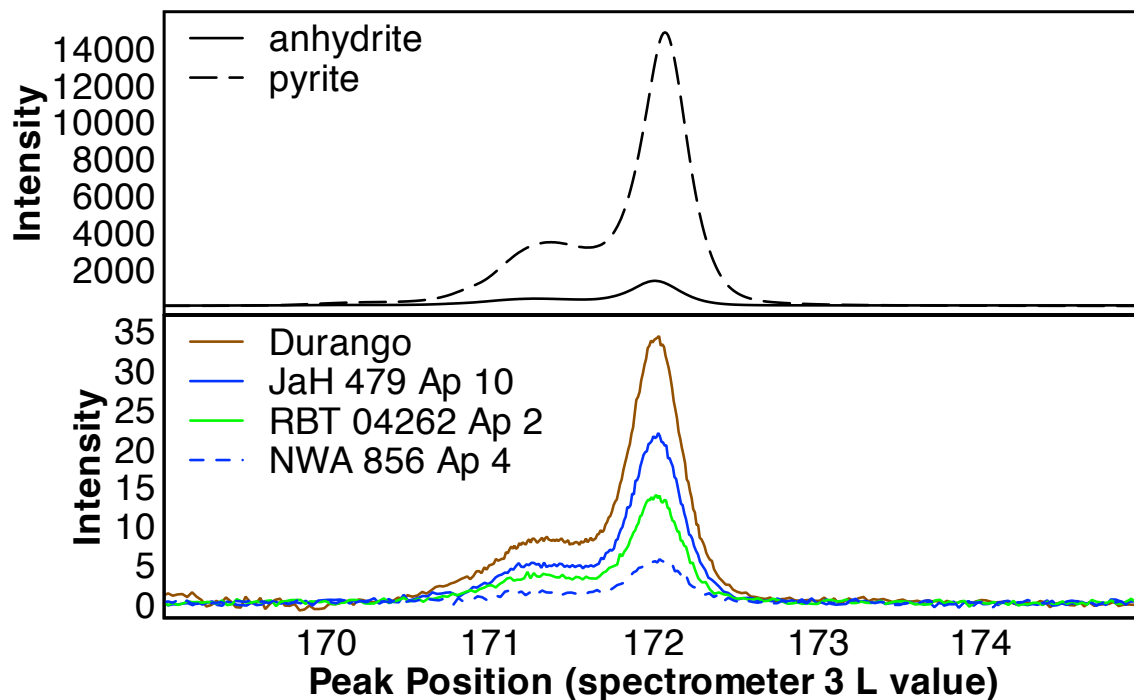


Figure 3.10. Spectrometer 3 spectra from session 1 illustrating the vast difference between peak intensities for various samples.

In either case, future work should include independently analyzed  $S^{6+}/S^{2-}$  ratios (such as from XANES) of either the anhydrite and pyrite, or the new synthetic standards in order to make a more quantitative determination of the proportions of sulfide and sulfate present.

### Sulfur Concentrations

Although the sulfur concentration estimates determined in this study match well with those determined in chapter II, it is not advisable that this method be used in place of traditional techniques to determine concentrations. The calibration curves used to calculate the S concentration vary from session to session, which means that additional standards would need to be used during each session to create a calibration curve, on top of which the method is much less robust than traditional techniques. This can be seen in table 3.5, which compares the concentration data of ion probe measurements from chapter II to the

Table 3.4. Background corrected peak intensities from spectrometer 3 in all sessions, and sulfur abundances (measured by ion probe in chapter II, unless otherwise noted) for all samples in this study.

Sample	<u>Session 1</u>			<u>Session 3</u>				S Abundance (wt % $\pm 2\sigma$ )	
	Peak Height			Peak Height					
	spec 2	spec 3	spec 5	spec 1	spec 2	spec 3	spec 5		
<b><u>Standards</u></b>									
<b>anhydrite</b>	200	1330	1130	320 280	570 500	1280 1200	1450 1230	23.55 <sup>a</sup>	
<b>pyrite</b>	2010	14850	14000	2375 2380	4300 4300	9700 9700	10500 10500	53.45 <sup>a</sup>	
<b>Durango</b>	14	34	32	5.3 5.5	9.1 9.3	19 20	19 20	0.10 $\pm$ 0.02 0.10 $\pm$ 0.02	
<b><u>Basaltic Shergottites</u></b>									
<b>JaH 479</b>	1	6.4	16	17				0.13 $\pm$ 0.02	
	3	6.4	15	16	5.1	8.7	20	23	0.21 $\pm$ 0.02
	8				2.7	4.6	10	12	0.10 $\pm$ 0.01
	9	6.3	15	13					0.12 $\pm$ 0.02
	10	9.3	21	21					0.14 $\pm$ 0.01
<b>NWA 856</b>	1				1.1	1.0	2.1	2.0	0.04 $\pm$ 0.01
	2	2.4	5.3	5.4					0.04 $\pm$ 0.06 <sup>b</sup>
	3				0.6	0.9	2.4	2.2	0.03 $\pm$ 0.00
	4	2.6	5.3	5.4					0.05 $\pm$ 0.07 <sup>b</sup>
<b>NWA 2986</b>	1	3.5	9.2	11					0.09 $\pm$ 0.01
	3				2.1	3.5	10	9.6	0.14 $\pm$ 0.08
	4				1.5	2.8	8.9	7.0	0.05 $\pm$ 0.00
<b>Shergotty</b>	3				1.2	1.7	4.1	3.5	0.03 $\pm$ 0.01 <sup>b</sup>
	6				2.8	4.7	10	13	0.06 $\pm$ 0.02
<b><u>Olivine-Phyric Shergottite</u></b>									
<b>RBT 04262</b>	1	6.7	17	16					0.13 $\pm$ 0.17 <sup>b</sup>
	2	5.7	14	12					0.11 $\pm$ 0.15 <sup>b</sup>
<b><u>Lherzolithic Shergottite</u></b>									
<b>NWA 1950</b>	1				0.5	0.9	1.9	2.0	0.01 $\pm$ 0.00
	2				0.5	0.8	1.9	2.0	0.01 $\pm$ 0.00

<sup>a</sup>Calculated by stoichiometry.

<sup>b</sup>Estimated in this study.

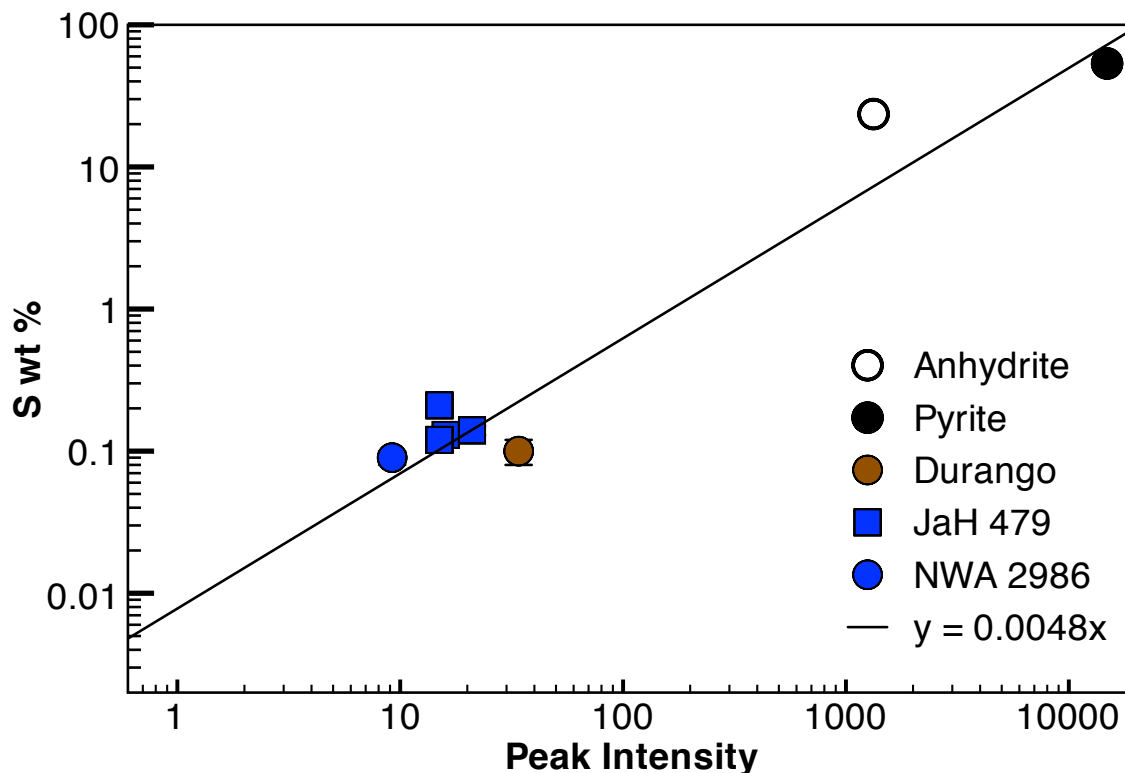


Figure 3.11. Background corrected peak intensities from spectrometer 3 in session 1 plotted against sulfur abundances measured in chapter II for apatites, and stoichiometrically calculated for anhydrite and pyrite. Error bars are  $2\sigma$  of concentrations determined from ion probe measurements. The best-fit line calculated by weighted, least-squares linear regression of the data is also shown.

concentration data calculated in this study. However, using this method to estimate sulfur abundances in order to corroborate them with sulfur abundances measured by more traditional methods may be a good contribution for evaluating the robustness of a measurement.

## Conclusions

Electron probe measurements of sulfur  $K\alpha$  X-rays show little variability in peak positions of apatites from basaltic and olivine-phyric shergottites, however this study was unable to illustrate reproducibility of relative peak positions of Durango within the two end member

Table 3.5. Concentration of standards and apatites calculated from this study compared to ion probe concentration data in chapter II.

Sample	Apatite	Session 1	Session 3	Known S
		Calculated S Abundance (wt% $\pm 2\sigma$ )	Calculated S Abundance (wt% $\pm 2\sigma$ )	
<b>Standards</b>				
anhydrite		6.34 $\pm$ 1.12	9.19 $\pm$ 0.37	23.55 <sup>a</sup>
			8.12 $\pm$ 0.45	
pyrite		70.59 $\pm$ 2.30	68.38 $\pm$ 0.17	53.45 <sup>a</sup>
			68.41 $\pm$ 0.15	
Durango		0.27 $\pm$ 0.37	0.14 $\pm$ 0.03	0.10 $\pm$ 0.02
			0.14 $\pm$ 0.02	0.10 $\pm$ 0.02
<b>Basaltic Shergottites</b>				
JaH 479	1	0.13 $\pm$ 0.16		0.13 $\pm$ 0.02
	3	0.12 $\pm$ 0.17	0.14 $\pm$ 0.01	0.21 $\pm$ 0.02
	8		0.07 $\pm$ 0.01	0.10 $\pm$ 0.01
	9	0.12 $\pm$ 0.17		0.12 $\pm$ 0.02
	10	0.18 $\pm$ 0.25		0.14 $\pm$ 0.01
NWA 856	1		0.02 $\pm$ 0.02	0.04 $\pm$ 0.01
	3		0.02 $\pm$ 0.00	0.03 $\pm$ 0.00
NWA 2986	1	0.07 $\pm$ 0.08		0.09 $\pm$ 0.01
	3		0.06 $\pm$ 0.01	0.14 $\pm$ 0.08
	4		0.05 $\pm$ 0.02	0.05 $\pm$ 0.00
Shergotty	6		0.08 $\pm$ 0.01	0.06 $\pm$ 0.02
<b>Lherzolic Shergottite</b>				
NWA 1950	1		0.01 $\pm$ 0.00	0.01 $\pm$ 0.00
	2		0.01 $\pm$ 0.00	0.01 $\pm$ 0.00

<sup>a</sup>Calculated by stoichiometry.

standards of anhydrite and pyrite from session to session. Because anhydrite and pyrite were the standards being used to determine sulfur speciation, the estimates of percent sulfide present in the apatites listed in tables 3.1 through 3.3 are not considered to be robust. However, because all of the apatite X-rays from basaltic shergottites have similar

peak wavelengths, and because all apatite peaks (from both Durango and SNCs) reside within the anhydrite and pyrite end member peaks, it is recommended that further efforts to resolve measuring sulfur speciation in apatites using the electron probe are worthwhile to pursue. I conclude that the most likely pursuit to resolve reproducibility of percent sulfide calculations would be to replace the standards (especially anhydrite which seems to be the least reproducible) with minerals more closely related to apatite and that are homogeneous (presumably the best materials to use would need to be synthesized in the laboratory).

Sulfur concentrations estimated in apatites from NWA 856, Shergotty, and RBT 04262 using this technique fall well within the range of sulfur abundances measured in basaltic and olivine-phyric shergottites in chapter II. However, this is not a feasible replacement for traditional abundance measurement techniques.

## BIBLIOGRAPHY

- Baker, D. R. and R. Moretti, 2011. Modeling the solubility of sulfur in magmas: A 50-year old geochemical challenge. In *Reviews in Mineralogy and Geochemistry* 73, 167 – 213. Mineralogical Society of America.
- Barrat, J. A., P. Gillet, V. Sautter, A. Jambon, M. Javoy, C. Göpel, M. Lesourd, F. Keller, and E. Petit, 2002. Petrology and chemistry of the basaltic shergottite North West Africa 480. *Meteoritics & Planetary Science* 37, 487 – 499.
- Barrat, J. A., A. Jambon, M. Bohn, P. Gillet, V. Sautter, C. Göpel, M. Lesourd, and F. Keller, 2002. Petrology and chemistry of the picritic shergottite North West Africa 1068 (NWA 1068). *Geochimica et Cosmochimica Acta* 66, 3505 – 3518.
- Basu Sarbadhikari, A., J. M. D. Day, Y. Liu, D. Rumble, and L. A. Taylor, 2009. Petrogenesis of olivine-phyric shergottite Larkman Nunatak 06319: Implications for enriched components in martian basalts. *Geochimica et Cosmochimica Acta* 73, 2190 – 2214.
- Beck, P., J. A. Barrat, P. Gillet, M. Wadhwa, I. A. Franchi, R. C. Greenwood, M. Bohn, J. Cotton, B. van de Moortèle, and B. Reynard, 2006. Petrography and geochemistry of the chassignite Northwest Africa 2737 (NWA 2737). *Geochimica et Cosmochimica Acta* 70, 2127 – 2139.
- Behrens, H. and J. D. Webster, 2011. Studies of sulfur in melts—Motivations and overview. In *Reviews in Mineralogy and Geochemistry* 73, 1 – 8. Mineralogical Society of America.

- Bibring, J. P., Y. Langevin, J. F. Mustard, F. Poulet, R. Arvidson, A. Gendrin, B. Gondet, N. Mangold, P. Pinet, F. Forget, M. Berthé, A. Gendrin, C. Gomez, D. Jouglet, A. Soufflot, M. Vincendon, M. Combes, P. Drossart, T. Encrenaz, T. Fouchet, R. Merchiorri, G. Belluci, F. Altieri, V. Formisano, F. Capaccioni, P. Cerroni, A. Coradini, S. Fonti, O. Korablev, V. Kottsov, N. Ignatiev, V. Moroz, D. Titov, L. Zasova, D. Loiseau, S. Douté, B. Schmitt, C. Sotin, E. Hauber, H. Hoffmann, R. Jaumann, U. Keller, T. Duxbury, and G. Neukum, 2006. Global mineralogical and aqueous Mars history derived from OMEGA/Mars Express data. *Science* 312, 400 – 404.
- Boctor, N. Z., C. M. Alexander, J. Wang, and E. Hauri, 2003. The sources of water in martian meteorites: Clues from hydrogen isotopes. *Geochimica et Cosmochimica Acta* 67, 3971 – 3989.
- Borg, L. E., L. E. Nyquist, H. Wiesmann, and Y. Reese, 2002. Constraints on the petrogenesis of martian meteorites from the Rb-Sr and Sm-Nd isotopic systematics of the lherzolithic shergottites ALH77005 and LEW88516. *Geochimica et Cosmochimica Acta* 66, 2037 – 2053.
- Borg, L. E., L. E. Nyquist, H. Wiesmann, C. Y. Shih, and Y. Reese, 2003. The age of Dar al Gani 476 and the differentiation history of the martian meteorites inferred from their radiogenic isotopic systematics. *Geochimica et Cosmochimica Acta* 67, 3519 – 3536.
- Bouvier, A., J. Blichert-Toft, J. Vervoort, and F. Albarède, 2005. The age of SNC meteorites and the antiquity of the martian surface. *Earth & Planetary Science Letters* 240, 221 – 233.

- Bouvier, A., J. Blichert-Toft, J. D. Vervoort, P. Gillet, and F. Albarède, 2008. The case for old basaltic shergottites. *Earth and Planetary Science Letters* 266, 105 – 124.
- Bouvier, A., J. Blichert-Toft, and F. Albarède, 2009. Martian meteorite chronology and the evolution of the interior of Mars. *Earth & Planetary Science Letters* 280, 285 – 295.
- Boyce, J. W., Y. Liu, G. R. Rossman, Y. Guan, J. M. Eiler, E. M. Stolper, and L. A. Taylor, 2010. Lunar apatite with terrestrial volatile abundances. *Nature* 466, 466 – 469.
- Boyce, J. W., J. M. Eiler, and M. B. Channon, 2012. An inversion-based self-calibration for SIMS measurements: Application to H, F, and Cl in apatite. *American Mineralogist* 97, 1116 – 1128.
- Brenan, J., 1994. Kinetics of fluorine, chlorine and hydroxyl exchanges in fluorapatite. *Chemical Geology* 110, 195 – 210.
- Bridges, J. C. and P. H. Warren, 2006. The SNC meteorites: Basaltic igneous processes on Mars. *Journal of the Geological Society* 163, 229 – 251.
- Bridges, J. C., D. C. Catling, J. M. Saxton, T. D. Swindle, I. C. Lyon, and M. M. Grady, 2001. Alteration assemblages in martian meteorites: Implications for near-surface processes. *Space Science Reviews* 96, 365 – 392.
- Carr, M. H., 2012. The fluvial history of Mars. *Philosophical Transactions of The Royal Society A* 370, 2193 – 2215.
- Carroll, M. K. and M. J. Rutherford, 1988. Sulfur speciation in hydrous experimental glasses of varying oxidation state: Results from measured wavelength shifts of sulfur X-rays. *American Mineralogist* 73, 845 – 849.

- Channon, M. B., M. Bonifacie, E. M. Stolper, and J. M. Eiler, 2009. Oxygen isotope compositions of mineral separates from SNC meteorites: Constraints on the petrogenesis of martian magmas. *LPSC XL* #2450.
- Channon, M. B., E. M. Stolper, and J. M. Eiler, 2010. Oxygen isotope compositions of mineral separates from SNC meteorites: Constraints on SNC parental magmas. *LPSC XLI* #2212.
- Christensen, P. R., R. V. Morris, M. D. Lane, J. L. Bandfield, and M. C. Malin, 2001. Global mapping of martian hematite mineral deposits: Remnants of water-driven processes on early Mars. *Journal of Geophysical Research* 106, 23,873 – 23,885.
- Clark, B. C. and A. K. Baird, 1979. Is the martian lithosphere sulfur rich? *Journal of Geophysical Research* 84, 8395 – 8403.
- Clayton, R. N. and T. K. Mayeda, 1963. The use of bromine pentafluoride in the extraction of oxygen from oxides and silicates for isotopic analysis. *Geochimica et Cosmochimica Acta* 27, 43 – 52.
- Clayton, R. N. and T. K. Mayeda, 1983. Oxygen isotopes in eucrites, shergottites, nakhlites, and chassignites. *Earth & Planetary Science Letters* 62, 1 – 6.
- Clayton, R. N. and T. K. Mayeda, 1986. Oxygen isotopes in Shergotty. *Geochimica et Cosmochimica Acta* 50, 979 – 982.
- Clayton, R. N. and T. K. Mayeda, 1996. Oxygen isotope studies of achondrites. *Geochimica et Cosmochimica Acta* 60, 1999 – 2017.
- Dann, J. C., A. H. Holzheid, T. L. Grove, and H. Y. McSween Jr., 2001. Phase equilibria of the Shergotty meteorite: Constraints on pre-eruptive water contents of martian

- magmas and fractional crystallization under hydrous conditions. *Meteoritics & Planetary Science* 36, 793 – 806.
- Davidson, J. P., J. M. Hora, J. M. Garrison, and M. A. Dungan, 2005. Crustal forensics in arc magmas. *Journal of Volcanology and Geothermal Research* 140, 157 – 170.
- Devine, J. D., H. Sigurdsson, A. N. Davis, and S. Self, 1984. Estimates of sulfur and chlorine yield to the atmosphere from volcanic eruptions and potential climatic effects. *Journal of Geophysical Research* 89, 6309 – 6325.
- Dohmen, R., H.-W. Becker, and S. Chakraborty, 2007. Fe-Mg diffusion in olivine I: Experimental determination between 700 1200 °C as a function of composition, crystal orientation and oxygen fugacity. *Physics & Chemistry of Minerals* 34, 389 – 407.
- Dreibus, G. and H. Wänke, 1985. Mars, a volatile-rich planet. *Meteoritics* 20, 367 – 381.
- Dreibus, G. and H. Wänke, 1987. Volatiles on Earth and Mars: A comparison. *Icarus* 71, 225 – 240.
- Edmunson, J., L. E. Borg, C. K. Shearer, and J. J. Papike, 2005. Defining the mechanisms that disturb the Sm-Nd isotopic systematics of the martian meteorites: Examples from Dar al Gani 476 and Allan Hills 77005. *Meteoritics & Planetary Science* 40, 1159 – 1174.
- Ehlmann, B. L., J. F. Mustard, S. L. Murchie, F. Poulet, J. L. Bishop, A. J. Brown, W. M. Calvin, R. N. Clark, D. J. Des Marais, and R. E. Milliken, 2008. Orbital identification of carbonate-bearing rocks on Mars. *Science* 322, 1828 – 1832.

- Eiler, J. M., 2001. Oxygen isotope variations of basaltic lavas and upper mantle rocks. In *Reviews in Mineralogy & Geochemistry* 43, 319 – 364. Mineralogical Society of America.
- Eiler, J. M., J. W. Valley, and E. M. Stolper, 1996. Oxygen isotope ratios in olivine from the Hawaii Scientific Drilling Project. *Journal of Geophysical Research* 101, 11807 – 11813.
- Elsenhimer, D. and J. W. Valley, 1993. Submillimeter scale zonation of  $\delta^{18}\text{O}$  in quartz and feldspar, Isle of Skye, Scotland. *Geochimica et Cosmochimica Acta* 57, 3669 – 3676.
- Farquhar, J. and M. H. Thiemens, 2000. Oxygen cycle of the martian atmosphere-regolith system:  $\Delta^{17}\text{O}$  of secondary phases in Nakhla and Lafayette. *Journal of Geophysical Research* 105, 11991 – 11997.
- Farquhar, J., M. H. Thiemens, and T. Jackson, 1998. Atmosphere-surface interactions on Mars:  $\Delta^{17}\text{O}$  measurements of carbonate from ALH 84001. *Science* 280, 1580 – 1582.
- Filiberto, J. and A. H. Treiman, 2009. Martian magmas contained abundant chlorine, but little water. *Geology* 37, 1087 – 1090.
- Floran, R. J., M. Prinz, P. F. Hlava, K. Keil, C. E. Nehru, and J. R. Hinthorne, 1978. The Chassigny meteorite: A cumulate dunite with hydrous amphibole-bearing melt inclusions. *Geochimica et Cosmochimica Acta* 42, 1213 – 1229.
- Foley, C. N., M. Wadhwa, L. E. Borg, P. E. Janney, R. Hines, and T. L. Grove, 2005. The early differentiation history of Mars from  $^{182}\text{W}$ - $^{142}\text{Nd}$  isotope systematics in the SNC meteorites. *Geochimica et Cosmochimica Acta* 69, 4557 – 4571.

- Franchi, I. A., I. P. Wright, A. S. Sexton, and C. T. Pillinger, 1999. The oxygen-isotopic composition of Earth and Mars. *Meteoritics & Planetary Science* 34, 657 – 661.
- Gaillard, F. and B. Scaillet, 2009. The sulfur content of volcanic gases on Mars. *Earth & Planetary Science Letters* 279, 34 – 43.
- Gillet, P., J. A. Barrat, P. Beck, B. Marty, R. C. Greenwood, I. A. Franchi, M. Bohn, and J. Cotton, 2005. Petrology, geochemistry, and cosmic-ray exposure age of Iherzolitic shergottite Northwest Africa 1950. *Meteoritics & Planetary Science* 40, 1175 – 1184.
- Gnos, E., B. Hofmann, I. A. Franchi, A. Al-Kathiri, M. Huser, and L. Moser, 2002. Sayh al Uhaymir 094: A new martian meteorite from the Oman desert. *Meteoritics & Planetary Science* 37, 835 – 854.
- Goodrich, C. A., 2003. Petrogenesis of olivine-phyric shergottites Sayh al Uhaymir 005 and Elephant Moraine A79001 lithology A. *Geochimica et Cosmochimica Acta* 67, 3735 – 3772.
- Goodrich, C. A., C. D. K. Herd, and L. A. Taylor, 2003. Spinels and oxygen fugacity in olivine-phyric and Iherzolitic shergottites. *Meteoritics & Planetary Science* 38, 1773 – 1792.
- Greenwood, J. P., R. E. Blake, and C. D. Coath, 2003. Ion microprobe measurements of  $^{18}\text{O}/^{16}\text{O}$  ratios of phosphate minerals in the martian meteorites ALH84001 and Los Angeles. *Geochimica et Cosmochimica Acta* 67, 2289 – 2298.
- Greenwood, J. P., S. Itoh, N. Sakamoto, E. P. Vicenzi, and H. Yurimoto, 2008. Hydrogen isotope evidence for loss of water from Mars through time. *Geophysical Research Letters* 35.

- Guan, Y., W. Hsu, L. A. Leshin, H. Wang, R. Wang, F. Zhang, C. Lin, and W. Zhang, 2003. Hydrogen isotopes of phosphates in the new martian meteorite GRV 99027. *LPSC XXXIV* #1830.
- Harvey, R. P., M. Wadhwa, H. Y. McSween Jr., and G. Crozaz, 1993. Petrography, mineral chemistry, and petrogenesis of Antarctic shergottite LEW88516. *Geochimica et Cosmochimica Acta* 57, 4769 – 4783.
- Haskin, L. A., A. Wang, B. L. Joliff, H. Y. McSween, B. C. Clark, D. J. Des Marais, S. M. McLellan, N. J. Tosca, J. A. Hurowitz, J. D. Farmer, A. Yen, S. W. Squyres, R. E. Arvidson, G. Klingelhöfer, C. Schröder, P. A. de Souza, D. W. Ming, R. Gellert, J. Zipfel, J. Brückner, J. F. Bell, K. Herkenhoff, P. R. Christensen, S. Ruff, D. Blaney, S. Gorevan, N. A. Cabrol, L. Crumpler, J. Grant, and L. Soderblom, 2005. Water alteration of rocks and soils on Mars at the Spirit rover site in Gusev crater. *Nature* 436, 66 – 69.
- Henning, P. A., E. Adolfsson, and J. Grins, 2000. The chalcogenide phosphate apatites  $\text{Ca}_{10}(\text{PO}_4)_6\text{S}$ ,  $\text{Sr}_{10}(\text{PO}_4)_6\text{S}$ ,  $\text{Ba}_{10}(\text{PO}_4)_6\text{S}$  and  $\text{Ca}_{10}(\text{PO}_4)_6\text{Se}$ . *Zeitschrift für Kristallographie* 215, 226 – 230.
- Herd, C. D. K., 2003. The oxygen fugacity of olivine-phyric martian basalts and the components within the mantle and crust of Mars. *Meteoritics & Planetary Science* 36, 1793 – 1805.
- Herd, C. D. K., 2006. Insights into the redox history of the NWA 1068/1110 martian basalt from mineral equilibria and vanadium oxybarometry. *American Mineralogist* 91, 1616 – 1627.

- Herd, C. D. K., J. J. Papike, and A. J. Brearley, 2001. Oxygen fugacity of martian basalts from electron microprobe oxygen and TEM-EELS analyses of Fe-Ti oxides. *American Mineralogist* 86, 1015 – 1024.
- Herd, C. D. K., L. E. Borg, J. H. Jones, and J. J. Papike, 2002. Oxygen fugacity and geochemical variations in the martian basalts: Implications for martian basalt petrogenesis and the oxidation state of the upper mantle of Mars. *Geochimica et Cosmochimica Acta* 66, 2025 – 2036.
- Herd, C. D. K., C. S. Schwandt, J. H. Jones, and J. J. Papike, 2002. An experimental and petrographic investigation of Elephant Moraine 79001 lithology A: Implications for its petrogenesis and the partitioning of chromium and vanadium in a martian basalt. *Meteoritics & Planetary Science* 37, 987 – 1000.
- Ikeda, Y., 1994. Petrography and petrology of the ALH-77005 shergottite. *Proceedings of the NIPR Symposium on Antarctic Meteorites* 7, 9 – 29.
- Jagoutz, E. and H. Wänke, 1986. Sr and Nd isotopic systematics of Shergotty meteorite. *Geochimica et Cosmochimica Acta* 50, 939 – 953.
- Jakosky, B. M. and J. H. Jones, 1997. The history of martian volatiles. *Reviews of Geophysics* 35, 1 – 16.
- Jambon, A., J. A. Barrat, V. Sautter, P. Gillet, C. Göpel, M. Javoy, J. L. Joron, and M. Lesourd, 2002. The basaltic shergottite Northwest Africa 856: Petrology and chemistry. *Meteoritics & Planetary Science* 37, 1147 – 1164.
- Jensen, H. B. and T. D. Glotch, 2011. Investigation of the near-infrared spectral character of putative martian chloride deposits. *Journal of Geophysical Research* 116.

- Johnson, M. C., M. J. Rutherford, and P. C. Hess, 1991. Chassigny petrogenesis: Melt compositions, intensive parameters and water contents of martian (?) magmas. *Geochimica et Cosmochimica Acta* 55, 349 – 366.
- Jugo, P. J., R. W. Luth, and J. P. Richards, 2005. Experimental data on the speciation of sulfur as a function of oxygen fugacity in basaltic melts. *Geochimica et Cosmochimica Acta* 69, 497 – 503.
- Karner, J. M., J. J. Papike, C. K. Shearer, G. McKay, L. Le, and P. Burger, 2007. Valence state partitioning of Cr and V between pyroxene-melt: Estimates of oxygen fugacity for martian basalt QUE 94201. *American Mineralogist* 92, 1238 – 1241.
- King, P. L. and S. M. McLennan, 2010. Sulfur on Mars. *Elements* 6, 107 – 112.
- Kusakabe, M. and Y. Matsuhisa, 2008. Oxygen three-isotope ratios of silicate reference materials determined by direct comparison with VSMOW-oxygen. *Geochemical Journal* 42, 309 – 317.
- Lapen, T. J., M. Richter, A. D. Brandon, V. Debaille, B. L. Beard, J. T. Shafer, and A. H. Peslier, 2010. A younger age for ALH84001 and its geochemical link to shergottite sources in Mars. *Science* 328, 347 – 351.
- Lentz, R. C. F., G. J. Taylor, and A. H. Treiman, 1999. Formation of a martian pyroxenite: A comparative study of the nakhlite meteorites and Theo's Flow. *Meteoritics & Planetary Science* 34, 919 – 932.
- Lentz, R. C. F., H. Y. McSween Jr., J. Ryan, and L. R. Riciputi, 2001. Water in martian magmas: Clues from light lithophile elements in shergottite and nakhlite pyroxenes. *Geochimica et Cosmochimica Acta* 65, 4551 – 4565.

- Leshin, L. A., 2000. Insights into martian water reservoirs from analyses of martian meteorite QUE94201. *Geophysical Research Letters* 27, 2017 – 2020.
- Longhi, J. and V. Pan, 1989. The parent magmas of the SNC meteorites. *Proceedings of the 19<sup>th</sup> Lunar and Planetary Science Conference*, 451 – 464.
- Lundberg, L. L., G. Crozaz, and H. Y. McSween Jr., 1990. Rare earth elements in minerals of the ALHA77005 shergottite and implications for its parent magma and crystallization history. *Geochimica et Cosmochimica Acta* 54, 2535 – 2547.
- McCanta, M. C., Rutherford, M. J., and J. H. Jones, 2004. An experimental study of rare earth element partitioning between a shergottite melt and pigeonite: Implications for the oxygen fugacity of the martian interior. *Geochimica et Cosmochimica Acta* 68, 1943 – 1952.
- McCanta, M. C., L. Elkins-Tanton, and M. J. Rutherford, 2009. Expanding the application of the Eu-oxybarometer to the lherzolitic shergottites and nakhlites: Implications for the oxidation state heterogeneity of the martian interior. *Meteoritics & Planetary Science* 44, 725 – 745.
- McCoy, T. J., M. Wadhwa, and K. Keil, 1999. New lithologies in the Zagami meteorite: Evidence for fractional crystallization of a single magma unit on Mars. *Geochimica et Cosmochimica Acta* 63, 1249 – 1262.
- McCubbin, F. M., N. J. Tosca, A. Smirnov, H. Nekvasil, A. Steele, M. Fries, and D. H. Lindsley, 2009. Hydrothermal jarosite and hematite in a pyroxene-hosted melt inclusion in martian meteorite Miller Range (MIL) 03346: Implications for magmatic-hydrothermal fluids on Mars. *Geochimica et Cosmochimica Acta* 73, 4907 – 4917.

- McCubbin, F. M., E. H. Hauri, S. M. Elardo, K. E. Vander Kaaden, J. Wang, and C. K. Shearer, 2012. Hydrous melting of the martian mantle produced both depleted and enriched shergottites. *Geology* 40, 683 – 686.
- McSween Jr., H. Y., 1994. What we have learned about Mars from SNC meteorites. *Meteoritics* 29, 757 – 779.
- McSween Jr., H. Y. and E. Jarosewich, 1983. Petrogenesis of the Elephant Moraine A79001 meteorite: Multiple magma pulses on the shergottite parent body. *Geochimica et Cosmochimica Acta* 47, 1501 – 1513.
- McSween Jr., H. Y. and A. H. Treiman, 1998. Martian meteorites. In *Reviews in Mineralogy and Geochemistry* 36, 6.1-6.53. Mineralogical Society of America.
- McSween Jr., H. Y., D. D. Eisenhour, L. A. Taylor, M. Wadhwa, and G. Crozaz, 1996. QUE94201 shergottite: Crystallization of a martian basaltic magma. *Geochimica et Cosmochimica Acta* 60, 4563 – 4569.
- McSween Jr., H. Y., T. L. Grove, R. C. F. Lentz, J. C. Dann, A. H. Holzheid, L. R. Riciputi, and J. G. Ryan, 2001. Geochemical evidence for magmatic water within Mars from pyroxenes in the Shergotty meteorite. *Nature* 409, 487 – 490.
- Miller, M. F., 2002. Isotopic fractionation and the quantification of  $^{17}\text{O}$  anomalies in the oxygen three-isotope system: An appraisal and geochemical significance. *Geochimica et Cosmochimica Acta* 66, 1881 – 1889.
- Miller, M. F., I. A. Franchi, A. S. Sexton, and C. T. Pillinger, 1999. High-precision  $\delta^{17}\text{O}$  isotope measurements of oxygen from silicates and other oxides: Method and applications. *Rapid Communications in Mass Spectrometry* 13, 1211 – 1217.

- Ming, D. W., D. W. Mittlefehldt, R. V. Morris, D. C. Golden, R. Gellert, A. Yen, B. C. Clark, S. W. Squyres, W. H. Farrand, S. W. Ruff, R. E. Arvidson, G. Klingelhöfer, H. Y. McSween, D. S. Rodionov, C. Schröder, P. A. de Souza, and A. Wang, 2006. Geochemical and mineralogical indicators for aqueous processes in the Columbia Hills of Gusev Crater, Mars. *Journal of Geophysical Research* 111, E2.
- Mittlefehldt, D. W., 1994. ALH84001, a cumulate orthopyroxenite member of the martian meteorite clan. *Meteoritics* 29, 214 – 221.
- Mittlefehldt, D. W., D. J. Lindstrom, M. M. Lindstrom, and R. R. Martinez, 1999. An impact-melt origin for lithology A of martian meteorite Elephant Moraine A79001. *Meteoritics & Planetary Science* 34, 357 – 367.
- Morris, R. V., S. W. Ruff, R. Gellert, D. W. Ming, R. E. Arvidson, B. C. Clark, D. C. Golden, K. Siebach, G. Klingelhöfer, C. Schröder, I. Fleischer, A. S. Yen, and S. W. Squyres, 2010. Identification of carbonate-rich outcrops on Mars by the Spirit rover. *Science* 329, 421 – 424.
- Mosenfelder, J. L., M. Le Voyer, G. R. Rossman, Y. Guan, D. R. Bell, P. D. Asimow, and J. M. Eiler, 2011. Analysis of hydrogen in olivine by SIMS: Evaluation of standards and protocol. *American Mineralogist* 96, 1725 – 1741.
- Mustard, J. F., S. L. Murchie, S. M. Pelkey, B. L. Ehlmann, R. E. Milliken, J. A. Grant, J. P. Bibring, F. Poulet, J. Bishop, E. Noe Dobrea, L. Roach, F. Seelos, R. E. Arvidson, S. Wiseman, R. Green, C. Hash, D. Humm, E. Malaret, J. A. McGovern, K. Seelos, T. Clancy, R. Clark, D. D. Marais, N. Izenberg, A. Knudson, Y. Langevin, T. Martin, P. McGuire, R. Morris, M. Robinson, T. Roush, M. Smith, G. Swayze, H. Taylor, T.

- Titus, and M. Wolff, 2008. Hydrated silicate minerals on Mars observed by the Mars Reconnaissance Orbiter CRISM instrument. *Nature* 454, 305 – 309.
- Nekvasil, H., J. Filiberto, F. M. McCubbin, and D. H. Lindsley, 2007. Alkalic parental magmas for chassignites? *Meteoritics & Planetary Science* 42, 979 – 992.
- Nyquist, L. E., D. D. Bogard, C. Y. Shih, A. Greshake, D. Stöffler, and O. Eugster, 2001. Ages and geologic histories of martian meteorites. *Space Science Reviews* 96, 105 – 164.
- Nyquist, L. E., D. D. Bogard, C. Y. Shih, J. Park, Y. D. Reese, and A. J. Irving, 2009. Concordant Rb-Sr, Sm-Nd, and Ar-Ar ages for Northwest Africa 1460: A 346Ma old basaltic shergottite related to “Iherzolitic” shergottites. *Geochimica et Cosmochimica Acta* 73, 4288 – 4309.
- Pan, Y. and M. E. Fleet, 2002. Compositions of the apatite-group minerals: Substitution mechanisms and controlling factors. In *Reviews in Mineralogy and Geochemistry* 48, 13 – 49. Mineralogical Society of America.
- Papike, J. J., J. M. Karner, C. K. Shearer, and P. V. Burger, 2009. Silicate mineralogy of martian meteorites. *Geochimica et Cosmochimica Acta* 73, 7443 – 7485.
- Parat, F. and F. Holtz, 2004. Sulfur partitioning between apatite and melt and effect of sulfur on apatite solubility at oxidizing conditions. *Contributions to Mineralogy and Petrology* 147, 201 – 212.
- Parat, F., F. Holtz, and M. J. Streck, 2011. Sulfur-bearing magmatic accessory minerals. In *Reviews in Mineralogy and Geochemistry* 73, 285 – 314. Mineralogical Society of America.

- Park, J., D. H. Garrison, and D. D. Bogard, 2009.  $^{39}\text{Ar}$ - $^{40}\text{Ar}$  ages of martian nakhlites. *Geochimica et Cosmochimica Acta* 73, 2177 – 2189.
- Patiño Douce, A. E. and M. Roden, 2006. Apatite as a probe of halogen and water fugacities in the terrestrial planets. *Geochimica et Cosmochimica Acta* 70, 3173 – 3196.
- Peng, G., J. F. Luhr, and J. J. McGee, 1997. Factors controlling sulfur concentrations in volcanic apatite. *American Mineralogist* 82, 1210 – 1224.
- Piccoli, P. M. and P. A. Candela, 2002. Apatite in igneous systems. In *Reviews in Mineralogy and Geochemistry* 48, 255 – 292. Mineralogical Society of America.
- Reed, B. C., 1992. Linear least-squares fits with errors in both coordinates. II: Comments on parameter variances. *American Journal of Physics* 60, 59 – 62.
- Reid, A. M. and T. E. Bunch, 1975. The nakhlites part II: Where, when, and how. *Meteoritics* 10, 317 – 324.
- Righter, K., K. Pando, and L. R. Danielson, 2009. Experimental evidence for sulfur-rich martian magmas: Implications for volcanism and surficial sulfur sources. *Earth & Planetary Science Letters* 288, 235 – 243.
- Roegge, J. S., M. J. Logsdon, H. S. Young, H. B. Barr, M. Borcsik, and H. D. Holland, 1974. Halogens in apatites from the Providencia area, Mexico. *Economic Geology* 69, 299 – 240.
- Roggensack, K., R. L. Hervig, S. B. McKnight, and S. N. Williams, 1997. Explosive basaltic volcanism from Cerro Negro Volcano: Influence of volatiles on eruptive style. *Science* 277, 1639 – 1642.

- Romanek, C. S., E. C. Perry, A. H. Treiman, R. A. Socki, J. H. Jones, and E. K. Gibson Jr., 1998. Oxygen isotopic record of silicate alteration in the Shergotty-Nakhla-Chassigny meteorite Lafayette. *Meteoritics & Planetary Science* 33, 775 – 784.
- Rosenbaum, J. M. and D. Matthey, 1995. Equilibrium garnet-calcite oxygen isotope fractionation. *Geochimica et Cosmochimica Acta* 59, 2839 – 2842.
- Rowe, M. C., A. J. R. Kent, and R. L. Nielsen, 2007. Determination of sulfur speciation and oxidation state of olivine hosted melt inclusions. *Chemical Geology* 236, 303 – 322.
- Rubin, A. E., P. H. Warren, J. P. Greenwood, R. S. Verish, L. A. Leshin, R. L. Hervig, R. N. Clayton, and T. K. Mayeda, 2000. Los Angeles: The most differentiated basaltic martian meteorite. *Geology* 28, 1011 – 1014.
- Rumble, D. and A. J. Irving, 2009. Dispersion of oxygen isotope compositions among 42 martian meteorites determined by laser fluorination: Evidence for assimilation of (ancient) altered crust. *LPSC XL #2293*.
- Rumble, D., J. Farquhar, E. D. Young, and C. P. Christensen, 1997. In situ oxygen isotope analysis with an excimer laser using F<sub>2</sub> and BrF<sub>5</sub> reagents and O<sub>2</sub> gas as analyte. *Geochimica et Cosmochimica Acta* 61, 4229 – 4234.
- Rumble, D., M. F. Miller, I. A. Franchi, and R. C. Greenwood, 2007. Oxygen three-isotope fractionation lines in terrestrial silicate minerals: An inter-laboratory comparison of hydrothermal quartz and eclogitic garnet. *Geochimica et Cosmochimica Acta* 71, 3592 – 3600.

- Ryerson, F. J., W. B. Durham, D. J. Cherniak, and W. A. Lanford, 1989. Oxygen diffusion in olivine: Effect of oxygen fugacity and implications for creep. *Journal of Geophysical Research* 94, 4105 – 4118.
- Sautter, V., J. A. Barrat, A. Jambon, J. P. Lorand, P. Gillet, M. Javoy, J. L. Joron, and M. Lesourd, 2002. A new martian meteorite from Morocco: The nakhlite North West Africa 817. *Earth & Planetary Science Letters* 195, 223 – 238.
- Scott, E. R. D., R. C. Greenwood, I. A. Franchi, and I. S. Sanders, 2009. Oxygen isotopic constraints on the origin and parent bodies of eucrites, diogenites, and howardites. *Geochimica et Cosmochimica Acta* 73, 5835 – 5853.
- Sharp, Z. D., 1990. A laser-based microanalytical method for the in situ determination of oxygen isotope ratios of silicates and oxides. *Geochimica et Cosmochimica Acta* 54, 1353 – 1357.
- Sharp, Z. D., C. K. Shearer, C. B. Agee, and K. D. McKeegan, 2011. The chlorine isotope composition of Mars. *LPSC XLII* #2534.
- Shearer, C. K., P. V. Burger, J. J. Papike, L. E. Borg, A. J. Irving, and C. Herd, 2008. Petrogenic linkages among martian basalts: Implications based on trace element chemistry of olivine. *Meteoritics & Planetary Science* 43, 1241 – 1258.
- Spicuzza, M. J., J. M. D. Day, L. A. Taylor, and J. W. Valley, 2007. Oxygen isotope constraints on the origin and differentiation of the moon. *Earth & Planetary Science Letters* 253, 254 – 265.
- Squyres, S. W., J. P. Grotzinger, R. E. Arvidson, J. F. Bell, W. Calvin, P. R. Christensen, B. C. Clark, J. A. Crisp, W. H. Farrand, K. E. Herkenhoff, J. R. Johnson, G. Klingelhöfer, A. H. Knoll, S. M. McLennan, H. Y. McSween, R. V. Morris, J. W.

- Rice, R. Rieder, and L. A. Soderblom, 2004. In situ evidence for an ancient aqueous environment at Meridiani Planum, Mars. *Science* 306, 1709 – 1714.
- Streck, M. J. and J. H. Dilles, 1998. Sulfur evolution of oxidized arc magmas as recorded in apatite from a porphyry copper batholith. *Geology* 26, 523 – 526.
- Symes, S. J. K., L. E. Borg, C. K. Shearer, and A. J. Irving, 2008. The age of the martian meteorite Northwest Africa 1195 and the differentiation history of the shergottites. *Geochimica et Cosmochimica Acta* 72, 1696 – 1710.
- Symonds, R. B., W. I. Rose, and M. H. Reed, 1988. Contribution of Cl- and F-bearing gases to the atmosphere by volcanoes. *Nature* 334, 415 – 418.
- Taylor, L. A., M. A. Nazarov, C. K. Shearer, H. Y. McSween Jr., J. Cahill, C. R. Neal, M. A. Ivanova, L. D. Barsukova, R. C. Lentz, and R. N. Clayton, 2002. Martian meteorite Dhofar 019: A new shergottite. *Meteoritics & Planetary Science* 37, 1107 – 1128.
- Taylor Jr., H. P., 1980. The effects of assimilation of country rocks by magmas on  $^{18}\text{O}/^{16}\text{O}$  and  $^{87}\text{Sr}/^{86}\text{Sr}$  systematics in igneous rocks. *Earth & Planetary Science Letters* 47, 243 – 254.
- Taylor Jr., H. P., M. B. Duke, L. T. Silver, and S. Epstein, 1965. Oxygen isotope studies of minerals in stony meteorites. *Geochimica et Cosmochimica Acta* 29, 489 – 512.
- Tepper, J. H. and S. M. Kuehner, 1999. Complex zoning in apatite from the Idaho batholith: A record of magma mixing and intracrystalline trace element diffusion. *American Mineralogist* 84, 581 – 595.

- Thordarson, T. and S. Self, 2003. Atmospheric and environmental effects of the 1783 – 1784 Laki eruption: A review and reassessment. *Journal of Geophysical Research* 108.
- Treiman, A. H., 1998. The history of Allan Hills 84001 revised: Multiple shock events. *Meteoritics & Planetary Science* 33, 753 – 764.
- Treiman, A. H., 2005. The nakhlite meteorites: Augite-rich igneous rocks from Mars. *Chemie der Erde* 65, 203 – 270.
- Treiman, A. H. and A. J. Irving, 2008. Petrology of martian meteorite Northwest Africa 998. *Meteoritics & Planetary Science* 43, 829 – 854.
- Treiman, A. H., M. D. Dyar, M. McCanta, S. K. Noble, and C. M. Pieters, 2007. Martian dunite NWA 2737: Petrographic constraints on geological history, shock events, and olivine color. *Journal of Geophysical Research* 112.
- Usui, T., H. Y. McSween Jr., and C. Floss, 2008. Petrogenesis of olivine-phyric shergottite Yamato 980459, revisited. *Geochimica et Cosmochimica Acta* 72, 1711 – 1730.
- Valley, J. W., N. Kitchen, M. J. Kohn, C. R. Niendorf, and M. J. Spicuzza, 1995. UWG-2, a garnet standard for oxygen isotope ratios: Strategies for high precision and accuracy with laser heating. *Geochimica et Cosmochimica Acta* 59, 5223 – 5231.
- Valley, J. W., J. M. Eiler, C. M. Graham, E. K. Gibson, C. S. Romanek, and E. M. Stolper, 1997. Low-temperature carbonate concretions in the martian meteorite ALH84001: Evidence from stable isotopes and mineralogy. *Science* 275, 1633 – 1638.

- Wadhwa, M., 2001. Redox state of Mars' upper mantle and crust from Eu anomalies in shergottite pyroxenes. *Science* 291, 1527 – 1530.
- Wadhwa, M. and G. Crozaz, 1995. Trace and minor elements in minerals of nakhlites and Chassigny: Clues to their petrogenesis. *Geochimica et Cosmochimica Acta* 59, 3629 – 3645.
- Wadhwa, M., R. C. F. Lentz, H. Y. McSween Jr., and G. Crozaz, 2001. A petrologic and trace element study of Dar al Gani 476 and Dar al Gani 489: Twin meteorites with affinities to basaltic and lherzolithic shergottites. *Meteoritics & Planetary Science* 36, 195 – 208.
- Wallace, P. J. and I. S. E. Carmichael, 1994. S speciation in submarine basaltic glasses as determined by measurements of SK $\alpha$  X-ray wavelength shifts. *American Mineralogist* 79, 161 – 167.
- Wallace, P. J. and T. M. Gerlach, 1994. Magmatic vapor source for sulfur dioxide released during volcanic eruptions: Evidence from Mount Pinatubo. *Science* 265, 497 – 499.
- Warren, P. H., J. P. Greenwood, and A. E. Rubin, 2004. Los Angeles: A tale of two stones. *Meteoritics & Planetary Science* 39, 137 – 156.
- Watson, L. L., I. D. Hutcheon, S. Epstein, and E. M. Stolper, 1994. Water on Mars: Clues from deuterium/hydrogen and water contents of hydrous phases in SNC meteorites. *Science* 265, 86 – 90.
- Webster, J. D., R. J. Kinzler, and E. A. Mathez, 1999. Chloride and water solubility in basalt and andesite melts and implications for magmatic degassing. *Geochimica et Cosmochimica Acta* 63, 729 – 738.

- Wiechert, U. H., A. N. Halliday, D. C. Lee, G. A. Snyder, L. A. Taylor, and D. Rumble, 2001. Oxygen isotopes and the moon-forming giant impact. *Science* 294, 345 – 348.
- Wiechert, U. H., A. N. Halliday, H. Palme, and D. Rumble, 2004. Oxygen isotope evidence for rapid mixing of the HED meteorite parent body. *Earth & Planetary Science Letters* 221, 373 – 382.
- Xirouchakis, D., D. S. Draper, C. S. Schwandt, and A. Lanzirotti, 2002. Crystallization conditions of Los Angeles, a basaltic martian meteorite. *Geochimica et Cosmochimica Acta* 66, 1867 – 1880.
- Zajacz, Z., P. A. Candela, P. M. Piccoli, and C. Sanchez-Valle, 2012. The partitioning of sulfur and chlorine between andesite melts and magmatic volatiles and the exchange coefficients of major cations. *Geochimica et Cosmochimica Acta* 89, 81 – 101.
- Zelenski, M. and Y. Taran, 2012. Volcanic emissions of molecular chlorine. *Geochimica et Cosmochimica Acta* 87, 210 – 226.
- Zipfel, J., P. Scherer, B. Spettel, G. Dreibus, and L. Schultz, 2000. Petrology and chemistry of the new shergottite Dar al Gani 476. *Meteoritics & Planetary Science* 35, 95 – 106.

*Appendix A*

## RAW DATA FOR CHAPTER I

Data for chapter I was acquired from 16 sessions on the Delta, and 8 sessions on the MAT 252. During the Delta sessions CO<sub>2</sub> was measured yielding only data for  $\delta^{18}\text{O}$ ; the raw data from those sessions can be found in table A.1. During the MAT 252 sessions O<sub>2</sub> was measured which resolves both  $\delta^{18}\text{O}$  and  $\delta^{17}\text{O}$ ; the raw data from those sessions can be found in table A.2. The abbreviations for the analyzed material in both tables are as follows: gt, garnet; px, pyroxene; cpx, clinopyroxene; opx, orthopyroxene; ol, olivine; and msk, maskelynite.

Table A.1. Raw data from all Delta sessions.

Sample	Material	$\delta^{45}\text{CO}_2$	$\sigma$	$\delta^{46}\text{CO}_2$	$\sigma$	Sample	Material	$\delta^{45}\text{CO}_2$	$\sigma$	$\delta^{46}\text{CO}_2$	$\sigma$
<b>20-Aug-08</b>											
UWG-2	gt	7.506	0.014	4.11	0.024	SCPX	opx	7.487	0.016	4.01	0.02
SCPX	opx	7.511	0.011	4.04	0.017	SCOL	ol	7.468	0.018	3.48	0.023
SCOL	ol	7.510	0.015	3.60	0.026	UWG-2	gt	7.508	0.012	4.04	0.018
UWG-2	gt	7.484	0.014	3.96	0.025	NWA 998	HCl cpx	7.482	0.016	3.20	0.019
SCPX	opx	7.577	0.012	4.09	0.02	NWA 998	HCl cpx	7.47	0.018	3.19	0.028
Lafayette	cpx	7.499	0.007	3.16	0.033	NWA 998	HCl cpx	7.474	0.01	3.16	0.014
UWG-2	gt	7.518	0.018	4.08	0.029	NWA 998	HCl cpx	7.469	0.016	3.06	0.032
NWA 1950	px	7.503	0.020	2.82	0.036	UWG-2	gt	7.45	0.014	3.98	0.018
NWA 1950	ol	7.474	0.011	2.65	0.031	SCPX	opx	7.493	0.014	4.02	0.024
UWG-2	gt	7.528	0.017	4.18	0.032	SCOL	ol	7.443	0.018	3.32	0.036
ALH A77005	ol	7.485	0.019	2.63	0.016	NWA 998	cpx	7.472	0.012	3.18	0.019
SCOL	ol	7.475	0.016	3.20	0.025	NWA 998	cpx	7.458	0.013	3.26	0.03
UWG-2	gt	7.470	0.026	3.82	0.042	NWA 998	cpx	7.484	0.018	3.25	0.03
SCPX	opx	7.505	0.010	4.02	0.024	NWA 998	cpx	7.478	0.014	3.22	0.027
SCOL	ol	7.503	0.018	3.57	0.029	UWG-2	gt	7.476	0.021	4.09	0.028
UWG-2	gt	7.503	0.021	4.04	0.037	SCPX	opx	7.479	0.007	3.93	0.021
<b>24-Aug-08</b>											

Table A.1 continued.

Sample	Material	$\delta^{45}\text{CO}_2$	$\sigma$	$\delta^{46}\text{CO}_2$	$\sigma$	Sample	Material	$\delta^{45}\text{CO}_2$	$\sigma$	$\delta^{46}\text{CO}_2$	$\sigma$
<b>28-Aug-08</b>											
UWG-2	gt	7.512	0.011	4.02	0.022	UWG-2	gt	7.526	0.019	4.21	0.02
UWG-2	gt	7.508	0.014	4.18	0.023	Lafayette	cpx	7.374	0.013	2.96	0.026
SCPX	opx	7.498	0.018	4.03	0.022	NWA 1950	ol	7.423	0.014	2.61	0.019
SCPX HCl	opx	7.498	0.014	4.08	0.016	UWG-2	gt	7.379	0.01	3.92	0.036
SCPX HF	opx	7.513	0.025	4.13	0.023	NWA 1950	px	7.445	0.14	2.96	0.037
NWA 998 HF	cpx	7.486	0.013	3.28	0.029	ALH A77005	ol	7.306	0.014	2.32	0.022
UWG-2	gt	7.491	0.018	4.09	0.037	UWG-2	gt	7.397	0.026	3.94	0.017
SCPX HCl	opx	7.454	0.019	3.88	0.027	Lafayette	cpx	7.378	0.014	2.91	0.025
SCPX HCl	opx	7.531	0.022	4.17	0.017	UWG-2	gt	7.44	0.016	3.88	0.026
SCPX HF	opx	7.503	0.021	4.05	0.028	NWA 1950	px	7.388	0.011	2.77	0.03
SCPX HF	opx	7.5	0.008	3.94	0.036	UWG-2	gt	7.409	0.009	3.91	0.031
UWG-2	gt	7.487	0.019	4.11	0.03	ALH A77005	ol	7.373	0.021	2.41	0.037
NWA 998 HF	cpx	7.448	0.016	3.15	0.027	Lafayette	ol	7.28	0.016	2.66	0.027
NWA 998 HF	cpx	7.451	0.018	3.12	0.029	UWG-2	gt	7.388	0.011	3.79	0.029
SCPX	opx	7.479	0.014	3.84	0.031	UWG-2	gt	7.368	0.014	3.71	0.029
UWG-2	gt	7.499	0.02	4.17	0.035	NWA 998	ol	7.329	0.015	2.57	0.036
SCPX	opx	7.491	0.019	4.04	0.033	UWG-2	gt	7.395	0.013	4.16	0.037
UWG-2	gt	7.502	0.016	4.06	0.019						
SCPX HCl	opx	7.498	0.012	4.11	0.042						
SCPX HCl	opx	7.472	0.022	3.94	0.028						
SCPX HF	opx	7.486	0.023	3.96	0.018						
NWA 998 HF	cpx	7.459	0.006	3.03	0.023						
UWG-2	gt	7.479	0.016	4.03	0.039						

Table A.1 continued.

Sample	Material	$\delta^{45}\text{CO}_2$	$\sigma$	$\delta^{46}\text{CO}_2$	$\sigma$	Sample	Material	$\delta^{45}\text{CO}_2$	$\sigma$	$\delta^{46}\text{CO}_2$	$\sigma$
<b>29-Jan-09</b>											
UWG-2	gt	7.346	0.014	3.72	0.042	UWG-2	gt	8.838	0.029	4.17	0.021
UWG-2	gt	7.419	0.011	3.83	0.027	SCOL	ol	8.849	0.016	4.14	0.012
NWA 998	ol	7.489	0.014	2.91	0.027	Lafayette	ol	8.819	0.027	3.24	0.023
UWG-2	gt	7.442	0.011	3.85	0.035	NWA 998	ol	8.777	0.017	3.15	0.034
UWG-2	gt	7.436	0.013	3.95	0.04	ALH A77005	ol	8.824	0.016	2.91	0.038
Lafayette	cpx	7.439	0.011	3.08	0.031	SCOL	ol	8.792	0.007	3.71	0.035
Lafayette	ol	7.437	0.026	2.97	0.036	UWG-2	gt	8.891	0.014	4.27	0.021
UWG-2	gt	7.45	0.015	3.77	0.031	SCPX	opx	8.831	0.013	4.24	0.02
<b>9-May-09</b>											
UWG-2	gt	8.802	0.018	4.09	0.03	NWA 2986	px	8.833	0.011	2.96	0.021
SCOL	ol	8.818	0.02	3.78	0.039	NWA 2986	msk	8.846	0.017	3.57	0.028
NWA 1950	ol	8.756	0.008	2.67	0.026	UWG-2	gt	8.908	0.02	4.31	0.03
NWA 1950	px	8.791	0.015	3.04	0.03	UWG-2	gt	8.826	0.02	4.22	0.025
UWG-2	gt	8.83	0.012	4.18	0.032	<b>1-Jul-09</b>					
UWG-2	gt	8.816	0.014	4.09	0.039	UWG-2	gt	8.748	0.023	4.21	0.032
SCOL	ol	8.809	0.009	3.61	0.016	SCPX	opx	8.747	0.012	4.11	0.028
Lafayette	ol	8.792	0.01	3.02	0.029	Shergotty	px	8.728	0.009	3.09	0.022
NWA 998	ol	8.799	0.017	2.92	0.016	NWA 2986	px	8.71	0.013	2.98	0.019
ALH A77005	ol	8.77	0.017	2.65	0.029	SCPX	opx	8.718	0.021	4.01	0.029
UWG-2	gt	8.817	0.008	4.11	0.02	UWG-2	gt	8.781	0.011	4.10	0.029
SCOL	ol	8.768	0.016	3.57	0.037	UWG-2	gt	8.734	0.019	4.11	0.025
UWG-2	gt	8.807	0.016	4.19	0.017	Shergotty	msk	8.746	0.021	3.42	0.022
						NWA 2986	msk	8.725	0.019	3.37	0.027
						UWG-2	gt	8.727	0.018	3.95	0.021
						UWG-2	gt	8.75	0.014	4.04	0.026

Table A.1 continued.

Sample	Material	$\delta^{45}\text{CO}_2$	$\sigma$	$\delta^{46}\text{CO}_2$	$\sigma$	Sample	Material	$\delta^{45}\text{CO}_2$	$\sigma$	$\delta^{46}\text{CO}_2$	$\sigma$
<b>13-Aug-09</b>											
UWG-2	gt	8.785	0.017	4.63	0.033	UWG-2	gt	8.819	0.02	4.599	0.023
SCPX	opx	8.767	0.012	4.53	0.025	SCOL	ol	8.794	0.017	4.018	0.029
ALH 84001	opx	8.777	0.017	3.96	0.029	DaG 476	px	8.801	0.011	3.505	0.016
Shergotty	px	8.765	0.022	3.57	0.027	NWA 2046	px	8.787	0.011	3.311	0.03
Nakhla	cpx	8.765	0.023	3.79	0.018	UWG-2	gt	8.779	0.017	4.392	0.029
SCPX	opx	8.775	0.01	4.44	0.022	SCOL	ol	8.783	0.018	3.978	0.02
UWG-2	gt	8.776	0.029	4.597	0.02	UWG-2	gt	8.794	0.011	4.535	0.018
UWG-2	gt	8.767	0.019	4.536	0.031	Nakhla	cpx	8.747	0.013	3.41	0.016
Shergotty	msk	8.781	0.011	4.112	0.021	NWA 2046	ol	8.765	0.013	3.214	0.029
ALH 84001	opx	8.765	0.014	3.699	0.036	SCOL	ol	8.751	0.015	3.731	0.016
SCPX	opx	8.784	0.011	4.43	0.028	UWG-2	gt	8.78	0.019	4.542	0.023
UWG-2	gt	8.776	0.017	4.607	0.041	<b>11-Nov-09</b>					
UWG-2	gt	8.774	0.011	4.554	0.026	UWG-2	gt	8.822	0.021	4.494	0.036
<b>10-Sep-09</b>											
UWG-2	gt	8.791	0.015	4.579	0.021	SCOL	ol	8.773	0.02	3.838	0.021
SCPX	opx	8.778	0.014	4.452	0.027	ALH A77005	px	8.797	0.018	3.413	0.021
ALH 84001	opx	8.798	0.016	3.749	0.031	Dho 019	px	8.796	0.015	3.599	0.045
Nakhla	cpx	8.758	0.021	3.461	0.027	UWG-2	gt	8.815	0.018	4.466	0.03
NWA 2046	px	8.779	0.012	3.48	0.023	SCOL	ol	8.781	0.011	3.879	0.023
SCPX	opx	8.791	0.025	4.351	0.035	DaG 476	px	8.801	0.016	3.459	0.026
UWG-2	gt	8.754	0.018	4.471	0.018	UWG-2	gt	8.817	0.015	4.349	0.013
UWG-2	gt	8.797	0.013	4.519	0.016	UWG-2	gt	8.804	0.018	4.399	0.013
NWA 2046	ol	8.754	0.02	2.875	0.019						
UWG-2	gt	8.79	0.011	4.451	0.02						

Table A.1 continued.

Sample	Material	$\delta^{45}\text{CO}_2$	$\sigma$	$\delta^{46}\text{CO}_2$	$\sigma$	Sample	Material	$\delta^{45}\text{CO}_2$	$\sigma$	$\delta^{46}\text{CO}_2$	$\sigma$
<b>19-Jan-10</b>											
UWG-2	gt	8.687	0.021	4.385	0.021	UWG-2	gt	8.8	0.009	4.519	0.016
SCPX	opx	8.795	0.008	4.166	0.037	SCOL	ol	8.791	0.022	3.783	0.033
UWG-2	gt	8.697	0.012	4.213	0.017	NWA 4468	px	8.782	0.012	3.413	0.021
Zagami	px	8.733	0.017	3.218	0.019	ALH A77005	px	8.77	0.013	3.15	0.036
SaU 005	px	8.778	0.026	3.43	0.022	UWG-2	gt	8.795	0.018	4.363	0.034
NWA 4468	px	8.721	0.017	3.179	0.025	SCPX	opx	8.785	0.016	4.183	0.021
UWG-2	gt	8.752	0.015	4.408	0.03	NWA 2046	ol	8.753	0.028	3.083	0.035
SCPX	opx	8.722	0.012	4.17	0.022	DaG 476	ol	8.79	0.015	4.039	0.034
SCOL	ol	8.792	0.019	3.971	0.018	UWG-2	gt		4.39		
SaU 005	ol	8.68	0.019	2.861	0.034	SCOL	ol	8.785	0.028	3.723	0.036
NWA 2737	ol	8.764	0.013	2.941	0.013	UWG-2	gt	8.79	0.02	4.408	0.026
UWG-2	gt	8.736	0.019	4.309	0.021	<b>11-May-11</b>					
SCOL	ol	8.743	0.009	3.687	0.015	UWG-2	gt	8.839	0.02	4.568	0.013
NWA 4468	msk	8.752	0.011	3.522	0.033	NWA 2986	msk	8.861	0.022	4.105	0.029
Zagami	msk	8.76	0.014	3.611	0.017	Shergotty	msk	8.83	0.031	3.947	0.02
						Zagami	msk	8.832	0.02	3.843	0.026
						NWA 4468	msk	8.837	0.019	3.64	0.039
						UWG-2	gt	8.822	0.021	4.399	0.04
						SCOL	ol	8.799	0.011	3.718	0.031
						DaG 476	ol	8.821	0.015	4	0.018
						DaG 476	px	8.797	0.024	3.677	0.033
						Zagami	px	8.79	0.012	3.259	0.012
						SCPX	px	8.801	0.014	4.297	0.011
						UWG-2	gt	8.811	0.021	4.436	0.032
						UWG-2	gt	8.829	0.015	4.465	0.022

Table A.2. Raw data from all MAT 252 sessions.

Sample	Material	$\delta^{33}\text{O}_2$	$\sigma$	$\delta^{34}\text{O}_2$	$\sigma$	Sample	Material	$\delta^{33}\text{O}_2$	$\sigma$	$\delta^{34}\text{O}_2$	$\sigma$
<b>9-Jun-09</b>						<b>30-Sep-09</b>					
UWG-2	gt	-11.17	0.06	-21.74	0.03	UWG-2	gt	-11.18	0.06	-21.80	0.05
UWG-2	gt	-11.10	0.04	-21.62	0.02	UWG-2	gt	-11.13	0.04	-21.69	0.05
SCPX	opx	-11.04	0.05	-21.52	0.04	SCOL	ol	-11.44	0.05	-22.24	0.06
NWA 998	cpx	-11.35	0.04	-22.67	0.03	NWA 1950	ol	-11.65	0.05	-23.21	0.09
SCOL	ol	-11.41	0.05	-22.18	0.02	UWG-2	gt	-11.28	0.04	-22.03	0.04
ALH A77005	ol	-11.59	0.05	-23.13	0.02	UWG-2	gt	-11.24	0.06	-21.84	0.07
SCOL	ol	-11.46	0.06	-22.22	0.03	<b>14-Oct-09</b>					
NWA 998	cpx	-11.36	0.05	-22.60	0.03	UWG-2	gt	-11.18	0.04	-21.79	0.07
SCPX	opx	-11.13	0.07	-21.63	0.03	UWG-2	gt	-11.16	0.05	-21.82	0.08
<b>17-Sep-09</b>						SCPX	opx	-11.19	0.04	-21.79	0.05
UWG-2	gt	-11.19	0.05	-21.79	0.05	ALH 84001	opx	-11.30	0.05	-22.61	0.04
UWG-2	gt	-11.15	0.14	-21.71	0.12	Shergotty	px	-11.46	0.04	-22.91	0.02
SCPX	px	-11.30	0.10	-21.98	0.10	UWG-2	gt	-11.20	0.07	-21.83	0.09
NWA 998	cpx	-11.31	0.08	-22.60	0.06	UWG-2	gt	-11.16	0.05	-21.76	0.07
NWA 998 HCl	cpx	-11.28	0.06	-22.56	0.04	<b>18-Nov-09</b>					
SCOL	ol	-11.47	0.08	-22.29	0.08	UWG-2	gt	-11.14	0.06	-21.78	0.04
UWG-2	gt	-11.14	0.09	-21.69	0.09	UWG-2	gt	-11.14	0.05	-21.72	0.04
<b>18-Sep-09</b>						SCOL	ol	-11.43	0.05	-22.28	0.04
UWG-2	gt	-11.29	0.07	-21.95	0.08	NWA 1950	ol	-11.62	0.06	-23.21	0.06
UWG-2	gt	-11.17	0.04	-21.76	0.06	Nakhla	cpx	-11.37	0.06	-22.75	0.06
SCOL	ol	-11.46	0.07	-22.30	0.07	SCOL	ol	-11.47	0.06	-22.31	0.05
NWA 998	cpx	-11.45	0.05	-22.84	0.05	UWG-2	gt	-11.16	0.04	-21.72	0.04
NWA 998 HF	cpx	-11.39	0.06	-22.77	0.07	UWG-2	gt	-11.16	0.05	-21.75	0.04
UWG-2	gt	-11.15	0.06	-21.68	0.07						

Table A.2 continued.

<b>Sample</b>	<b>Material</b>	$\delta^{33}\text{O}_2$	$\sigma$	$\delta^{34}\text{O}_2$	$\sigma$
<b>13-May-10</b>					
UWG-2	gt	-11.14	0.08	-21.78	0.05
UWG-2	gt	-11.15	0.09	-21.80	0.05
NWA 4468	px	-11.33	0.07	-22.75	0.04
NWA 2986	px	-11.47	0.06	-22.94	0.04
UWG-2	gt	-11.14	0.08	-21.80	0.04
<b>18-May-10</b>					
UWG-2	gt	-11.15	0.06	-21.82	0.03
UWG-2	gt	-11.16	0.04	-21.81	0.03
Lafayette	cpx	-11.37	0.04	-22.77	0.02
Zagami	px	-11.46	0.04	-22.99	0.02
NWA 2737	ol	-11.58	0.04	-23.22	0.02
UWG-2	gt	-11.17	0.03	-21.85	0.03

*Appendix B*

## RAW DATA AND CALIBRATION CURVES FOR CHAPTER II

Data for chapter II was acquired from one SIMS session and five NanoSIMS sessions. I analyzed SNC apatites in the SIMS session, which occurred in January of 2011. The raw data from the SIMS session can be found in table B.1, and the calibration curves can be found in figures B.1 – B.4. I analyzed SNC apatites over three NanoSIMS sessions, and the last two of the five NanoSIMS sessions were used for analyzing SNC and terrestrial olivines, as well as terrestrial apatite. The NanoSIMS sessions occurred during June and December of 2011, and February, May, and June of 2012 and the raw data can be found in tables B.2 – B.6 (respectively), and the calibration curves can be found in figures B.5 – B.23 (respectively).

Table B.1. Raw data from the January 2011 SIMS session.

Sample	$^{12}\text{C}/^{18}\text{O}$	$\sigma$	$^{16}\text{OH}/^{18}\text{O}$	$\sigma$	$^{19}\text{F}/^{18}\text{O}$	$\sigma$	$^{31}\text{P}/^{18}\text{O}$	$\sigma$	$^{32}\text{S}/^{18}\text{O}$	$\sigma$	$^{35}\text{Cl}/^{18}\text{O}$	$\sigma$	Cl+F+OH
<b>In-House Standards</b>													
Durango 0_1	0.000	0.000	0.359	0.004	99.562	0.705	15.536	0.110	1.641	0.014	5.835	0.048	1.03
Durango 0_2	0.000	0.000	0.363	0.004	99.094	0.834	15.587	0.167	1.603	0.020	5.674	0.062	1.02
<b>External Standards</b>													
Synthetic FAp 1	0.000	0.000	0.060	0.002	106.694	1.082	16.116	0.121	0.010	0.001	0.003	0.001	1.01
Synthetic FAp 2	0.000	0.000	0.053	0.004	107.039	0.779	15.961	0.129	0.010	0.001	0.005	0.000	1.01
Synthetic ClAp 1	0.000	0.000	0.022	0.001	0.020	0.001	16.276	0.152	0.010	0.001	109.704	1.189	1.09
Synthetic ClAp 2	0.000	0.000	0.013	0.001	0.020	0.001	16.365	0.125	0.003	0.001	109.830	0.004	1.09
<b>Samples</b>													
JaH 479 Msk 1_1	0.000	0.000	0.008	0.001	0.437	0.067	0.009	0.001	0.000	0.000	0.435	0.070	
JaH 479 Ap 1_1	0.011	0.001	2.069	0.083	42.209	0.336	14.876	0.089	2.097	0.106	33.033	0.480	0.95
<sup>3</sup> JaH 479 Ap 2_1a	0.075	0.004	5.517	0.115	30.584	1.443	14.224	0.492	3.698	0.096	22.633	0.178	1.11
JaH 479 Ap 3_1	0.013	0.001	2.407	0.053	41.603	0.182	14.969	0.066	3.339	0.076	30.134	0.411	0.95
<sup>1</sup> JaH 479 Ap 4_1	0.017	0.001	2.680	0.033	18.502	0.271	18.056	0.387	2.039	0.055	44.445	0.829	
<sup>1</sup> JaH 479 Ap 5_1	0.145	0.026	2.990	0.056	39.585	0.644	19.533	0.123	2.661	0.056	26.800	0.256	
<b>In-House Standards</b>													
Durango 0_3	0.000	0.000	0.361	0.003	96.783	0.418	15.673	0.048	1.541	0.017	5.437	0.050	1.00
Durango 0_4	0.000	0.000	0.367	0.003	96.677	0.520	15.521	0.058	1.530	0.011	5.406	0.044	1.00
<b>External Standard</b>													
Synthetic ClAp 3	0.000	0.000	0.013	0.001	0.019	0.001	16.248	0.071	0.003	0.000	100.536	0.376	1.00
<b>Samples</b>													
JaH 479 Msk 2_1	0.000	0.000	0.003	0.000	0.341	0.075	0.010	0.000	0.000	0.000	0.306	0.057	
JaH 479 Ap 2_1b	0.036	0.013	4.305	0.357	36.299	1.272	14.165	0.267	1.563	0.123	16.764	0.342	0.98
<sup>1</sup> JaH 479 Ap 2_1c	0.029	0.003	4.353	0.120	32.288	1.636	17.412	0.639	1.658	0.057	16.660	0.223	

<sup>1</sup>Discarded due to inconsistent  $^{31}\text{P}/^{18}\text{O}$ .<sup>3</sup>Discarded due to Cl+F+OH either <0.85 or >1.10.

Table B.1 continued.

Sample	$^{12}\text{C}/^{18}\text{O}$	$\sigma$	$^{16}\text{OH}/^{18}\text{O}$	$\sigma$	$^{19}\text{F}/^{18}\text{O}$	$\sigma$	$^{31}\text{P}/^{18}\text{O}$	$\sigma$	$^{32}\text{S}/^{18}\text{O}$	$\sigma$	$^{35}\text{Cl}/^{18}\text{O}$	$\sigma$	Cl+F+OH
<b>Samples</b>													
JaH 479 Ap 6_1a	0.118	0.011	2.859	0.072	48.201	0.220	14.514	0.090	1.450	0.221	22.307	0.253	0.98
JaH 479 Ap 6_1b	0.081	0.005	3.107	0.098	49.974	0.751	14.941	0.189	1.537	0.142	23.590	0.639	1.04
JaH 479 Ap 7_1a	0.084	0.004	2.057	0.040	39.528	0.281	15.060	0.069	2.480	0.146	32.472	0.203	0.92
<sup>2</sup> JaH 479 Ap 7_1b	1.485	0.174	2.304	0.039	42.245	0.531	14.813	0.153	2.699	0.079	33.918	0.395	
<sup>2</sup> JaH 479 Ap 7_1c	0.724	0.086	2.354	0.129	44.125	1.683	14.848	0.541	2.719	0.102	34.533	1.184	
JaH 479 Ap 8_1	0.024	0.004	2.339	0.025	50.819	0.246	14.984	0.070	1.598	0.042	21.299	0.388	0.94
JaH 479 Ap 8_2	0.008	0.001	1.888	0.020	51.948	0.266	14.874	0.096	1.251	0.029	23.396	0.265	0.92
JaH 479 Ap 8_3	0.015	0.001	2.402	0.032	40.402	0.269	14.800	0.079	1.991	0.045	28.791	0.203	0.93
JaH 479 Ap 9_1	0.021	0.001	1.816	0.024	54.793	0.420	15.217	0.072	1.603	0.046	23.156	0.159	
JaH 479 Ap 9_2a	0.046	0.011	2.618	0.237	51.838	0.466	14.704	0.220	2.099	0.126	25.739	0.563	
<sup>1</sup> JaH 479 Ap 9_2b	0.026	0.006	2.494	0.220	47.817	0.797	18.230	1.144	2.057	0.186	27.686	1.127	
JaH 479 Ap 10_1	0.024	0.001	2.429	0.063	40.126	0.380	14.818	0.097	2.287	0.030	27.403	0.411	0.91
JaH 479 Ap 11_1	0.015	0.001	1.804	0.047	68.519	0.698	14.459	0.124	1.610	0.063	18.606	0.370	1.02
<sup>3</sup> NWA 2986 Ap 1_1	0.010	0.001	2.520	0.015	4.121	0.020	15.077	0.066	1.376	0.098	27.566	0.079	0.59
NWA 2986 Ap 1_2	0.012	0.002	2.643	0.042	35.358	0.435	15.658	0.118	1.361	0.040	27.718	0.256	0.89
NWA 2986 Ap 2_1	0.078	0.007	2.152	0.031	25.007	0.337	14.486	0.116	0.974	0.012	43.320	1.116	0.90
NWA 2986 Ap 3_1	0.022	0.003	1.588	0.028	49.291	0.316	15.175	0.154	2.268	0.616	26.380	0.161	0.90
NWA 2986 Ap 4_1	0.011	0.001	1.526	0.022	35.019	0.358	14.068	0.167	0.835	0.016	38.302	0.665	0.88
NWA 2986 Ap 5_1	0.023	0.001	2.183	0.020	36.831	0.342	15.382	0.176	0.857	0.016	29.106	0.624	0.87
<b>In-House Standards</b>													
Durango 0_5	0.000	0.000	0.343	0.003	98.813	0.475	15.526	0.065	1.564	0.021	5.681	0.054	1.02
Durango 0_6	0.000	0.000	0.342	0.003	99.012	0.564	15.525	0.080	1.537	0.014	5.701	0.032	1.02

<sup>1</sup>Discarded due to inconsistent  $^{31}\text{P}/^{18}\text{O}$ .<sup>2</sup>Discarded due to a positive correlation of C and OH.<sup>3</sup>Discarded due to Cl+F+OH either  $<0.85$  or  $>1.10$ .

Table B.1 continued.

Sample	$^{12}\text{C}/^{18}\text{O}$	$\sigma$	$^{16}\text{OH}/^{18}\text{O}$	$\sigma$	$^{19}\text{F}/^{18}\text{O}$	$\sigma$	$^{31}\text{P}/^{18}\text{O}$	$\sigma$	$^{32}\text{S}/^{18}\text{O}$	$\sigma$	$^{35}\text{Cl}/^{18}\text{O}$	$\sigma$	CI+F+OH
<b>External Standard</b>													
Synthetic CIAp 4	0.000	0.000	0.012	0.001	0.019	0.001	16.107	0.083	0.002	0.000	101.347	0.814	1.01
<b>Samples</b>													
NWA 1950 Ap 1_1	0.000	0.000	0.360	0.005	57.260	0.311	15.299	0.433	0.273	0.006	33.705	0.229	0.91
NWA 1950 Ap 1_2	0.116	0.098	0.491	0.040	72.119	0.584	15.586	0.136	0.155	0.008	25.543	1.067	0.98
<sup>1</sup> NWA 1950 Ap 1_3	0.008	0.001	0.195	0.010	17.780	0.343	8.822	0.155	0.070	0.005	6.228	0.271	
NWA 1950 Ap 2_1a	0.161	0.040	1.331	0.041	82.928	0.598	16.409	0.136	0.089	0.007	4.522	0.060	0.97
NWA 1950 Ap 2_1b	0.188	0.028	1.396	0.015	81.875	0.901	15.457	0.111	0.095	0.004	6.894	0.070	0.99
NWA 998 Ap 1_1	0.015	0.002	0.334	0.005	49.353	0.299	15.587	0.076	0.036	0.002	45.168	0.431	0.95
NWA 998 Ap 2_1a	0.034	0.001	0.330	0.010	52.193	0.255	16.024	0.104	0.016	0.004	45.047	0.349	0.97
<sup>1</sup> NWA 998 Ap 2_1b	3.485	2.948	0.679	0.257	51.056	0.507	17.433	0.763	0.067	0.009	42.420	0.748	
NWA 998 Ap 3_1	0.212	0.018	0.535	0.007	48.661	0.287	15.453	0.081	0.113	0.007	45.891	0.289	0.97
<b>External Standards</b>													
Ap004 1	0.000	0.000	2.544	0.012	67.372	0.274	15.037	0.084	2.212	0.028	5.775	0.063	0.97
Ap004 2	0.000	0.000	2.536	0.011	67.348	0.253	14.976	0.088	2.203	0.029	5.792	0.059	0.96
Ap005 1	0.000	0.000	1.955	0.019	68.500	0.483	15.371	0.106	0.873	0.010	14.037	0.091	0.99
Ap005 2	0.000	0.000	1.960	0.017	68.511	0.430	15.506	0.079	0.886	0.010	14.025	0.064	0.99
Ap003 1	0.000	0.000	0.203	0.003	98.900	0.319	15.333	0.067	2.193	0.032	6.293	0.027	1.01
Ap003 2	0.000	0.000	0.206	0.002	99.756	0.447	15.254	0.073	2.246	0.025	6.341	0.043	1.02
<b>Samples</b>													
NWA856 Msk 1_1	0.000	0.000	0.006	0.001	0.002	0.000	0.009	0.001	0.000	0.000	0.001	0.000	
NWA856 crack	18.458	4.196	1.785	0.191	0.029	0.001	0.038	0.004	0.054	0.005	0.927	0.236	
NWA856 crack	15.607	1.125	1.705	0.036	9.174	0.262	7.954	0.402	0.693	0.072	17.213	0.400	
NWA856 crack	47.482	5.707	12.993	0.610	53.304	3.897	30.520	5.805	0.654	0.053	58.183	3.375	
NWA 856 Ap 1_1	0.078	0.009	2.835	0.058	17.697	0.165	15.548	0.154	0.465	0.037	49.488	0.368	0.97

<sup>1</sup>Discarded due to inconsistent  $^{31}\text{P}/^{18}\text{O}$ .

Table B.1 continued.

Sample	$^{12}\text{C}/^{18}\text{O}$	$\sigma$	$^{16}\text{OH}/^{18}\text{O}$	$\sigma$	$^{19}\text{F}/^{18}\text{O}$	$\sigma$	$^{31}\text{P}/^{18}\text{O}$	$\sigma$	$^{32}\text{S}/^{18}\text{O}$	$\sigma$	$^{35}\text{Cl}/^{18}\text{O}$	$\sigma$	Cl+F+OH
Samples													
NWA 856 Ap 1_2	0.084	0.006	2.937	0.097	16.691	0.421	14.823	0.411	0.713	0.034	43.728	0.930	0.91
<sup>3</sup> NWA 856 Ap 2_1	0.028	0.001	1.819	0.010	6.803	0.081	14.879	0.072	0.424	0.007	19.957	0.109	0.46
NWA 856 Ap 3_1	0.423	0.023	1.799	0.010	54.956	0.262	14.520	0.128	0.396	0.006	19.791	0.083	0.91
<sup>3</sup> NWA 856 Ap 4_1	0.249	0.017	2.366	0.031	37.217	24.914	14.446	0.155	0.225	0.025	17.080	0.151	0.78
<sup>3</sup> NWA 856 Ap 5_1	0.064	0.006	2.115	0.013	6.575	0.066	14.442	0.283	0.384	0.008	20.134	0.096	0.49
<sup>3</sup> NWA 856 Ap 6_1	0.175	0.020	2.659	0.030	6.748	0.058	15.243	0.137	0.211	0.004	10.773	0.305	0.46

<sup>3</sup>Discarded due to Cl+F+OH either <0.85 or >1.10.

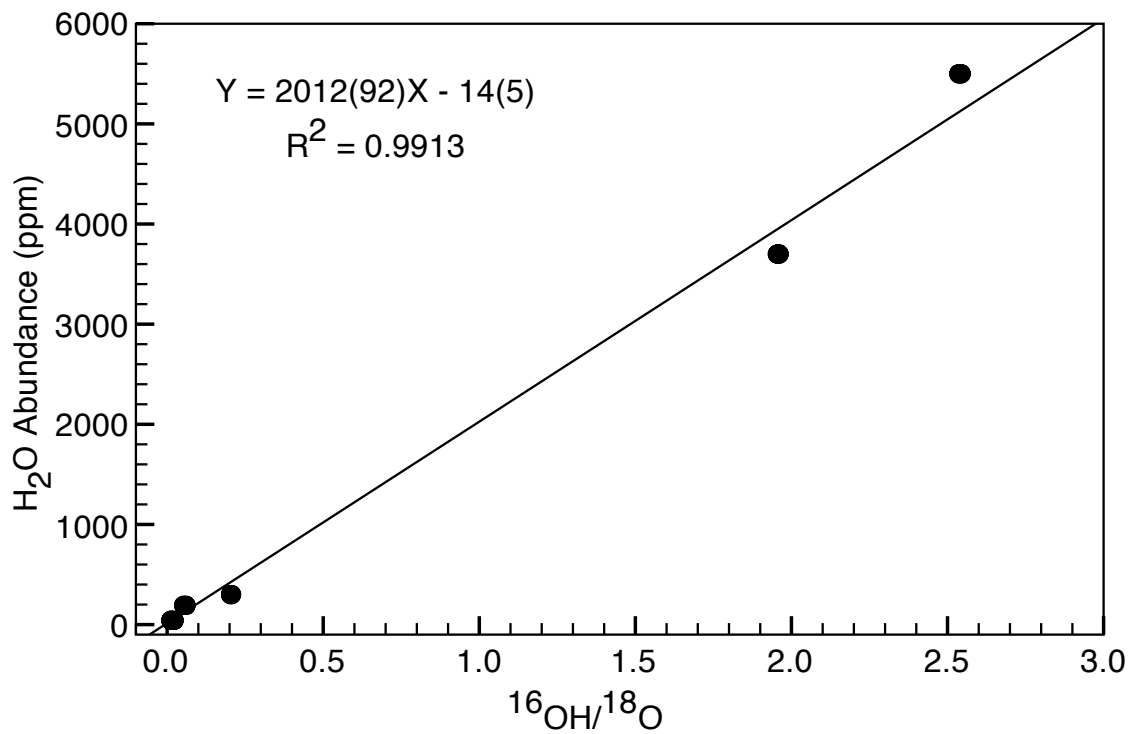


Figure B.1. Calibration curve for OH during the January 2011 SIMS session.

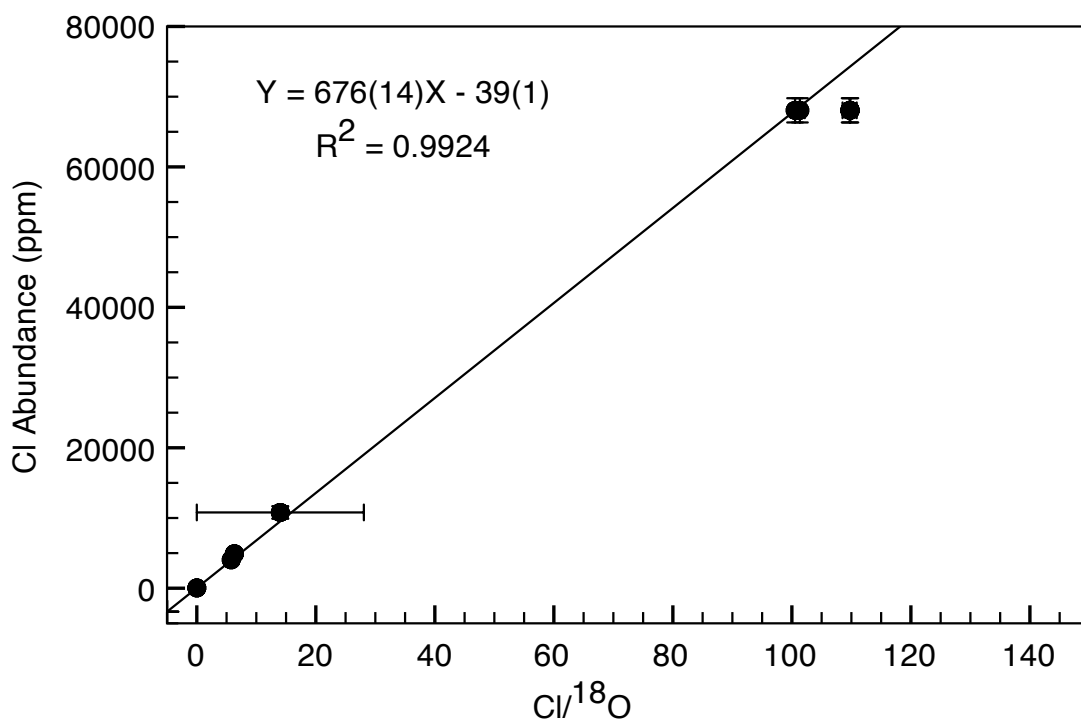


Figure B.2. Calibration curve for Cl during the January 2011 SIMS session.

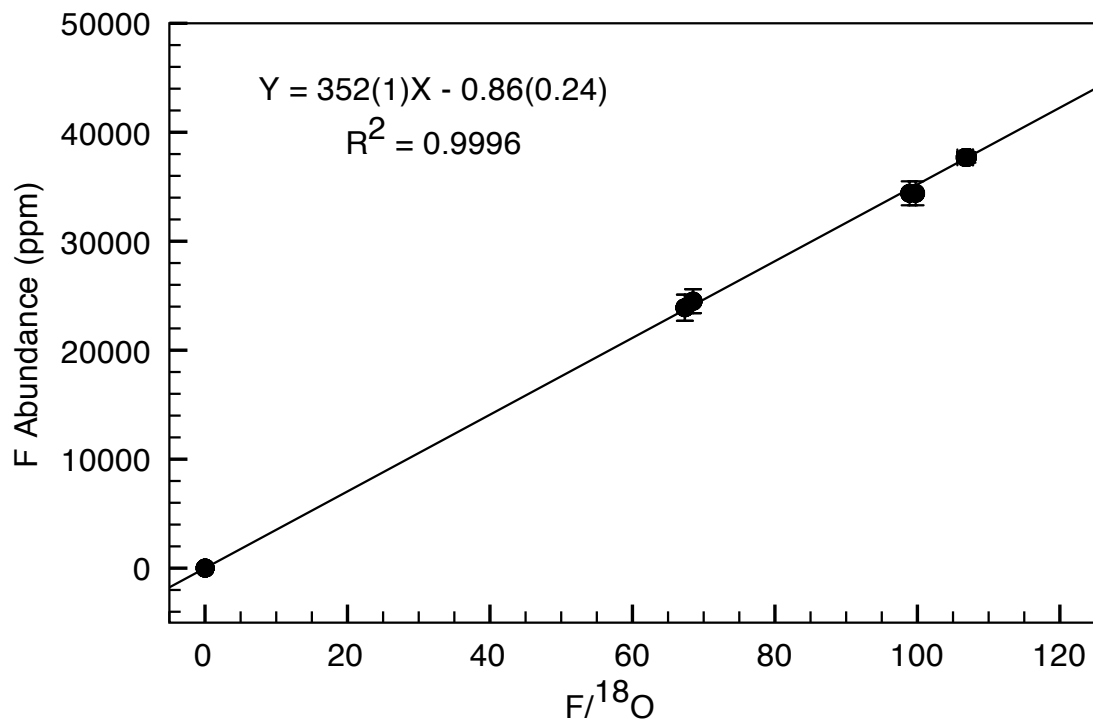


Figure B.3. Calibration curve for F during the January 2011 SIMS session.

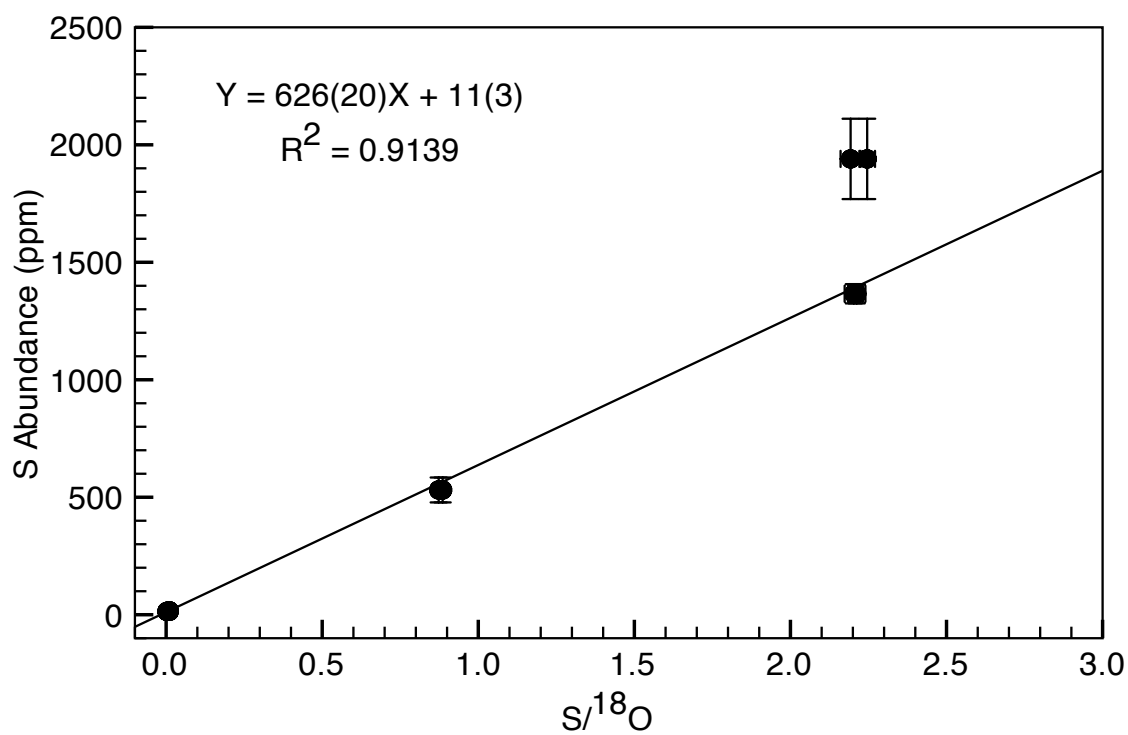


Figure B.4. Calibration curve for S during the January 2011 SIMS session.

Table B.2. Raw data from the June 2011 NanoSIMS session.

Sample	$^{12}\text{C}/^{18}\text{O}$	$\sigma$	$^{16}\text{OH}/^{18}\text{O}$	$\sigma$	$^{19}\text{F}/^{18}\text{O}$	$\sigma$	$^{31}\text{P}/^{18}\text{O}$	$\sigma$	$^{32}\text{S}/^{18}\text{O}$	$\sigma$	$^{35}\text{Cl}/^{18}\text{O}$	$\sigma$	Cl+F+OH
<b>External Standards</b>													
Ap018 1	0.015	0.002	0.462	0.011	58.803	0.728	16.929	0.251	6.508	0.093	0.851	0.017	1.01
Ap018 2	0.014	0.002	0.484	0.012	58.181	0.881	16.906	0.321	6.323	0.104	0.739	0.017	1.00
Ap018 3	0.015	0.002	0.590	0.014	55.637	0.701	16.735	0.285	6.096	0.100	0.592	0.013	1.00
Ap004 1	0.012	0.002	0.956	0.017	41.001	0.535	16.904	0.236	1.827	0.031	3.359	0.054	0.96
Ap004 2	0.013	0.002	0.932	0.017	40.638	0.493	16.806	0.233	1.803	0.030	3.281	0.046	0.95
Ap004 3	0.012	0.001	0.949	0.016	40.732	0.505	16.784	0.288	1.802	0.033	3.293	0.048	0.96
Ap003 1	0.019	0.002	0.129	0.004	62.154	0.843	18.054	0.256	1.987	0.030	3.742	0.058	1.00
Ap003 2	0.017	0.002	0.128	0.004	61.761	0.776	17.915	0.270	1.971	0.028	3.689	0.056	0.99
Ap003 3	0.019	0.005	0.139	0.011	61.768	0.725	17.950	0.220	2.018	0.025	3.702	0.050	1.00
<b>In-House Standards</b>													
Durango 1_1	0.003	0.001	0.194	0.007	58.719	0.768	18.679	0.269	1.312	0.023	3.416	0.055	0.97
Durango 1_2	0.002	0.001	0.191	0.007	58.894	0.883	18.489	0.301	1.297	0.025	3.381	0.059	0.97
Durango 1_3	0.001	0.000	0.191	0.008	58.731	0.838	18.211	0.324	1.271	0.023	3.336	0.059	0.97
Durango 1_4	0.002	0.001	0.177	0.006	57.124	0.694	18.303	0.293	1.246	0.021	3.153	0.050	0.94
<b>External Standards</b>													
Ap003 4	0.020	0.002	0.134	0.005	62.084	0.782	17.800	0.213	2.040	0.035	3.705	0.056	1.00
Ap004 4	0.014	0.002	0.891	0.016	38.922	0.515	17.551	0.257	1.845	0.034	3.351	0.052	0.92
Ap005 1	0.005	0.001	0.694	0.015	39.519	0.523	17.244	0.248	0.697	0.016	9.998	0.145	0.97
<b>In-House Standards</b>													
Durango 2_1	0.003	0.001	0.159	0.005	56.569	0.711	18.149	0.220	1.306	0.023	2.927	0.039	0.92
Durango 2_2	0.003	0.001	0.154	0.005	56.428	0.799	18.130	0.258	1.311	0.021	2.890	0.047	0.92
<b>Samples</b>													
NWA 2737 Ap 1_1	0.004	0.001	0.325	0.009	39.488	0.547	18.189	0.257	0.011	0.001	21.812	0.319	1.06
<sup>2</sup> NWA 2737 Ap 1_2	0.018	0.002	0.480	0.013	39.781	0.556	17.746	0.284	0.080	0.004	20.014	0.328	

<sup>2</sup>Discarded due to a positive correlation of C and OH.

Table B.2 continued.

Sample	$^{12}\text{C}/^{18}\text{O}$	$\sigma$	$^{16}\text{OH}/^{18}\text{O}$	$\sigma$	$^{19}\text{F}/^{18}\text{O}$	$\sigma$	$^{31}\text{P}/^{18}\text{O}$	$\sigma$	$^{32}\text{S}/^{18}\text{O}$	$\sigma$	$^{35}\text{Cl}/^{18}\text{O}$	$\sigma$	Cl+F+OH
<b>Samples</b>													
NWA 2737 Ap 2_1a	0.003	0.001	0.339	0.010	41.877	0.549	18.236	0.257	0.043	0.003	20.075	0.265	1.06
NWA 2737 Ap 2_1b	0.002	0.001	0.338	0.008	41.988	0.597	17.930	0.256	0.039	0.003	20.223	0.303	1.07
<sup>2</sup> NWA 2737 Ap 2_2a	0.012	0.002	0.530	0.056	41.025	0.725	17.406	0.320	0.576	0.101	19.729	0.259	
NWA 2737 Ap 1_3	0.003	0.001	0.272	0.009	41.249	0.609	17.946	0.275	0.007	0.001	17.250	0.266	0.99
<b>In-House Standards</b>													
Durango 2_3	0.004	0.001	0.194	0.009	62.383	0.979	17.689	0.238	1.316	0.023	3.384	0.064	1.02
Durango 2_4	0.004	0.001	0.202	0.006	64.082	0.904	17.635	0.265	1.341	0.025	3.395	0.055	1.04
Durango 2_5	0.004	0.001	0.184	0.006	61.214	0.849	17.480	0.257	1.264	0.024	3.102	0.046	0.99
Durango 2_6	0.008	0.002	0.197	0.006	62.959	0.695	17.616	0.292	1.325	0.022	3.300	0.046	1.02
<b>Sample</b>													
<sup>1</sup> NWA 2737 Ap 2_2b	0.001	0.001	0.430	0.013	48.692	0.957	14.917	0.290	0.060	0.004	15.009	0.510	
<b>In-House Standards</b>													
Durango 2_7	0.001	0.000	0.180	0.006	61.565	0.721	18.028	0.211	1.364	0.024	3.258	0.048	1.00
Durango 2_8	0.001	0.000	0.181	0.005	61.963	0.879	17.903	0.277	1.349	0.027	3.212	0.052	1.00
<b>Sample</b>													
<sup>2</sup> NWA 2737 Ap 2_2c	0.111	0.006	0.530	0.012	37.546	0.655	17.427	0.308	0.601	0.016	21.747	0.369	
<b>In-House Standards</b>													
Durango 3_1	0.001	0.000	0.175	0.005	65.542	0.769	17.152	0.213	1.354	0.023	3.493	0.056	1.05
Durango 3_2	0.001	0.000	0.137	0.004	61.793	0.857	17.743	0.266	1.399	0.022	3.470	0.055	0.99
Durango 3_3	0.001	0.000	0.130	0.004	60.696	0.635	17.364	0.187	1.336	0.019	3.279	0.040	0.97

<sup>1</sup>Discarded due to inconsistent  $^{31}\text{P}/^{18}\text{O}$ .<sup>2</sup>Discarded due to a positive correlation of C and OH.

Table B.2 continued.

Sample	$^{12}\text{C}/^{18}\text{O}$	$\sigma$	$^{16}\text{OH}/^{18}\text{O}$	$\sigma$	$^{19}\text{F}/^{18}\text{O}$	$\sigma$	$^{31}\text{P}/^{18}\text{O}$	$\sigma$	$^{32}\text{S}/^{18}\text{O}$	$\sigma$	$^{35}\text{Cl}/^{18}\text{O}$	$\sigma$	Cl+F+OH
<b>Samples</b>													
<sup>3</sup> Shergotty Ap 3_1	0.161	0.007	1.226	0.023	3.134	0.043	17.755	0.199	0.581	0.017	38.900	0.484	1.13
<sup>3</sup> Shergotty Ap 3_2	1.223	0.200	1.213	0.068	6.553	0.068	17.465	0.187	0.452	0.016	36.281	0.476	1.13
<sup>3</sup> Shergotty Ap 3_3	1.784	0.124	1.588	0.032	4.014	0.052	17.790	0.198	0.417	0.009	35.952	0.416	1.20
Shergotty Ap 5_1	0.301	0.042	1.138	0.035	24.836	0.244	17.295	0.189	0.622	0.011	21.453	0.242	1.10
Shergotty Ap 5_2	0.221	0.013	1.132	0.024	24.932	0.285	17.450	0.197	0.628	0.012	21.458	0.241	1.10
Shergotty Ap 6_1	0.002	0.001	1.028	0.023	21.129	0.245	17.343	0.190	0.902	0.026	22.634	0.282	1.04
Shergotty Ap 6_2	0.056	0.009	1.109	0.023	23.506	0.272	17.454	0.192	0.788	0.118	20.893	0.290	1.07
Shergotty Ap 6_3	0.089	0.037	1.123	0.016	23.681	0.249	17.102	0.202	0.665	0.011	20.964	0.243	1.07
<b>In-House Standard</b>													
Durango 3_4	0.001	0.000	0.179	0.006	65.209	0.729	17.065	0.203	1.358	0.024	3.439	0.055	1.05
<b>External Standards</b>													
Ap003 5	0.012	0.001	0.133	0.004	66.883	0.609	16.986	0.173	1.986	0.021	3.800	0.040	1.06
Ap004 5	0.010	0.001	1.113	0.016	44.447	0.516	16.611	0.186	1.885	0.024	3.721	0.045	1.06
Ap005 2	0.006	0.001	0.862	0.016	42.887	0.485	17.156	0.179	0.726	0.011	11.064	0.120	1.09
<b>In-House Standard</b>													
Durango 1_5	0.001	0.000	0.203	0.005	63.878	0.706	17.403	0.203	1.283	0.019	3.496	0.045	1.04

<sup>3</sup>Discarded due to Cl+F+OH either <0.85 or >1.10.

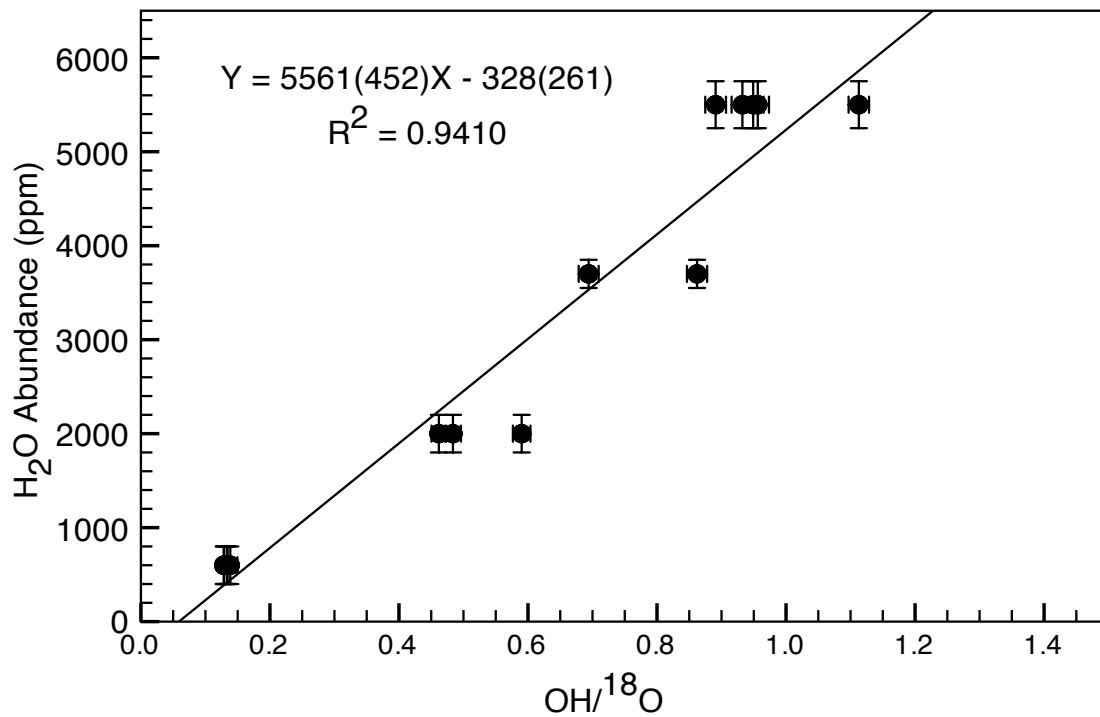


Figure B.5. Calibration curve for OH during the June 2011 NanoSIMS session.

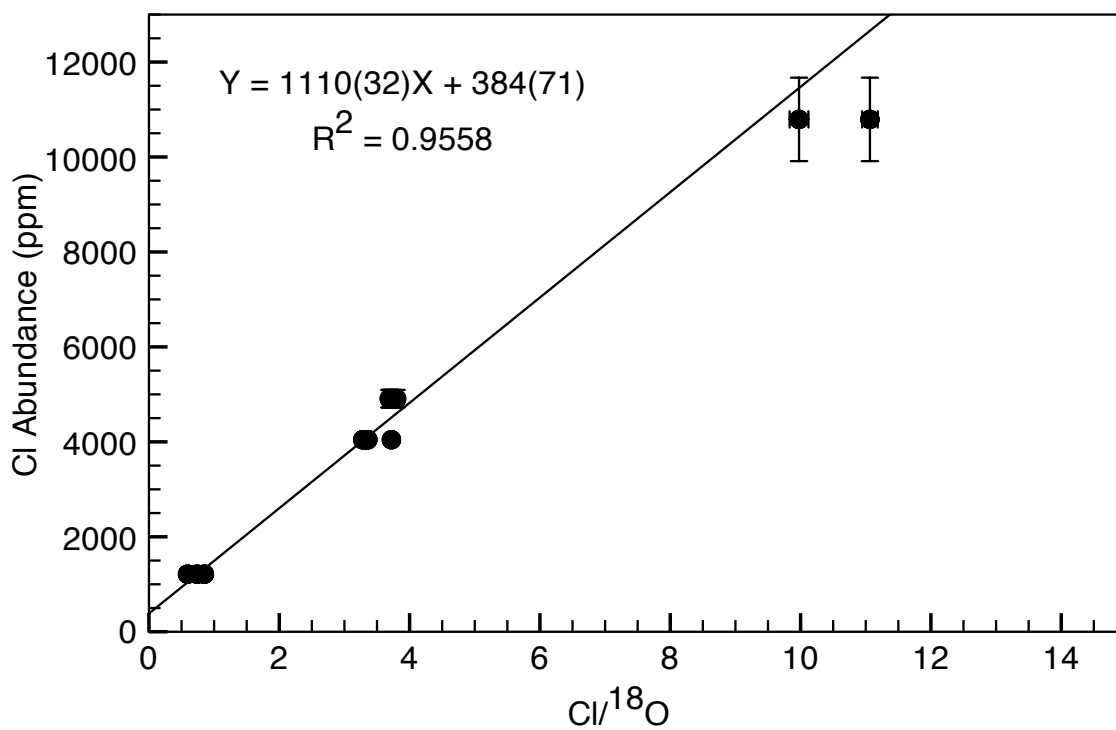


Figure B.6. Calibration curve for Cl during the June 2011 NanoSIMS session.

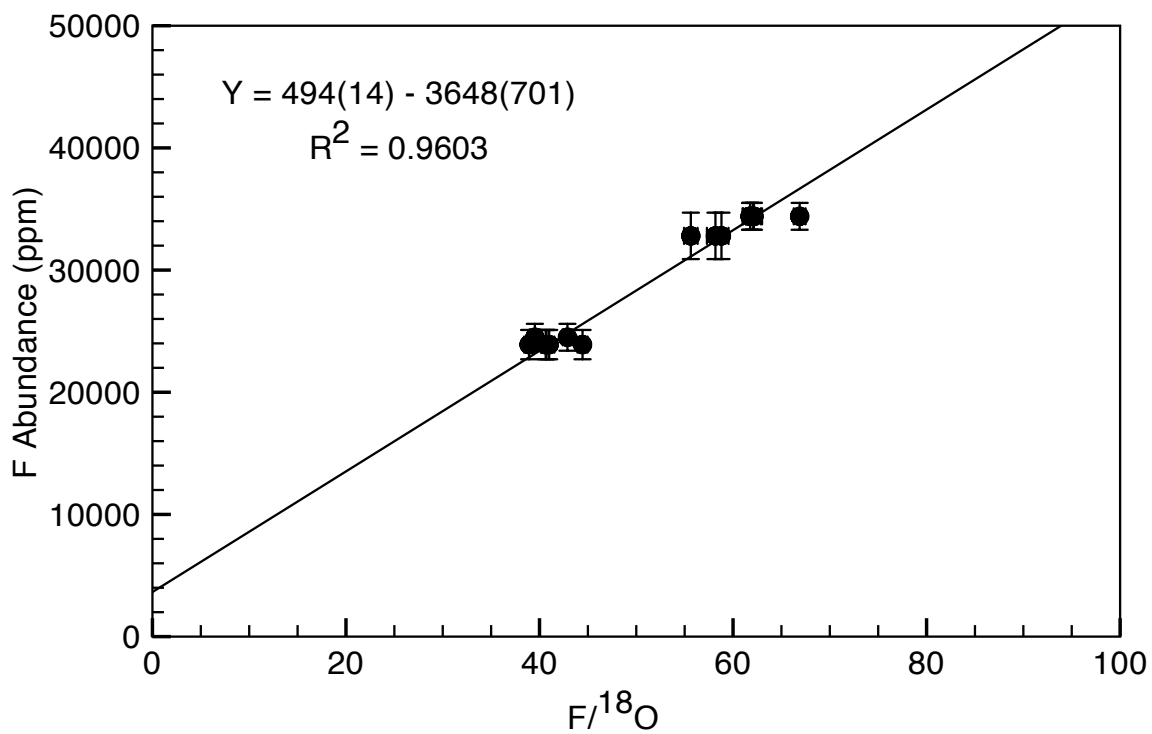


Figure B.7. Calibration curve for F during the June 2011 NanoSIMS session.

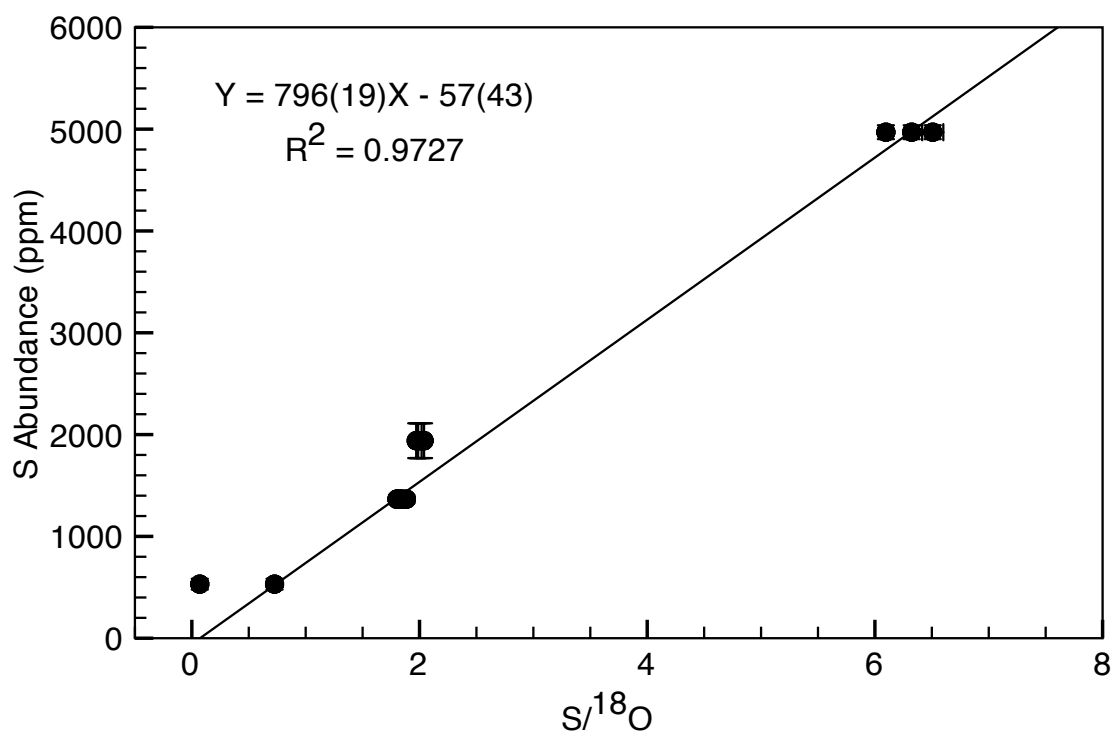


Figure B.8. Calibration curve for S during the June 2011 NanoSIMS session.

Table B.3. Raw data from the December 2011 NanoSIMS session.

Sample	$^{12}\text{C}/^{18}\text{O}$	$\sigma$	$^{16}\text{OH}/^{18}\text{O}$	$\sigma$	$^{19}\text{F}/^{18}\text{O}$	$\sigma$	$^{32}\text{S}/^{18}\text{O}$	$\sigma$	$^{35}\text{Cl}/^{18}\text{O}$	$\sigma$	Cl+F+OH
<b>External Standards</b>											
Ap005 1	0.001	0.000	1.020	0.015	46.182	0.651	0.706	0.012	8.487	0.087	0.92
Ap005 2	0.002	0.001	1.020	0.019	47.321	0.627	0.712	0.012	8.558	0.123	0.94
Ap005 3	0.001	0.000	1.008	0.017	48.113	0.652	0.712	0.011	8.591	0.106	0.94
Ap004 1	0.008	0.001	1.319	0.020	48.589	0.615	1.809	0.223	3.639	0.044	0.93
Ap004 2	0.008	0.001	1.284	0.020	48.387	0.603	1.783	0.026	3.590	0.047	0.92
Ap004 3	0.008	0.001	1.300	0.019	48.601	0.568	1.748	0.025	3.664	0.047	0.93
Ap003 1	0.001	0.000	0.215	0.006	72.938	0.903	2.412	0.044	5.207	0.061	0.98
Ap003 2	0.001	0.000	0.224	0.006	73.254	1.269	2.263	0.144	5.073	0.075	0.99
Ap018 1	0.040	0.008	0.680	0.014	69.462	0.937	5.750	0.087	0.916	0.017	0.98
Ap018 2	0.011	0.001	0.694	0.012	70.010	0.902	5.851	0.085	0.905	0.016	0.98
Ap018 3	0.010	0.001	0.703	0.014	70.104	0.956	5.662	0.082	0.912	0.017	0.99
<b>In-House Standards</b>											
Durango 1_1	0.004	0.001	0.310	0.011	75.952	1.031	1.296	0.025	3.175	0.064	1.00
Durango 1_2	0.001	0.000	0.302	0.009	76.289	1.124	1.285	0.024	3.783	0.059	1.01
Durnago 1_3	0.001	0.000	0.300	0.009	76.037	0.971	1.302	0.021	3.790	0.053	1.01
<b>External Standards</b>											
Ap003 3	0.002	0.001	0.250	0.009	75.753	0.800	1.845	0.029	3.431	0.049	0.99
Ap003 4	0.001	0.000	0.222	0.007	75.289	0.901	1.862	0.023	4.126	0.053	0.99
<b>In-House Standard</b>											
Durango 3_1	0.008	0.005	0.259	0.026	72.379	1.378	0.944	0.022	2.529	0.050	0.95
<b>Sample</b>											
NWA 6710 Ap 2_1	0.085	0.007	2.635	0.047	34.010	0.547	0.261	0.008	0.252	0.009	0.99
<b>In-House Standard</b>											
Durango 3_2	0.017	0.003	0.236	0.012	72.088	1.057	1.277	0.031	3.430	0.059	0.95

Table B.3 continued.

Sample	$^{12}\text{C}/^{18}\text{O}$	$\sigma$	$^{16}\text{OH}/^{18}\text{O}$	$\sigma$	$^{19}\text{F}/^{18}\text{O}$	$\sigma$	$^{32}\text{S}/^{18}\text{O}$	$\sigma$	$^{35}\text{Cl}/^{18}\text{O}$	$\sigma$	Cl+F+OH
<b>Samples</b>											
<sup>3</sup> NWA 6710 Ap 9_1a	0.049	0.009	2.761	0.049	37.712	0.522	0.512	0.053	3.878	0.067	1.11
<sup>2</sup> NWA 6710 Ap 1a_1	0.584	0.096	2.718	0.049	38.964	0.572	0.883	0.024	2.544	0.042	
NWA 6710 Ap 1a_2	0.070	0.005	2.666	0.100	39.736	0.889	0.652	0.016	1.750	0.055	1.08
NWA 6710 Ap 1b_1	0.058	0.005	2.385	0.048	35.661	0.517	0.353	0.009	3.985	0.077	1.02
<sup>3</sup> NWA 6710 Ap 1c_1	0.043	0.003	2.364	0.036	28.308	0.391	0.731	0.019	16.252	0.230	1.12
<b>In-House Standard</b>											
Durango 3_5	0.006	0.004	0.338	0.012	74.524	1.133	1.486	0.033	3.773	0.072	1.00

<sup>2</sup>Discarded due to a positive correlation of C and OH.

<sup>3</sup>Discarded due to Cl+F+OH either <0.85 or >1.10.

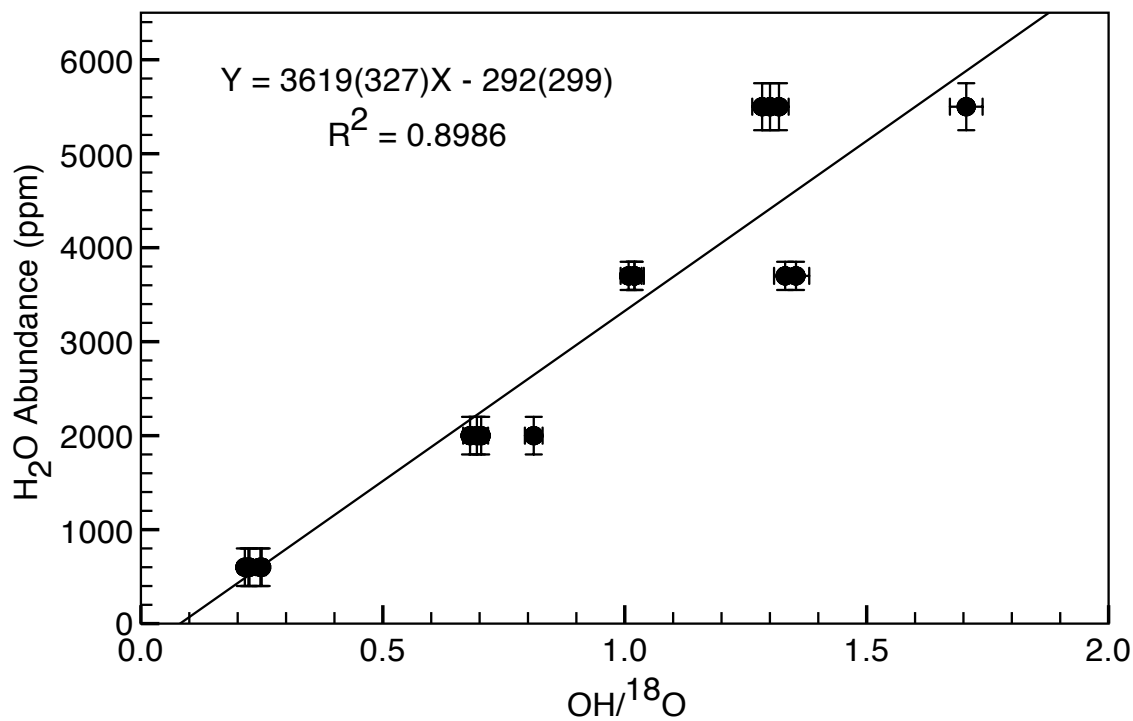


Figure B.9. Calibration curve for OH during the December 2011 NanoSIMS session.

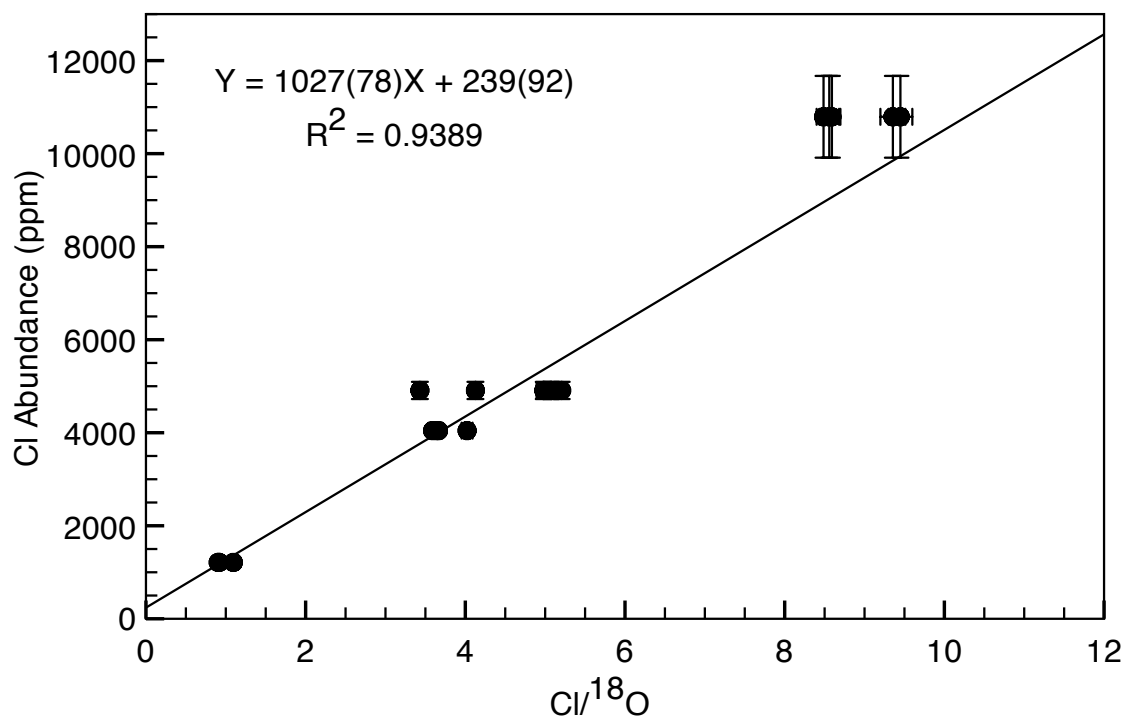


Figure B.10. Calibration curve for Cl during the December 2011 NanoSIMS session.

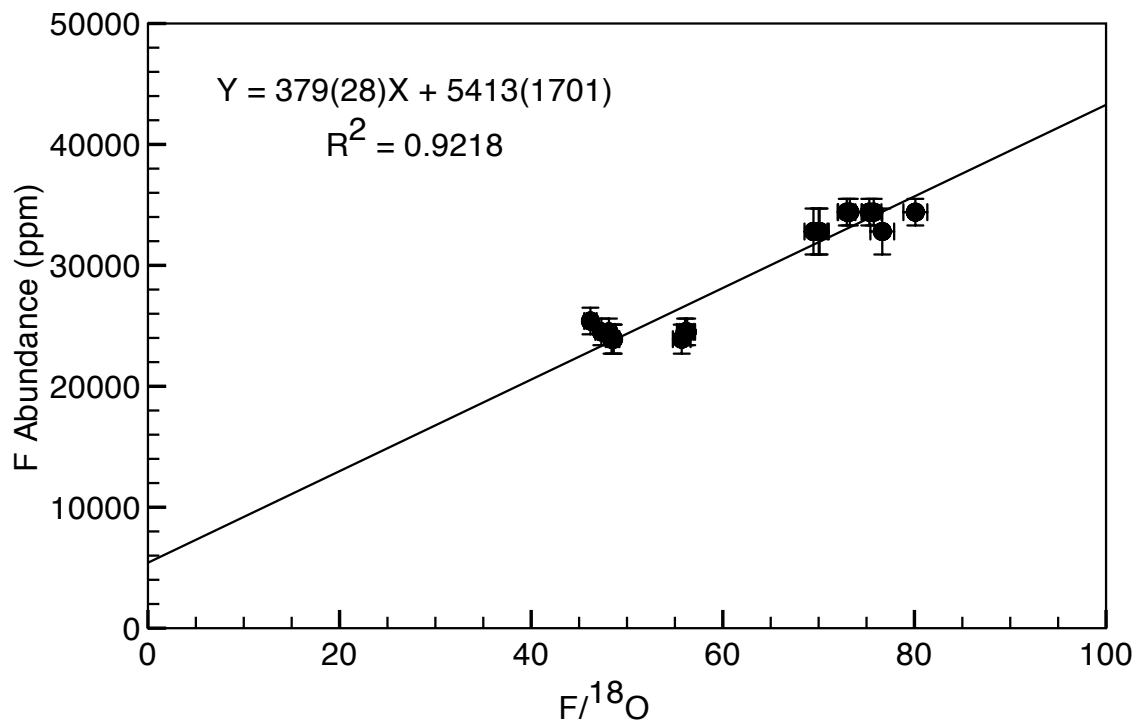


Figure B.11. Calibration curve for F during the December 2011 NanoSIMS session.

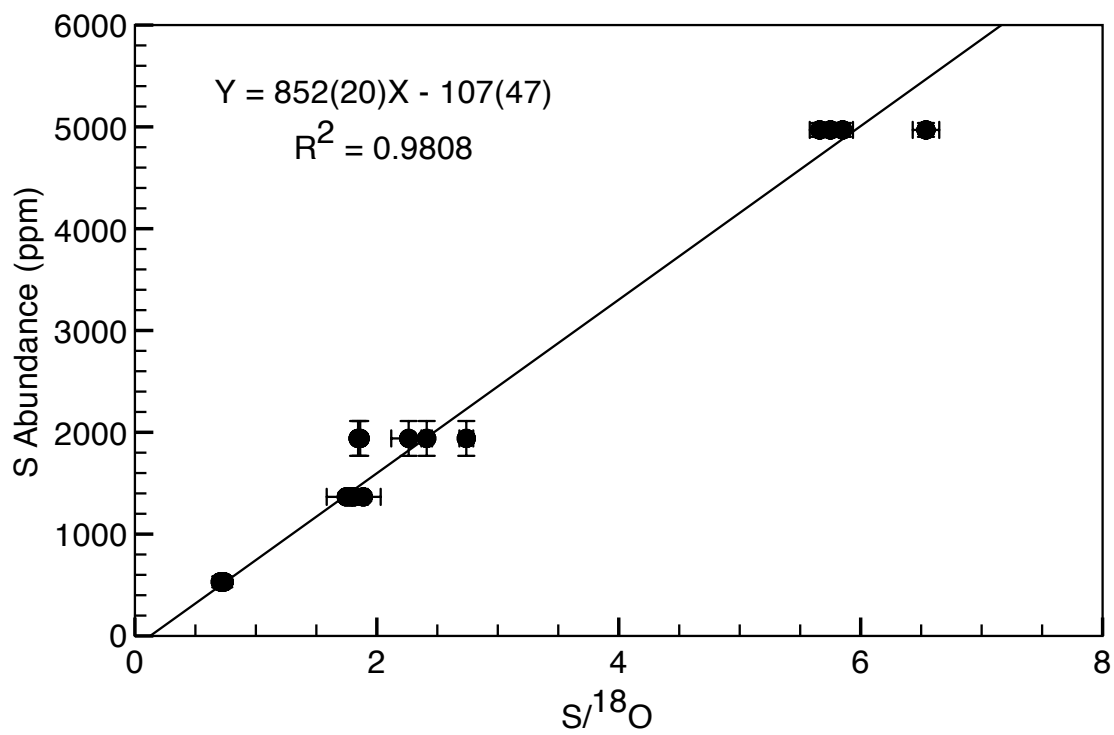


Figure B.12. Calibration curve for S during the December 2011 NanoSIMS session.

Table B.4. Raw data from the February 2012 NanoSIMS session.

Sample	$^{12}\text{C}/^{18}\text{O}$	$\sigma$	$^{16}\text{OH}/^{18}\text{O}$	$\sigma$	$^{19}\text{F}/^{18}\text{O}$	$\sigma$	$^{31}\text{P}/^{18}\text{O}$	$\sigma$	$^{32}\text{S}/^{18}\text{O}$	$\sigma$	$^{35}\text{Cl}/^{18}\text{O}$	$\sigma$	Cl+F+OH
<b>External Standards</b>													
Ap003 1	0.001	0.000			71.231	1.089	15.824	0.243	1.019	0.012	2.102	0.044	
Ap003 2	0.003	0.001			71.128	1.137	15.741	0.240	1.064	0.025	2.102	0.047	
Ap003 3	0.001	0.000			71.108	1.147	15.764	0.258	1.026	0.026	2.097	0.046	
Ap004 1	0.008	0.001			50.073	0.698	15.618	0.232	1.093	0.021	1.967	0.038	
Ap004 2	0.008	0.001			49.364	0.665	15.611	0.218	1.087	0.021	1.912	0.037	
Ap004 3	0.008	0.001			49.187	0.742	15.606	0.239	1.075	0.019	1.885	0.036	
Ap005 1	0.001	0.000			48.182	0.749	15.795	0.274	0.427	0.011	5.602	0.121	
Ap005 2	0.001	0.001			47.638	0.732	15.792	0.257	0.425	0.011	5.417	0.102	
Ap005 3	0.001	0.000	0.641	0.017	48.329	0.624	15.687	0.201	0.426	0.011	5.547	0.097	1.03
Ap005 4	0.002	0.001	0.601	0.019	47.461	0.679	15.748	0.245	0.419	0.012	5.195	0.103	1.00
Ap005 5	0.002	0.001	0.619	0.017	47.662	0.767	15.780	0.244	0.433	0.013	5.276	0.117	1.01
Ap018 1	0.013	0.002	0.346	0.012	69.135	1.064	15.158	0.226	3.732	0.070	0.528	0.014	1.02
Ap018 2	0.013	0.002	0.357	0.009	68.426	0.999	15.202	0.242	3.747	0.060	0.505	0.011	1.01
Ap018 3	0.013	0.002	0.372	0.011	67.960	1.000	15.323	0.225	3.714	0.058	0.464	0.014	1.01
Ap004 4	0.008	0.001	0.861	0.018	49.942	0.723	15.727	0.229	1.094	0.020	1.945	0.029	1.02
Ap004 5	0.008	0.001	0.820	0.023	49.229	0.694	15.691	0.209	1.078	0.022	1.892	0.042	0.99
Ap004 6	0.009	0.001	0.819	0.024	49.147	0.791	15.670	0.244	1.075	0.022	1.880	0.043	0.99
Ap003 4	0.001	0.000	0.084	0.004	71.809	0.977	15.602	0.233	1.124	0.019	2.216	0.045	1.01
Ap003 5	0.002	0.001	0.083	0.004	70.565	0.935	15.631	0.219	1.140	0.023	2.137	0.040	0.99
Ap003 6	0.001	0.000	0.085	0.005	70.718	1.152	15.719	0.250	1.134	0.025	2.135	0.048	1.00
<b>In-House Standards</b>													
Durango 1_1	0.002	0.001	0.156	0.006	68.779	1.029	16.143	0.237	0.767	0.015	1.773	0.040	0.99
Durango 1_2	0.002	0.001	0.153	0.006	69.820	0.944	16.147	0.225	0.773	0.015	1.868	0.036	1.00
Durango 1_3	0.011	0.002	0.172	0.006	68.736	1.020	16.015	0.248	0.788	0.019	1.779	0.037	0.99

Table B.4 continued.

Sample	$^{12}\text{C}/^{18}\text{O}$	$\sigma$	$^{16}\text{OH}/^{18}\text{O}$	$\sigma$	$^{19}\text{F}/^{18}\text{O}$	$\sigma$	$^{31}\text{P}/^{18}\text{O}$	$\sigma$	$^{32}\text{S}/^{18}\text{O}$	$\sigma$	$^{35}\text{Cl}/^{18}\text{O}$	$\sigma$	CH+F+OH
<b>External Standards</b>													
Ap005_6	0.001	0.000	0.589	0.016	46.586	0.638	15.215	0.208	0.412	0.011	5.354	0.086	0.99
Ap005_7	0.002	0.001	0.569	0.014	45.888	0.674	15.425	0.236	0.407	0.008	5.089	0.085	0.96
<b>Samples</b>													
<sup>3</sup> JaH 479 Ap 2_2	0.004	0.001	1.273	0.050	25.136	0.358	15.508	0.226	1.119	0.019	11.093	0.195	1.12
JaH 479 Ap 2_3	0.085	0.042	1.090	0.026	29.907	0.422	15.256	0.219	0.960	0.023	8.604	0.170	1.04
<b>In-House Standards</b>													
Durango 4_1	0.004	0.001	0.223	0.008	74.869	1.062	16.172	0.231	0.894	0.020	1.930	0.041	1.09
Durango 4_2	0.014	0.002	0.233	0.008	73.648	1.170	16.339	0.253	0.928	0.019	1.999	0.038	1.08
Durango 5_1	0.000	0.000	0.114	0.005	72.086	0.932	16.493	0.223	0.888	0.016	1.844	0.041	1.01
Durango 5_2	0.001	0.000	0.111	0.005	71.144	1.000	16.530	0.240	0.866	0.019	1.781	0.032	1.00
Durango 5_3	0.001	0.000	0.111	0.006	70.872	0.881	16.460	0.200	0.868	0.016	1.758	0.033	1.00
<b>Samples</b>													
<sup>3</sup> Dho 019 Ap 1_1	0.077	0.004	1.280	0.029	17.013	0.217	15.463	0.200	1.083	0.023	18.585	0.293	1.28
<sup>3</sup> Dho 019 Ap 1_2	0.059	0.003	1.742	0.054	16.031	0.236	15.430	0.223	2.104	0.039	16.749	0.293	1.37
Dho 019 Px 1_1	0.000	0.000	0.116	0.010	0.004	0.001	0.001	0.000	0.000	0.000	0.001	0.000	0.000
Dho 019 Msk 1_1	0.002	0.001	0.074	0.007	0.001	0.000	0.004	0.001	0.000	0.000	0.001	0.000	0.000
Dho 019 Ol 1_1	0.001	0.000	0.155	0.008	0.001	0.000	0.037	0.002	0.000	0.000	0.000	0.000	0.000
<sup>1</sup> Dho 019 Ap 2_1	0.125	0.007	1.884	0.048	12.253	0.279	14.122	0.213	2.297	0.096	21.776	0.421	1.29
<sup>3</sup> Dho 019 Ap 2_2	0.073	0.004	1.128	0.055	16.552	0.425	15.294	0.230	1.316	0.048	20.963	0.493	1.03
Dho 019 Ap 2_3	0.057	0.005	1.579	0.040	17.341	0.241	15.283	0.236	1.621	0.075	15.410	0.336	1.03
Dho 019 Ap 2_4	0.029	0.003	1.140	0.023	16.740	0.235	15.645	0.229	0.691	0.018	17.054	0.257	0.99
Dho 019 Msk 2_1	0.002	0.001	0.234	0.008	0.001	0.000	0.013	0.002	0.000	0.000	0.001	0.000	0.000

<sup>1</sup>Discarded due to inconsistent <sup>31</sup>P/<sup>18</sup>O.<sup>3</sup>Discarded due to CH+F+OH either <0.85 or >1.10.

Table B.4 continued.

Sample	$^{12}\text{C}/^{18}\text{O}$	$\sigma$	$^{16}\text{OH}/^{18}\text{O}$	$\sigma$	$^{19}\text{F}/^{18}\text{O}$	$\sigma$	$^{31}\text{P}/^{18}\text{O}$	$\sigma$	$^{32}\text{S}/^{18}\text{O}$	$\sigma$	$^{35}\text{Cl}/^{18}\text{O}$	$\sigma$	Cl+F+OH
<b>Samples</b>													
Dho 019 Px 2_1	0.357	0.020	0.287	0.026	0.017	0.002	0.014	0.003	0.020	0.002	0.009	0.002	
Dho 019 Ol 2_1	0.001	0.000	0.213	0.015	0.001	0.000	0.091	0.004	0.000	0.000	0.000	0.000	
<b>In-House Standards</b>													
Durango 5_4	0.001	0.000	0.108	0.005	70.755	0.941	16.183	0.228	0.861	0.016	1.793	0.037	1.00
Durango 5_5	0.001	0.000	0.108	0.005	69.268	1.001	16.185	0.230	0.821	0.017	1.674	0.033	0.97
Durango 5_6	0.001	0.000	0.115	0.006	69.028	0.989	16.108	0.228	0.828	0.019	1.672	0.034	0.97
Durango 2_1	0.002	0.000	0.192	0.010	68.510	0.947	15.284	0.227	0.698	0.014	1.541	0.028	0.99
Durango 2_2	0.003	0.001	0.194	0.007	67.258	0.796	15.290	0.193	0.654	0.014	1.529	0.025	0.98
Durango 2_3	0.007	0.002	0.201	0.007	67.059	1.095	15.215	0.234	0.666	0.016	1.535	0.030	0.98
<b>Samples</b>													
<sup>3</sup> NWA 6710 Ap 9_1b	0.043	0.005	2.101	0.037	35.854	0.438	15.195	0.186	0.195	0.008	1.729	0.031	1.27
NWA 6710 Ap 9_2	0.021	0.002	1.480	0.044	33.192	0.523	15.305	0.232	0.245	0.014	2.181	0.053	1.04
NWA 6710 Px 1_1	0.003	0.001	0.517	0.031	0.013	0.002	0.006	0.001	0.005	0.001	0.003	0.001	
NWA 6710 Msk 1_1	0.001	0.000	0.210	0.011	0.001	0.000	0.012	0.002	0.000	0.000	0.001	0.000	
NWA 6710 Ol 1_1	0.000	0.000	0.438	0.020	0.000	0.000	0.039	0.002	0.000	0.000	0.001	0.000	
NWA 6710 Ap 11_1	0.011	0.001	1.199	0.031	26.569	0.393	15.404	0.222	0.205	0.007	7.522	0.137	1.03
NWA 6710 Ap 11_2	0.043	0.004	1.181	0.029	27.719	0.403	15.229	0.239	0.214	0.007	6.063	0.105	0.99
NWA 6710 Px 2_1	0.018	0.013	0.491	0.028	0.004	0.001	0.006	0.001	0.001	0.000	0.009	0.002	
NWA 6710 Msk 2_1	0.000	0.000	1.211	0.029	0.001	0.000	0.018	0.002	0.001	0.001	0.006	0.001	
<sup>3</sup> NWA 6710 Ap 5_1	0.036	0.006	1.885	0.061	33.239	0.433	14.946	0.190	0.262	0.019	3.505	0.077	1.22
<sup>3</sup> NWA 6710 Ap 5_2	0.020	0.002	1.640	0.037	32.126	0.548	15.163	0.242	0.229	0.008	3.868	0.079	1.13
<b>In-House Standards</b>													
Durango 2_4	0.006	0.002	0.182	0.007	68.345	0.967	15.235	0.200	0.742	0.017	1.593	0.033	0.99
Durango 2_5	0.006	0.002	0.153	0.006	69.099	1.157	15.269	0.239	0.718	0.018	1.176	0.021	0.97

<sup>3</sup>Discarded due to Cl+F+OH either <0.85 or >1.10.

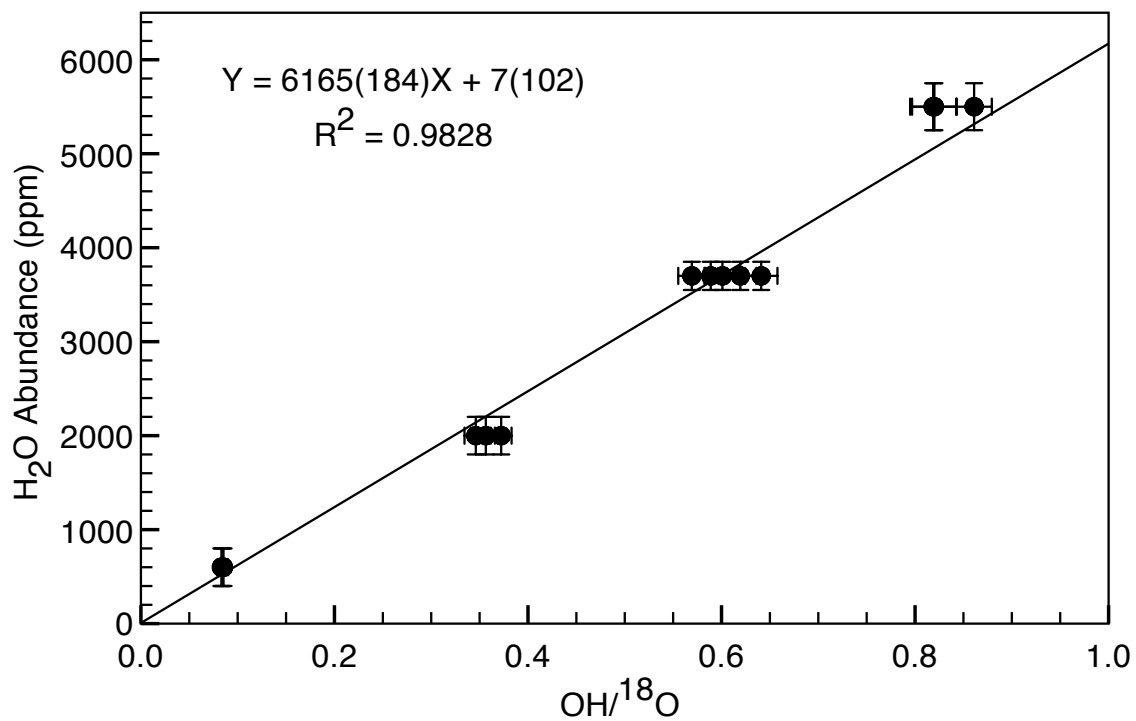


Figure B.13. Calibration curve for OH during the February 2012 NanoSIMS session.

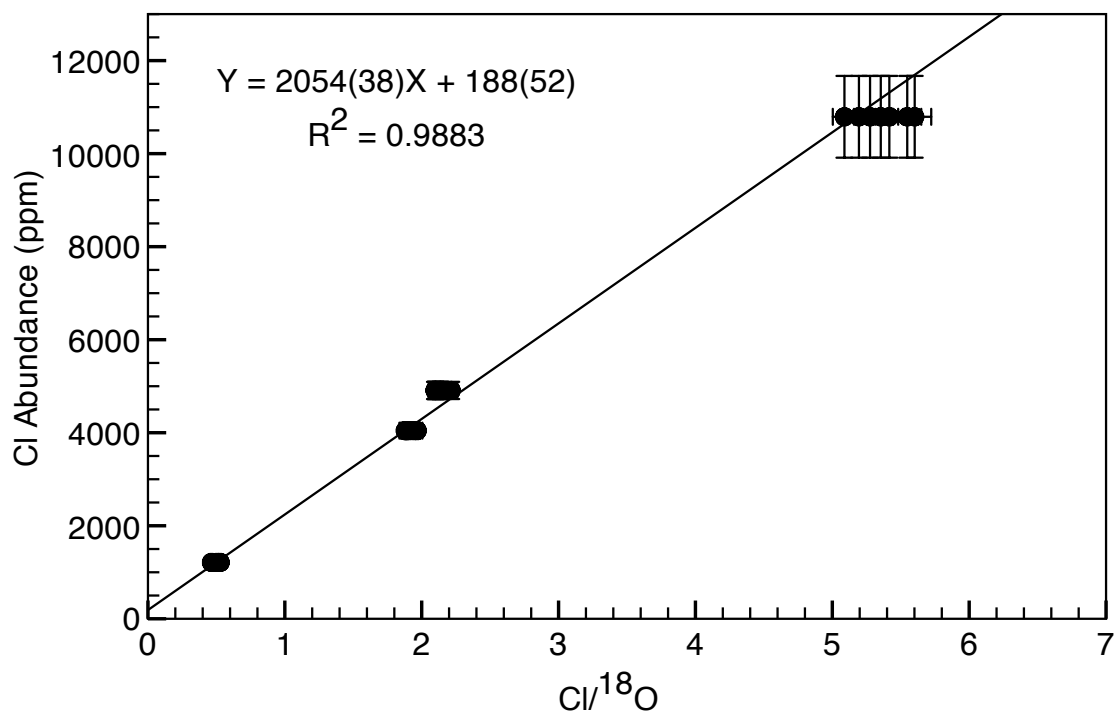


Figure B.14. Calibration curve for Cl during the February 2012 NanoSIMS session.

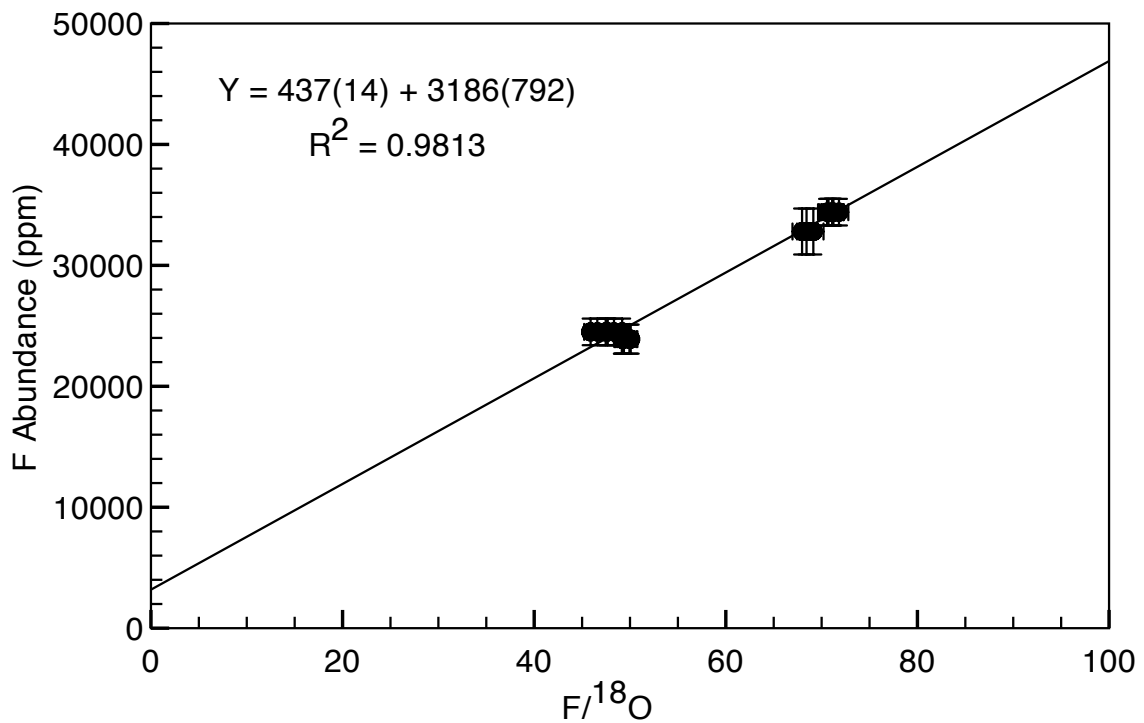


Figure B.15. Calibration curve for F during the February 2012 NanoSIMS session.

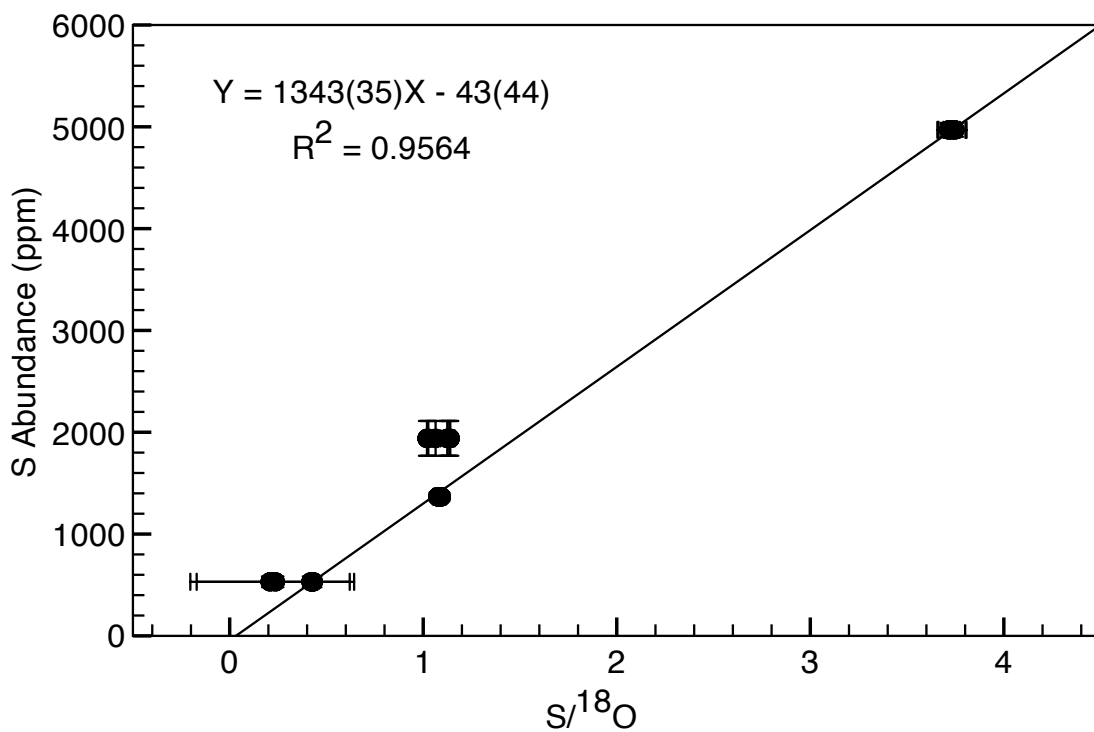


Figure B.16. Calibration curve for S during the February 2012 NanoSIMS session.

Table B.5. Raw data from the May 2012 NanoSIMS session.

Sample	$^{12}\text{C}/^{18}\text{O}$	$\sigma$	$^{16}\text{OH}/^{18}\text{O}$	$\sigma$	$^{32}\text{S}/^{18}\text{O}$	$\sigma$	$^{35}\text{Cl}/^{18}\text{O}$	$\sigma$	$^{37}\text{Cl}/^{18}\text{O}$	$\sigma$
<b>External Standards</b>										
Ap003 1	0.001	0.000	0.155	0.003	1.361	0.012	2.660	0.023	0.542	0.006
Ap003 2	0.001	0.000	0.148	0.002	1.291	0.014	2.493	0.026	0.462	0.006
Ap003 3	0.001	0.000	0.146	0.003	1.296	0.017	2.429	0.028	0.426	0.006
Ap004 1	0.008	0.000	1.277	0.012	1.408	0.015	2.925	0.032	0.612	0.006
Ap004 2	0.008	0.000	1.242	0.011	1.371	0.013	2.827	0.027	0.567	0.006
Ap004 3	0.008	0.000	1.237	0.012	1.361	0.015	2.810	0.032	0.559	0.006
Ap005 1	0.001	0.000	0.943	0.010	0.524	0.007	6.296	0.071	1.327	0.012
Ap005 2	0.001	0.000	0.918	0.010	0.487	0.007	5.953	0.070	1.243	0.011
Ap005 3	0.001	0.000	0.906	0.011	0.478	0.007	5.813	0.067	1.189	0.009
Ap018 1	0.013	0.001	0.527	0.006	4.618	0.046	0.651	0.006	0.142	0.002
Ap018 2	0.078	0.017	0.576	0.011	4.626	0.038	0.667	0.006	0.141	0.003
Ap018 3	0.013	0.001	0.544	0.006	4.499	0.037	0.637	0.007	0.134	0.003
<b>In-House Standards</b>										
Synthetic OI 1	0.001	0.000	0.041	0.001	0.001	0.000	0.003	0.001	0.001	0.000
Synthetic OI 2	0.001	0.000	0.044	0.001	0.002	0.000	0.005	0.001	0.001	0.000
Synthetic OI 3	0.001	0.000	0.041	0.001	0.002	0.000	0.004	0.001	0.001	0.000
<b>Samples</b>										
NWA 6710 Px 1 (In)	0.229	0.031	0.191	0.005	0.012	0.001	0.014	0.003	0.003	0.001
NWA 6710 Px 2 (In)	0.158	0.007	0.146	0.005	0.009	0.001	0.006	0.001	0.001	0.000
NWA 6710 OI 1_1 (In)	0.153	0.011	0.154	0.003	0.008	0.001	0.008	0.001	0.002	0.000
NWA 6710 OI 2_1 (In)	0.263	0.014	0.146	0.006	0.040	0.002	0.003	0.001	0.001	0.000
NWA 6710 Msk 3 (In)	0.006	0.001	0.027	0.003	0.006	0.001	0.002	0.001	0.000	0.000
NWA 6710 Msk 4 (In)	0.005	0.001	0.029	0.003	0.004	0.001	0.001	0.001	0.000	0.000
NWA 6710 OI 3_1 (In)	0.045	0.066	0.073	0.022	0.004	0.002	0.004	0.001	0.001	0.000
NWA 6710 OI 4_1 (In)	0.259	0.012	0.093	0.004	0.014	0.002	0.004	0.000	0.001	0.000

Table B.5 continued.

Sample	$^{12}\text{C}/^{18}\text{O}$	$\sigma$	$^{16}\text{OH}/^{18}\text{O}$	$\sigma$	$^{32}\text{S}/^{18}\text{O}$	$\sigma$	$^{35}\text{Cl}/^{18}\text{O}$	$\sigma$	$^{37}\text{Cl}/^{18}\text{O}$	$\sigma$
<b>Samples</b>										
NWA 6710 Px 5 (In)	0.064	0.006	0.033	0.004	0.009	0.002	0.001	0.000	0.000	0.000
NWA 6710 Px 6 (In)	0.225	0.014	0.046	0.005	0.028	0.010	0.006	0.001	0.002	0.001
<b>In-House Standards</b>										
Synthetic OI 4	0.001	0.000	0.020	0.001	0.003	0.002	0.005	0.002	0.001	0.001
Synthetic OI 5	0.001	0.000	0.020	0.001	0.001	0.000	0.003	0.000	0.001	0.000
Synthetic OI 6	0.002	0.000	0.020	0.001	0.005	0.001	0.004	0.001	0.001	0.000
<b>Samples</b>										
NWA 1950 OI 1_1 (In)	0.034	0.015	0.055	0.003	0.001	0.000	0.001	0.000	0.000	0.000
NWA 1950 OI 3_1 (In)	0.140	0.052	0.086	0.006	0.046	0.010	0.001	0.000	0.000	0.000
NWA 1950 Px 1 (In)	0.291	0.052	0.278	0.016	0.092	0.040	0.009	0.001	0.002	0.000
NWA 1950 Px 2 (In)	0.032	0.002	0.079	0.004	0.005	0.001	0.004	0.001	0.001	0.000
NWA 1950 Px 3 (In)	0.006	0.001	0.047	0.005	0.001	0.000	0.001	0.000	0.000	0.000
<b>In-House Standards</b>										
Synthetic OI 7	0.003	0.001	0.023	0.001	0.006	0.001	0.007	0.002	0.001	0.000
Synthetic OI 8	0.004	0.001	0.024	0.001	0.014	0.001	0.009	0.001	0.001	0.000
Synthetic OI 9	0.003	0.001	0.023	0.001	0.003	0.001	0.006	0.001	0.001	0.000
Synthetic OI 10	0.001	0.000235	0.014	0.001	0.001	0.000	0.002	0.000	0.000	0.000
Synthetic OI 11	0.002	0.000	0.015	0.001	0.013	0.002	0.016	0.002	0.004	0.001
<b>Sample</b>										
NWA 6710 OI 5_1 (In)	0.144	0.015	0.121	0.008	0.071	0.008	0.015	0.002	0.004	0.001
<b>In-House Standard</b>										
Synthetic OI 12	0.002	0.000	0.013	0.001	0.002	0.000	0.003	0.000	0.001	0.000
<b>Sample</b>										
JaH 479 OI 2_1 (In)	0.027	0.002	0.146	0.011	0.007	0.001	0.004	0.001	0.001	0.000

Table B.5 continued.

Sample	$^{12}\text{C}/^{18}\text{O}$	$\sigma$	$^{16}\text{OH}/^{18}\text{O}$	$\sigma$	$^{32}\text{S}/^{18}\text{O}$	$\sigma$	$^{35}\text{Cl}/^{18}\text{O}$	$\sigma$	$^{37}\text{Cl}/^{18}\text{O}$	$\sigma$
<b>In-House Standards</b>										
Synthetic OI 13	0.001	0.000	0.015	0.001	0.001	0.000	0.004	0.000	0.001	0.000
Synthetic OI 14	0.001	0.000	0.015	0.001	0.000	0.000	0.001	0.000	0.000	0.000
Synthetic OI 15	0.001	0.000	0.010	0.001	0.000	0.000	0.004	0.000	0.001	0.000
<b>Samples</b>										
NWA 1950 OI 1_2 (In)	0.030	0.003	0.045	0.002	0.003	0.001	0.001	0.000	0.000	0.000
NWA 1950 OI 4_1 (In)	0.002	0.000	0.016	0.001	0.000	0.000	0.000	0.000	0.000	0.000
NWA 1950 OI 5_1 (In)	0.051	0.002	0.038	0.001	0.009	0.001	0.001	0.000	0.000	0.000
NWA 1950 OI crack 1 (In)	0.951	0.113	0.818	0.090	0.718	0.070	0.055	0.010	0.013	0.002
NWA 1950 OI crack 2 (In)	0.902	0.239	0.292	0.030	0.098	0.015	0.270	0.065	0.067	0.016
NWA 1950 OI 6_1 (In)	0.166	0.007	0.106	0.003	0.009	0.001	0.001	0.000	0.000	0.000
NWA 6710 OI 1_2 (In)	0.117	0.004	0.098	0.002	0.009	0.002	0.003	0.000	0.001	0.000
NWA 6710 OI crack (In)	0.299	0.031	0.301	0.013	0.208	0.011	0.015	0.001	0.003	0.000
JaH 479 OI 4_1 (In)	0.052	0.007	0.202	0.027	0.035	0.004	0.011	0.002	0.002	0.000
JaH 479 OI 5_1 (In)	0.030	0.002	0.139	0.005	0.073	0.014	0.008	0.001	0.001	0.000
JaH 479 OI crack (In)	0.426	0.074	1.180	0.033	0.390	0.064	0.302	0.015	0.067	0.003
<b>In-House Standard</b>										
Synthetic OI 16	0.001	0.000	0.013	0.001	0.000	0.000	0.004	0.000	0.001	0.000
<b>External Standards</b>										
grr1017 1	0.000	0.000	0.011	0.001	0.000	0.000	0.000	0.000	0.000	0.000
grr1017 2	0.001	0.000	0.011	0.001	0.001	0.000	0.000	0.000	0.000	0.000
grr999a 1	0.000	0.000	0.013	0.001	0.000	0.000	0.000	0.000	0.000	0.000
grr999a 2	0.001	0.000	0.015	0.001	0.001	0.000	0.000	0.000	0.000	0.000
grr999a 3	0.001	0.000	0.013	0.001	0.001	0.000	0.000	0.000	0.000	0.000

Table B.5 continued.

Sample	$^{12}\text{C}/^{18}\text{O}$	$\sigma$	$^{16}\text{OH}/^{18}\text{O}$	$\sigma$	$^{32}\text{S}/^{18}\text{O}$	$\sigma$	$^{35}\text{Cl}/^{18}\text{O}$	$\sigma$	$^{37}\text{Cl}/^{18}\text{O}$	$\sigma$
<b>External Standards</b>										
grr997 1	0.000	0.000	0.013	0.001	0.000	0.000	0.000	0.000	0.000	0.000
grr997 2	0.001	0.000	0.013	0.001	0.000	0.000	0.000	0.000	0.000	0.000
grr997 3	0.001	0.000	0.012	0.001	0.000	0.000	0.000	0.000	0.000	0.000
grr1012-1 1	0.001	0.000	0.030	0.001	0.000	0.000	0.000	0.000	0.000	0.000
grr1012-1 2	0.001	0.000	0.029	0.001	0.001	0.000	0.000	0.000	0.000	0.000
grr1012-1 3	0.001	0.000	0.029	0.001	0.001	0.000	0.000	0.000	0.000	0.000
grr1629-2 1	0.000	0.000	0.016	0.001	0.000	0.000	0.000	0.000	0.000	0.000
grr1629-2 2	0.001	0.000	0.015	0.001	0.000	0.000	0.000	0.000	0.000	0.000
grr1629-2 3	0.001	0.000	0.015	0.001	0.000	0.000	0.000	0.000	0.000	0.000
grr1695-2 1	0.001	0.000	0.015	0.001	0.000	0.000	0.000	0.000	0.000	0.000
grr1695-2 2	0.001	0.000	0.015	0.001	0.000	0.000	0.000	0.000	0.000	0.000
grr1695-2 3	0.002	0.000	0.014	0.001	0.000	0.000	0.000	0.000	0.000	0.000
rom177 1	0.001	0.000	0.023	0.001	0.000	0.000	0.000	0.000	0.000	0.000
rom177 2	0.014	0.001	0.022	0.001	0.000	0.000	0.000	0.000	0.000	0.000
rom177 3	0.001	0.000	0.021	0.001	0.000	0.000	0.000	0.000	0.000	0.000
grr1784e 1	0.001	0.000	0.017	0.001	0.000	0.000	0.000	0.000	0.000	0.000
grr1784e 2	0.001	0.000	0.016	0.001	0.000	0.000	0.000	0.000	0.000	0.000
grr1784e 3	0.065	0.005	0.018	0.001	0.001	0.000	0.001	0.000	0.000	0.000

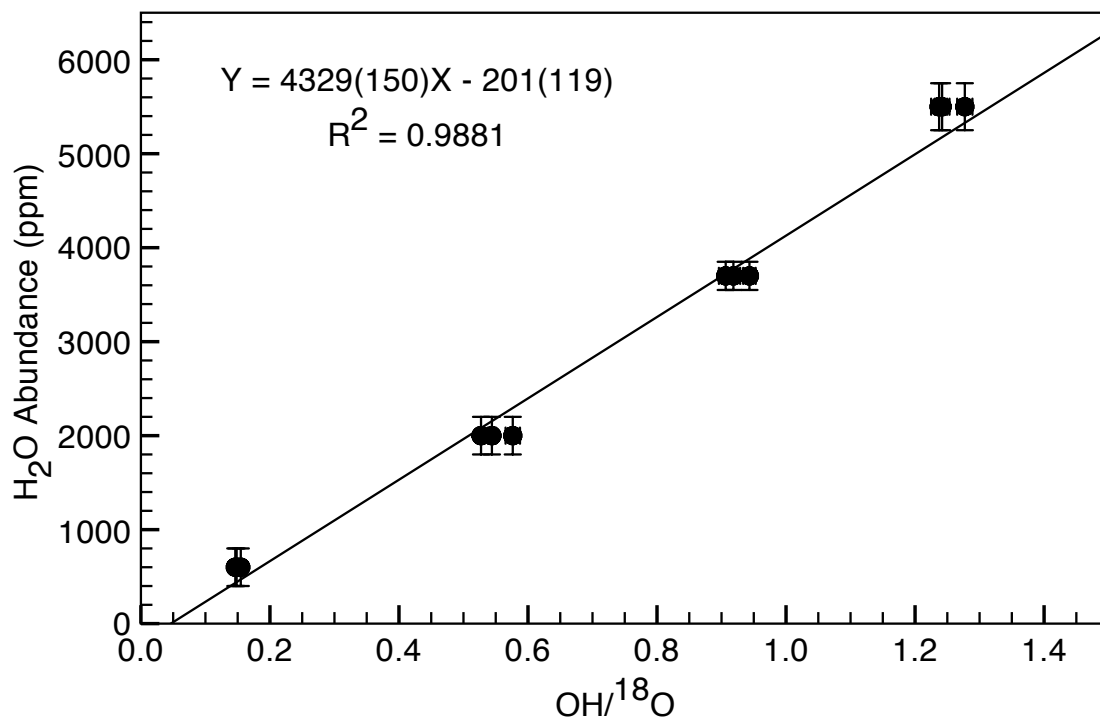


Figure B.17. Calibration curve for OH in apatite during the May 2012 NanoSIMS session.

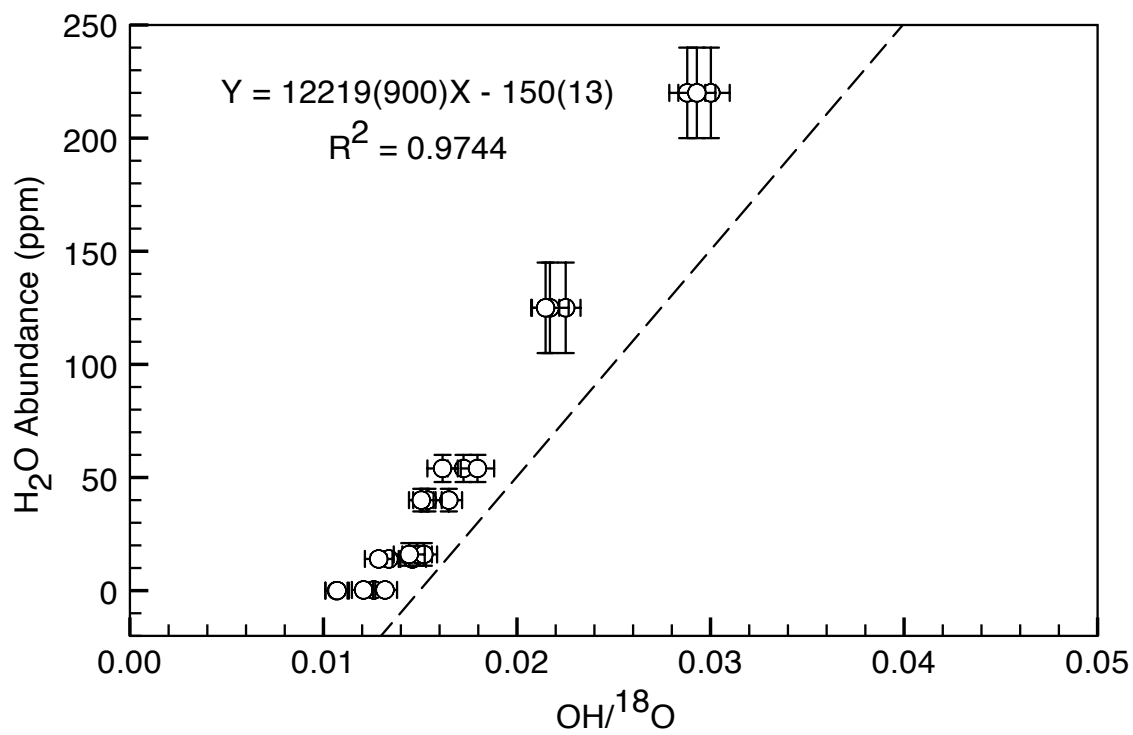


Figure B.18. Calibration curve for OH in olivine during the May 2012 NanoSIMS session.

Table B.6. Raw data from the June 2012 NanoSIMS session.

Sample	$^{12}\text{C}/^{18}\text{O}$	$\sigma$	$^{16}\text{OH}/^{18}\text{O}$	$\sigma$	$^{19}\text{F}/^{18}\text{O}$	$\sigma$	$^{31}\text{P}/^{18}\text{O}$	$\sigma$	$^{32}\text{S}/^{18}\text{O}$	$\sigma$	$^{35}\text{Cl}/^{18}\text{O}$	$\sigma$	Cl+F+OH
<b>External Standards</b>													
Ap018 1	0.016	0.002	0.678	0.012			13.313	0.161	5.390	0.077	0.565	0.011	
Ap018 2	0.015	0.001	0.672	0.011			13.257	0.174	5.379	0.076	0.535	0.014	
Ap018 3	0.015	0.002	0.689	0.014			13.254	0.194	5.373	0.083	0.510	0.014	
Ap018 4	0.013	0.002	0.573	0.010	68.893	0.787	13.402	0.158	4.949	0.058	0.586	0.012	0.99
Ap018 5	0.013	0.002	0.550	0.011	69.677	0.753	13.402	0.152	4.871	0.056	0.576	0.011	0.99
Ap018 6	0.012	0.001	0.613	0.013	68.932	0.822	13.413	0.161	5.009	0.058	0.535	0.012	0.99
Ap005 1	0.001	0.001	0.994	0.017	50.275	0.654	13.894	0.184	0.546	0.014	4.749	0.068	0.99
Ap005 2	0.002	0.001	0.995	0.017	50.211	0.652	13.727	0.193	0.537	0.011	4.583	0.074	0.98
Ap005 3	0.002	0.001	0.982	0.017	50.202	0.718	13.950	0.203	0.551	0.013	4.814	0.074	0.99
Ap004 1	0.009	0.001	1.266	0.023	49.130	0.647	13.339	0.181	1.313	0.021	1.755	0.030	0.95
Ap004 2	0.009	0.001	1.366	0.022	50.702	0.540	13.461	0.153	1.402	0.019	1.998	0.028	0.99
Ap004 3	0.008	0.001	1.375	0.022	50.869	0.552	13.599	0.142	1.440	0.022	2.089	0.031	1.00
Ap003 2	0.001	0.000	0.152	0.005	73.586	0.888	13.975	0.178	1.497	0.023	2.341	0.035	1.00
Ap003 3	0.002	0.000	0.153	0.005	74.170	0.921	14.076	0.199	1.509	0.026	2.385	0.035	1.01
Ap003 4	0.002	0.001	0.152	0.005	73.871	0.884	13.923	0.169	1.482	0.025	2.340	0.038	1.00
<b>In-House Standards</b>													
Durango 1_4	0.001	0.000	0.224	0.006	70.152	0.886	13.542	0.181	0.882	0.017	1.613	0.024	0.96
Durango 1_5	0.002	0.001	0.231	0.007	71.305	0.966	13.584	0.170	0.910	0.017	1.672	0.027	0.97
Durango 5_1	0.011	0.001	0.176	0.006	72.484	0.975	13.999	0.196	1.090	0.020	1.754	0.031	0.98
Durango 5_2	0.012	0.002	0.175	0.005	72.809	0.774	13.843	0.156	1.061	0.017	1.717	0.025	0.98
Durango 5_3	0.012	0.002	0.172	0.006	72.170	0.695	13.894	0.161	1.067	0.018	1.705	0.028	0.97
Durango 5_4	0.015	0.002	0.173	0.005	73.459	0.772	13.768	0.139	1.063	0.016	1.764	0.022	0.99
Durango 5_5	0.016	0.002	0.173	0.005	73.308	0.871	13.758	0.162	1.079	0.016	1.736	0.028	0.98
Durango 5_6	0.018	0.002	0.178	0.006	73.862	0.995	13.772	0.177	1.082	0.019	1.745	0.027	0.99

Table B.6 continued.

Sample	$^{12}\text{C}/^{18}\text{O}$	$\sigma$	$^{16}\text{OH}/^{18}\text{O}$	$\sigma$	$^{19}\text{F}/^{18}\text{O}$	$\sigma$	$^{31}\text{P}/^{18}\text{O}$	$\sigma$	$^{32}\text{S}/^{18}\text{O}$	$\sigma$	$^{35}\text{Cl}/^{18}\text{O}$	$\sigma$	Cl+F+OH
<b>Samples</b>													
NMNH 116771-178 Ap 1_1	0.002	0.001	0.402	0.010	71.035	0.857	13.454	0.157	0.163	0.006	1.752	0.024	1.01
NMNH 116771-178 Ap 1_2	0.001	0.000	0.381	0.009	72.383	0.833	13.923	0.167	0.201	0.006	1.803	0.027	1.02
NMNH 116771-178 OI 1_1	0.001	0.000	0.037	0.003	0.294	0.007	0.007	0.001	0.000	0.000	0.000	0.000	
NMNH 116771-178 OI 1_2	0.001	0.000	0.039	0.003	0.341	0.008	0.002	0.001	0.001	0.000	0.000	0.000	
NMNH 116771-178 Ap 2_1	0.001	0.000	0.389	0.009	72.946	0.928	13.837	0.177	0.217	0.006	1.835	0.029	1.03
NMNH 116771-178 OI 2_1	0.002	0.000	0.046	0.003	0.005	0.001	0.008	0.001	0.001	0.000	0.000	0.000	
NMNH 116771-178 OI 4_1	0.001	0.000	0.033	0.002	0.362	0.007	0.002	0.001	0.000	0.000	0.000	0.000	
NMNH 116771-178 Ap 5_1	0.001	0.000	0.372	0.008	72.998	0.806	14.053	0.165	0.152	0.005	1.899	0.028	1.03
NMNH 116771-178 Ap 5_2	0.001	0.000	0.375	0.011	72.197	0.798	13.748	0.170	0.095	0.004	1.812	0.028	1.02
NMNH 116771-178 OI 5_1	0.001	0.000	0.053	0.004	0.006	0.001	0.006	0.001	0.000	0.000	0.000	0.000	
<b>In-House Standards</b>													
Durango 5_7	0.001	0.000	0.165	0.006	75.607	0.877	13.739	0.151	1.117	0.016	1.963	0.026	1.02
Durango 5_8	0.002	0.001	0.168	0.005	76.000	0.844	13.624	0.160	1.113	0.019	1.904	0.025	1.02
<b>External Standards</b>													
grr997 1	0.001	0.000	0.016	0.002	0.002	0.001	0.001	0.000	0.002	0.000	0.001	0.000	
grr997 2	0.003	0.001	0.018	0.002	0.003	0.001	0.001	0.000	0.003	0.001	0.001	0.000	
<b>Samples</b>													
San Carlos OI 1_1 (In)	0.001	0.000	0.014	0.001	0.003	0.001	0.026	0.002	0.001	0.000	0.000	0.000	
San Carlos OI 1_2 (In)	0.002	0.001	0.015	0.001	0.004	0.001	0.026	0.002	0.002	0.000	0.000	0.000	
San Carlos OI 1_3 (In)	0.001	0.001	0.016	0.002	0.003	0.001	0.025	0.002	0.002	0.001	0.000	0.000	
San Carlos OI 2_1 (In)	0.002	0.001	0.017	0.001	0.003	0.001	0.017	0.002	0.001	0.000	0.000	0.000	
San Carlos OI 2_2 (In)	0.003	0.001	0.017	0.002	0.004	0.001	0.016	0.002	0.002	0.001	0.000	0.000	

Table B.6 continued.

Sample	$^{12}\text{C}/^{18}\text{O}$	$\sigma$	$^{16}\text{OH}/^{18}\text{O}$	$\sigma$	$^{19}\text{F}/^{18}\text{O}$	$\sigma$	$^{31}\text{P}/^{18}\text{O}$	$\sigma$	$^{32}\text{S}/^{18}\text{O}$	$\sigma$	$^{35}\text{Cl}/^{18}\text{O}$	$\sigma$	Cl+F+OH
<b>External Standards</b>													
grr1012-1 1	0.002	0.001	0.035	0.002	0.128	0.005	0.008	0.001	0.003	0.001	0.005	0.001	0.005
grr1012-1 2	0.003	0.001	0.035	0.002	0.128	0.005	0.008	0.001	0.004	0.001	0.001	0.001	0.000
grr1017 1	0.002	0.001	0.013	0.002	0.002	0.001	0.000	0.000	0.004	0.001	0.001	0.001	0.000
grr1017 2	0.005	0.001	0.014	0.001	0.003	0.001	0.000	0.000	0.007	0.002	0.001	0.001	0.001
grr999a 1	0.001	0.000	0.017	0.002	0.006	0.001	0.007	0.001	0.001	0.000	0.000	0.000	0.000
grr999a 2	0.002	0.001	0.018	0.002	0.007	0.001	0.007	0.001	0.002	0.001	0.000	0.000	0.000
grr1695-2 1	0.001	0.000	0.020	0.002	0.002	0.001	0.004	0.001	0.002	0.001	0.000	0.000	0.000
grr1695-2 2	0.002	0.001	0.021	0.002	0.002	0.001	0.004	0.001	0.002	0.001	0.000	0.000	0.000
grr1629-2 1	0.001	0.001	0.020	0.002	0.003	0.001	0.000	0.000	0.002	0.001	0.000	0.000	0.000
grr1629-2 2	0.006	0.002	0.021	0.002	0.003	0.001	0.000	0.000	0.003	0.001	0.000	0.000	0.000
grr1784e 1	0.002	0.001	0.022	0.003	0.004	0.001	0.001	0.000	0.003	0.001	0.000	0.000	0.000
grr1784e 2	0.002	0.001	0.022	0.002	0.004	0.001	0.001	0.000	0.003	0.001	0.001	0.001	0.000
rom177 1	0.002	0.001	0.032	0.002	0.106	0.004	0.013	0.001	0.002	0.001	0.001	0.001	0.000
rom177 2	0.002	0.001	0.030	0.002	0.112	0.004	0.013	0.002	0.002	0.001	0.000	0.000	0.000
<b>In-House Standards</b>													
Durango 5_9	0.003	0.001	0.167	0.006	75.576	0.913	13.690	0.346	1.127	0.026	1.925	0.041	1.02
Durango 5_10	0.003	0.001	0.169	0.006	75.723	0.955	13.704	0.184	1.118	0.022	1.880	0.029	1.02

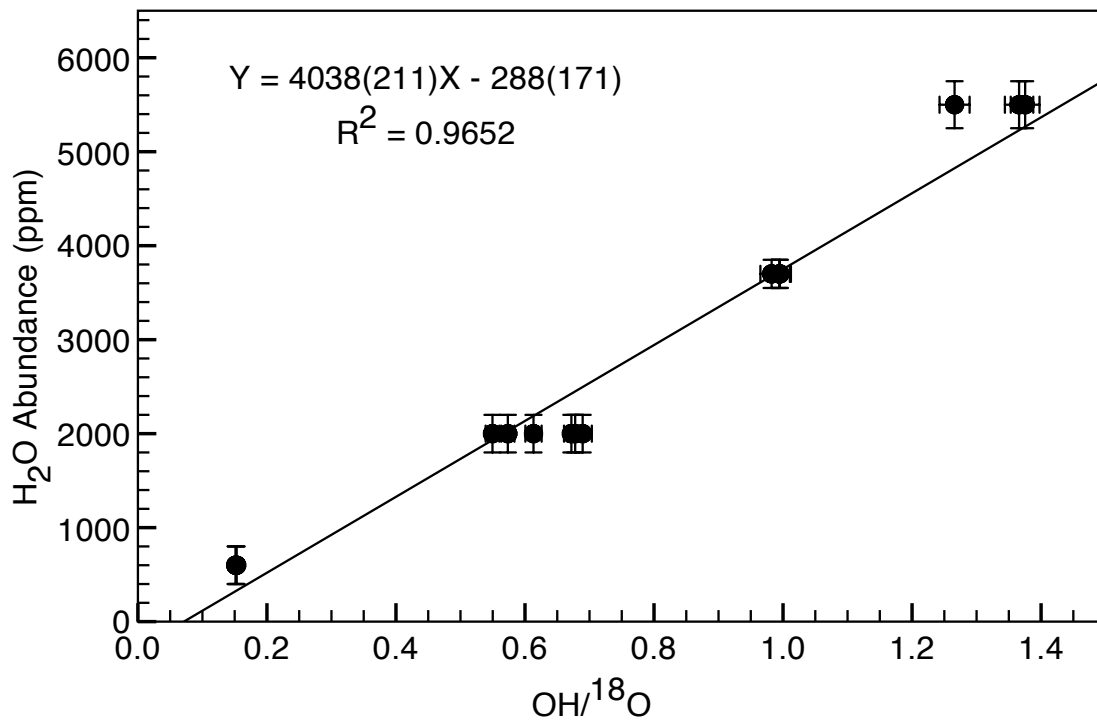


Figure B.19. Calibration curve for OH in apatite during the June 2012 NanoSIMS session.

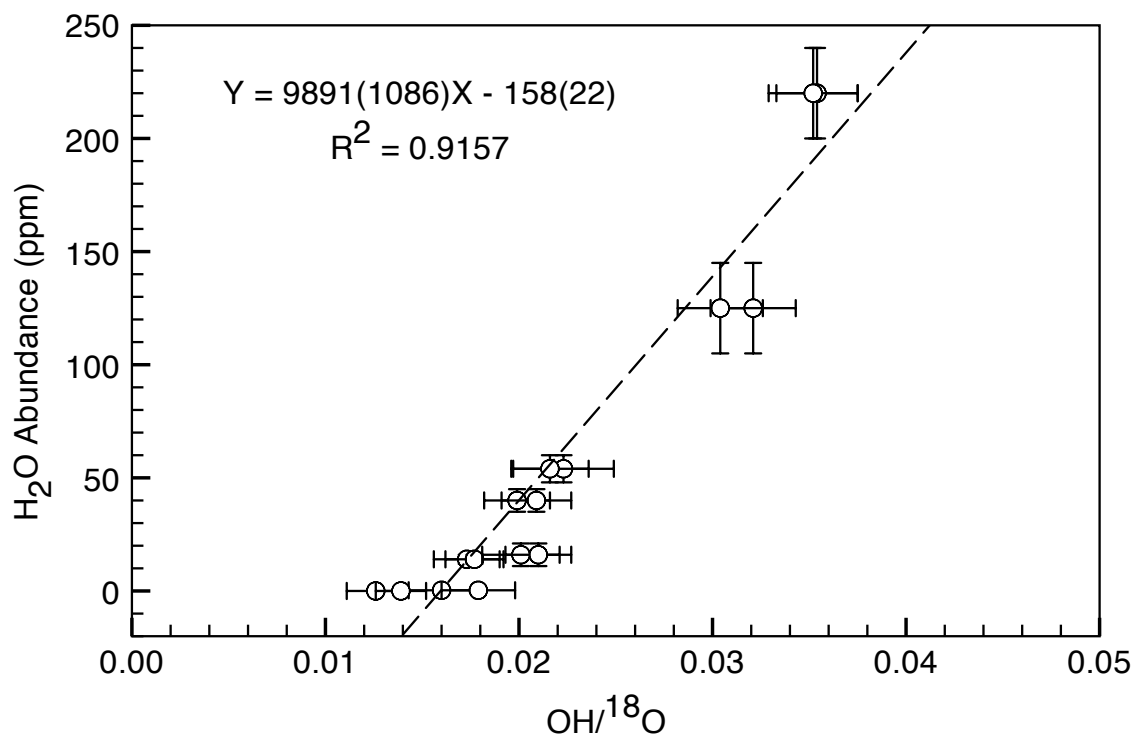


Figure B.20. Calibration curve for OH in olivine during the June 2012 NanoSIMS session.

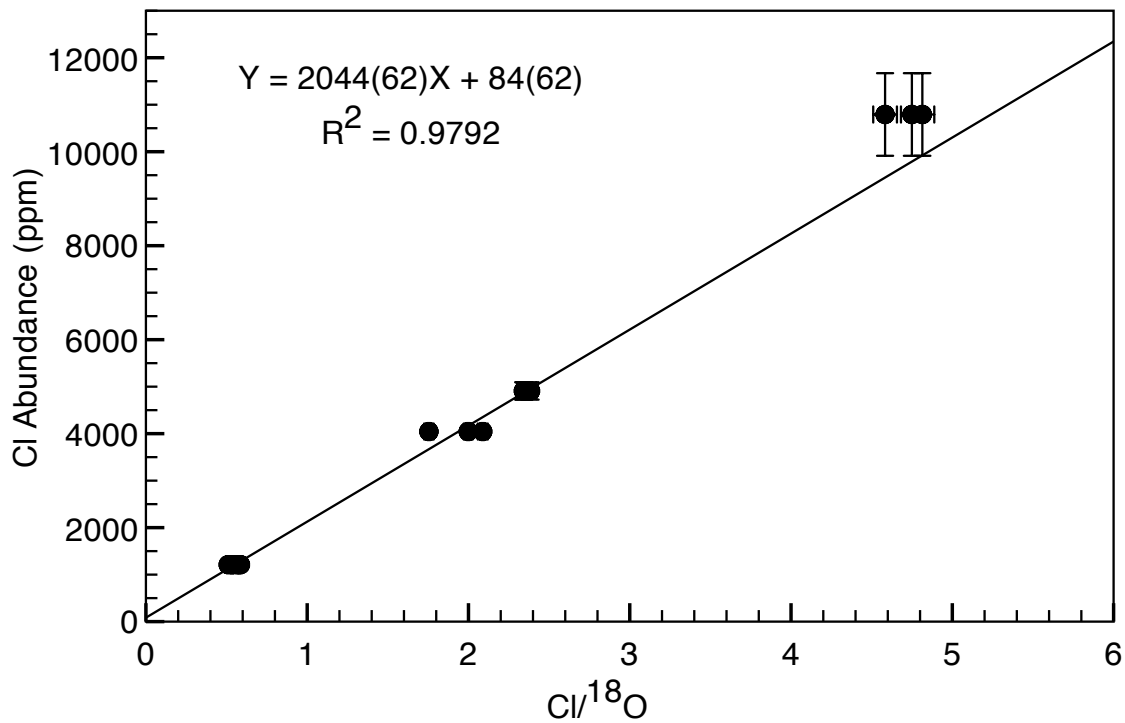


Figure B.21. Calibration curve for Cl in apatite during the June 2012 NanoSIMS session.

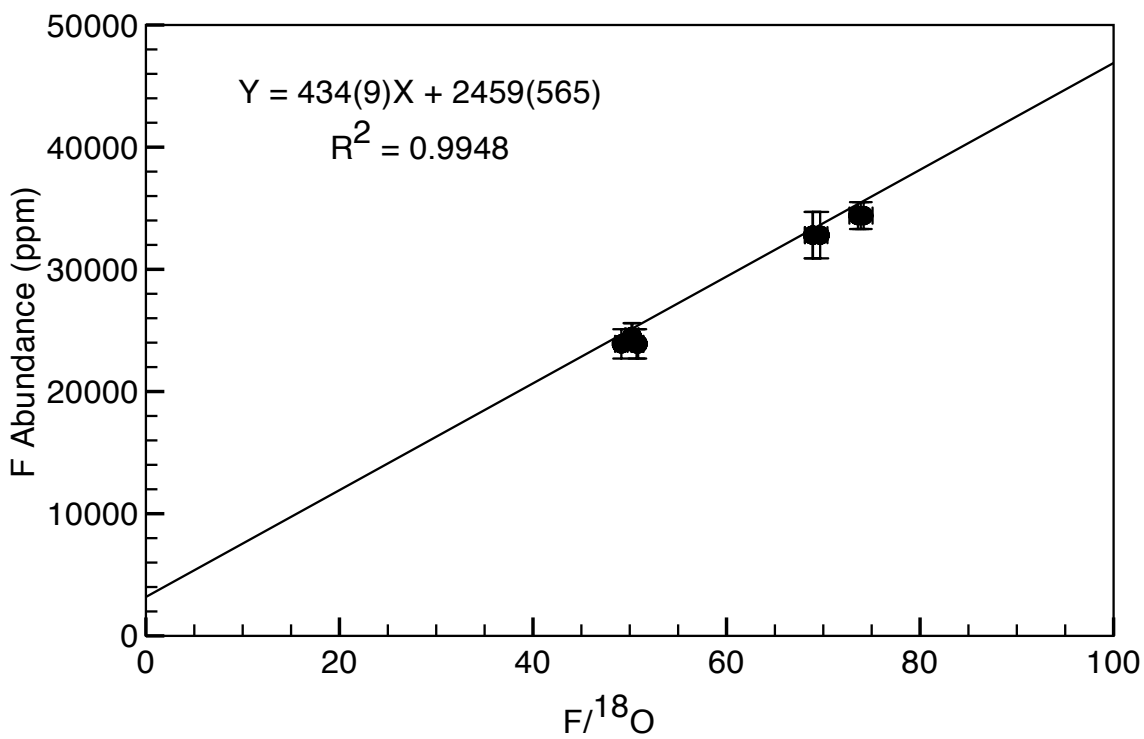


Figure B.22. Calibration curve for F in apatite during the June 2012 NanoSIMS session.

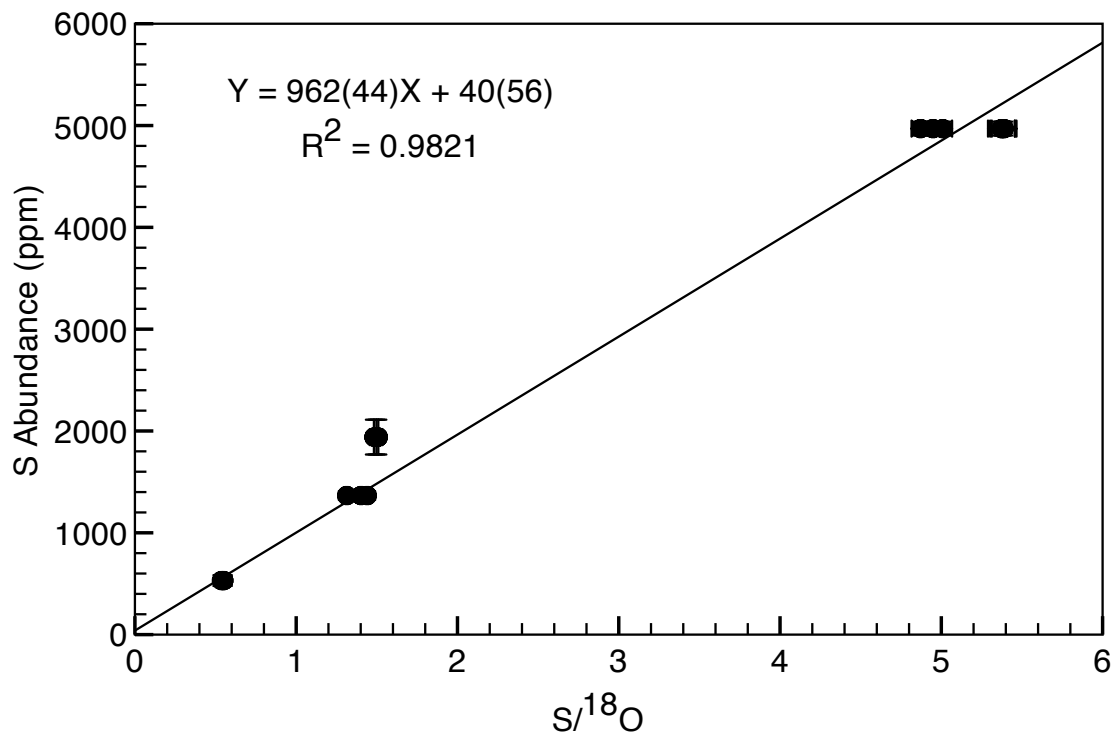


Figure B.23. Calibration curve for S in apatite during the June 2012 NanoSIMS session.

*Appendix C*

SUPPLEMENTARY DATA, SPECTRA, AND CALIBRATION CURVES FOR  
CHAPTER III

Data for chapter III was acquired over 3 electron probe sessions. Four analyses from sessions 1 in chapter III were removed because their peak positions (percent sulfide) relative to the standards were significantly different from spectrometer to spectrometer within the session (table C.1). Figures C.1 – C.17 show spectra of the SNCs from all spectrometers other than 3 (those spectra are found in chapter III) during sessions 1 and 3. The vertical scale of all the spectra figures is arbitrary intensity; the scale was changed for each spectrum such that the peak heights would match and peak positions could be more easily compared. The calibration curves used to convert peak intensities to sulfur concentration for all spectrometers in each session (except for spectrometer 3 in session 1, which can be found in chapter III) are shown in figures C.18 – C.23. Table C.2 lists all the calculated sulfur concentration data for each spectrometer in sessions 1 and 3.

Table C.1. Analyses from session 1 that were removed because of inconsistent percent sulfide calculations between spectrometers.

<b>Sample</b>	<b>Apatite</b>	<b>spec 2</b>	<b>spec 3</b>	<b>spec 5</b>	<b>spec 2</b>	<b>spec 3</b>	<b>spec 5</b>
<b><u>Session 1</u></b>							
<b>NWA 856</b>	1	172.142	172.023	172.080	84	26	14
	5	172.082	172.039	172.090	-19	52	31
<b>NWA 2986</b>	2	172.267	172.176	172.054	300	277	-31
	3	172.190	172.101	172.000	167	154	-122

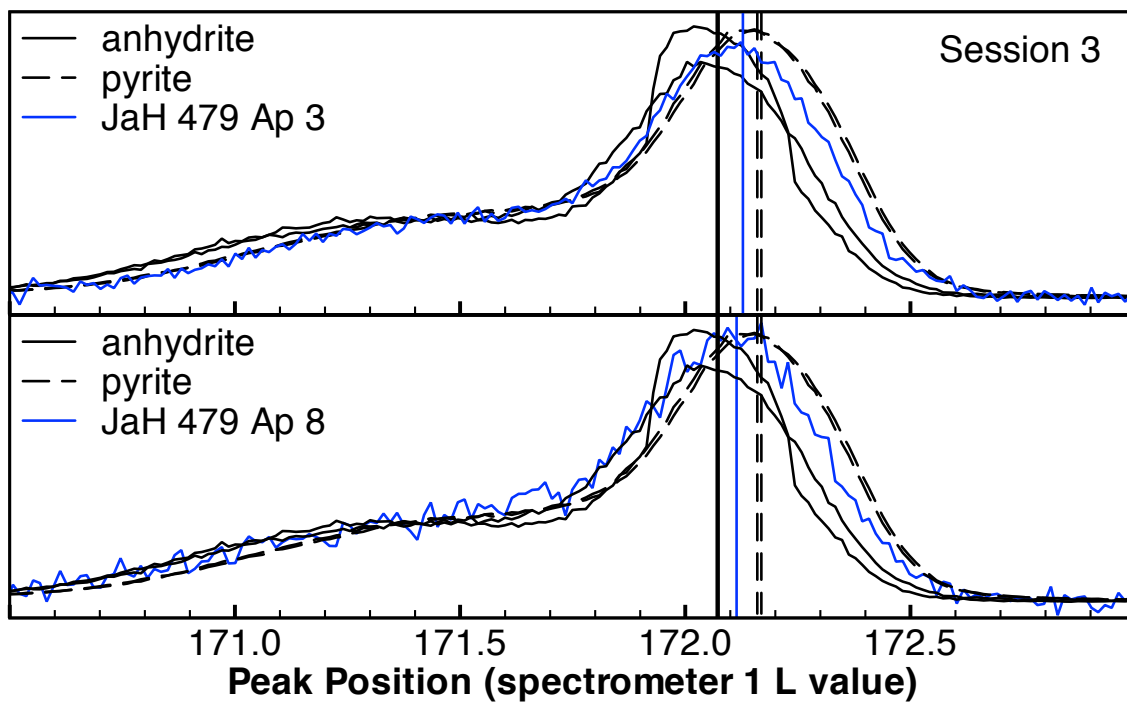


Figure C.1. Spectrometer 1 spectra of apatite grains from basaltic shergottite JaH 479 measured during session 3.

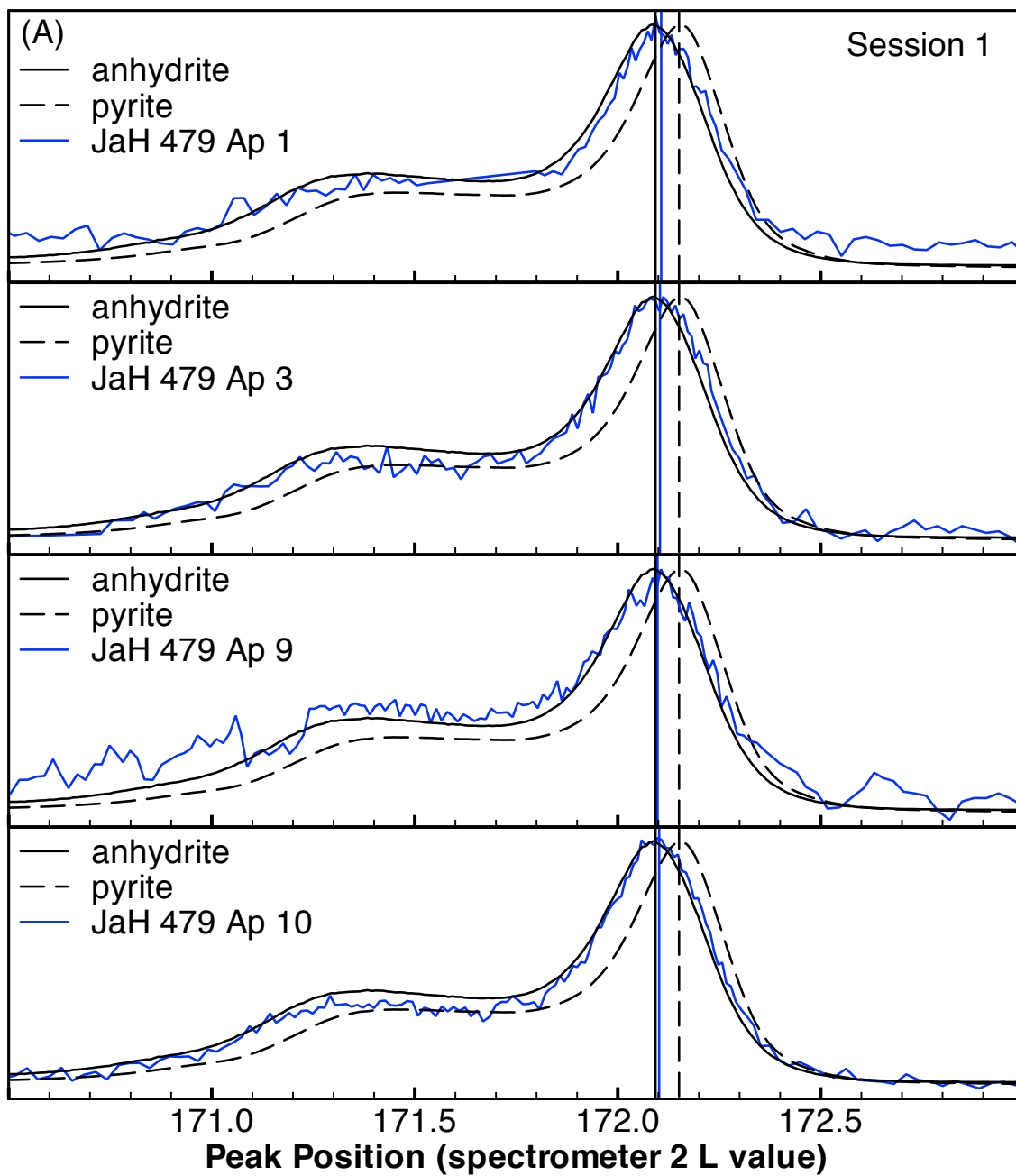


Figure C.2. Spectrometer 2 spectra of apatite grains from basaltic shergottite JaH 479 measured during session 1 and session 3. (A) session 1, and (B) session 3.

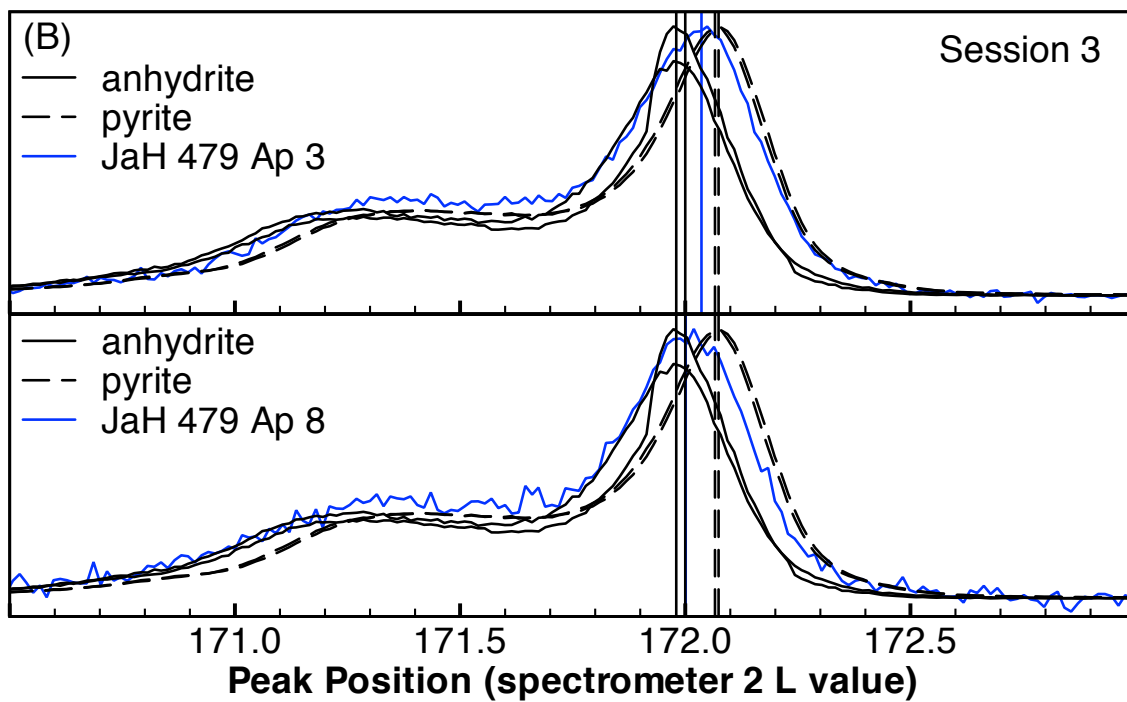


Figure C.2 continued.

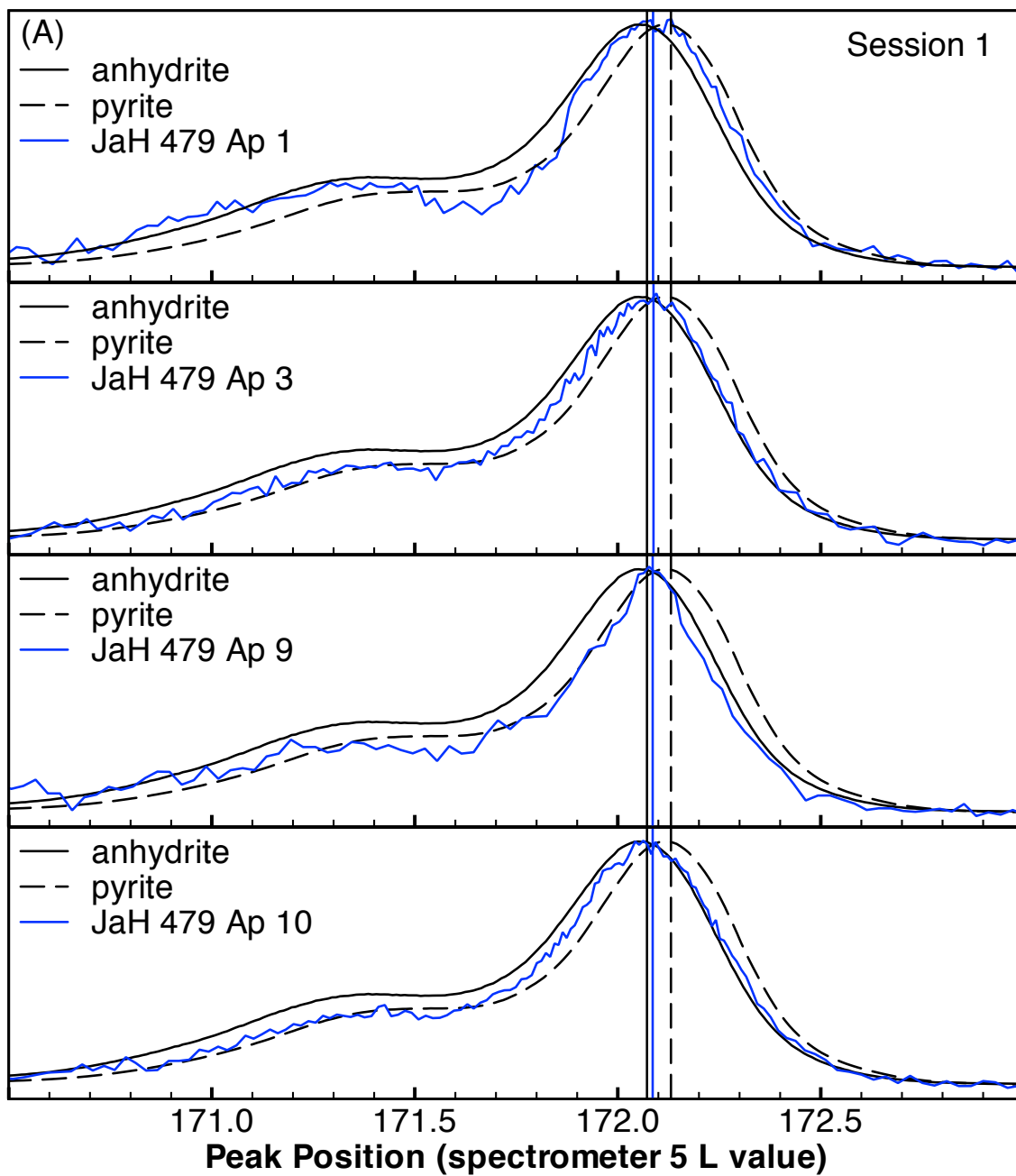


Figure C.3. Spectrometer 5 spectra of all apatite grains from basaltic shergottite JaH 479 measured during session 1 and session 3. (A) session 1, and (B) session 3.

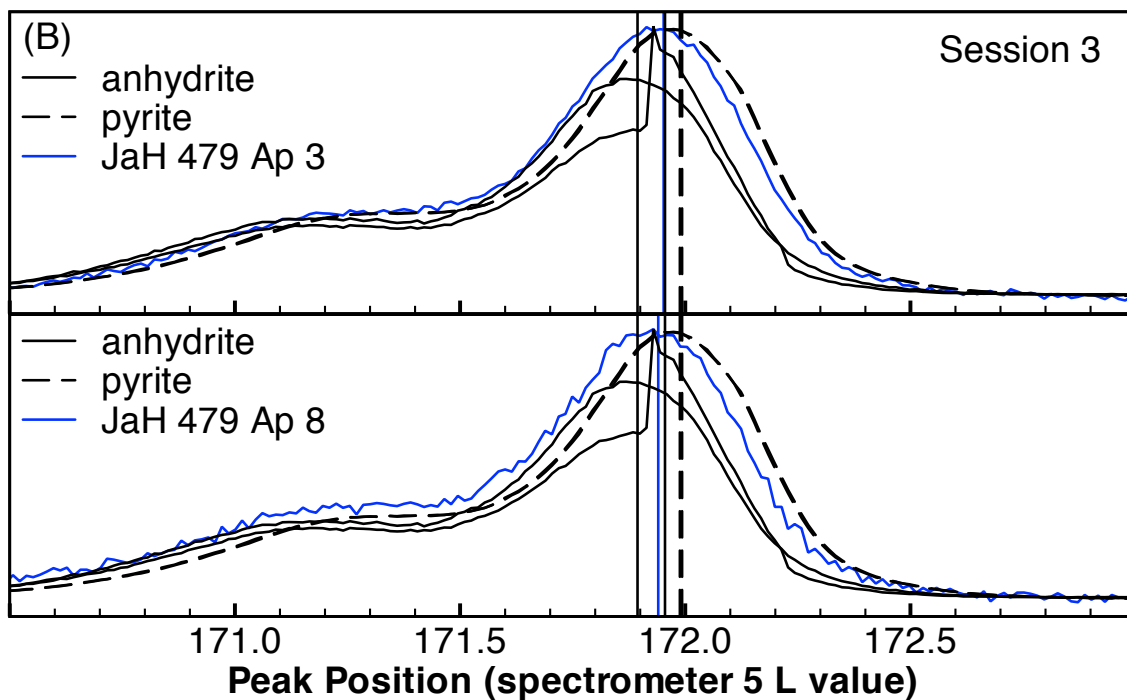


Figure C.3 continued.

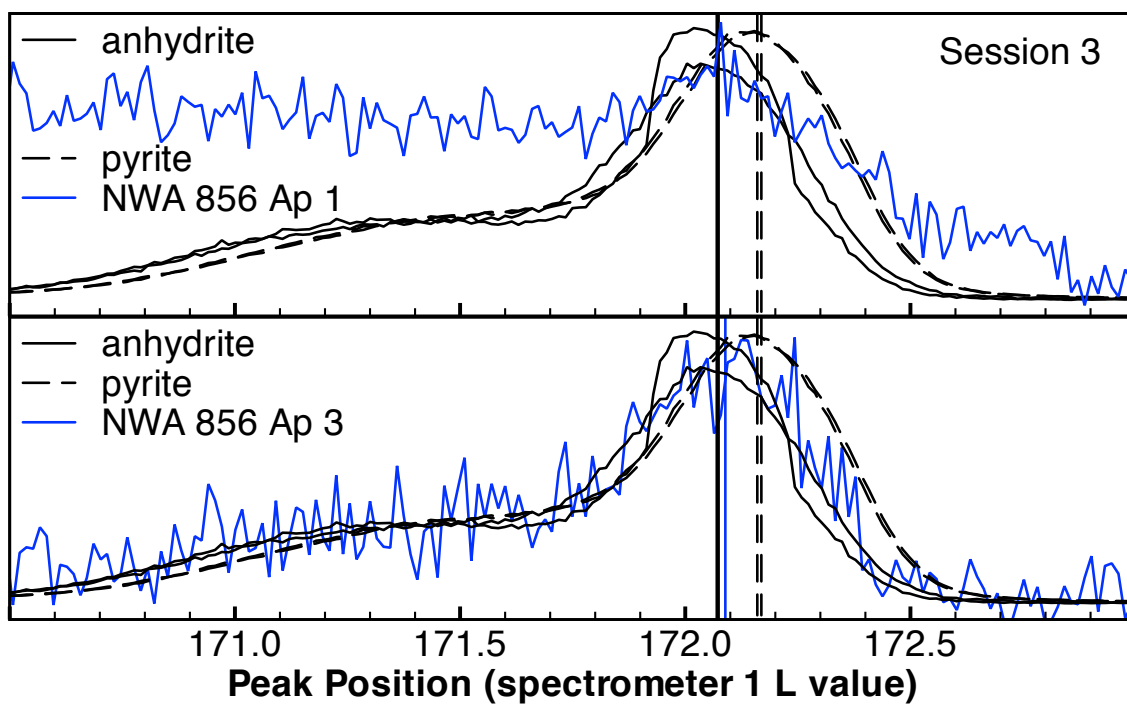


Figure C.4. Spectrometer 1 spectra of all apatite grains from basaltic shergottite NWA 856 measured during session 3.

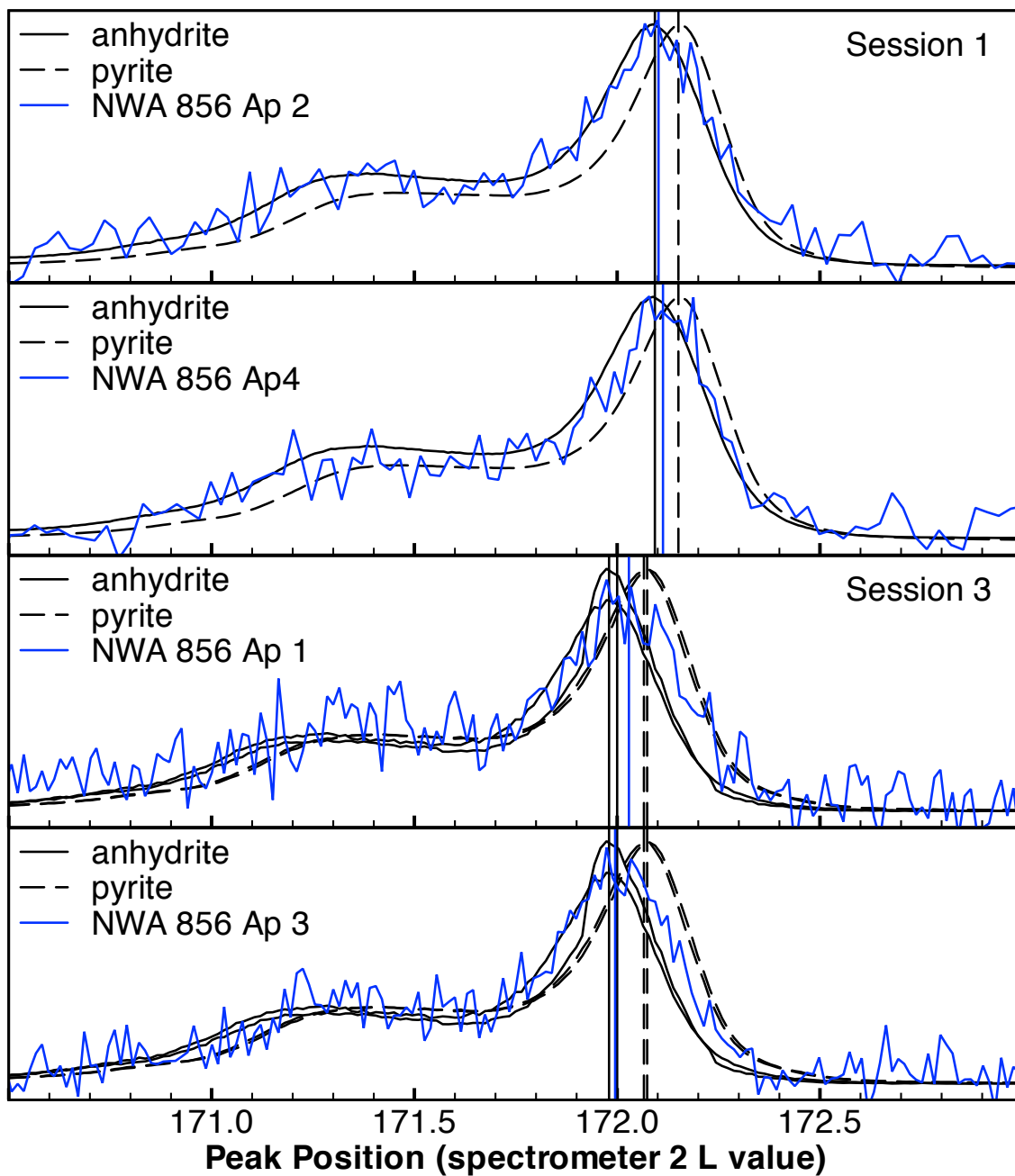


Figure C.5. Spectrometer 2 spectra of all apatite grains from basaltic shergottite NWA 856 measured during session 1 and session 3.

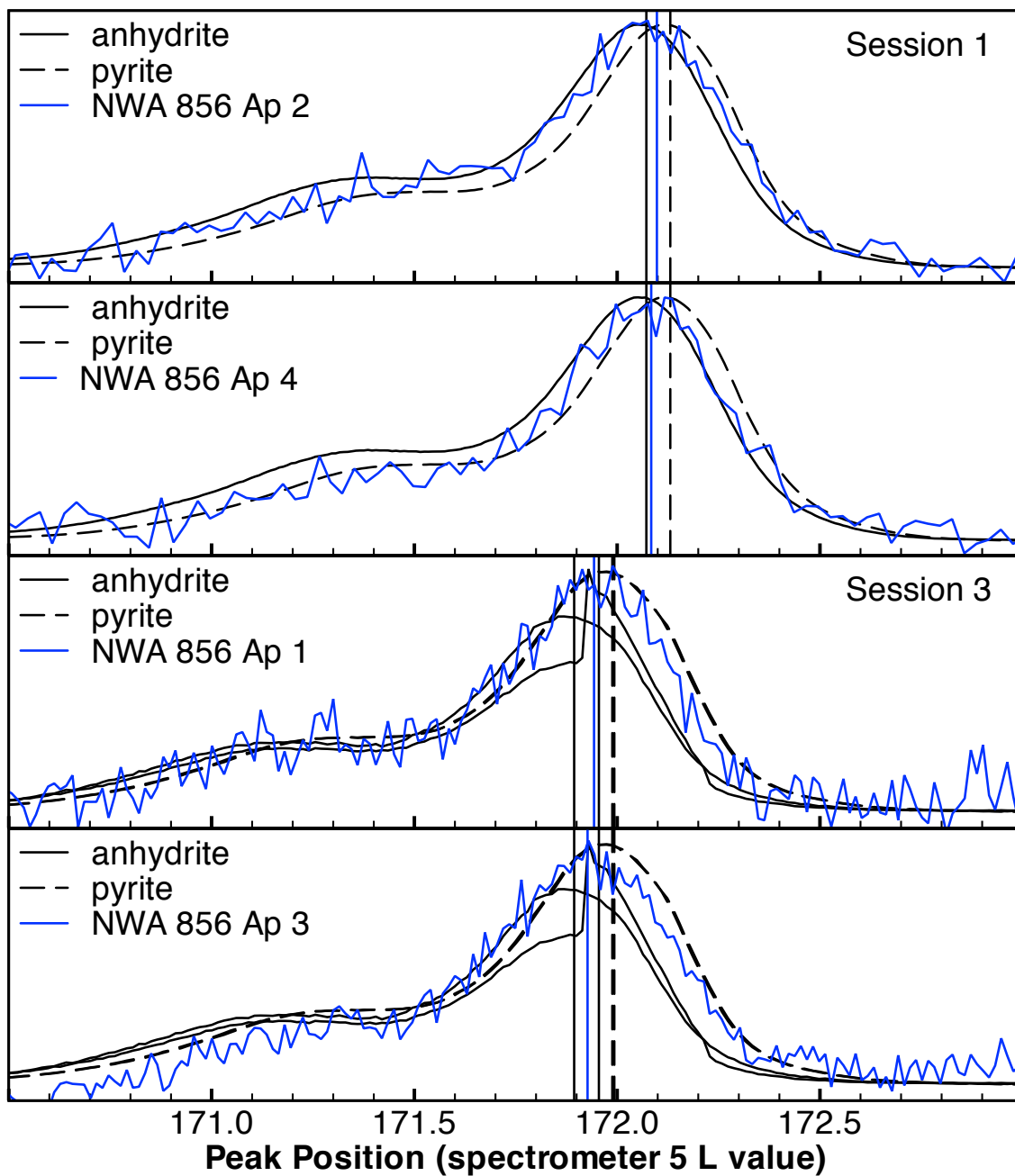


Figure C.6. Spectrometer 5 spectra of all apatite grains from basaltic shergottite NWA 856 measured during sessions 1 and 3.

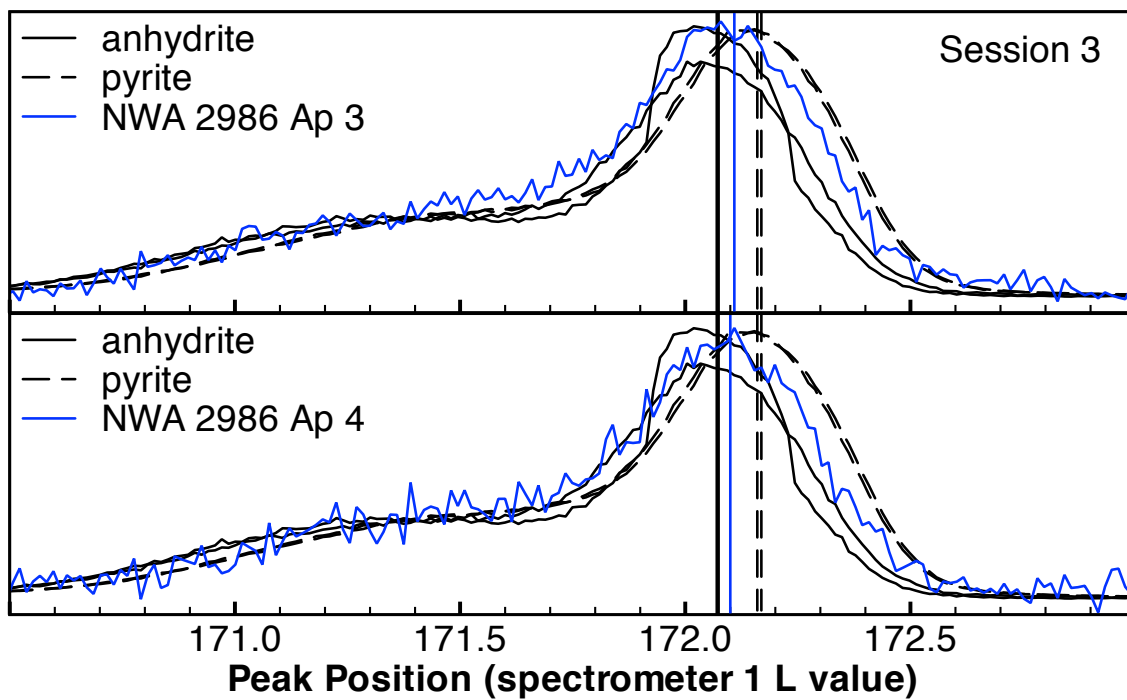


Figure C.7. Spectrometer 1 spectra of all apatite grains from basaltic shergottite NWA 2986 measured during session 3.

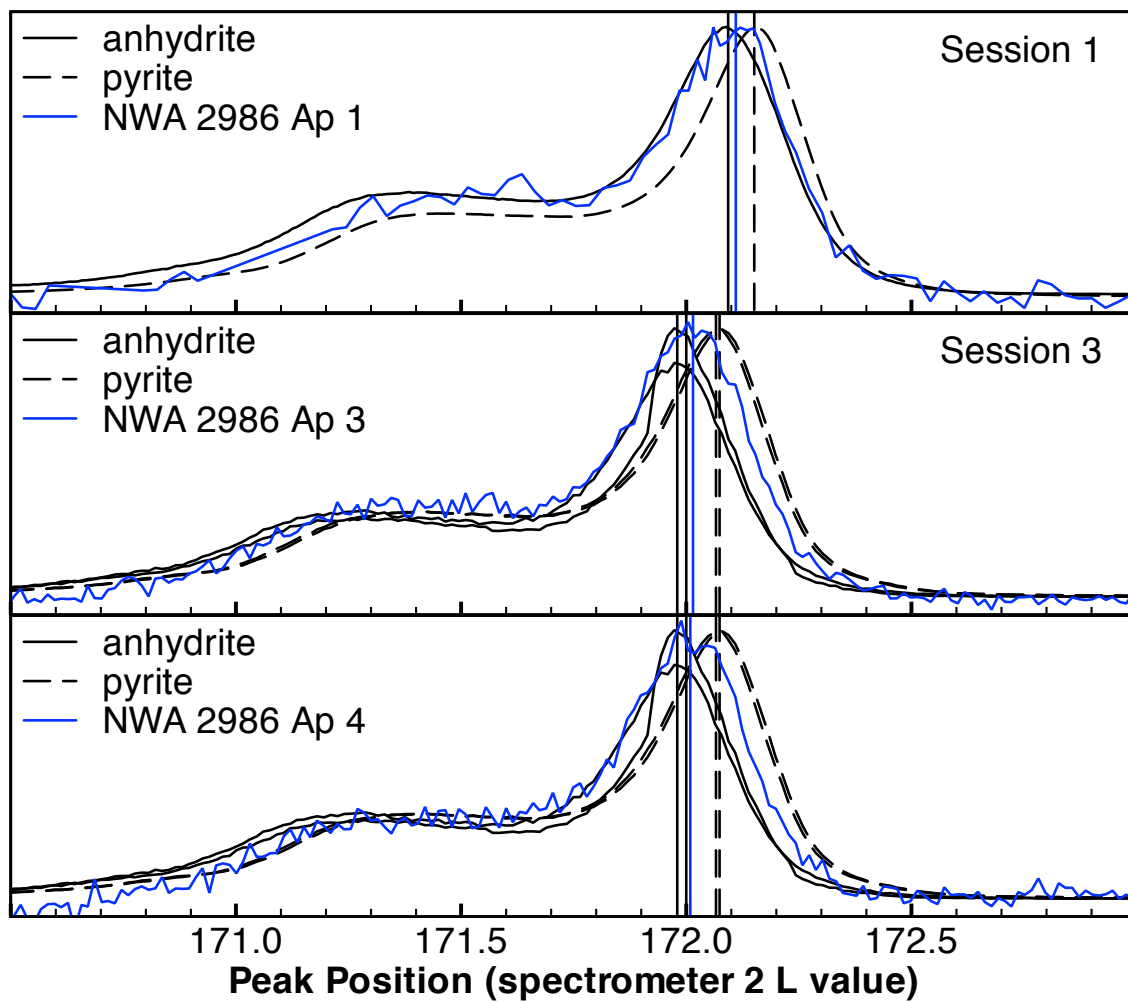


Figure C.8. Spectrometer 2 spectra from all apatite grains from basaltic shergottite NWA 2986 measured during sessions 1 and 3.

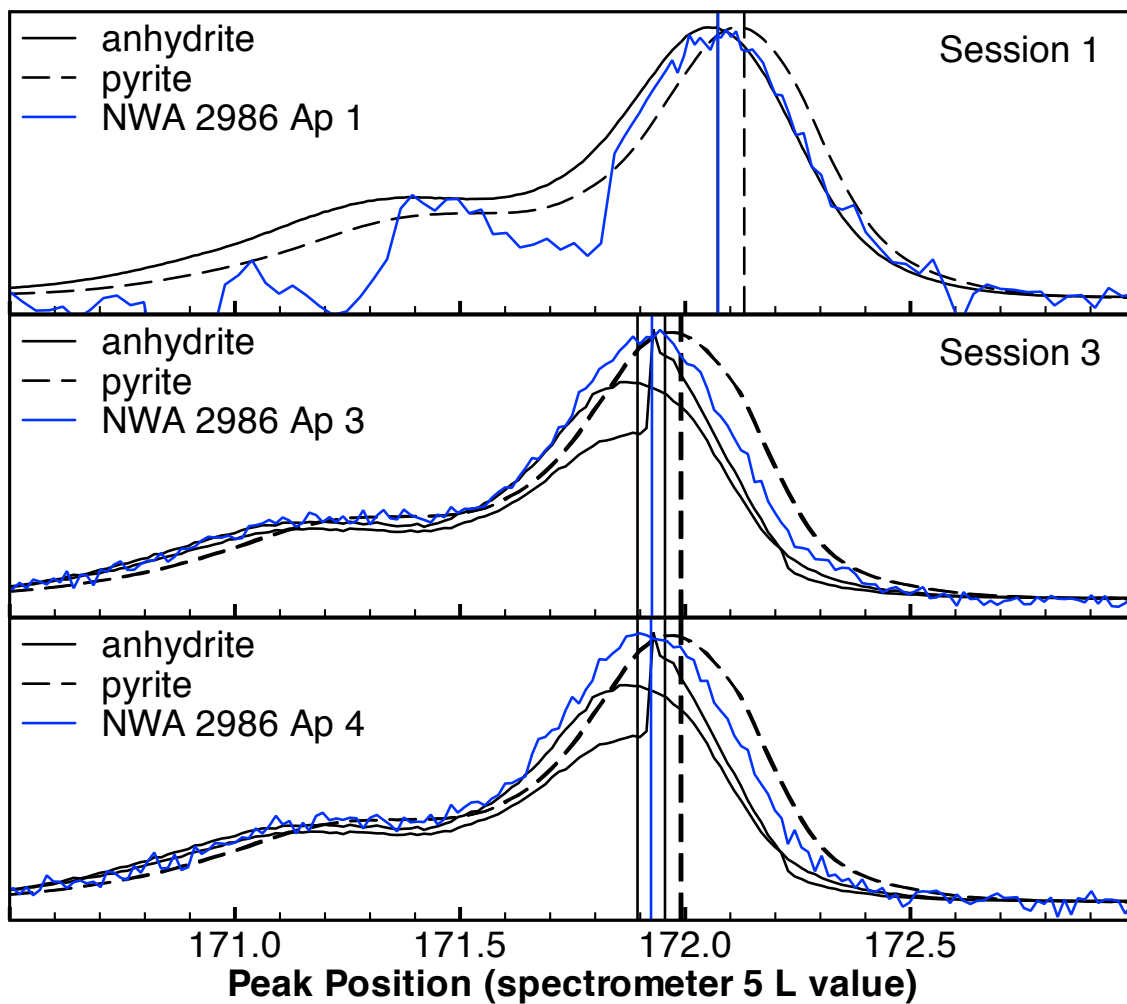


Figure C.9. Spectrometer 5 spectra of all apatite grains from basaltic shergottite NWA 2986 measured during sessions 1 and 3.

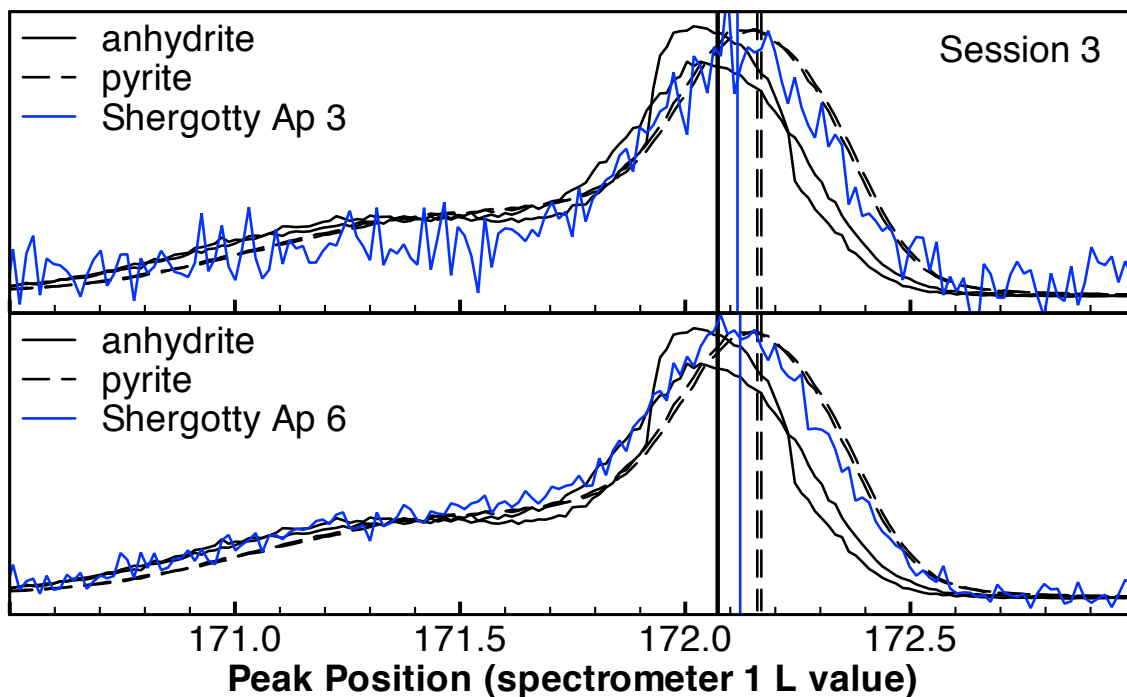


Figure C.10. Spectrometer 1 spectra of all apatite grains from basaltic shergottite Shergotty measured during session 3.

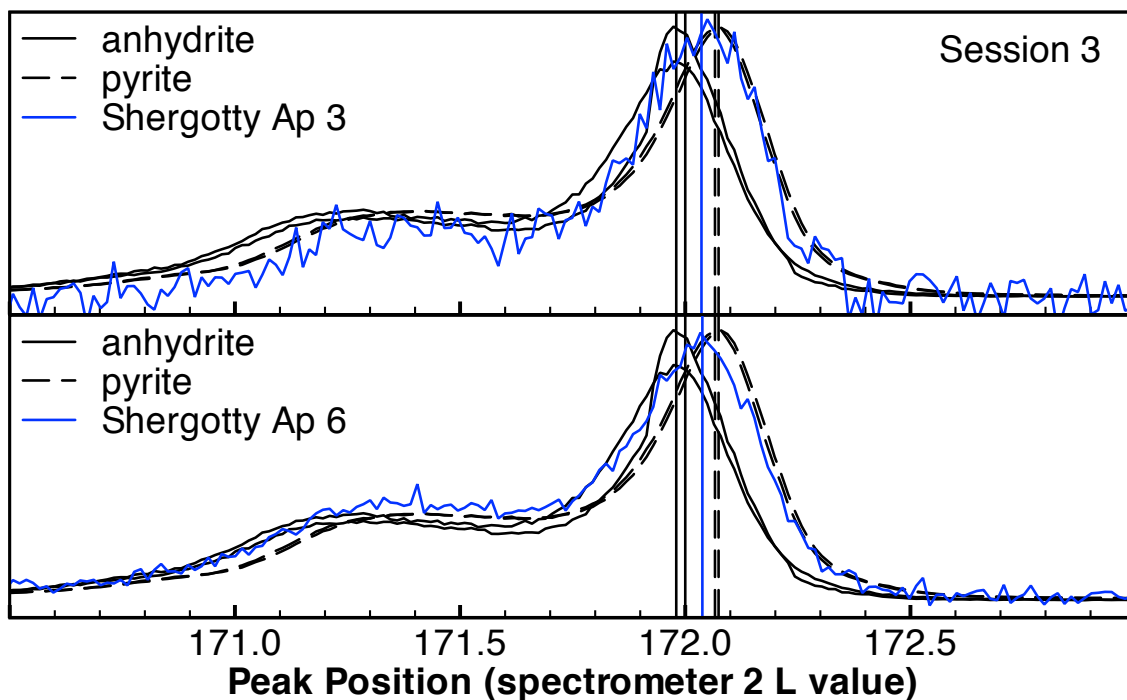


Figure C.11. Spectrometer 2 spectra of all apatite grains from basaltic shergottite Shergotty measured during session 3.

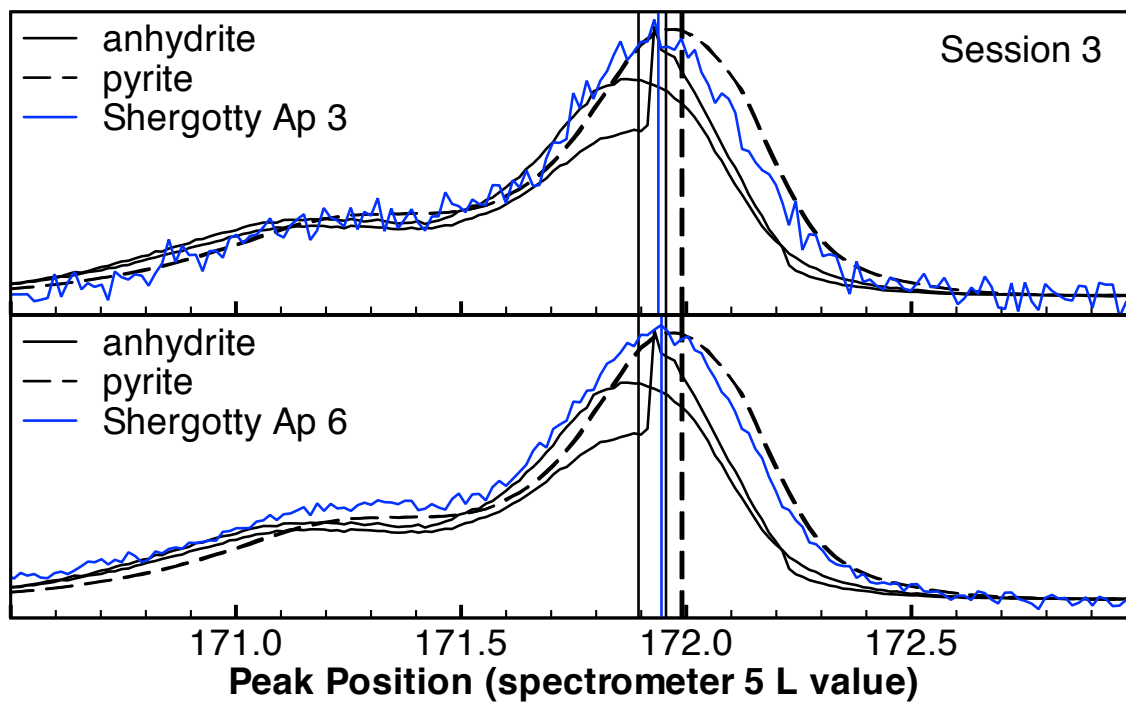


Figure C.12. Spectrometer 5 spectra of all apatite grains from basaltic shergottite Shergotty measured during session 3.

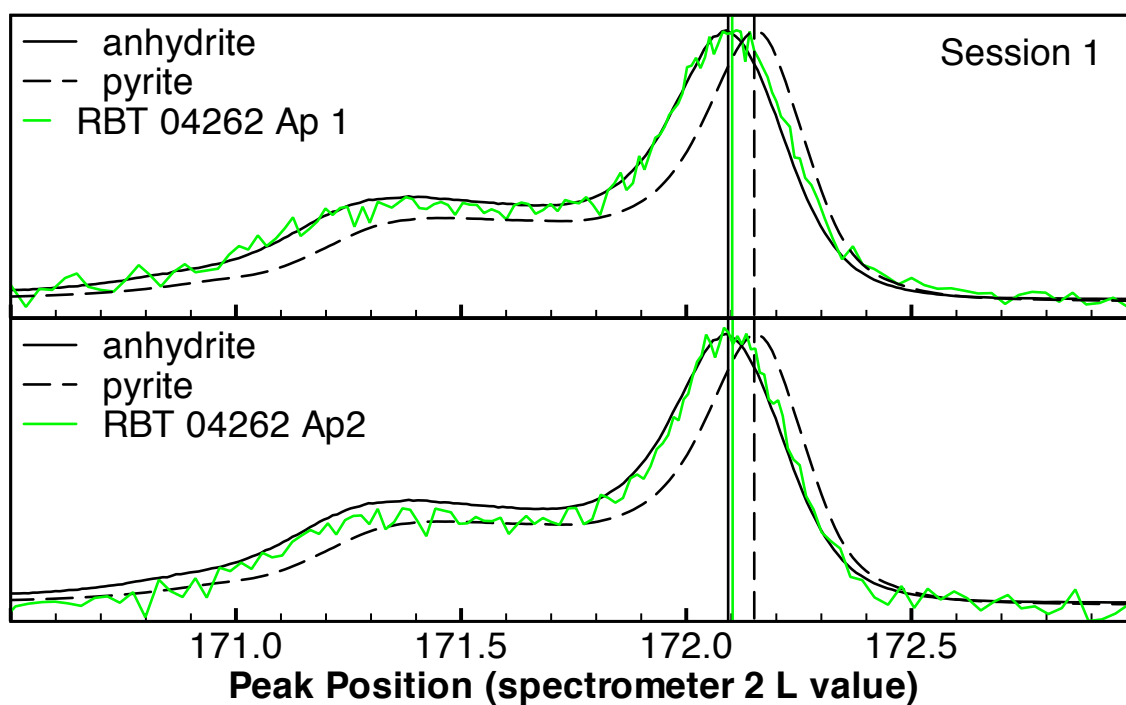


Figure C.13. Spectrometer 2 spectra of all apatite grains from olivine-phyric shergottite RBT 04262 measured during session 1.

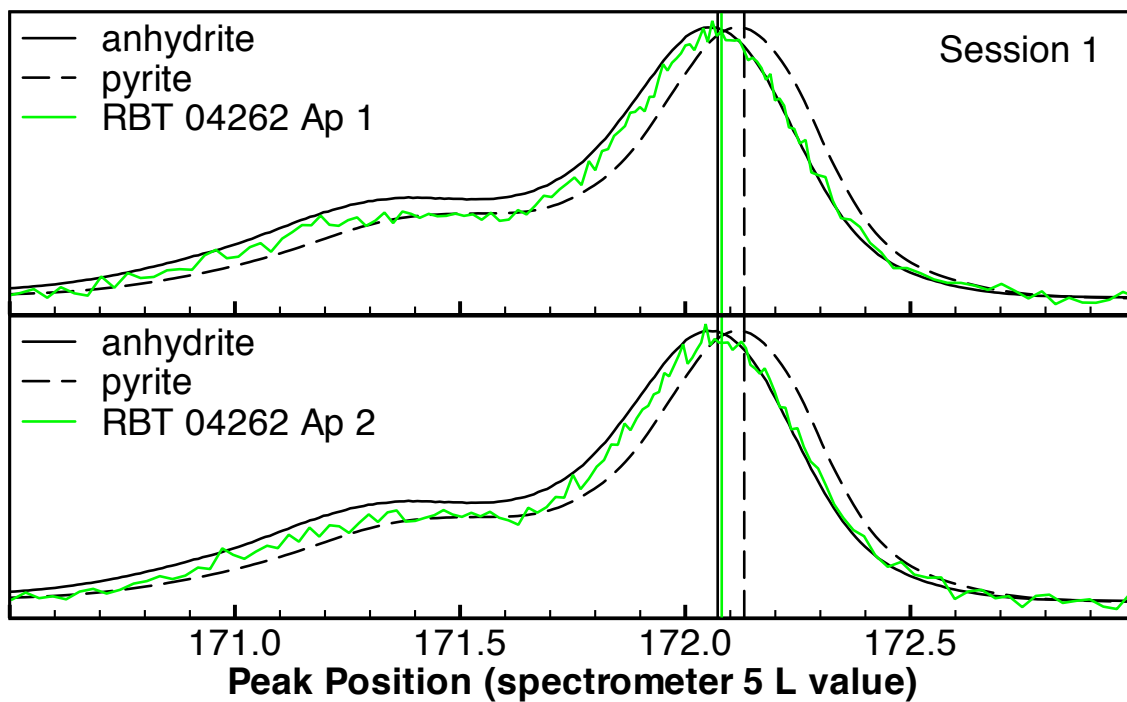


Figure C.14. Spectrometer 5 spectra of all apatite grains from olivine-phyric shergottite RBT 04262 measured during session 1.

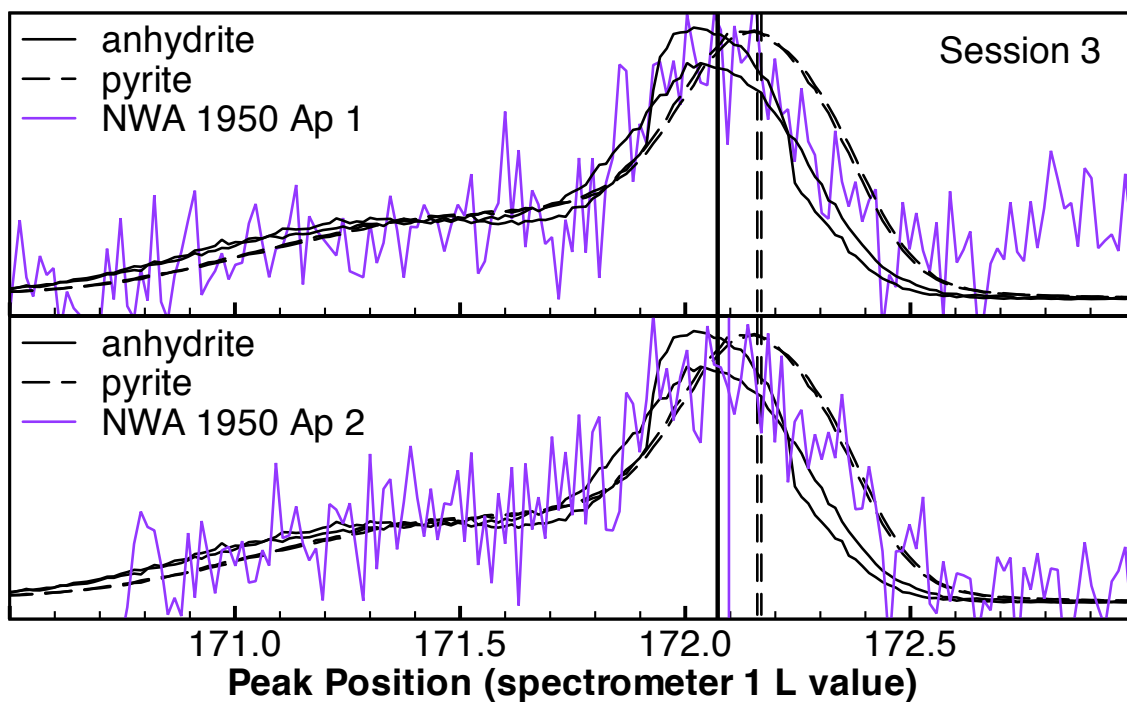


Figure C.15. Spectrometer 1 spectra of all apatites from ilherzolitic shergottite NWA 1950 measured during session 3.

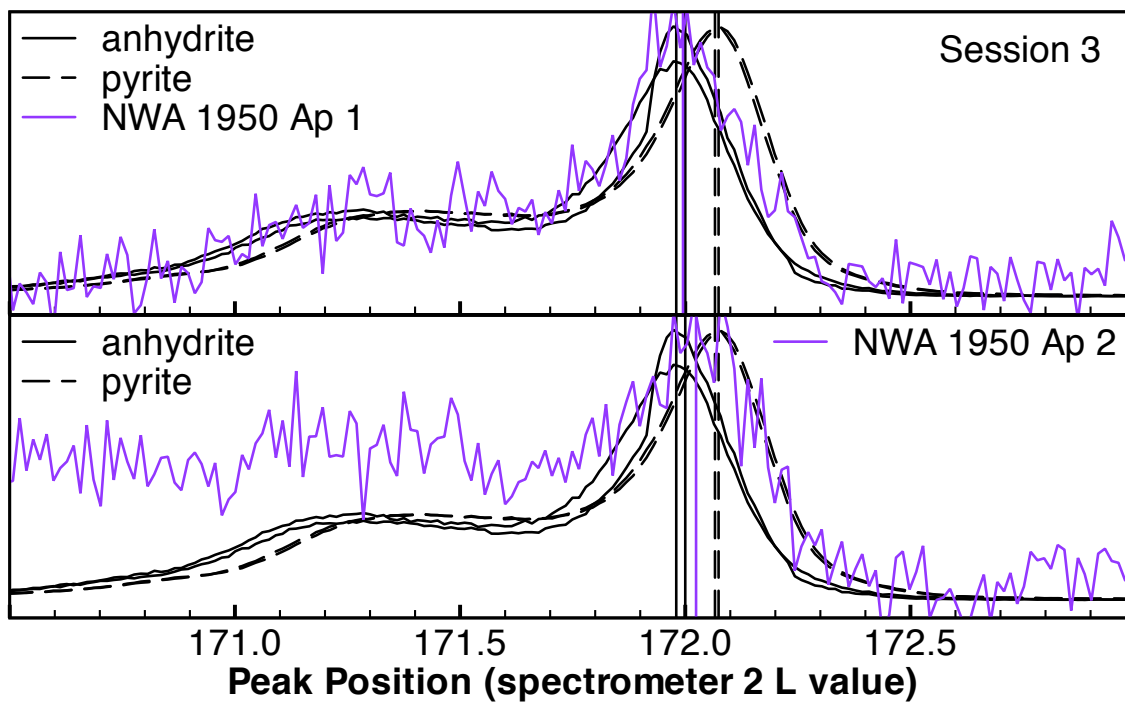


Figure C.16. Spectrometer 2 spectra of all apatites from Iherzolitic shergottite NWA 1950 measured during session 3.

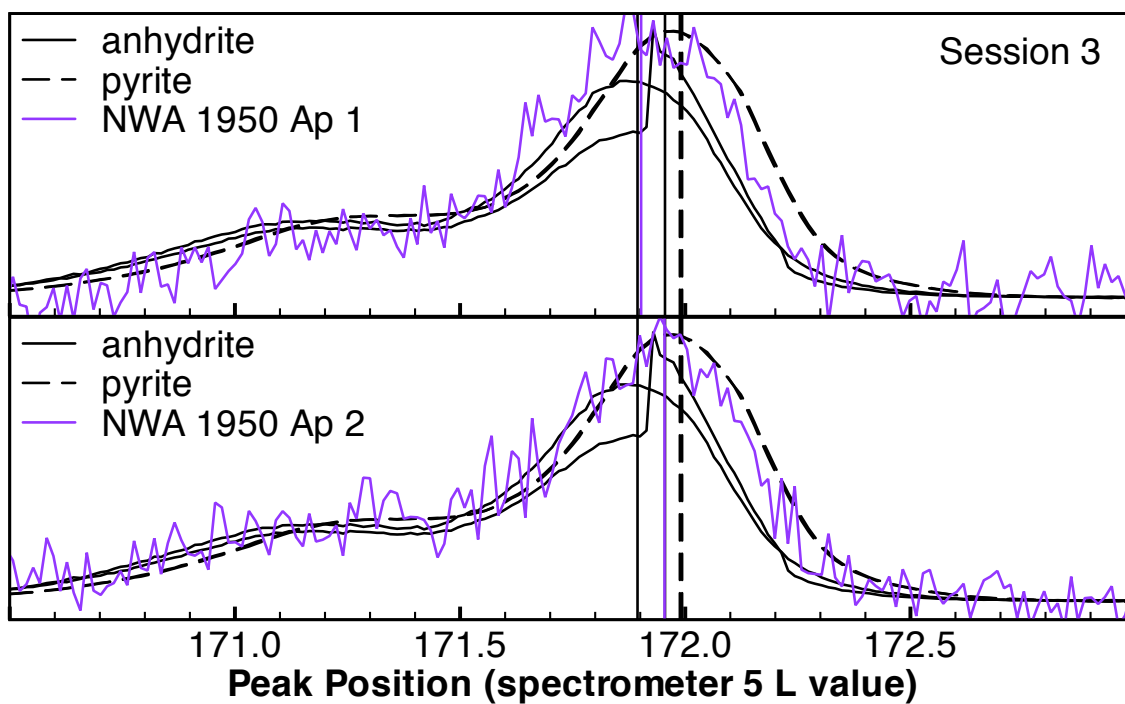


Figure C.17. Spectrometer 5 spectra of all apatites from Iherzolitic shergottite NWA 1950 measured during session 3.

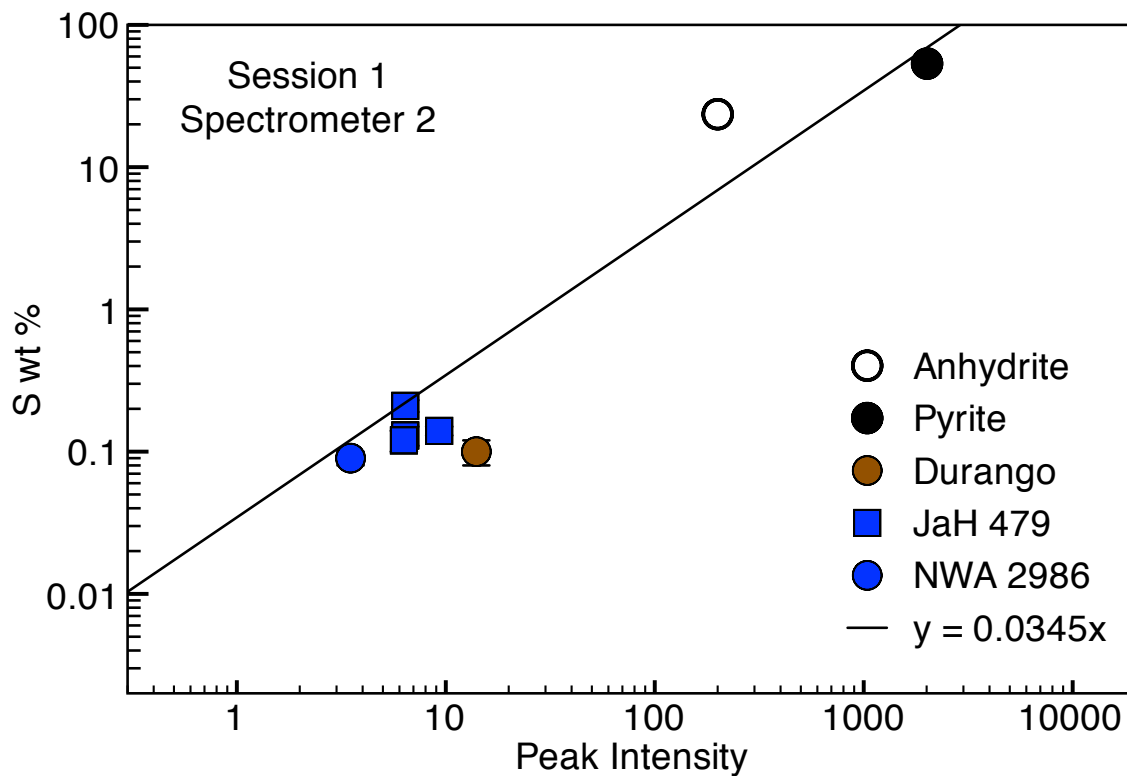


Figure C.18. Background corrected peak intensities from spectrometer 2 in session 1 plotted against sulfur abundances measured in chapter II for apatites, and stoichiometrically calculated for anhydrite and pyrite. Error bars are  $2\sigma$  of concentrations determined from ion probe measurements. The best-fit line calculated by a weighted, least-squares linear regression of the data is also shown.

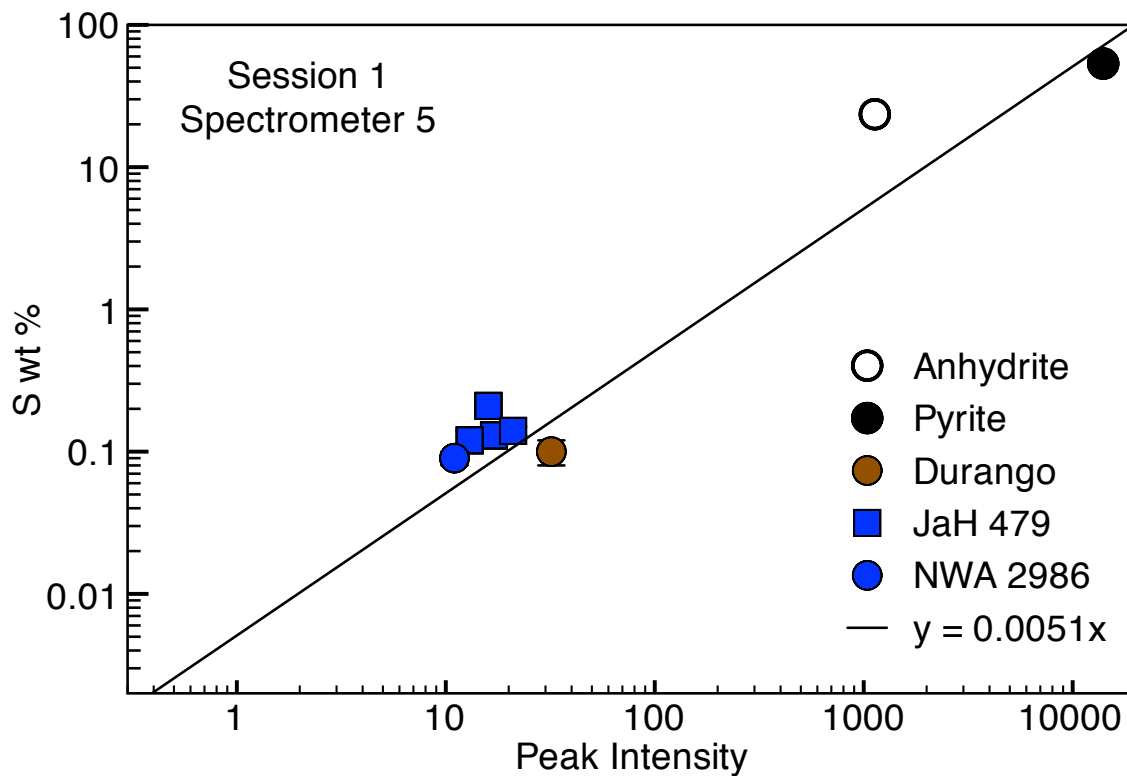


Figure C.19. Background corrected peak intensities from spectrometer 5 in session 1 plotted against sulfur abundances measured in chapter II for apatites, and stoichiometrically calculated for anhydrite and pyrite. Error bars are  $2\sigma$  of concentrations determined from ion probe measurements. The best-fit line calculated by a weighted, least-squares linear regression of the data is also shown.

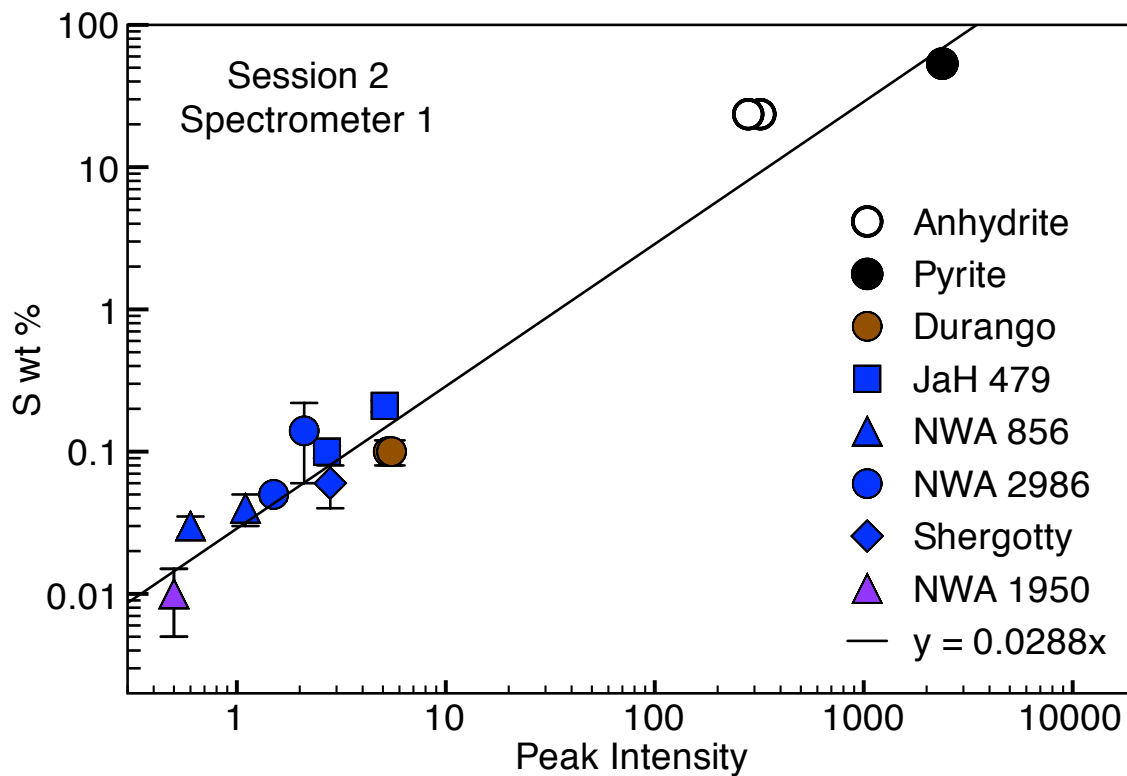


Figure C.20. Background corrected peak intensities from spectrometer 1 in session 2 plotted against sulfur abundances measured in chapter II for apatites, and stoichiometrically calculated for anhydrite and pyrite. Error bars are  $2\sigma$  of concentrations determined from ion probe measurements. The best-fit line calculated by a weighted, least-squares linear regression of the data is also shown.

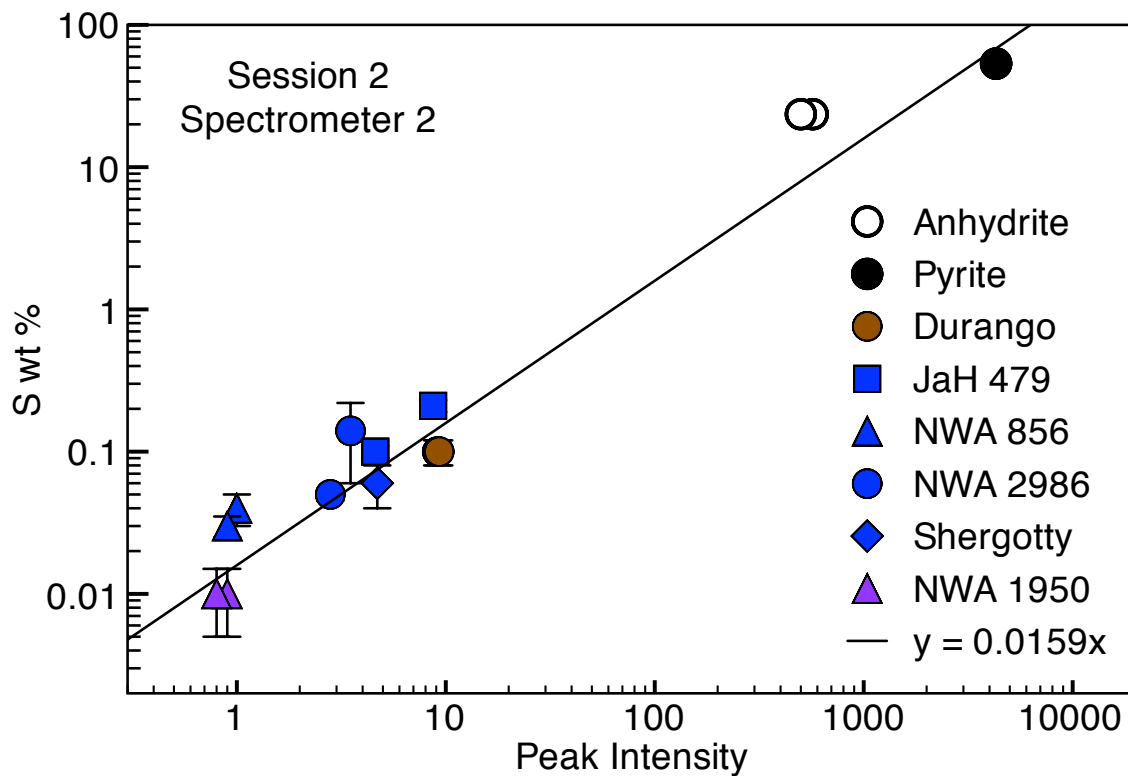


Figure C.21. Background corrected peak intensities from spectrometer 2 in session 2 plotted against sulfur abundances measured in chapter II for apatites, and stoichiometrically calculated for anhydrite and pyrite. Error bars are  $2\sigma$  of concentrations determined from ion probe measurements. The best-fit line calculated by a weighted, least-squares linear regression of the data is also shown.

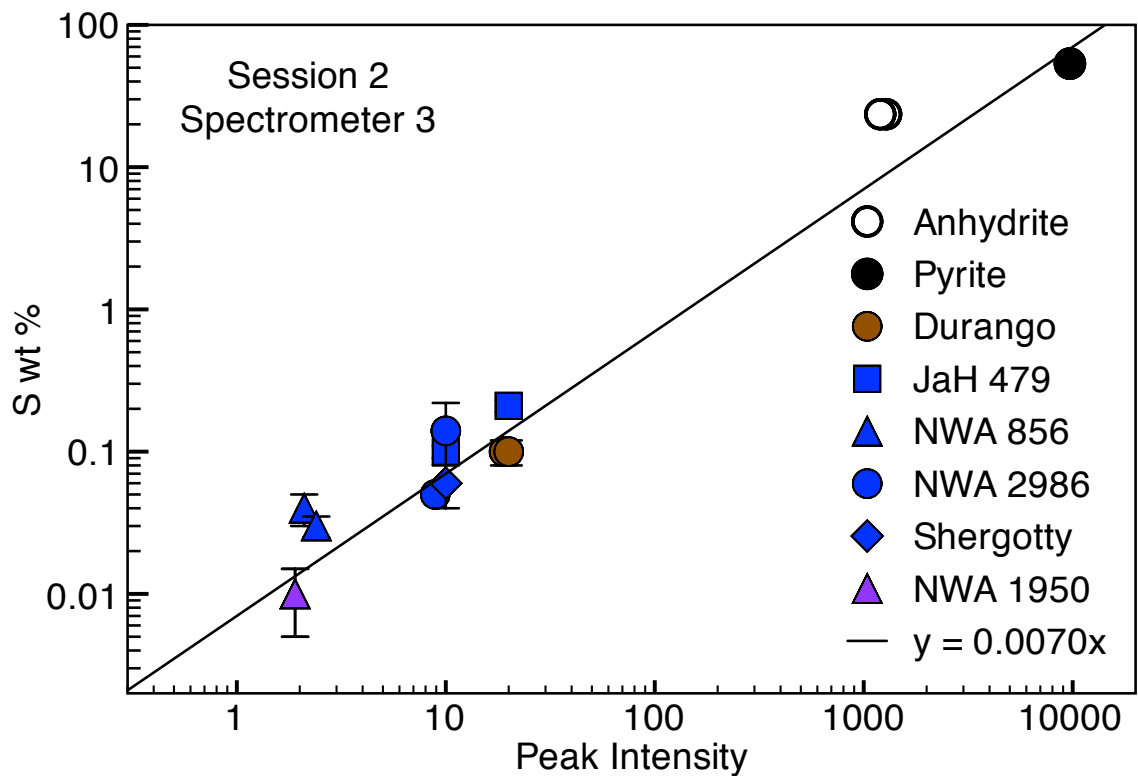


Figure C.22. Background corrected peak intensities from spectrometer 3 in session 2 plotted against sulfur abundances measured in chapter II for apatites, and stoichiometrically calculated for anhydrite and pyrite. Error bars are  $2\sigma$  of concentrations determined from ion probe measurements. The best-fit line calculated by a weighted, least-squares linear regression of the data is also shown.

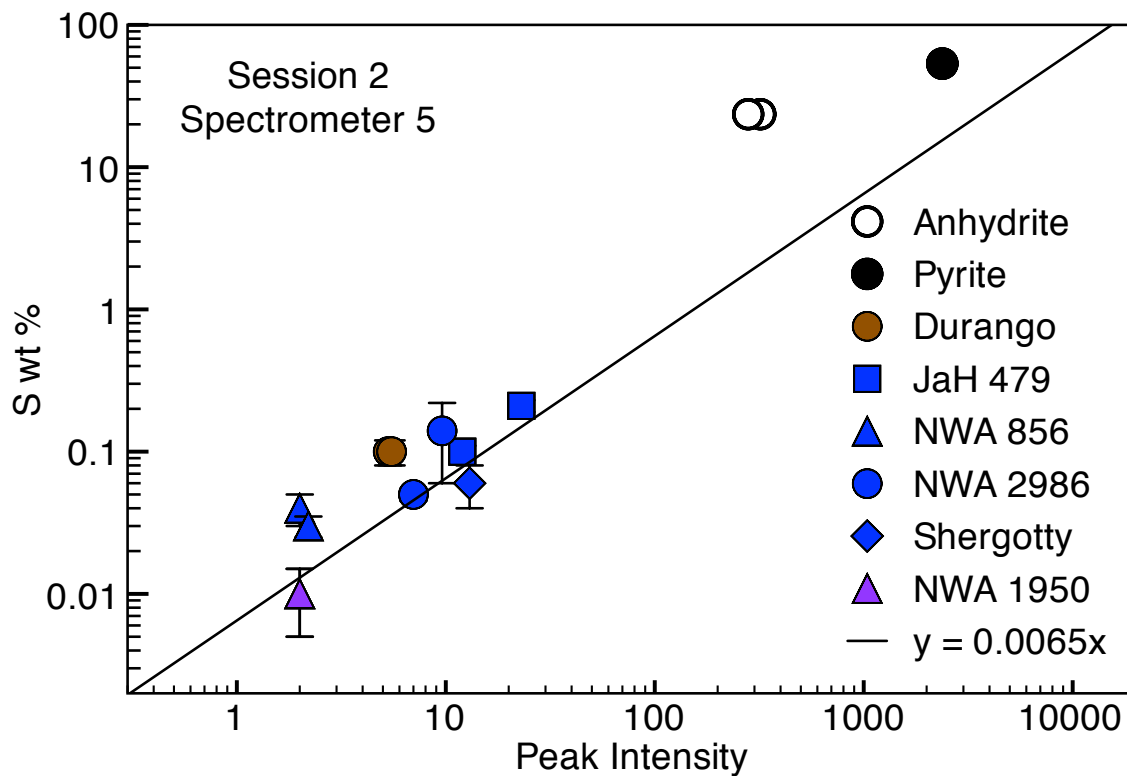


Figure C.23. Background corrected peak intensities from spectrometer 5 in session 2 plotted against sulfur abundances measured in chapter II for apatites, and stoichiometrically calculated for anhydrite and pyrite. Error bars are  $2\sigma$  of concentrations determined from ion probe measurements. The best-fit line calculated by a weighted, least-squares linear regression of the data is also shown.

Table C.2. Calculated sulfur concentration data for each spectrometer per session.

Sample	Calculated S Abundance (wt%)							Known S Abundance (wt% $\pm 2\sigma$ )	
	Session 1			Session 3					
	spec 2	spec 3	spec 5	spec 1	spec 2	spec 3	spec 5		
<b>Standards</b>									
<b>anhydrite</b>	6.90	6.36	5.77	9.20	9.08	9.02	9.44	23.55 <sup>a</sup>	
				8.05	7.97	8.45	8.01		
<b>pyrite</b>	69.31	70.97	71.51	68.30	68.50	68.34	68.36	53.45 <sup>a</sup>	
				68.45	68.50	68.34	68.36		
<b>Durango</b>	0.48	0.16	0.16	0.15	0.14	0.13	0.12	0.10 $\pm$ 0.02	
				0.16	0.15	0.14	0.13	0.10 $\pm$ 0.02	
<b>Basaltic Shergottites</b>									
<b>JaH 479</b>	1	0.22	0.08	0.09				0.13 $\pm$ 0.02	
	3	0.22	0.07	0.08	0.15	0.14	0.14	0.15	0.21 $\pm$ 0.02
	8				0.08	0.07	0.07	0.08	0.10 $\pm$ 0.01
	9	0.22	0.07	0.07					0.12 $\pm$ 0.02
	10	0.32	0.10	0.11					0.14 $\pm$ 0.01
<b>NWA 856</b>	1				0.03	0.02	0.01	0.01	0.04 $\pm$ 0.01
	2	0.08	0.03	0.03					
	3				0.02	0.01	0.02	0.01	0.03 $\pm$ 0.00
	4	0.09	0.03	0.03					
<b>NWA 2986</b>	1	0.12	0.04	0.06					0.09 $\pm$ 0.01
	3				0.06	0.06	0.07	0.06	0.14 $\pm$ 0.08
	4				0.04	0.04	0.06	0.05	0.05 $\pm$ 0.00
<b>Shergotty</b>	3				0.03	0.03	0.03	0.02	
	6				0.08	0.07	0.07	0.08	0.06 $\pm$ 0.02
<b>Olivine-Phyric Shergottite</b>									
<b>RBT 04262</b>	1	0.23	0.08	0.08					
	2	0.20	0.07	0.06					
<b>Lherzolithic Shergottite</b>									
<b>NWA 1950</b>	1				0.01	0.01	0.01	0.01	0.01 $\pm$ 0.00
	2				0.01	0.01	0.01	0.01	0.01 $\pm$ 0.00

<sup>a</sup>Calculated by stoichiometry.